Constraints on the Prompt Emission Mechanism of Gamma-Ray Bursts using Time-Resolved Spectroscopy

A dissertation submitted for the degree of
Doctor of Natural Sciences (Dr. rer. nat.)

by

Hoi-Fung Yu

to

Technische Universität München

and

Max-Planck-Institut für extraterrestrische Physik

December 2015

Technische Universität München

Technische Universität München
Max-Planck-Institut für extraterrestrische Physik

Constraints on the Prompt Emission Mechanism of Gamma-Ray Bursts using Time-Resolved Spectroscopy

Hoi-Fung Yu

Vollständiger Abdruck der von der Fakultät für Physik der Technischen Universität München zur Erlangung des akademischen Grades eines

Doktors der Naturwissenschaften

genehmigten Dissertation.

Vorsitzender:		Univ.-Prof. Dr. Alejandro Ibarra
Prüfer der Dissertation:	1.	Priv.-Doz. Dr. Jochen Greiner
	2.	Univ.-Prof. Dr. Elisa Resconi

Die Dissertation wurde am 03.12.2015 bei der Technischen Universität München eingereicht und durch die Fakultät für Physik am 04.02.2016 angenommen.

To my beloved,

Pik-Ying Peggy Chan.

願聞顯據
以窮理實
浮詞虛貶
竊非所懼

祖沖之《駁議》(462)

I will listen to the evidence,
To pursue the truth.
Fancy words and false demeaning,
Are not what I fear.

Zou Cung-Zi, *Refutation* (462)

For small creatures such as we the vastness is bearable only through love.

Carl Sagan, *Contact* (1985)

Tell your son to stop trying to fill your head with science - for to fill your heart with love is enough!

Richard Feynman, *No Ordinary Genius: The Illustrated Richard Feynman* (1996)

We are going to die, and that makes us the lucky ones. Most people are never going to die because they are never going to be born.

Richard Dawkins, *Unweaving the Rainbow* (1998)

我藏起來的秘密
在每一天清晨裡
暖成咖啡
安靜的拿給妳

小柯〈不要說話〉
陳奕迅《不想放手》(2008)

The secrets that I hide,
In mornings of every day,
I warm and make them into coffee,
Silently pass to you.

Little Or, *Don't Talk*
Eason Chan, *Don't Wanna Let Go* (2008)

Abstract

Since the birth of gamma-ray astronomy, large number of gamma-ray bursts (GRBs) has been observed. These short, cosmological flashes of high-energy gamma-rays ($\sim 10^{51}$ - 10^{53} erg s^{-1}) are believed to associate with exploding massive stars. Gamma-ray bursts can be used to probe the physical and chemical environment of the early Universe at redshifts $z > 10$, thus the study of GRBs is one of the most important in contemporary high-energy astrophysics. Through research efforts in the past half century, large amount of high-quality gamma-ray data have been obtained. However, a coherent understanding of the GRB prompt emission mechanism is still missing mainly due to the difficulty in interpreting the data. In this dissertation, I study the emission mechanism of the GRB prompt emission phase by time-resolved spectroscopy using the high-resolution data obtained by the *Fermi* Gamma-ray Space Telescope Gamma-ray Burst Monitor (GBM). I present detailed time-resolved spectral analysis of the brightest GBM GRBs. A novel quantity is invented to measure the spectral sharpness which can be used to compare directly to theory. It is found that the conventional explanation of the prompt emission phase by optically thin synchrotron emission is inconsistent with a majority of observed spectra. Emission mechanism other than non-thermal synchrotron radiation is likely required to achieve a full explanation of the GRB prompt emission phase.

Zusammenfassung

Seit Beginn der Gammastrahlen-Astronomie wurde eine Vielzahl an Gammastrahlenblitzen (Gamma-Ray Bursts, GRBs) beobachtet. Diese kurzlebigen, kosmologischen Strahlenblitze aus hochenergetischen Gammastrahlen ($\sim 10^{51}$ - 10^{53} erg s^{-1}) werden im heutigen Verständnis mit explodierenden massereichen Sternen in Verbindung gesetzt. Mithilfe von GRBs kann die physikalische und chemische Umgebung des frühen Universums bei Rotverschiebungen von $z > 10$ untersucht werden, was die Erforschung von GRBs zu einer der wichtigsten Studien der heutigen Hochenergie-Astrophysik macht. Durch die Forschung im letzten halben Jahrhundert wurde eine große Menge an hochwertigen Messdaten im Bereich der Gammastrahlung gesammelt. Jedoch fehlt noch das vollständige Verständnis der prompten Emission von GRBs , was hauptsächlich an der Schwierigkeit beim Interpretieren der Messdaten liegt. In dieser Doktorarbeit untersuche ich den Emissionsmechanismus der prompten Emissionsphase von GRBs durch zeitaufgelöste Spektroskopie anhand der hochauflösenden Messdaten des *Fermi* Gamma-ray Space Telescope Gamma-ray Burst Monitor (GBM). Ich präsentiere detailierte zeitaufgelöste Spektralanalysen der hellsten GBM GRBs. Eine neue Größe zum Messen der spektralen Schärfe, welche sich für den direkten Vergleich mit der Theorie eignet, wird eingeführt. Dabei ergibt sich, dass die konventionelle Erklärung der prompten Emissionsphase durch optisch dünne Synchrotronstrahlung inkonsistent mit der Mehrheit der beobachteten Spektren ist. Es werden wahrscheinlich andere Emissionsmechanismen als die nichtthermische Synchrotronstrahlung benötigt, um eine vollständige Erklärung für die prompte Emissionsphase von GRBs zu erhalten.

Contents

Chapter 1

Gamma-Ray Bursts

"I can live with doubt, and uncertainty, and not knowing. I think it is much more interesting to live not knowing than have answers which might be wrong. ... It doesn't frighten me."

- Richard Feynman

Gamma-ray bursts are among the most interesting and mysterious objects in the observable Universe. Today, we know that they are cosmological transient gamma-ray sources isotropically distributed across the sky, associated with exploding massive stars or compact object mergers. However, we still do not know exactly what causes a GRB and how it emits the enormous energy (typically $\sim 10^{53}$ erg within tens of seconds) that can outshine the total energy output in the entire history of a galaxy.

An understanding of the emission mechanism of GRBs provides information of, for instance, the dynamics of the relativistic outflows in the GRB jet, microphysics parameters in the emission regions, structure and dynamics of the progenitor and the central engine (believed to be either a black hole or a magnetar), chemical and physical properties of the circum-burst and interstellar medium, host galaxy properties, and ultimately the evolution of the universe. The last item in the list is one of the most important aspects of modern cosmology, which requires observational data from high redshift sources.

Simply because they are extremely bright in the gamma-ray frequencies, GRBs easily hold the record of the highest observed redshift among all kinds of cosmological sources known to date. Moreover, the plausible linkage of GRBs to supernovae provides prospect of including GRBs into the so-called cosmological ladder. Therefore, researches on the emission mechanism of the observed

gamma-rays from GRBs are of great importance and interest to not only high-energy astrophysicists, but also to cosmologists and many scientists in the research fields of fundamental natural science.

In this dissertation, I present my works as tiny contributions to the quest of revealing the true GRB physics. Using the *Fermi* GBM data, I first performed time-resolved spectroscopy on a few energetic GBM GRBs to investigate the emission mechanism of the prompt emission phase. In Ch. 2, I present the first *Fermi* GBM GRB time-resolved spectral catalog (Yu et al. submitted). In Ch. 3 (Yu et al. 2015a), we find that the conventional synchrotron emission models require additional balckbodies or fine-tuned microphysics parameters to be able to get over the "line-of-death" problem. In Ch. 4 (Yu et al. 2015b), we find that most of the spectra are indeed inconsistent with a purely optically thin synchrotron emission model by a novel measured quantity. Before going into the details of my researches, let's do a revision on various emission mechanism models of GRBs.

Unless otherwise stated, in all following chapters, cgs units are used and errors are given at the 1σ confidence level.

1.1 A Brief History of GRB Research

The story begins 48 years ago.

For a long period of time, before the birth of high-energy astronomy, astronomers used to think that the gamma-ray sky stays relatively constant except for statistical background fluctuations. In the year of 1967, a group of satellites, named the *Vela* Satellite Network, were launched to identify gamma-ray signatures emitted by nuclear weapons on Earth. The *Vela* satellites quickly detected a number of mysterious gamma-ray flashes. Localization analysis results (Klebesadel et al. 1973) showed that these gamma-rays are originated neither from the Earth nor the Sun, ruling out the possibility of nuclear tests or solar origin. This new kind of extraterrestrial gamma-ray sources is named gamma-ray bursts.

The Earth's atmosphere has been protecting lifes on Earth from harmful gamma-rays for billions of years. In order to study and understand these short (typically around tens of seconds) but luminous events, scientists have to launch detectors into space. Research progress has much advanced when the *Compton* gamma-ray Observatory[1] was launched in 1991, with the highly sensitive Burst and Transient Source Explorer (BATSE) instrument (Fishman et al. 1989; Meegan et al. 1992)

[1] `http://heasarc.gsfc.nasa.gov/docs/cgro/cossc/`

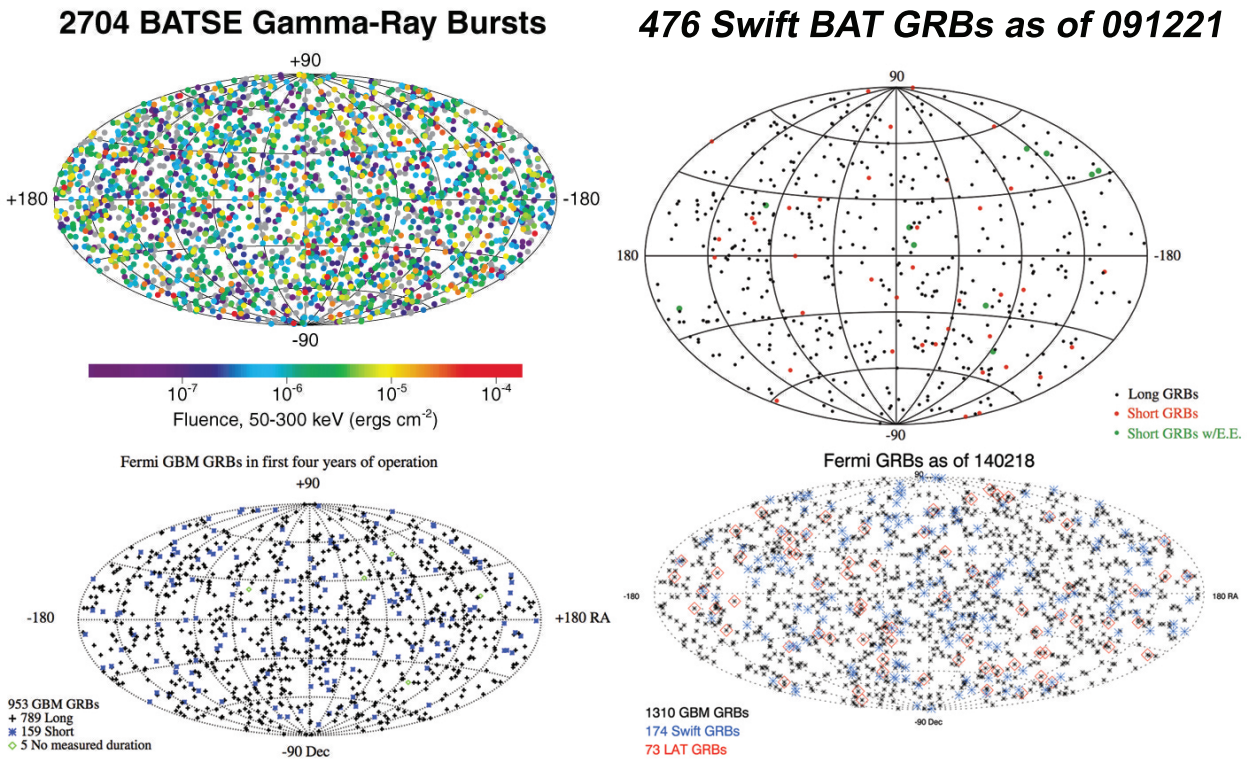

Figure 1.1: Distributions of GRBs on the sky. From top left to bottom right: 2,704 BATSE GRBs of the complete *CGRO* mission; 476 *Swift* BAT GRBs as of 21 December 2009 (Sakamoto et al. 2011); 953 *Fermi* GBM GRBs as of 13 July 2012 (von Kienlin et al. 2014); 1,310 *Fermi* GBM GRBs, 174 *Swift* GRBs, and 73 *Fermi* LAT GRBs as of 18 February 2014.

on board specially constructed to monitor and locate GRBs. In contrast to pointed gamma-ray telescopes, BATSE provides all-sky monitoring in the gamma-ray energy range of 25 keV - 2 MeV where most observed early gamma-rays, i.e., the prompt emission, from GRBs typically reside. The near real-time localization of GRBs from BATSE has facilitated quick multi-wavelength follow-up observations by various ground- and space-based telescopes and led to an increased interest of GRB physics in the high-energy astrophysical research community.

More and more GRBs are detected such that statistical studies of these transients can finally be conducted. By plotting their duration (the time period that accumulates from 5% to 95% of the emission, T_{90}) against the hardness ratio (ratio of the observed energy in different energy bands), Kouveliotou et al. (1993) discovered that there are two kinds of GRBs - the long/soft GRBs ($T_{90} > 2$ s and low-energy photons rich) and the short/hard GRBs ($T_{90} < 2$ s and high-energy photons rich).

The short duration of GRBs, the observed millisecond variabilities in their lightcurves, and

their high-energy gamma-ray emissions all suggest that the central engines of GRBs must be small and compact. Therefore, astrophysicists first speculated that GRBs are originated from small scale objects in the solar system or compact sources within our Milky Way Galaxy, e.g., galactic neutron stars or black holes.

In contrast, BATSE data showed that GRBs are distributed isotropically across the sky (Briggs et al. 1996; Hakkila et al. 1994; Tegmark et al. 1996). Figure 1.1 shows examples of GRB sky maps taken from the *CGRO*,[2] *Swift*, and *Fermi* mission.[3] This discovery is a strong evidence against theories of GRBs being originated from galactic sources or the supermassive black hole at the galactic center, because we do not see GRBs on only the galactic plane. Therefore, despite the non-detection of expected nuclear emission lines which prevented the measurement of cosmological redshift, it is strongly suggested that GRBs are of extragalactic origins (e.g., van den Bergh 1983; Paczynski 1986). This is later confirmed by Metzger et al. (1997) who reported the redshift of GRB 970508 measured from its optical afterglow spectrum. Nowadays, it is believed that long GRBs are results of gravitational collapse of massive stars (Woosley 1993, 1996; MacFadyen & Woosley 1999), which is further supported by the discovery of GRB-Supernova connection (see, e.g., Hjorth & Bloom 2012), while short GRBs are results of compact mergers, happened in distant galaxies billions of years ago. Both scenarios result in a central black hole which powers the GRB by accretion of surrounding matter (or a magnetar suggested by recent studies, see, e.g., Greiner et al. 2015).

Since GRBs are confirmed to be cosmological sources, the emitting materials must be extremely energetic and relativistic (GRB luminosities are typically 10^{51} - 10^{53} erg s^{-1}). Astrophysicists found the extreme energetics of GRBs puzzling - what kind of emission mechanism can produce such powerful emissions that are still observable in the gamma-ray energy bands over a distance of billions of light-years? One natural explanation is the so-called fireball model (Goodman 1986; Meszaros et al. 1993; Meszaros & Rees 1993; Rees & Meszaros 1992, 1994; Tavani 1996; Piran 1999), in which the observed gamma-rays are emitted by outflow matter ejected from the central engine. Since the prompt emission is observed in gamma-ray frequencies, the emitting matter is beamed and extremely relativistic. If the outflow environment is optically thick, a thermal spectrum due to photospheric radiation should result (Paczynski 1986). The thermal spectrum is expected to be a blackbody, on top another non-thermal component (e.g., Ryde 2005). However, spectral analysis showed little signs of blackbodies (e.g., Goodman 1986). Instead broken power-law

[2] `http://heasarc.gsfc.nasa.gov/docs/cgro/batse/`
[3] `http://fermi.gsfc.nasa.gov/ssc/observations/types/grbs/`

shapes are found in the spectra of almost every GRB. Power laws are signatures of non-thermal radiation processes, and the simplest among them is synchrotron radiation emitted by populations of relativistic electrons gyrating around the local magnetic field (see, e.g., Rybicki & Lightman 1979).

Surprisingly, when the first BATSE GRB spectral catalog (Band et al. 1993; Ford et al. 1995; Preece et al. 1996, 1998b) was published, about 30% of the time-resolved prompt emission spectra are shown to be inconsistent with synchrotron emission models. This is the so-called synchrotron "line-of-death" problem (Katz 1994a; Tavani 1995; Crider et al. 1998; Preece et al. 1998a, 2002). Well, it is not a majority, maybe some minor modifications can be made to save the synchrotron emission models, most people thought. The fact is that even after decades of research efforts, still not a single synchrotron emission model can explain all these "outliners".

In 2004 the *Swift* satellite[4] was launched into orbit, on board which has a gamma-ray burst dedicated instrument, the Burst Alert Telescope (BAT, Barthelmy 2000; Barthelmy et al. 2005), used to monitor GRBs in a large field-of-view (2 steradians) in the 15 - 150 keV energy range. When a GRB is detected, the BAT can request the spacecraft to slew towards the burst position and conduct follow-up observations with the high precision X-Ray Telescope (XRT, Burrows et al. 2000; Hill et al. 2000) in the 0.3 - 10 keV energy range and the Ultraviolet/Optical Telescope (UVOT). *Swift* has revolutionized afterglow studies, however BAT's upper energy boundary is usually below the peak energy in the prompt spectrum of a few hundred keV, it is difficult to draw strong conclusion on the prompt emission mechanism using the *Swift* data alone.

Many afterglow (when the ejected shells collide with the interstellar medium and circum-burst material blown away by the progenitor star) spectra are obtained by the BAT and XRT in X rays, and also by many ground-based optical and radio telescopes thanks to the rapid and precise localization of bursts by XRT circulated near real-time to the gamma-ray research community via the Gamma-ray Coordinates Network[5] (GCN). Sari et al. (1998) derived the expected spectral behavior if the observed afterglow emission is emitted from shocked electrons via synchrotron radiation (Paczynski & Rhoads 1993; Katz 1994b; Waxman 1997a,b; Wijers et al. 1997; Katz & Piran 1997; Mészáros et al. 1998). The derived spectral slopes and evolutions of the spectral breaks are compared to and agreed nicely with the observed afterglow spectra. It is very tempting to explain the prompt emission and afterglow emission using the same radiation process, although a fraction of the prompt emission spectra appear to be inconsistent with simple synchrotron theories.

[4] `http://swift.gsfc.nasa.gov`
[5] `http://gcn.gsfc.nasa.gov/gcn3_archive.html`

The model to explain the prompt-afterglow emission, i.e., emission from colliding shells *internal* to the jet of ejected matter vs. emission from collisions between shells and the *external* medium, is known as the internal-external shock model.

Another very important GRB dedicated instrument is the Gamma-ray Burst Monitor (GBM, Bissaldi et al. 2009; Meegan et al. 2009) on board the *Fermi* Gamma-ray Space Telescope[6], which was launched into orbit in 2008. The GBM provides all-sky monitoring and high temporal and spectral resolution data of GRBs in the energy range of 8 keV - 40 MeV. It is complemented by another instrument, the Large Area Telescope (LAT, Atwood et al. 2009), which covers more energetic photons in the energy range of 20 MeV - 300 GeV. Its unprecedented wide energy coverage has made *Fermi* an excellent telescope for studying the prompt emission properties of GRBs. The data obtained by GBM have improved the understanding of GRBs by the research community in recent years. For example, Burgess et al. (2011) fit a physical model to the GBM GRB data for the first time, a big advancement to GRB spectral analysis since in the past only empirical fit functions were used. It was found that a physical model with a synchrotron and a thermal component can fit a few bright bursts adequately (Burgess et al. 2011, 2014a).

Multi-mission and multi-wavelength observations are hot topics for GRB studies. For example, many gamma-ray satellites joined together to form the Interplanetary Network[7] (IPN). The localization of gamma-ray sources is difficult due to low photon statistics, the uncertainty is usually large (a few degrees or more, see Connaughton et al. 2015). If a gamma-ray source is observed simultaneously by multiple telescopes, a much smaller error contour of the gamma-ray source position on the sky can be obtained by overlapping the locations deduced by each instrument, which is known as the method of triangulation. Multi-mission inter-calibration can also be done, providing more precise and accurate gamma-ray energetics of the GRB.

Ground-based GRB dedicated instruments play an important role in multi-wavelength studies of GRBs. For instance, the Gamma-Ray Burst Optical/Near-Infrared Detector (GROND, Greiner et al. 2008) mounted on the MPG 2.2 m Telescope on the mountain of La Silla, Chile, can observe GRB afterglow simultaneously in 7 frequency bands from optical to near-infrared. High-quality optical and near-infrared multi-band photometry obtained by the GROND instrument can determine redshift and host galaxy properties (e.g., gas and dust extinction, metallicity, etc.) of GRBs. The multi-band data obtained by GROND also makes broad band spectral energy distribution (SED) possible, which is essential to distinguish different theories and scenarios of the prompt and

[6] `http://fermi.gsfc.nasa.gov`
[7] `http://ipnpr.jpl.nasa.gov/index.cfm`

afterglow emission mechanism. Although it was suggested that the optical emission during the prompt emission period might not be related to the gamma-ray emission (e.g., Akerlof et al. 2000), some recent simultaneous GROND and gamma-ray observations during the prompt phase did show similarities (e.g., Elliott et al. 2014; Greiner et al. 2014).

Despite these progresses, more conundrums have also been found. Photons of GeV energies have been observed in the LAT data (e.g., Axelsson et al. 2012), usually delayed relative to the keV emission. Several empirical relations between the spectral parameters and the GRB's energetics are observed (e.g., Amati et al. 2002, 2008; Amati 2010; Ghirlanda et al. 2010; Yonetoku et al. 2004), but physical explanations are still lacking. Bursts with redshifts $z > 9$ are found (see, e.g., Tanvir 2013). Numbers of observed dark bursts (GRBs without afterglow emission, see, e.g., Fynbo et al. 2001; Lazzati et al. 2002; Greiner et al. 2011) and orphan afterglows (GRBs without prompt emission, see, e.g., Rhoads 1997; Huang et al. 2002; Cenko et al. 2013) are increasing. Delayed X-ray flares and optical flares in the afterglow light curves are similar to the gamma-ray pulses in the prompt lightcurves (e.g., Racusin et al. 2008; Ackermann et al. 2014; Elliott et al. 2014; Greiner et al. 2014), suggesting plausible connection between the two emission phases. Extended emission in GeV has been observed, in which the temporal property might indicate a separate emission region (e.g., Abdo et al. 2010). Most interestingly, a third kind of GRBs are proposed (Gendre et al. 2013; Stratta et al. 2013; Levan et al. 2014; Greiner et al. 2014, 2015) - ultra-long GRBs which the prompt emission phase can last for hours or longer. Connection between ultra-long GRBs and super-luminous supernovae suggests that the central engines of GRBs may not be black holes, but highly magnetized neutron stars called magnetars (Greiner et al. 2015).

1.2 GRB Prompt Emission Models

In the fireball model, when the matter in the accretion disk around the central black hole is being accreted inwards, a bipolar jet structure is formed because of angular momentum conservation. Inside the jet there are shells of materials traveling outwards at relativistic speeds. When a faster shell catches up and collides with a slower shell, shock waves will be formed which transform internal energy of the bulk of ejected materials to the kinetic energy of electrons. Since electrons are much easier to accelerate than baryons, it is generally believed that the prompt emission of GRBs is due to leptonic process(es). In this section, I review some of these processes.

1.2.1 Synchrotron Radiation

Consider a single electron (e.g., Dermer & Menon 2009). If a magnetic field is present, the electron experiences a Lorentz force

$$\vec{F} = \frac{\mathrm{d}}{\mathrm{d}t}(\gamma m_\mathrm{e}\vec{v}) = q_\mathrm{e}\left(\vec{E} + \frac{1}{c}\vec{v}\times\vec{B}\right), \tag{1.1}$$

where q_e is the electron charge, m_e the electron rest mass, $\gamma = 1/\sqrt{1-\beta}$ the Lorentz factor, $\vec{v} = \vec{\beta}c$ the velocity, c the speed of light, $\vec{E}$ the electric field, and $\vec{B}$ the magnetic field.

Assuming the net electric field is negligible, there is no work done on the electron. Therefore, we have the equations of motion in the direction parallel and perpendicular to the magnetic field as

$$\frac{\mathrm{d}\vec{v}_\parallel}{\mathrm{d}t} = 0\,,\ \frac{\mathrm{d}\vec{v}_\perp}{\mathrm{d}t} = \frac{q_\mathrm{e}}{\gamma m_\mathrm{e}c}\vec{v}_\perp\times\vec{B}\,. \tag{1.2}$$

Since γ is constant, v is constant. According to Eqn. (1.2), $v_\parallel$ is constant and thus $v_\perp$ is also constant. Therefore, the electron accelerates only in the direction normal to $\vec{v}_\perp$ and $\vec{B}$. Thus, the motion is a combination of uniform linear motion and uniform circular motion, which is a helical motion along $\vec{B}$.

We can define the angular frequency of the motion

$$\omega_\mathrm{L} = \frac{q_\mathrm{e}B}{\gamma m_\mathrm{e}c}\,, \tag{1.3}$$

which is known as the Larmor frequency. The Larmor radius of gyration is thus

$$r_\mathrm{L} = \frac{v_\perp}{\omega_\mathrm{L}} = \frac{\beta_\perp\gamma m_\mathrm{e}c^2}{q_\mathrm{e}B}\,. \tag{1.4}$$

We can compute the synchrotron power radiated by the electron

$$P = \frac{2q_\mathrm{e}^4B^2\gamma^2\beta_\perp^2}{3m_\mathrm{e}^2c^3}\,. \tag{1.5}$$

The average power can be found by averaging the pitch angle α between the velocity $\beta = \beta_\perp/\sin\alpha$ and the magnetic field. Since

$$\langle\beta_\perp^2\rangle = \frac{\beta^2}{4\pi}\int\sin^2\alpha\,\mathrm{d}\Omega = \frac{2\beta^2}{3}\,, \tag{1.6}$$

we have the average synchrotron radiation power formula

$$\langle P \rangle = \frac{4}{3}\sigma_{\rm T} c \beta^2 \gamma^2 U_{\rm B} \,. \tag{1.7}$$

Here $\sigma_{\rm T} = 8\pi q_{\rm e}^4 / 3 m_{\rm e}^2 c^4$ is the Thomson cross section and $U_{\rm B} = B^2/8\pi$ is the magnetic energy density.

It is interesting to compute the synchrotron spectrum. Because of the relativistic beaming effect, the radiation received by the observer will appear to be concentrated in a cone (with opening angle $\sim 1/\gamma$) about the electron velocity $\vec{v}$ from a small arc of each gyration. We also know that the variation in the electric field of the observed beaming radiation depends only on $\gamma\theta$, where θ is the polar angle about $\vec{v}$. From geometry and the Larmor formulae, it can be shown that

$$\gamma\theta \approx 2\gamma^3 \omega_{\rm L} t \sin\alpha \,, \tag{1.8}$$

and the observed pulse width

$$\Delta T \approx \frac{1}{\gamma^3 \omega_{\rm L} \sin\alpha} \,. \tag{1.9}$$

By Fourier transformation of the electric field we can obtain the power spectrum which is expected to extend orders above the characteristic frequency

$$\omega_{\rm c} \equiv \frac{3}{2}\gamma^3 \omega_{\rm L} \sin\alpha \,. \tag{1.10}$$

So we have the electric field

$$E(\omega) \propto \int_{-\infty}^{\infty} f(\omega_{\rm c} t) e^{i\omega t} {\rm d}t \propto \int_{-\infty}^{\infty} f(\xi) e^{i\omega\xi/\omega_{\rm c}} {\rm d}\xi \,. \tag{1.11}$$

The latter proportionality by changing variable $\xi = \omega_{\rm c} t$.

Since the power is proportional to $|E(\omega)|^2$, from Eqn. (1.11) it must be of the form

$$P(\omega) = C\mathcal{F}\left(\frac{\omega}{\omega_{\rm c}}\right) \,. \tag{1.12}$$

Here $\mathcal{F}$ is a dimensionless function and C is a constant of proportionality which carries all the

physical dimensions. Here, we just quote the standard textbook result (Rybicki & Lightman 1979):

$$P(\omega) = \frac{\sqrt{3}}{2\pi} \frac{q_{\rm e}^3 B \sin\alpha}{m_{\rm e} c^2} \mathcal{F}\left(\frac{\omega}{\omega_{\rm c}}\right) , \tag{1.13}$$

where

$$\mathcal{F}(x) = x \int_x^\infty K_{5/3}(\epsilon) {\rm d}\epsilon \tag{1.14}$$

is known as the synchrotron kernel. Here $K_{5/3}$ is the modified Bessel function of fractional order 5/3.

The synchrotron spectrum of a single electron is simply proportional to $\mathcal{F}$.[8] It can be shown that the limits of $\mathcal{F}(x)$ can be approximated by simpler analytical functions for $x \ll 1$ and $x \gg 1$ (see, e.g., van Eerten & Wijers 2009), for the ease of computation.

The monochromatic flux of the synchrotron emission spectrum can be obtained, given the electron population $n_{\rm e}$, as

$$F_\nu \propto \int_1^\infty n_{\rm e}(\gamma_{\rm e})\, \mathcal{F}\left(\frac{\nu}{\nu_{\rm e}}\right) {\rm d}\gamma_{\rm e} , \tag{1.15}$$

where $\gamma_{\rm e}$ is the Lorentz factor of the electron and $\nu_{\rm e} \propto \omega_{\rm L}$ is the synchrotron frequency of the electron. Notice that Eqn. (1.15) either describes an instantaneously generated spectrum and 90 degrees pitch angle between magnetic field and electron velocity, or a situation where magnetic field and particle population remain unchanged.

Mathematically, the synchrotron emission spectrum of a single electron is the sharpest possible case of optically thin synchrotron emission theory. However, under realistic conditions, there is no reason to believe that the observed emission originates from only one electron. Thus, it is more realistic to consider a Maxwellian population of electrons, since it is an efficient distribution of electron energies. The resulting spectrum is sharper than the synchrotron spectrum from a power-law distribution of electron population with typical electron population index $p \sim 2.3$ (e.g., Bednarz & Ostrowski 1998; Kirk et al. 2000; Achterberg et al. 2001; Curran et al. 2010; Ryan et al. 2015). For a Maxwellian population of electrons with the temperature parameterized by the thermal Lorentz factor $\gamma_{\rm th}$, we have

$$n_{\rm e} \propto \left(\frac{\gamma_{\rm e}}{\gamma_{\rm th}}\right)^2 \exp\left(-\frac{\gamma_{\rm e}}{\gamma_{\rm th}}\right) , \tag{1.16}$$

[8] This already assumes integration over emission direction (see Rybicki & Lightman 1979, Eqns. 6.29 - 31). If a single electron were viewed from a single angle, a sharper spectrum would mathematically result.

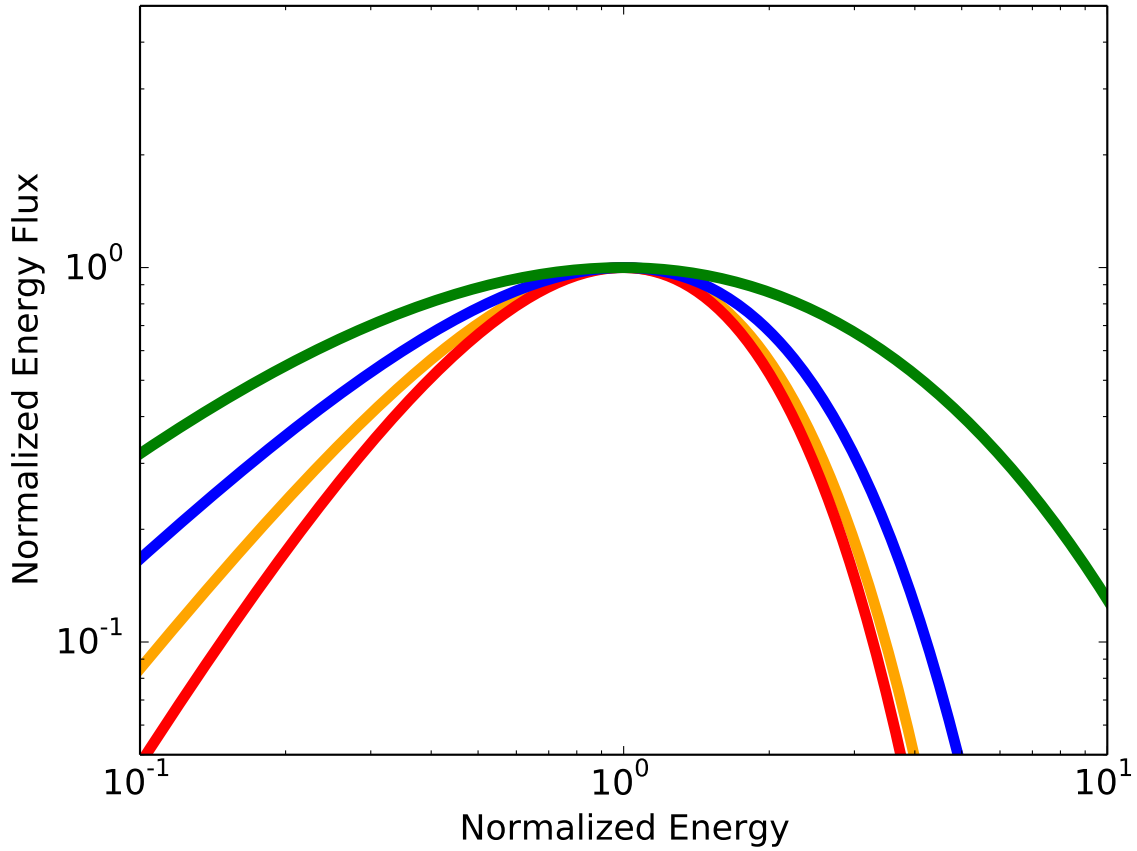

Figure 1.2: Normalized synchrotron spectra for various cases. The green curve shows the Maxwellian synchrotron function, blue shows the single electron synchrotron integrating over all emission directions, and orange and red show the single electron cases of polarization directions perpendicular and parallel to the projection of the magnetic field on the sky, respectively.

and the Maxwellian synchrotron spectrum

$$F_\nu \propto \int_1^\infty \left(\frac{\gamma_\mathrm{e}}{\gamma_\mathrm{th}}\right)^2 \exp\left(-\frac{\gamma_\mathrm{e}}{\gamma_\mathrm{th}}\right) \mathcal{F}\left(\frac{\nu}{\nu_\mathrm{e}}\right) \mathrm{d}\gamma_\mathrm{e}\,. \tag{1.17}$$

Since $\nu_\mathrm{e} \propto \gamma_\mathrm{e}^2$, by changing the variable $\nu = \xi\nu_\mathrm{th} \propto \xi\gamma_\mathrm{th}^2$, it can be shown that

$$F_\nu \propto \gamma_\mathrm{th}\,\xi^{\frac{3}{2}} \int_{\frac{1}{\gamma_\mathrm{th}}}^\infty x^{-\frac{5}{2}} \exp\left(-\xi^{\frac{1}{2}} x^{-\frac{1}{2}}\right) \mathcal{F}(x)\,\mathrm{d}x\,, \tag{1.18}$$

which allows us to normalize the spectrum in units of ξ. Again, note that Eqn. (1.17) represents one of the sharpest cases among synchrotron spectra for multiple electrons, but that the assumptions

of a single temperature and magnetic field are still unrealistic. The normalized νF_ν spectra of the aforementioned synchrotron functions are ploted in Fig. 1.2. Observed emission will contain a mixture of these and lead to smoother spectra.

Another reasonable assumption for the electron population is a power-law distribution of the electron energies:

$$n_\mathrm{e} \propto \gamma_\mathrm{e}^{-p} : \gamma_\mathrm{e} \geq \gamma_\mathrm{min} \,, \tag{1.19}$$

and the synchrotron spectrum with electron population index p is

$$F_\nu \propto \int_{\gamma_\mathrm{min}}^{\infty} \gamma_\mathrm{e}^{-p} \, \mathcal{F}\left(\frac{\nu}{\nu_\mathrm{e}}\right) \, \mathrm{d}\gamma_\mathrm{e} \,, \tag{1.20}$$

where γ_min is the minimum injection energy of the electron population. The F_ν spectrum can be solved as

$$F_\nu \propto \nu^{\frac{1-p}{2}} \int_0^{\frac{\nu}{\nu_\mathrm{min}}} \left(\frac{\nu}{\nu_\mathrm{e}}\right)^{\frac{p-3}{2}} \mathcal{F}\left(\frac{\nu}{\nu_\mathrm{e}}\right) \, \mathrm{d}\left(\frac{\nu}{\nu_\mathrm{e}}\right) \,, \tag{1.21}$$

where ν_min is the minimum injection frequency of the electron population. As with temperature, the observed spectrum will be smoother due to a mixture of ν_min values in the emission. If we substitute the approximation of $\mathcal{F}(x) \sim x^{1/3}$ for $x \ll 1$, we can recover the famous 1/3 low-energy spectral slope below ν_min for any value of p.

In reality, electron cooling should exist, as more energetic electrons lose their energy faster due to radiative losses and cool down. One could consider, in addition to the minimum injection energy break ν_min, the cooling break ν_cool.

The optically thin synchrotron shock model (SSM) predicts two different scenarios, namely fast cooling and slow cooling (see, e.g., Sari et al. 1998; Preece et al. 2002), depending on the injection and evolution of the relativistic electron population. Both of them consist of a lower and a higher frequency break, fixed by the values of the cooling frequency ν_cool and the minimum injection frequency ν_min for the relativistic electrons. The electrons in the shock are accelerated to a minimum energy γ_min. Assuming a power-law behavior for the electron energy distribution $n(\gamma_\mathrm{e}) \propto \gamma_\mathrm{e}^{-p}$, where $\gamma_\mathrm{e} \geq \gamma_\mathrm{min}$, the emission spectrum also has a power-law shape. As long as $p > 2$, the distribution is characterized by its lower cutoff at γ_min, and the integrated energy of the population does not diverge at high electron energies.

There is a critical energy γ_cool such that electrons with energies above γ_cool emit a significant amount of their energy via synchrotron cooling. The values of γ_cool and γ_min correspond to ν_cool

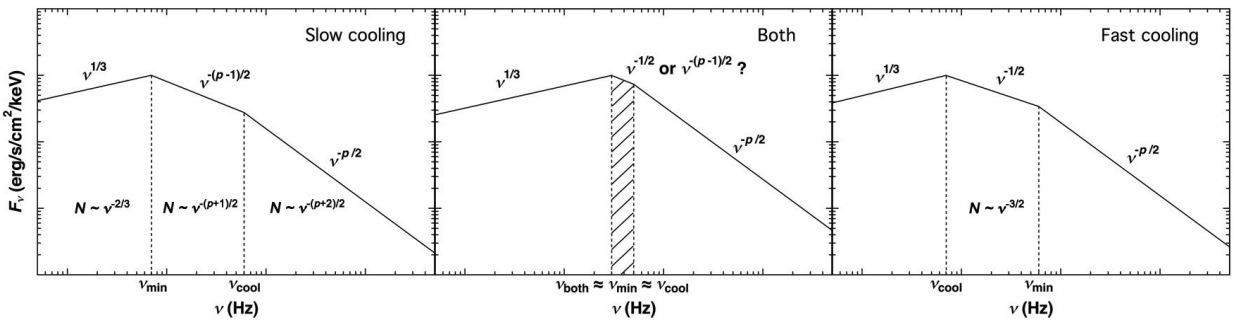

Figure 1.3: Schematic spectra for the SSM cooling scenarios. The left, middle, and right panels show the "slow", "both", and "fast" cases in the energy flux space. The shaded region represents the possible location of $\nu_{\rm both}$ (i.e., $E_{\rm p}$) when fitting the observed spectrum using a model with smoothly jointed power laws. The photon distribution slopes are also indicated for each case.

and $\nu_{\rm min}$, and the slow-cooling spectrum is given by

$$F_{\nu,{\rm slow}} \propto \begin{cases} \nu^{1/3} : \nu_{\rm min} > \nu \,, \\ \nu^{-(p-1)/2} : \nu_{\rm cool} > \nu > \nu_{\rm min} \,, \\ \nu^{-p/2} : \nu > \nu_{\rm cool} \,, \end{cases} \tag{1.22}$$

while the fast-cooling spectrum is given by

$$F_{\nu,{\rm fast}} \propto \begin{cases} \nu^{1/3} : \nu_{\rm cool} > \nu \,, \\ \nu^{-1/2} : \nu_{\rm min} > \nu > \nu_{\rm cool} \,, \\ \nu^{-p/2} : \nu > \nu_{\rm min} \,. \end{cases} \tag{1.23}$$

Subtracting 1 from the spectral indices will give the power-law photon indices (i.e., α and β), which lead to a synchrotron line-of-death $\alpha = -2/3$ for both scenarios and a second line-of-death $\alpha = -3/2$ (Preece et al. 1998a) for the fast-cooling scenario. Figure 1.3 shows the schematic spectra for the slow- and fast-cooling scenario, as well as the so-called "both" case where $\nu_{\rm cool}/\nu_{\rm min}$ (slow cooling) or $\nu_{\rm min}/\nu_{\rm cool}$ (fast cooling) is close to unity. The both case can be considered to describe an intermediate case of moderately fast cooling.

1.2.2 Compton Scattering

Compton scattering is one of the most important photon-particle interactions for high-energy astrophysics, because it describes the resulting photon spectrum when an external source of photons scattered by a population of particles (electrons for most of the cases). Compton scattering is

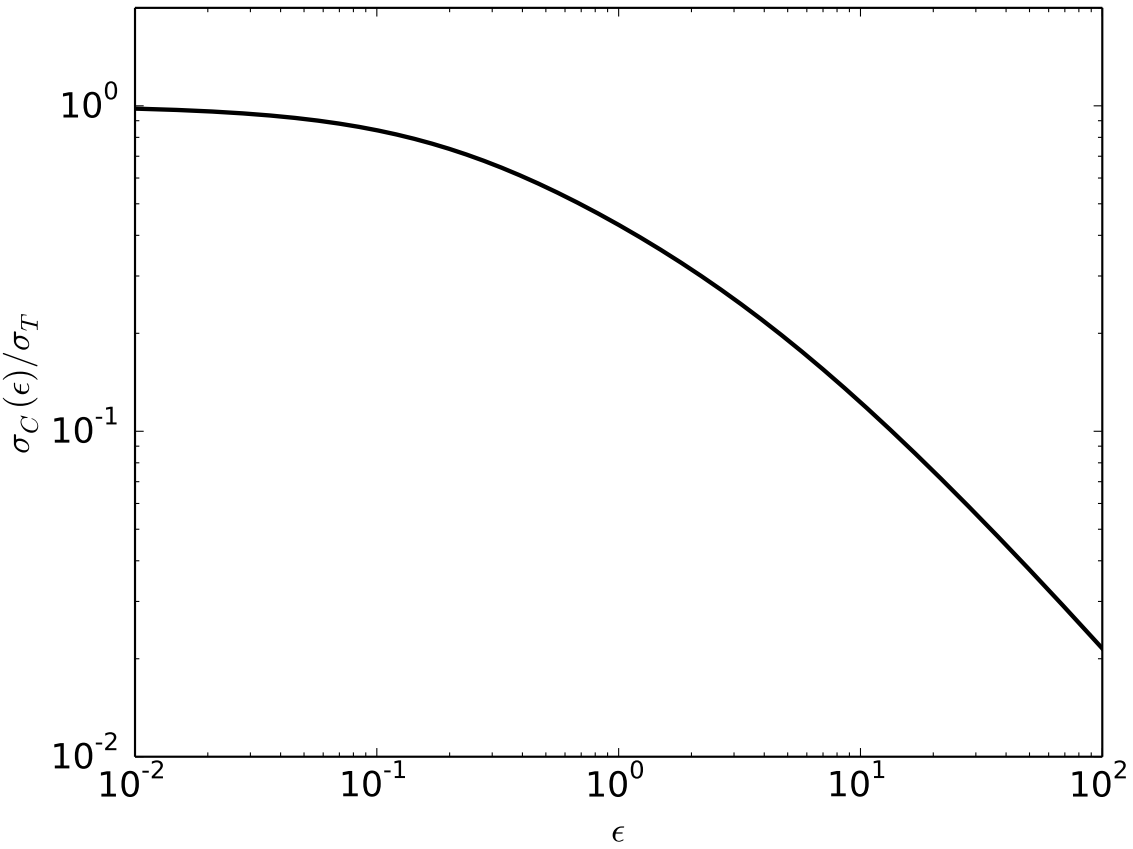

Figure 1.4: Compton cross section $\sigma_{\rm C}$ as a function of dimensionless photon energy ϵ, normalized by the Thomson cross section $\sigma_{\rm T} = 6.6525^{-25}$ cm^2.

the generalization of Thompson scattering when the incident and scattered photon have the same energy. The term inverse Compton scattering is used for the process of a low-energy photon up-scattered by an energetic electron.

Consider the simplest case of a single photon interacting with a single electron. In the rest frame of the electron, we have the equations of energy and momentum conservation:

$$\begin{cases} 1 + \epsilon = \epsilon' + \gamma \,, \\ \epsilon = \epsilon' \cos\theta_{\rm ph} + \beta\gamma \sin\theta_{\rm e} \,, \\ \epsilon' \sin\theta_{\rm ph} = \beta\gamma \sin\theta_{\rm e} \,. \end{cases} \tag{1.24}$$

Here the above quantities are all in units of electron rest mass $m_{\rm e}c^2$, ϵ and ϵ' are the dimensionless

energy of the incident and scattered photon, $\theta_{\rm ph}$ is the angle between the incident and scattered direction of the photon, and $\theta_{\rm e}$ is the angle between the incident photon and scattered electron direction. Solving these equations gives the scattered photon energy ϵ' as a function of $\theta_{\rm ph}$ and ϵ.

When $\epsilon \ll 1$, $\epsilon \approx \epsilon'$ which is independent of $\theta_{\rm ph}$ and defines the Thompson regime. When $\epsilon \gg 1$, quantum effects are important, which defines the Klein-Nishina regime. We quote the total cross section of Compton scattering, aka. the Klein-Nishina formula (Klein & Nishina 1929):

$$\sigma_{\rm C} = \frac{\pi r_{\rm e}^2}{\epsilon^2}\left[4 + \frac{2\epsilon^2(1+\epsilon)}{(1+2\epsilon)^2} + \frac{\epsilon^2 - 2\epsilon - 2}{\epsilon}\ln(1+2\epsilon)\right], \tag{1.25}$$

where $r_e = q_{\rm e}^2/m_{\rm e}c^2$ is the classical electron radius. We plot $\sigma_{\rm C}$ as a function of ϵ in Fig. 1.4. It shows that Compton scattering is most important for low-energy photons.

The exact spectrum of Compton scattering depends on the incident photon spectrum and electron distribution and involves complicated convolution of the photon and electron density. Examples for various photon and electron distributions have been derived in standard textbooks (e.g., Rybicki & Lightman 1979; Longair 1981; Dermer & Menon 2009; Ghisellini 2013), while the most general derivation can be found in Jones (1968) and Blumenthal & Gould (1970). In most astrophysical applications, we are often interested in the case of an isotropic radiation field scattered by a power-law population of electrons (Eqn. 1.19). The result is a power law which increases from low energies to a peak, followed by a steep power-law decay, and the slopes of which depend on p.

The Compton spectral shape mimics a power-law exponential cutoff, which is observed in many GRB spectra (see Ch. 2). However, if the typically observed spectral peak of GRBs in the sub-MeV energy range is due to inverse Compton scattering, then there should be no emission in the optical wavelengths. This is because the effect of Eqn. (1.25) will be amplified by multiple scattering, aka. the Comptonization process. The simultaneous optical and gamma-ray observations of, e.g., GRB 121217A (Elliott et al. 2014) and GRB 130925A (Greiner et al. 2014) might indicate inconsistency with the Compton scattering hypothesis.

1.2.3 Synchrotron Self-Compton

If the synchrotron radiation is inverse Compton scattered by the same emitting particle itself, the process is called synchrotron self-Compton (SSC). In a dense astrophysical emission region, one would expect SSC to take place.

To compute the SSC flux, we have to go back to look for the synchrotron emission function

before averaging the emission direction. Crusius & Schlickeiser (1986) derived a general analytical result for isotropic electron population in a randomly oriented magnetic field,

$$\nu F_\nu^{\rm syn} = \frac{\sqrt{3}\delta_{\rm D}^4 \nu' q_{\rm e}^3 B}{4\pi d_{\rm L}^2 m_{\rm e} c^2} \int_1^\infty n'_{\rm e}(\gamma') R(x) {\rm d}\gamma' \,, \tag{1.26}$$

where $\delta_{\rm D} = [\gamma(1-\beta\cos\theta)]^{-1}$ is the relativistic Doppler factor. All primed quantities are measured in the comoving frame. The function

$$R(x) = \frac{x}{2} \int_0^\pi \int_{x/\sin\theta}^\infty K_{5/3}(\epsilon) {\rm d}\epsilon {\rm d}\theta \tag{1.27}$$

can be approximated in the asymptotic limits as

$$R(x) = \begin{cases} \frac{\sqrt[3]{2}\Gamma^2(1/3)}{5} \sqrt[3]{x} : x \ll 1 \,, \\ \frac{\pi}{2} e^{-x} \left(1 - \frac{99}{162x}\right) : x \gg 1. \end{cases} \tag{1.28}$$

Here Γ is the gamma function and $K_{5/3}$ is the Bessel function of fractional order 5/3.

The SSC flux is obtained by convolving the synchrotron flux with the Compton scattering emission function. Finke et al. (2008) derived the form of the SSC flux in the observer frame as

$$\nu F_\nu^{\rm SSC} = \frac{9}{16\pi} \frac{(1+z)^2 \sigma_{\rm T} \nu_{\rm s}'^2}{\delta_{\rm D}^2 c^2 t_{\rm min}^2} \int_0^\infty \frac{\nu F_\nu^{\rm syn}}{\nu'^3} \int_{\gamma'_{\rm min}}^{\gamma'_{\rm max}} \frac{n'_{\rm e}(\gamma')}{\gamma'^2} \mathcal{F}_{\rm C}(q, \Gamma_{\rm e}) {\rm d}\gamma' {\rm d}\nu' \,, \tag{1.29}$$

where z is the redshift, $\sigma_{\rm T} = 8\pi r_{\rm e}^2/3$ is the Thomson cross section, $t_{\rm min}$ is the minimum variability timescale, $\nu'_{\rm s}$ is the frequency of the Compton scattered photon. The Compton scattering kernel $\mathcal{F}_{\rm C}(q,\, \Gamma_{\rm e})$ is a function of photon and electron distribution. It is first derived by Jones (1968) and then by Blumenthal & Gould (1970):

$$\mathcal{F}_{\rm C}(q,\, \Gamma_{\rm e}) = \left[2q \ln q + (1+2q)(1-q) + \frac{1}{2} \frac{\Gamma_{\rm e}^2 q^2 (1-q)}{1+\Gamma_{\rm e} q} \right] H\left(q;\, \frac{1}{4\gamma'^2},\, 1\right) . \tag{1.30}$$

Here, $H(x;\, x_1,\, x_2) = 1$ for $x_1 \le x \le x_2$ and $H(x;\, x_1,\, x_2) = 0$ elsewhere is the Heaviside function, $\Gamma_{\rm e} = 4h\nu'\gamma'$ where h is the Planck constant, and

$$q = \frac{h\nu'_{\rm s}/\gamma'}{\Gamma_{\rm e}(1 - h\nu'_{\rm s}/\gamma')} \,. \tag{1.31}$$

The integration limits $\gamma'_{\rm max}$ and $\gamma'_{\rm min}$ can be obtained using the Heaviside function of q.

The SSC spectrum is predicted to be wider than the seed synchrotron spectrum (e.g., Ghisellini 2013). Thus it is believed that SSC cannot explain the observed GRB prompt emission spectra (see, e.g., Baring & Braby 2004; Axelsson & Borgonovo 2015; Yu et al. 2015b).

A comprehensive review of GRB physics can be found in Piran (2004). Recent reviews on the emission mechanism of GRBs can also be found in, e.g., Zhang (2014) and Pe'er (2015).

1.3 *Fermi* Gamma-ray Burst Monitor

The *Fermi* Gamma-ray Space Telescope, launched in June 2008, harbors two scientific instruments, namely the Gamma-ray Burst Monitor (GBM, Meegan et al. 2009) and the Large Area Telescope (LAT, Atwood et al. 2009). The GBM is a sensitive scintillation array covering the energy range from 8 keV to 40 MeV, while the LAT is sensitive in the complementary energy range from 30 MeV to 300 GeV. The GBM consists of twelve thallium activated sodium iodide (NaI(Tl), hereafter NaI) detectors covering the energy range from 8 keV to 1 MeV and two bismuth germanate (BGO) detectors covering the energy range from 200 keV to 40 MeV. This provides spectral coverage over three orders of magnitude, which makes the GBM a powerful observing instrument for GRB prompt emission.

The GBM observes the whole sky which is not occulted by the Earth (> 8 sr) and provides real-time locations for GRB triggers. The arrangement of the NaI detectors allows GBM to locate GRBs in a real-time manner; and the two BGO detectors are placed on opposite sides of the spacecraft in order to cover all bursts coming from any direction in the sky. These real-time locations are circulated via the Gamma-ray Coordination Network[9] (GCN) which allows ground-based follow-up observations. Occasionally, an Autonomous Repoint Request (ARR) can be accepted by the Flight Software (FSW) which allows *Fermi* to slew towards the direction of the source, so that it can be observed with the LAT.

The GBM generates three kinds of scientific data. The first type is CTIME which provides coarse spectral resolution of 8 energy channels and fine temporal resolution of 0.256 s during the nominal time period, i.e., before the trigger and 600 s after the trigger; during the trigger period, the resolution is increased to 64 ms. The second type is CSPEC which provides coarse temporal resolution at nominal (4.096 s) and trigger (1.024 s) period, and high spectral resolution of 128 pseudo-logarithmically scaled energy channels. The third type is time-tagged event (TTE) data

[9] `http://gcn.gsfc.nasa.gov/gcn3_archive.html`

which stores individual photon events tagged with arrival time (resolution of 2 μs), photon energy channel (128 pseudo-logarithmic energy channels), and detector number (NaI 0 - 11 and BGO 0 - 1). TTE data were stored on board GBM in a recycling buffer. After 26 November 2012[10] this data type became continuous. When GBM is triggered, the spacecraft will transmit pre- and post-trigger TTE data (about 300 s in duration) to the ground as science data.

1.4 Heuristic Fit Functions

Conventionally, heuristic models are fit to the observed GRB prompt emission spectra. These mathematical functions are empirical in origin. The most popular models are the Band function, the smoothly broken power law, the cutoff power law, and the simple power law. The Planck function (i.e., a blackbody) may be occasionally added to one of these models in some bursts (e.g., Mészáros et al. 2002; Ryde 2005; Guiriec et al. 2011; Axelsson et al. 2012; Guiriec et al. 2013; Burgess et al. 2014a,b; Pe'er et al. 2015).

1.4.1 Band Function

The Band function (BAND) is a model in which a power law with high-energy exponential cutoff and a high-energy power law are joined together by a smooth transition. It is an empirical function proposed by Band et al. (1993), which fits most of the observed GRB spectra. Parametrized by the peak energy $E_{\rm p}$ (despite the fact that there may not be a peak in the νF_ν space when the high-energy photon index $\beta \geq -2$) in the observed νF_ν spectrum, the photon model of BAND is defined as

$$f_{\rm BAND}(E) = A \begin{cases} \left(\frac{E}{100\ {\rm keV}}\right)^{\alpha} \exp\left[-\frac{(\alpha+2)E}{E_{\rm p}}\right] : E < E_{\rm c}\,, \\ \left(\frac{E}{100\ {\rm keV}}\right)^{\beta} \exp\left(\beta-\alpha\right) \left(\frac{E_{\rm c}}{100\ {\rm keV}}\right)^{\alpha-\beta} : E \geq E_{\rm c}\,, \end{cases} \tag{1.32}$$

where

$$E_{\rm c} = \left(\frac{\alpha-\beta}{\alpha+2}\right) E_{\rm p}\,. \tag{1.33}$$

In Eqns. (1.32) and (1.33), A is the normalization factor at 100 keV in units of ph s^{-1} cm^{-2} keV^{-1}, α is the low-energy power-law photon index, β is the high-energy power-law photon index, $E_{\rm p}$ is the peak energy in the νF_ν space in units of keV, and $E_{\rm c}$ is the characteristic energy in units of keV.

[10] `http://fermi.gsfc.nasa.gov/ssc/data/access/gbm/`

Note that the *peak energy* $E_{\rm p}$ represents the position of the peak in the model curve in the νF_ν space, and the *characteristic energy* $E_{\rm c}$ represents the position where the low-energy power law with an exponential cutoff ends and the pure high-energy power law starts. These two energies should be distinguished from the *break energy* $E_{\rm b}$ which represents the position where the low-energy power law joins the high-energy power law. Therefore, we should not compare the Band function's $E_{\rm p}$ or $E_{\rm c}$ to the smoothly broken power law's $E_{\rm b}$. We can compute the break energy where the two power laws join together for the Band function. The derivation is already given by Kaneko et al. (2006), here we only give the resulting equation:

$$E_{\rm b} = \left(\frac{\alpha-\beta}{\alpha+2}\right)\frac{E_{\rm p}}{2} + \frac{1}{2}E_{\rm lb}\,, \tag{1.34}$$

in units of keV. Here $E_{\rm lb}$ is the lower boundary of the detector. In the asymptotic limit, this term vanishes and therefore $E_{\rm b}$ is proportional to $E_{\rm p}$.

1.4.2 Smoothly Broken Power Law

The smoothly broken power law (SBPL) is a model of two power laws joined by a smooth transition. It was first parameterized by Ryde (1999) and then re-parameterized by Kaneko et al. (2006):

$$f_{\rm SBPL}(E) = A\left(\frac{E}{100\ {\rm keV}}\right)^b 10^{(a-a_{\rm piv})}\,, \tag{1.35}$$

where

$$\begin{cases} a = m\Delta\ln\left(\frac{e^q+e^{-q}}{2}\right), a_{\rm piv} = m\Delta\ln\left(\frac{e^{q_{\rm piv}}+e^{-q_{\rm piv}}}{2}\right)\,, \\ m = \frac{\beta-\alpha}{2}, b = \frac{\alpha+\beta}{2}\,, \\ q = \frac{\log(E/E_{\rm b})}{2}, q_{\rm piv} = \frac{\log(100\ {\rm keV}/E_{\rm b})}{2}\,. \end{cases} \tag{1.36}$$

In Eqns. (1.35) and (1.36), A is the normalization factor at 100 keV in units of ph s^{-1} cm^{-2} keV^{-1}, α and β are the low- and high-energy power-law photon indices respectively, $E_{\rm b}$ is the break energy in units of keV, and Δ is the break scale. Unlike the Band function, the break scale is not coupled to the power-law indices, so SBPL is a five-parameters model if we let Δ free to vary. In this dissertation, we follow Kaneko et al. (2006), Goldstein et al. (2012), and Gruber et al. (2014) to fix $\Delta = 0.3$.

The peak energy of SBPL in the νF_ν space can be found at

$$E_{\rm p} = 10^x E_{\rm b}\,, x = \Delta \tanh^{-1}\left(\frac{\alpha+\beta+4}{\alpha-\beta}\right)\,. \tag{1.37}$$

Note that Eqn. (1.37) is only valid for $\alpha > -2$ and $\beta < -2$.

1.4.3 Cutoff Power Law

The cutoff power law, aka. the Comptonized model (COMP), is a power-law model with a high-energy exponential cutoff. Note that when $\beta \to -\infty$, BAND reduces to COMP:

$$f_{\rm COMP}(E) = A\left(\frac{E}{100\ {\rm keV}}\right)^{\alpha} \exp\left[-\frac{(\alpha+2)E}{E_{\rm p}}\right]\,, \tag{1.38}$$

where A is the normalization factor at 100 keV in units of ph s^{-1} cm^{-2} keV^{-1}, α is the power-law photon index, and $E_{\rm p}$ is the peak energy in the νF_ν space in units of keV.

1.4.4 Power Law

The power law (PL) is defined as

$$f_{\rm PL}(E) = A\left(\frac{E}{100\ {\rm keV}}\right)^{\alpha}\,, \tag{1.39}$$

where A is the normalization factor at 100 keV in units of ph s^{-1} cm^{-2} keV^{-1}, and α is the power-law photon index.

1.4.5 Planck Function

The Planck function, aka. the blackbody model (BB), is defined as

$$f_{\rm BB}(E) = A\left[\frac{(E/1\ {\rm keV})^2}{\exp(E/kT)-1}\right]\,, \tag{1.40}$$

where A is the normalization factor at 1 keV in units of photons s^{-1} cm^{-2} keV^{-1} and kT is the temperature of the blackbody in units of keV.

1.4.6 Synchrotron Fit Function

Empirical model fitting is the dominant technique for the past few decades of GRB spectroscopy researches. One can obtain the best-fit parameter and then interpret the values by physics. However, the conventional models aforementioned have no direct connection to the physical processes that they are trying to describe. In this work, a semi-empirical model is formulated to account for the characteristic power-law indices for the two synchrotron cooling cases.

The synchrotron fit function (SYNC) is a modified triple power-law with sharp breaks defined as

$$f_{\rm SYNC}(E) = A \begin{cases} \left(\frac{E}{100\ {\rm keV}}\right)^{\alpha} : E < E_{\rm b,1}, \\ \left(\frac{E_{\rm b,1}}{100\ {\rm keV}}\right)^{\alpha-\beta} \left(\frac{E}{100\ {\rm keV}}\right)^{\beta} : E_{\rm b,1} \leq E < E_{\rm b,2}, \\ \left(\frac{E_{\rm b,1}}{100\ {\rm keV}}\right)^{\alpha-\beta} \left(\frac{E_{\rm b,2}}{100\ {\rm keV}}\right)^{\beta-\gamma} \left(\frac{E}{100\ {\rm keV}}\right)^{\gamma} : E \geq E_{\rm b,2}\,, \end{cases} \tag{1.41}$$

where A is the normalization factor at 100 keV in units of photons $\rm s^{-1}\ cm^{-2}\ keV^{-1}$, α, β, and γ are the power-law indices of the three segments (from low to high energy), and $E_{\rm b,1}$ and $E_{\rm b,2}$ are the two break energies in units of keV. Here we fix $\alpha = -2/3$ and $\beta - \gamma = 1/2$ to create a SYNC-slow model for the slow-cooling scenario (Eq. 1.22). This makes it a four-parameter model with freely varying A, $E_{\rm b,1}$, $E_{\rm b,2}$, and β (or equivalently, γ). We also fix $\alpha = -2/3$ and $\beta = -3/2$ to create a SYNC-fast model for the fast-cooling scenario (Eq. 1.23). This also makes a four-parameter model with freely varying A, $E_{\rm b,1}$, $E_{\rm b,2}$, and γ.

Chapter 2

The *Fermi* GBM GRB Time-Resolved Spectral Catalog

"[I do not] carry such information in my mind since it is readily available in books. ... The value of a college education is not the learning of many facts but the training of the mind to think."

- Albert Einstein

Gamma-ray bursts (GRBs) are the most energetic explosions known to humankind. Although discovered in 1967 (Klebesadel et al. 1973) by the *Vela* Satellite Network, the physics of GRBs still remains unsolved, e.g., the nature of the emission mechanism of the so-called prompt emission phase. Today, we know that GRBs are gamma-ray emissions from cosmological sources (Metzger et al. 1997) distributed isotropically across the sky (Meegan et al. 1992; Pendleton et al. 1994; Briggs et al. 1996). The two kinds of GRBs, long/soft and short/hard (Kouveliotou et al. 1993), are thought to have different origins. It is generally believed that long/soft (duration $T_{90} > 2$ s and low-energy photon rich) GRBs are the result of gravitational collapse events from massive progenitors, and short/hard ($T_{90} < 2$ s and high-energy photon rich) GRBs originate from compact merger events.

A powerful method to discern the physical properties and emission mechanisms of GRBs is through detailed spectral analysis. However, the spectral properties of individual GRB may be significantly different. Therefore, analysis of large sample of burst spectra is necessary to obtain a coherent physical picture. Such large spectral catalogs, some time-integrated and some time-resolved, have been published for many hard X-ray or gamma-ray observing instruments, e.g., the

CGRO/BATSE (25 keV - 2 MeV, Pendleton et al. 1994; Preece et al. 2000; Kaneko et al. 2006; Goldstein et al. 2013), *BeppoSAX*/GRBM (40 - 700 keV, Frontera et al. 2009), *Swift*/XRT (0.2 - 10 keV, Evans et al. 2009), *Swift*/BAT (15 - 150 keV, Sakamoto et al. 2008, 2011), *Fermi*/LAT (20 MeV - 300 GeV, Ackermann et al. 2013), and *Fermi*/GBM (time-integrated, 8 keV - 40 MeV, Nava et al. 2011; Goldstein et al. 2012; Gruber et al. 2014; von Kienlin et al. 2014).

This chapter presents the first *Fermi* GBM GRB time-resolved spectral catalog. In contrast to previous time-resolved spectral catalogs of other instruments, the broad energy range covered by the GBM allows a sensitive investigation at energies of a few hundred keV where the peaks or breaks of the prompt emission spectra are located. This catalog presents time-resolved fit parameters using standard fit functions, parameter-parameter and parameter-uncertainty correlations, spectral evolutionary trends over time, in particular the peak energy $E_{\rm p}$ evolution, distributions of spectral slopes (given in photon indices α and β), and plausible blackbody components. We present in Ch. 4 a novel measure of the sharpness of the spectral peak using this catalog burst sample (Yu et al. 2015b). The measure places a strong constraint on the physics of prompt emission models, ruling out an optically thin synchrotron origin for the peak or break of the spectrum in a large majority of cases.

This chapter is structured as follows. We describe the characteristics of GBM and the methods of data selection and reduction in Sect. 2.1. The fitting models used in this catalog is described in Sect. 1.4. The spectral analysis procedure is given in Sect. 2.2, and the fitting results are presented in Section 2.3. We summarize our results and conclude in Sect. 2.4. Individual best-fit spectra are tabulated in Appendix A.

2.1 *Fermi* GBM Data Reduction

2.1.1 Detector Selection

We apply the same detector selection criteria used in all official GBM GRB time-integrated spectral catalogs (Goldstein et al. 2012; Gruber et al. 2014; von Kienlin et al. 2014). The detectors with viewing angle larger than 60 degrees or blocked by the LAT or solar panels are removed (Bissaldi et al. 2009; Goldstein et al. 2012; Gruber et al. 2014). For every spectrum, a maximum of three NaIs with one BGO are used in the analysis. If more than three NaIs satisfied these criteria, the NaIs with the smallest viewing angles are used in order to avoid binning bias towards the lower energies (Goldstein et al. 2012).

2.1.2 Data Type Selection

There are three different types of data generated by GBM. The first type is CTIME which provides coarse spectral resolution of 8 energy channels and fine temporal resolution of 0.256 s during the nominal time period, i.e., before the trigger and 600 s after the trigger; during the trigger period, the resolution is increased to 64 ms. The second type is CSPEC which provides coarse temporal resolution at nominal (4.096 s) and trigger (1.024 s) period, and high spectral resolution of 128 pseudo-logarithmically scaled energy channels. The third type is time-tagged event (TTE) data which stores individual photon events tagged with arrival time (resolution of 2 μs), photon energy channel (128 pseudo-logarithmic energy channels), and detector number (NaI 0 - 11 and BGO 0 - 1). TTE data were stored on board GBM in a recycling buffer. After 26 November 2012[1] this data type became continuous. When GBM is triggered, the spacecraft will transmit pre- and post-trigger TTE data (about 300 s in duration) to the ground as science data. Therefore, for the 15 bursts with evident precursor or emission longer than 300 s, we use the CSPEC data (about 8,000 s in duration).

2.1.3 Energy Channel Selection and Background Fitting

To account for the poor transparency for gamma-rays of the silicone pad in front of the NaI crystal and of the Multi Layer Insulation (MLI) around the detectors (Bissaldi et al. 2009), the energy channels below 8 keV and the overflow channels above 900 keV are removed. A similar cutoff criterion is also used in the BGOs so that only energy channels between 250 keV and 40 MeV are used. An effective energy range from 8 keV to 40 MeV is used for the spectral analysis in this chapter.

For each burst, a polynomial with order 2 - 4 is fit to every energy channel according to two user-defined background intervals, before and after the emission period. The background model is then interpolated across the emission period. This is done by varying the selected intervals and order of polynomial until the χ^2 statistics is minimised over all energy channels. The resulting background intervals are then loaded to all detectors, generating the background model to be used in the spectral analysis. The background intervals used in this catalog are identical to those used in Gruber et al. (2014).

[1] `http://fermi.gsfc.nasa.gov/ssc/data/access/gbm/`

2.1.4 Burst and Spectrum Selection

We first select all the bursts detected by GBM in the first 4 years (i.e., from 14 July 2008 to 13 July 2012), which is the same GRB subset as used in the 4-yr GBM GRB time-integrated spectral catalog (Gruber et al. 2014; von Kienlin et al. 2014). The GBM triggered on 954 GRBs in this period of time (one of them triggered GBM twice, see von Kienlin et al. 2014). Time-resolved spectral analysis requires bright bursts with sufficiently high signal-to-noise spectra. This bright subsample is selected by applying the following criteria: 10 keV - 1 MeV energy fluence $f > 4 \times 10^{-5}$ erg cm^{-2} and/or 10 keV - 1 MeV peak photon flux $F_{\rm p} > 20$ ph s^{-1} cm^{-2} (in either 64, 256, or 1,024 ms binning timescales). These criteria are satisfied by 134 bursts out of the 954. Sixteen among them are of the short burst class.

In order to alleviate the problem that the spectra from the brightest bursts dominate the statistics, we further require each event to have at least 5 time bins in the light curves when binned with signal-to-noise ratio (S/N) = 30. This optimal S/N is found by iterating the binning process on characteristic bursts drawn from various fluence and peak-flux level, which does not significantly merge peaks and valleys in the light curves while providing the highest number of time bins. As a result, 81 bursts satisfy these criteria; among them there is only one short burst (GRB 120323A; GBM trigger #120323507). In total, 1,802 time-resolved time bins and spectra were obtained.

Four different empirical models are fit to each spectrum, namely the Band function (BAND), smoothly broken power law (SBPL), cutoff power law (COMP), and power law (PL). See Sect. 1.4 for function definitions. This results in a compilation of $1,802 \times 4 = 7,208$ spectral fits. Compared to the 4-yr GBM GRB time-integrated spectral catalog (Gruber et al. 2014; von Kienlin et al. 2014), the catalog presented here includes a lower number of GRBs (81 vs. 943), however, the number of high-resolution spectra is higher (1,491, see Sect. 2.3, vs. 943).

For all the aforementioned mathematical functions, the resulting spectrum has a peak in the νF_ν space if and only if $\alpha > -2$ and $\beta < -2$. Since the Band function presumes $\alpha > \beta$, for the BAND fits with $\alpha \leq -2$, the spectrum decreases monotonically, and for those with $\beta \geq -2$, the spectrum increases monotonically. For the SBPL fits with $\alpha \leq -2$ or $\beta \geq -2$, $E_{\rm p}$ is not calculated because Eqn. (1.37) is invalid. Similarly, for the COMP fits with $\alpha \leq -2$, $E_{\rm p}$ is just a break and the spectrum decreases monotonically, and obviously not there for the PL model.

2.2 Spectral Analysis Method

The light curves are binned according to the procedure described in Sect. 2.1, resulting in a total of 1,802 time bins and $1,802 \times 4 = 7,208$ spectra. Time-resolved spectral analysis is performed using the official GBM spectral analysis software RMFIT[2] v4.3BA. RMFIT employs a modified forward-folding technique based on the Levenberg-Marquardt algorithm. During the fitting process, the fitting models are converted into counts. These counts are then compared to the observed counts and RMFIT iterates itself until a best fit is found according to the chosen statistics for minimization.

In order to fold the model spectra into count space in the forward-folding process, detector response matrices (DRMs) are generated using the GBM response matrices v2.0. These DRMs contain information about the angular dependence of the detector efficiency, effective area of the detectors, partial energy deposition, energy dispersion, nonlinearity in the detectors, and atmospheric and spacecraft scattering of photons into the detectors. Therefore, they are functions of photon energies, angular dependence between spacecraft and the source, and angle between spacecraft orientation relative to the Earth. In order to account for the orientation change of the detectors relative to the burst direction because of the slew of the spacecraft, DRMs are generated for every 2 degrees on the sky and grouped into RSP2 files for each burst. This means each DRM is weighted by the counts in the detectors for every 2 degrees of spacecraft slew.

The chosen statistics for minimization in the fitting process is the so-called Castor C-Statistics (CSTAT). This is a modified statistical function based on the original Cash statistics (Cash 1979). Since the background is Poissonian, the net count statistics is non-Gaussian, CSTAT is preferable over the traditional χ^2 statistics. However, CSTAT does not provide a goodness-of-fit measure as χ^2, because there is no standard probability distribution for the likelihood of CSTAT. As a result, test statistics must be calculated and compared to the resulting CSTAT values by simulating the fitting model a large number of times, which allows us to reject a model up to a certain confidence level. Theoretically, this should be done for each burst separately, but due to the infeasibility of generating large number of simulated spectra for all bursts, we adopt the values given in Gruber et al. (2014) for models (8.58 for PL vs. COMP, and 11.83 for COMP vs. BAND or SBPL) with various numbers of free parameters. These values, what we call the critical ΔCSTAT or $\Delta\text{CSTAT}_{\text{crit}}$, are listed in Table 1 of Gruber et al. (2014).

[2]The public version of the RMFIT software is available at `http://fermi.gsfc.nasa.gov/ssc/data/analysis/rmfit/`

2.3 Time-Resolved Spectral Analysis Results

2.3.1 General Statistics

Table 2.1: Best-fit statistics for the GOOD and BEST samples. For each sample the number of spectra N and the percentage of the fraction of the spectra are given for each fitting model. ALL represents the overall population of spectra (i.e., BAND + SBPL + COMP + PL).

	GOOD		BEST	
Model	N	percentage	N	percentage
BAND	939	52.1%	139	9.3%
SBPL	1,201	66.6%	170	11.4%
COMP	1,276	70.8%	1,030	69.1%
PL	1,488	82.6%	152	10.2%
ALL	1,802	-	1,491	-

We define the GOOD sample of spectra by the following criteria: for a parameter Q, the relative error $\sigma_Q/Q \leq 0.4$, except for all power-law indices. For models that have two power-law indices, the low-energy index error has to satisfy $\sigma_\alpha \leq 0.4$, and the high-energy power-law index has to satisfy $\sigma_\beta \leq 1.0$. For the single power law, the index error criterion is the same as α's. These criteria are the same as used in the 4-yr *Fermi* GBM GRB time-integrated spectral catalog (Gruber et al. 2014). We also define the BEST sample as: for each spectrum, the GOOD models that have the lowest CSTAT after correcting the values by $\Delta\mathrm{CSTAT}_{\mathrm{crit}}$ (see Sect. 2.2). Therefore, if the spectrum has no GOOD model, it has no BEST model either. Vice versa, if it has a BEST model, it must have at least one GOOD model. The fit results of the BEST model of all spectra for all GRBs[3] are listed in Table A.1.

We note that BAND's E_{b} and SBPL's E_{p} are computed instead of fit parameters. Therefore, we compute $\sigma_{E_{\mathrm{b}}}$ of BAND and $\sigma_{E_{\mathrm{p}}}$ of SBPL by performing Monte-Carlo simulations using the errors of the best-fitting model parameters. We randomly draw new values of the model parameters from a uniform probability function sharing the same 1σ width. This process is repeated to generate 10,000 realizations, and a cumulative distribution function (CDF) is constructed. The errors

[3]In this chapter, the names of the bursts are given according to the *Fermi* GBM trigger designation that is assigned for each new trigger detected. The first 6 digits indicate the year, month, and day of the month, and the last 3 digits indicate the fraction of the day. For more details, please see the online *Fermi* GBM burst catalog at `http://heasarc.gsfc.nasa.gov/W3Browse/fermi/fermigbrst.html`

Table 2.2: The mean and median values of the best-fit parameters for the GOOD and BEST samples. The mean values are computed by simply taking the averages of each parameter, and their errors are given by the standard deviations. The errors of the medians are given by the 1σ errors of each parameter by constructing the CDFs. ALL indicates parameter properties after combining the distributions. [a]We note that the GOOD ALL values may contain multiple GOOD fit parameters from a single spectrum. [b]Due to the very different parameter behavior of PL, we give also the ALL without PL values which better reflect the statistics of the overall distribution of more complex models.

		GOOD[a]		BEST	
Parameter	Model	Mean	Median	Mean	Median
α	BAND	-0.665 ± 0.329	$-0.691^{+0.329}_{-0.267}$	-0.603 ± 0.300	$-0.639^{+0.298}_{-0.205}$
	SBPL	-0.853 ± 0.268	$-0.862^{+0.242}_{-0.256}$	-0.763 ± 0.362	$-0.741^{+0.241}_{-0.396}$
	COMP	-0.790 ± 0.315	$-0.777^{+0.275}_{-0.264}$	-0.802 ± 0.312	$-0.810^{+0.287}_{-0.297}$
	PL	-1.414 ± 0.199	$-1.378^{+0.151}_{-0.237}$	-1.674 ± 0.169	$-1.648^{+0.147}_{-0.216}$
	ALL	-0.971 ± 0.407	$-0.953^{+0.374}_{-0.429}$	-0.867 ± 0.413	$-0.823^{+0.304}_{-0.413}$
	ALL w/o PL[b]	-0.778 ± 0.312	$-0.795^{+0.289}_{-0.278}$	-0.776 ± 0.323	$-0.773^{+0.272}_{-0.320}$
β	BAND	-2.503 ± 0.329	$-2.477^{+0.377}_{-0.425}$	-2.214 ± 0.272	$-2.183^{+0.224}_{-0.311}$
	SBPL	-2.598 ± 0.486	$-2.410^{+0.282}_{-0.643}$	-2.412 ± 0.573	$-2.272^{+0.317}_{-0.573}$
	ALL	-2.556 ± 0.450	$-2.509^{+0.396}_{-0.482}$	-2.323 ± 0.472	$-2.217^{+0.262}_{-0.412}$
$E_{\rm p}$	BAND	313.18 ± 302.84	$230.00^{+207.60}_{-91.00}$	306.03 ± 256.35	$229.00^{+200.40}_{-105.40}$
(keV)	SBPL	292.17 ± 274.72	$208.20^{+234.07}_{-80.43}$	252.92 ± 234.49	$162.38^{+258.46}_{-85.50}$
	COMP	428.50 ± 464.70	$297.20^{+314.10}_{-131.90}$	408.99 ± 440.73	$280.35^{+310.95}_{-115.85}$
	ALL	349.55 ± 369.96	$244.69^{+268.21}_{-101.09}$	380.20 ± 409.48	$264.30^{+298.70}_{-114.18}$
$E_{\rm b}$	BAND	219.75 ± 230.59	$162.39^{+133.30}_{-63.68}$	173.54 ± 146.47	$134.29^{+97.10}_{-52.96}$
(keV)	SBPL	206.00 ± 188.40	$182.70^{+86.70}_{-86.54}$	151.96 ± 174.16	$116.85^{+81.95}_{-71.86}$
	ALL	212.04 ± 208.04	$161.70^{+116.50}_{-64.12}$	161.67 ± 162.39	$129.23^{+89.08}_{-69.92}$

are then obtained by taking the 1σ width of the resulting CDFs. This procedure generates the most conservative error values because the uniform probability function has the largest standard deviation.

The fit statistics for the GOOD and BEST sample are listed in Table 2.1. It can be seen that the simple power law can produce a GOOD fit in 82.6% of the total 1,802 spectra. The COMP and

SBPL can produce similar fractions of GOOD fits (70.8% and 66.6% respectively), and the BAND can only produce a GOOD fit in around half of the sample spectra (52.1%). This indicates that the conventional Band function may not be the optimal mathematical fit function for the majority of time-resolved spectra (e.g., Giblin et al. 1999; González et al. 2012; Sacahui et al. 2013).

Looking at the BEST sample, COMP has the largest fraction of BEST fits (69.1%), SBPL and PL have 11.4% and 10.2% respectively, and BAND gives the lowest fraction, only 9.3%. However, we note that these resulting statistics do not necessarily imply that the Comptonized model is generally favored over the Band function. Kaneko et al. (2006) and Goldstein et al. (2012) showed that there appeared to be a strong correlation between the S/N and the complexity of the BEST model. Therefore, we cannot rule out the possibility that this observed preference is due to poor count statistics at the high energies.

The mean and median values of the parameter distributions in the GOOD and BEST samples are shown in Table 2.2. The "Mean" columns show the average value of each parameter distribution and their errors are given by the standard deviations. The "Median" columns show the median and 1σ errors of each parameter by constructing the CDFs. It can be seen that the mean and median values of α and β agree well within the error bars, while those of $E_{\rm p}$ and $E_{\rm b}$ show only marginal agreements within the error bars. The latter can be attributed to the log-normal, rather then Gaussian, distribution of $E_{\rm p}$ and $E_{\rm b}$, as shown in Figs. 2.1 and 2.2.

In Fig. 2.1 we show the distributions of the GOOD sample best-fit parameters. The top left panel shows the GOOD distributions of the low-energy power-law index α. It can be seen that there are two peaks in the ALL population. The peak at $\alpha \approx -0.7$ is due to the populations of BAND, SBPL, and COMP collectively. The peak at $\alpha \approx -1.4$ is due to the population of PL alone. The significantly softer values of PL's α can also be seen in Table 2.2. Moreover, it is observed that no GOOD value of PL's α lies above $\alpha = -0.8$.

The top right panel shows the GOOD distributions of the high-energy power-law index β. It can be seen that both the BAND's and SBPL's β show very similar distributions, with a broad and asymmetric peak of the populations at $\beta \approx -2.5$. Only 7.6% of the overall population of $\beta \geq -2$, which implies that there is no peak in the νF_ν space and the spectrum increases monotonically, therefore an extra break must exist above the GBM's observing energy range.

The bottom left panel shows the GOOD distributions for the νF_ν peak energy $E_{\rm p}$. We note that $E_{\rm p}$ for SBPL is not a fit parameter but computed quantity by Eqn. (1.37). We also note that the spectrum can increase or decrease monotonically if the conditions described in Sect. 2.1.4 are

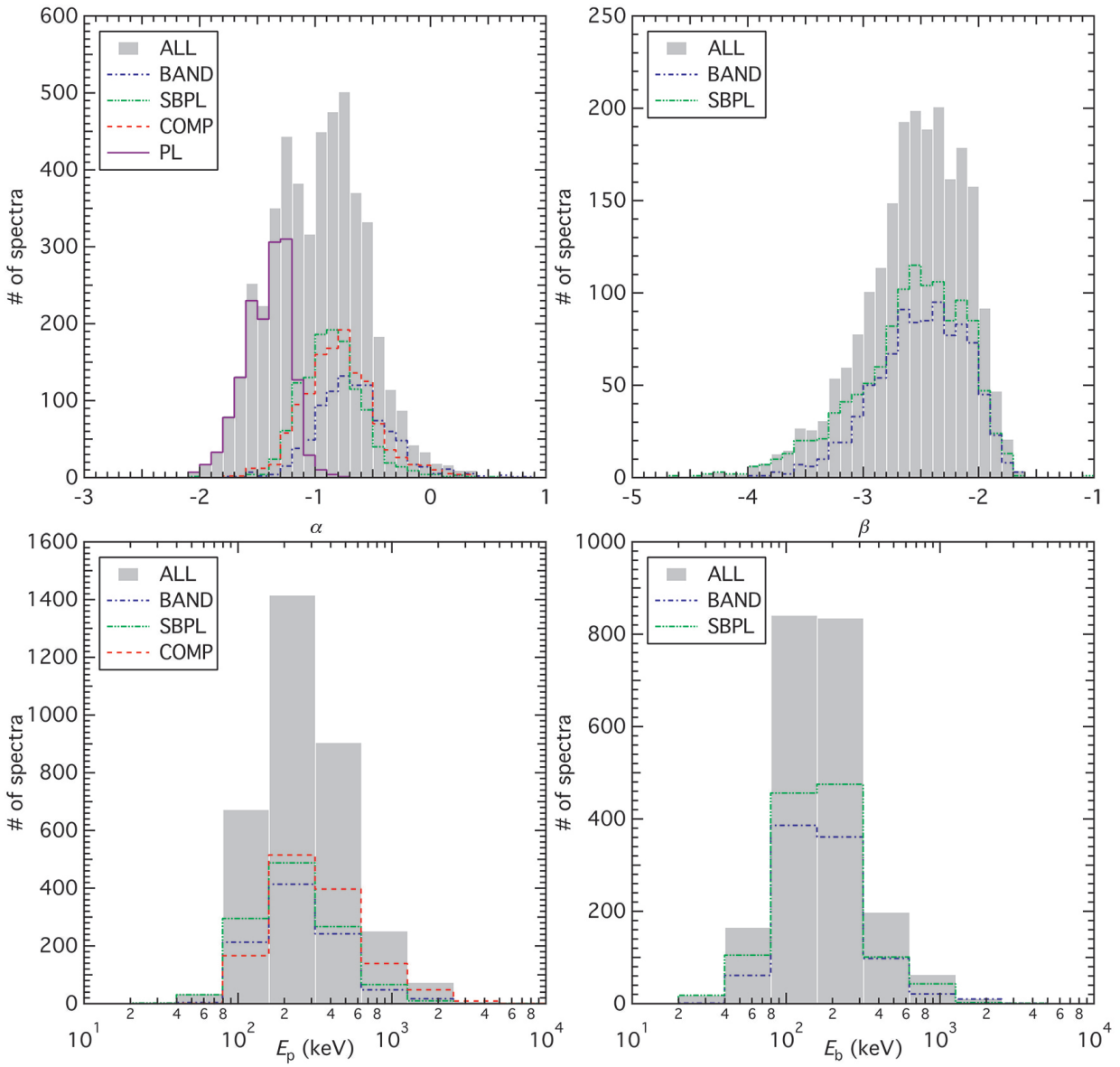

Figure 2.1: The distributions of the GOOD sample spectral parameters. The BAND parameter populations are shown by the blue dash-dotted lines, the SBPL by the green dash-double dotted lines, the COMP by the red dashed lines, and the PL by the purple solid lines. The overall populations (ALL) are shown by the grey solid histograms. Top left panel: distributions of α. Top right panel: distributions of β. Bottom left panel: distributions of $E_{\rm p}$. Bottom right panel: distributions of $E_{\rm b}$.

satisfied. It can be seen that the $E_{\rm p}$ populations of all three different fit functions are very similar, with a peak at $E_{\rm p} \approx 250$ keV. Only 3.9% of the overall population of $E_{\rm p} \geq 1$ MeV.

The bottom right panel shows the GOOD distributions for the break energy $E_{\rm b}$. We note that

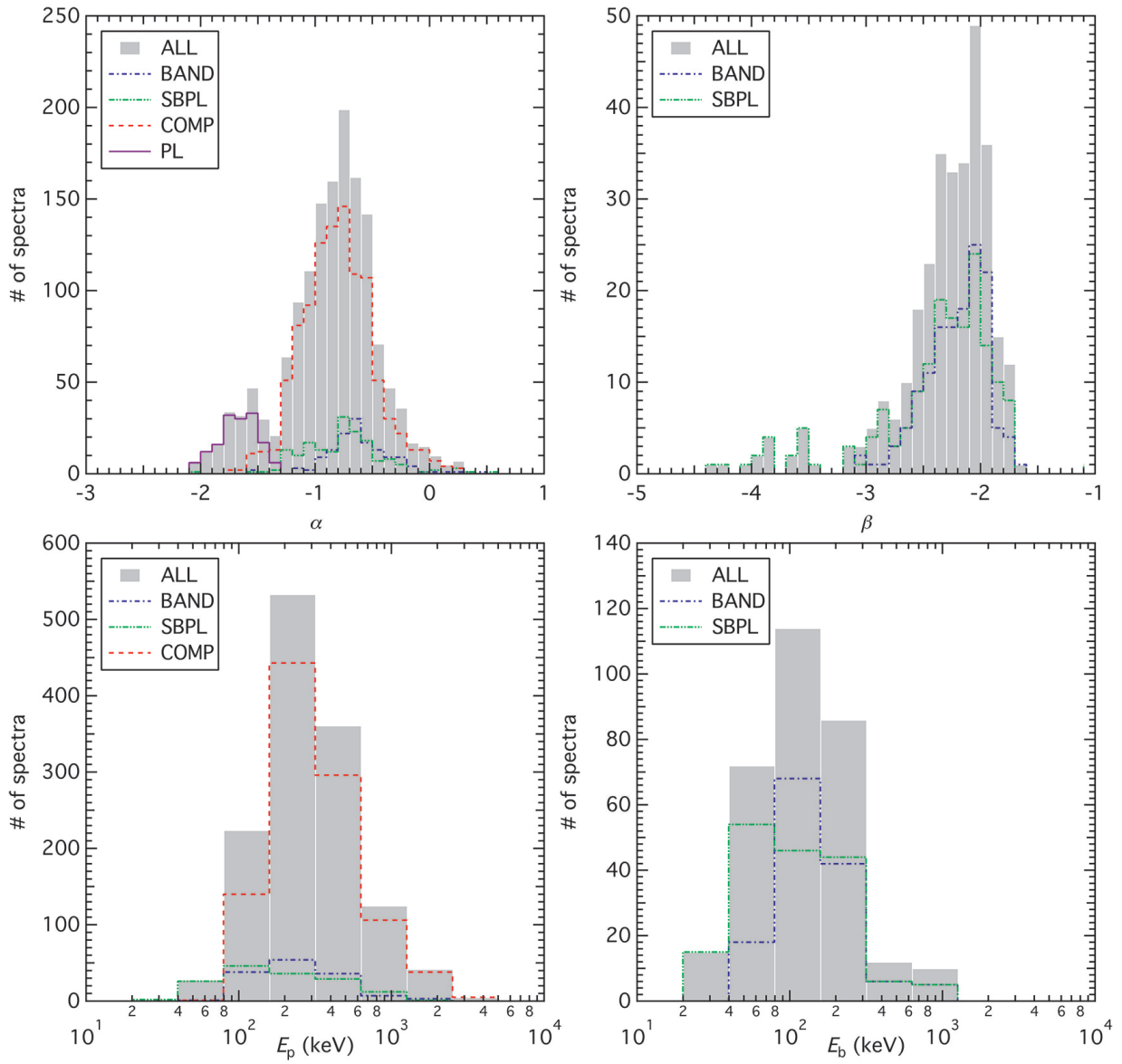

Figure 2.2: The distributions of the BEST sample spectral parameters. The BAND parameter populations are shown by the blue dash-dotted lines, the SBPL by the green dash-double dotted lines, the COMP by the red dashed lines, and the PL by the purple solid lines. The overall populations (ALL) are shown by the grey solid histograms. Top left panel: distributions of α. Top right panel: distributions of β. Bottom left panel: distributions of $E_{\rm p}$. Bottom right panel: distributions of $E_{\rm b}$.

$E_{\rm b}$ for BAND is not a fit parameter but computed quantity by Eqn. (1.34). It can be seen that the $E_{\rm b}$ populations of the two different fit functions are very similar, with a peak at $E_{\rm b} \approx 150$ keV, lower than the peak of the distribution of $E_{\rm p} \approx 250$ keV.

In Fig. 2.2 we show the distributions of the BEST sample best-fit parameters. The top left panel shows the BEST distributions of the low-energy power-law index α. It can be seen that there are two peaks in the ALL population, resulting from the two-peak distribution from the GOOD distribution. The majority of the values of α for BAND, SBPL, and COMP are similar to that of the GOOD distribution (≈ -2.5 up to -0.5). The peak at $\alpha \approx -0.7$, excluding those values from PL, is dominated by the COMP model. It can be seen that the population of BAND's α is slightly harder that that of the SBPL's which also shows a larger spread. The significantly softer values of PL's α in the BEST sample has a smaller spread than that in the GOOD sample, with no value lies above $\alpha = -1.3$. Therefore, the distinct behaviors of PL's to the other fit function's α is evident.

The top right panel shows the BEST distributions of the high-energy power-law index β. It can be seen that the BAND's β becomes more concentrated between -3.1 and -1.6, while the SBPL's β extend to much steeper values of about -4.4. The peak of the populations shifted to harder values at $\beta \approx -2.1$, comparing to the GOOD sample. As a result, 21% of the overall population of $\beta \geq -2$ (no peak in the νF_ν space).

The bottom left panel shows the BEST distributions for the νF_ν peak energy $E_{\rm p}$. It can be seen that the $E_{\rm p}$ population of COMP dominates the overall distribution, and that the COMP population extends to higher energies (up to about 5 MeV) than the BAND and SBPL populations, which instead extend to lower energies (down to about 20 keV). We do not find any spectrum with very large $E_{\rm p}$, with only 4.8% of the overall population of $E_{\rm p} \geq 1$ MeV.

The bottom right panel shows the distributions for the break energy $E_{\rm b}$. It can be seen that the $E_{\rm b}$ population of BAND has a clear peak at $E_{\rm b} \approx 150$ keV, while the $E_{\rm b}$ population of SBPL has a broad peak (from 40 keV to 300 keV).

These general statistics suggests that when performing spectral analysis of GRBs, one should not assume a Band spectrum (e.g., Giblin et al. 1999; González et al. 2012; Sacahui et al. 2013). Instead, one should always try different fit functions and compare the fit statistics to find the best description to the data. Similar statistical behaviors are also observed in the time-integrated spectral catalogs (Goldstein et al. 2012; Gruber et al. 2014).

2.3.2 Parameter-Parameter Scatter Plots

Figure 2.3 shows the scatter plots between the best-fit parameters of the BEST sample. The top left panel shows the plot of β against α. Trends can neither be found between α and β for individual models nor the overall population as a whole. It can be seen that SBPL's β population extend to

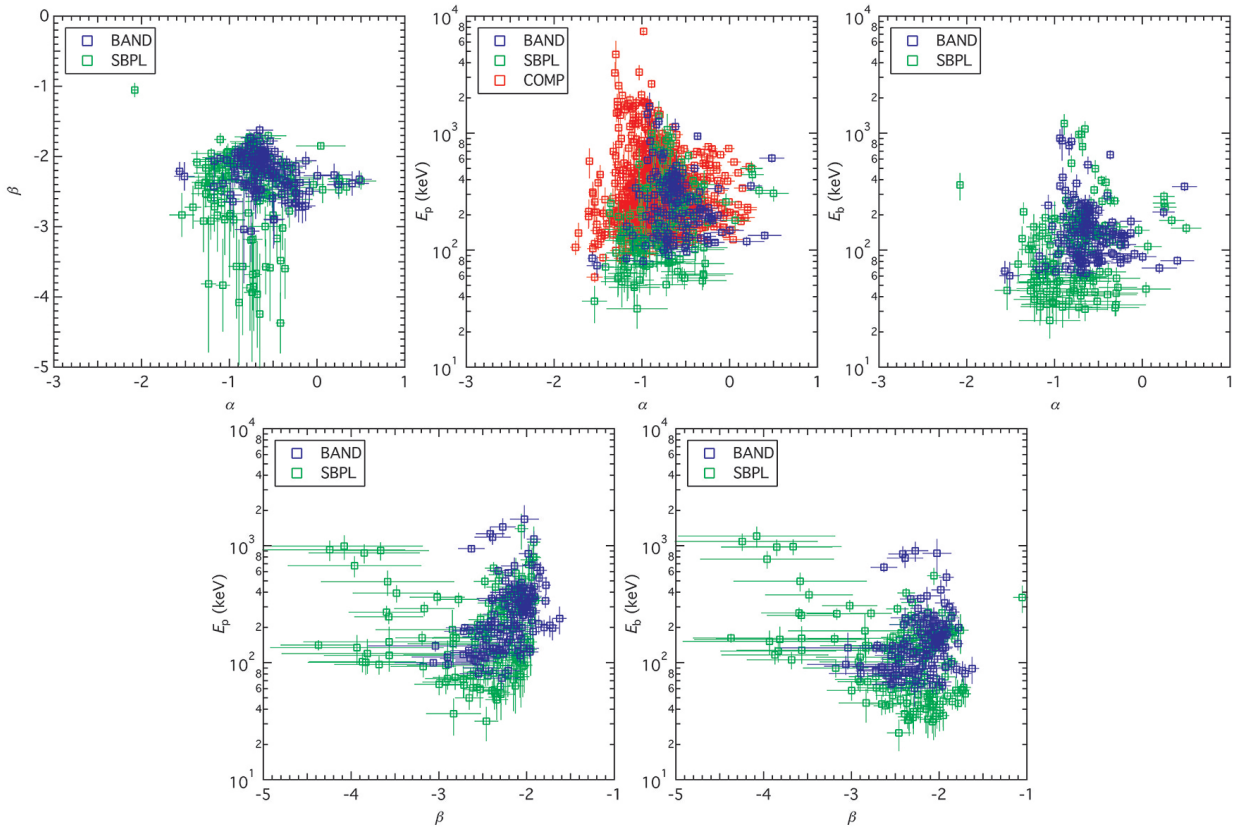

Figure 2.3: The scatter plots between the BEST sample spectral parameters. The blue, red, and green data points represent BAND, COMP, and SBPL fits, respectively. Top left panel: β against α. Top middle panel: $E_{\rm p}$ against α. Top right panel: $E_{\rm b}$ against α. Bottom left panel: $E_{\rm p}$ against β. Bottom right panel: $E_{\rm b}$ against β.

steeper values and have larger error bars in the same range of values of α. The larger error for steeper β shows that the SBPL tends to mimic a COMP spectrum, in which β is poorly constrained due to less photon statistics at the higher energies.

The top middle panel shows the plot of $E_{\rm p}$ against α. Trends can neither be found between α and $E_{\rm p}$ for individual models nor the overall population as a whole. It can be seen that while the data points seem to occupy the same region, SBPL's $E_{\rm p}$ extends to lower energies and COMP's $E_{\rm p}$ extends to higher energies, for similar range of values for α.

The top right panel shows the plot of $E_{\rm b}$ against α. Similar to the plot of $E_{\rm p}$, no trends can be found for $E_{\rm b}$, and SBPL's $E_{\rm b}$ extends to lower energies for similar range of values of α. This is because, according to Eqns. (1.34) and (1.37), $E_{\rm p}$ is proportional to $E_{\rm b}$.

The bottom left panel shows the plot of $E_{\rm p}$ against β, and the bottom right panel shows the

plot of $E_{\rm b}$ against β. Since $E_{\rm p}$ is proportional to $E_{\rm b}$, the two plots show similar behaviors. A slight trend may exist between $E_{\rm p}$ against β in the population of BAND: steeper β tends to have lower $E_{\rm p}$. However, this trend is not seen in the population of SBPL.

These plots show that the SBPL produces larger uncertainties for steeper β, and has difficulties to constrain the high-energy power-law behavior in comparison to the Band function.

2.3.3 Parameter-Uncertainty Scatter Plots

Figure 2.4 shows the scatter plots between the best-fit parameters and uncertainties of the parameters of the BEST sample. The top left panel shows the plot of σ_α against α. It is seen that the SBPL gives the most scatter and large errors (extend to almost $\sigma_\alpha = 0.4$), while other models give relatively small errors of $\sigma_\alpha < 0.2$. The PL gives the smallest $\sigma_\alpha \leq 0.1$. A clear trend for σ_α can be seen: σ_α tends to be larger when α increases (i.e., becomes harder).

The top middle panel shows the plot of σ_β against β. A clear trend is observed that σ_β becomes larger when β decreases (i.e., becomes softer/steeper). The trend is indeed expected because the high-energy power-law slope becomes less constrained when the BAND or SBPL mimics a COMP model, i.e., when there are less photon statistics at the high energies which leads to a cutoff behavior.

The top right panel shows the plot of $\sigma_{E_{\rm p}}$ against $E_{\rm p}$. It is observed that $\sigma_{E_{\rm p}}$ of SBPL is systematically larger than that of BAND and COMP for the same value of $E_{\rm p}$. The values of $\sigma_{E_{\rm p}}$ for BAND and COMP also tend to lie above the dashed line, implying that $\sigma_{E_{\rm p}}$ becomes larger when $E_{\rm p}$ increases. We note that $E \approx 900$ keV is the upper energy boundary of the NaIs, so that there are only data contributed by the BGOs beyond this limit, providing less photon statistics and thus increases the uncertainty in determining the spectral peak position.

The bottom left panel shows the plot of $\sigma_{E_{\rm b}}$ against $E_{\rm b}$. Comparing to the peak energies, $\sigma_{E_{\rm b}}$ of the break energies $E_{\rm b}$ have similar trends for both the BAND and SBPL fits. The errors lie systematically above the dashed line for both models.

It is also of interest to investigate how the position of the spectral peak affects the uncertainties in the spectral slopes. The bottom middle panel shows the plot of σ_α against $E_{\rm p}$. A clear trend is observed that the low-energy power-law slope becomes more uncertain when the spectrum peaks at lower energies. This is because the low-energy spectral slope is determined by the photon statistics below the peak energy. When the peak energy is smaller, there are relatively fewer data points to constrain the value of the low-energy power-law slope. It is also observed that for the same value of $E_{\rm p}$, σ_α tends to be larger for the SBPL fits than that for the BAND or COMP fits.

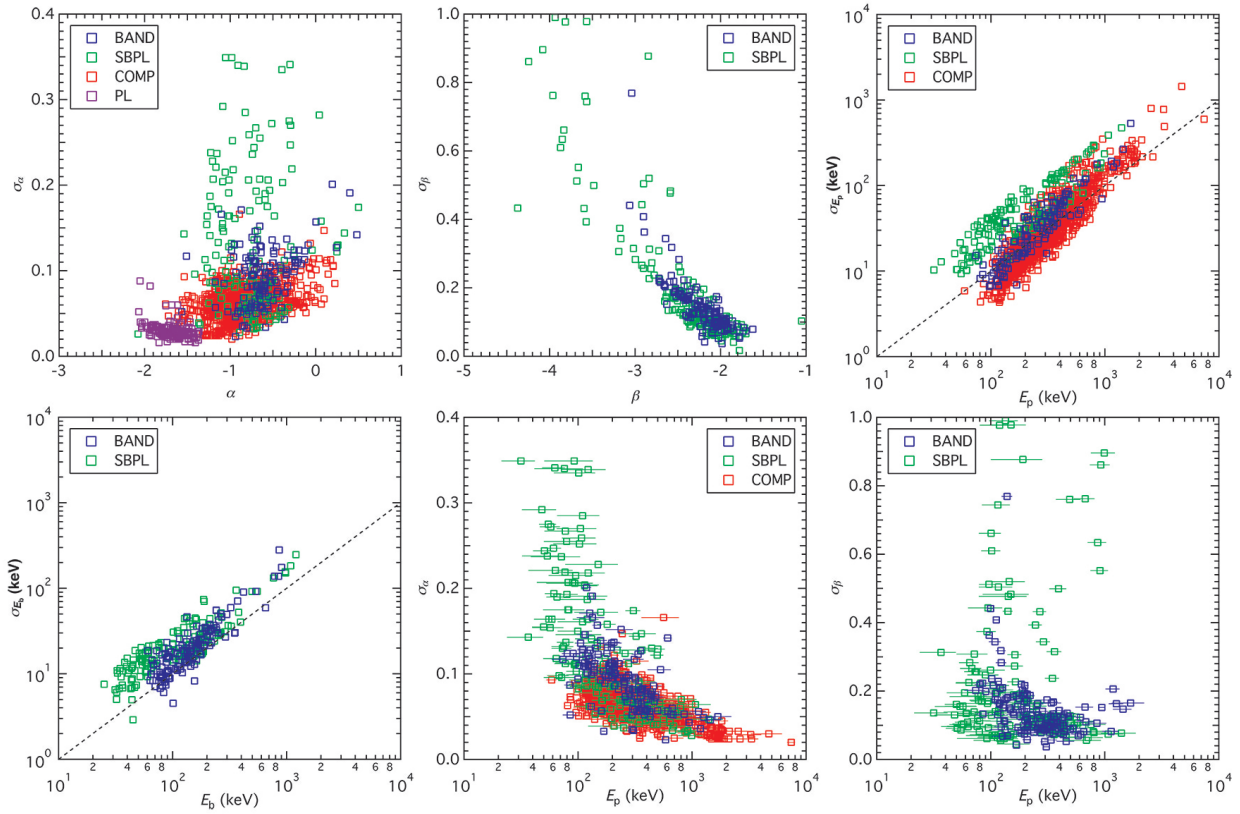

Figure 2.4: The scatter plots between the BEST sample spectral parameters and uncertainties. The blue, red, green, and purple data points represent BAND, COMP, SBPL, and PL fits, respectively. The dashed lines show $y = 0.1x$. Top left panel: σ_α against α. Top middle panel: σ_β against β. Top right panel: σ_{E_p} against E_p. Bottom left panel: σ_{E_b} against E_b. Bottom middle panel: σ_α against E_p. Bottom right panel: σ_β against E_p.

The bottom right panel shows the plot of σ_β against E_p. A trend is observed that higher values of E_p tend to produce smaller σ_β, which is weaker in comparison to the plot of σ_α against E_p. This shows that the high-energy power-law slope is not as strongly coupled to the peak position as the low-energy power-law slope.

These plots again show that the smoothly broken power-law model produces the highest degree of uncertainties in the best-fit parameters. This is not limited in the high-energy power-law index β, as shown in Fig. 2.3. Figure 2.4 shows that SBPL's peak position significantly affects the uncertainties of both power-law indices, more so than the other models. The slight offsets of the best-fit parameters from different fit functions are expected because they have intrinsically different parametrical formulae. In general, we observe good consistency in the parameter space occupation, indicating that the minima in the parameter spaces are well defined and our results are statistically

reliable.

2.3.4 $E_{\rm p}$ Evolution

Time-resolved spectral analysis of GRBs has shown that there are two different kinds of $E_{\rm p}$ evolutionary trends (e.g., Ford et al. 1995), namely the intensity tracking and the hard-to-soft behavior. Intensity tracking bursts show evidence that the values of $E_{\rm p}$ follow similar trends of the intensity (either photon flux or energy flux) in their light curves. Hard-to-soft bursts show evidence that $E_{\rm p}$ decays (in general) monotonically with time.

We compute the Spearman's Rank Correlation Coefficient ρ (Spearman 1904) between $E_{\rm p}$ and (1) the 1 keV - 1 MeV photon flux, $\rho_{\rm ph}$, (2) the 1 keV - 1 MeV energy flux, $\rho_{\rm en}$, and (3) the time, $\rho_{\rm t}$. A positive value indicates a positive correlation, a negative value indicates a negative correlation, and a value of zero means no correlation. The process is repeated for different confidence levels of 90%, 95%, and 99%. We note that the confidence levels are *not* the probabilities to find ρ within the confidence intervals. They are the *proportions* to find the real ρ within the confidence intervals when the spectral analysis process is repeated. For example, the 99% confidence interval of ρ means that if the spectral analysis is repeated a large number of times, we will find on average, in 99 out of 100 times, that the real ρ lies within the 99% confidence interval. However, we will never know if we have picked the lucky ones, because we have no way to know the actual value of ρ. Therefore, the confidence level of a confidence interval provides a sense of how often a correlation is expected to be found.

First, we distinguish the $E_{\rm p}$ evolutionary trends by machine. For each confidence level of the ρ's, we check the following logical criteria:[4] (1) if $\rho_{\rm ph}$ *or* $\rho_{\rm en} > 0.5$, *and* it is not consistent with zero within the confidence interval; *and* $\rho_{\rm t} \geq -0.5$ *or* it is consistent with zero within the confidence interval, then we define the trend as intensity tracking ("in.track."); (2) if $\rho_{\rm ph} \leq 0.5$ *and* $\rho_{\rm en} \leq 0.5$, *or* they are consistent with zero within their confidence intervals; *and* $\rho_{\rm t} < -0.5$ and it is not consistent with zero within the confidence interval, then we define the trend as hard-to-soft ("h.t.s."); (3) everything else are defined as undetermined ("undeter."). The values and confidence intervals of the ρ's, and the machine-decided kinds of trends are listed in Cols. (3) - (14) of Table A.2.

Then, we distinguish the $E_{\rm p}$ evolutionary trends by human eyes (Col. 15 of Table A.2). We plot

[4]We iterated the machine-based decision process for many different logical criteria, and found that the stated criteria provide a fairly robust determination of the trends comparing to human decisions. See main text and Table A.2.

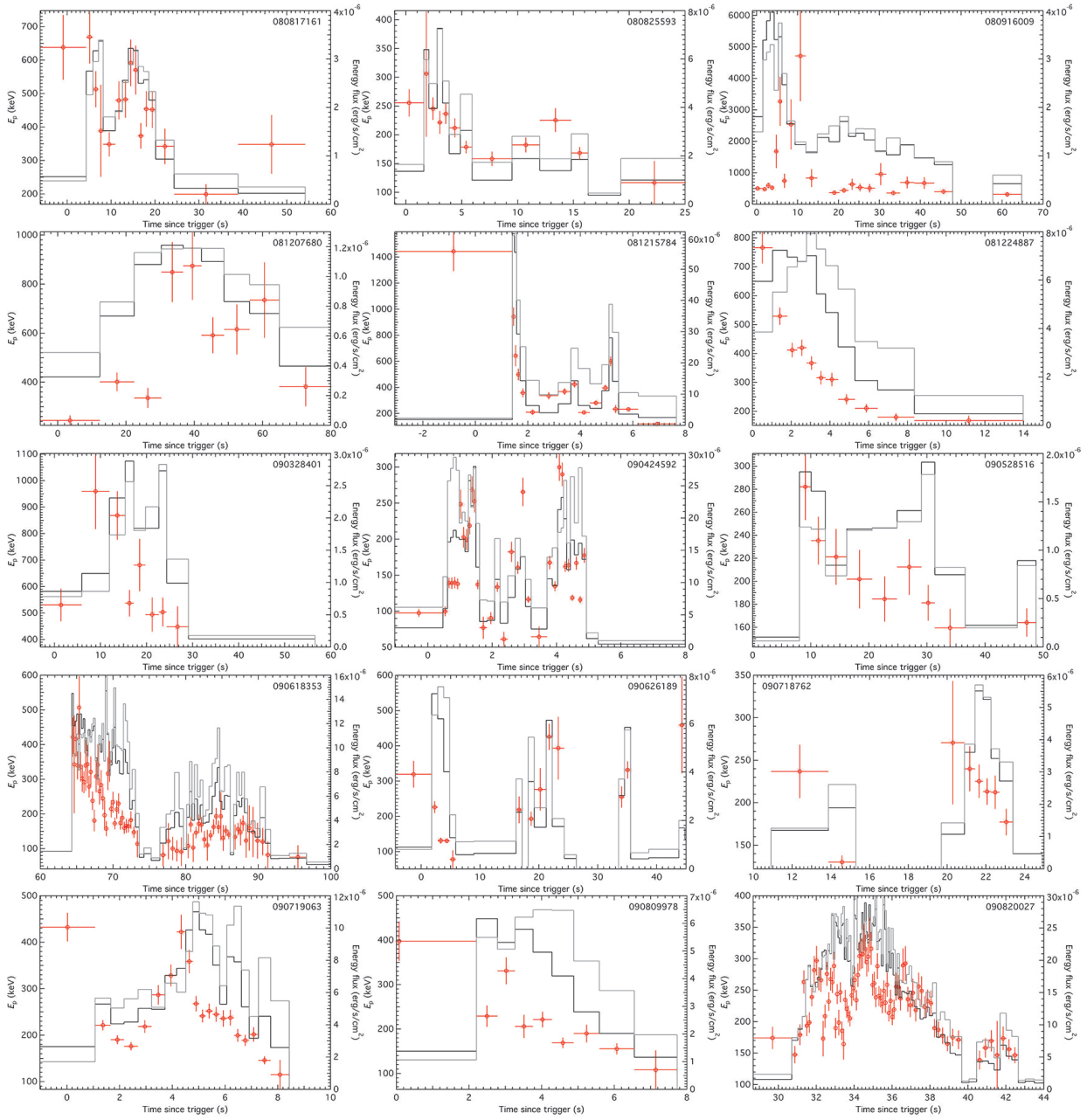

Figure 2.5: $E_{\rm p}$ evolutions (red data points, left axis) of individual burst with the 10 keV - 1 MeV energy flux (black histograms, right axis) and the 10 keV - 1 MeV photon flux (grey histograms, arbitrary units) overlaid.

the $E_{\rm p}$ evolutions (red data points, left axis) in Figs. 2.5 - 2.8, with the 10 keV - 1 MeV energy flux (black histograms, right axis) and the 10 keV - 1 MeV photon flux (grey histograms, arbitrary units) light curves overlaid. We note that we only plot and compare the 57 bursts with $E_{\rm p}$ in at

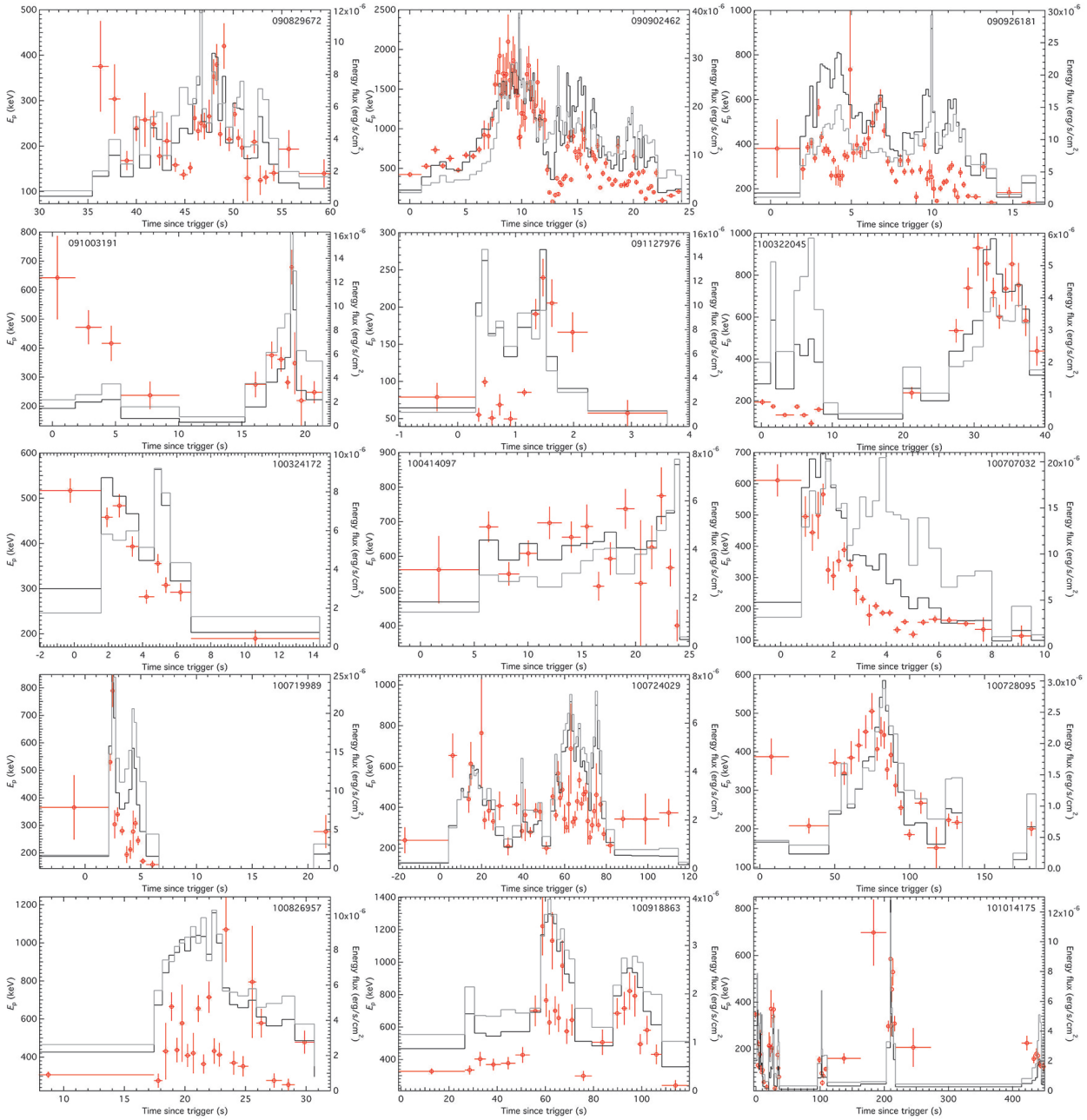

Figure 2.6: Same as Fig. 2.5.

least 6 time bins or more. We find that the machine-based decision process is quite robust, in that only 2 bursts (3.5%) are mis-attributed to the opposite kind ("h.t.s." vs. "in.track."), namely GRB 100719989 (Fig. 2.6) and GRB 111216389 (Fig. 2.7). The brightness of the first peak relative to the second peak of GRB 100719989 mimics a trend that $E_{\rm p}$ is decaying with time. In contrast,

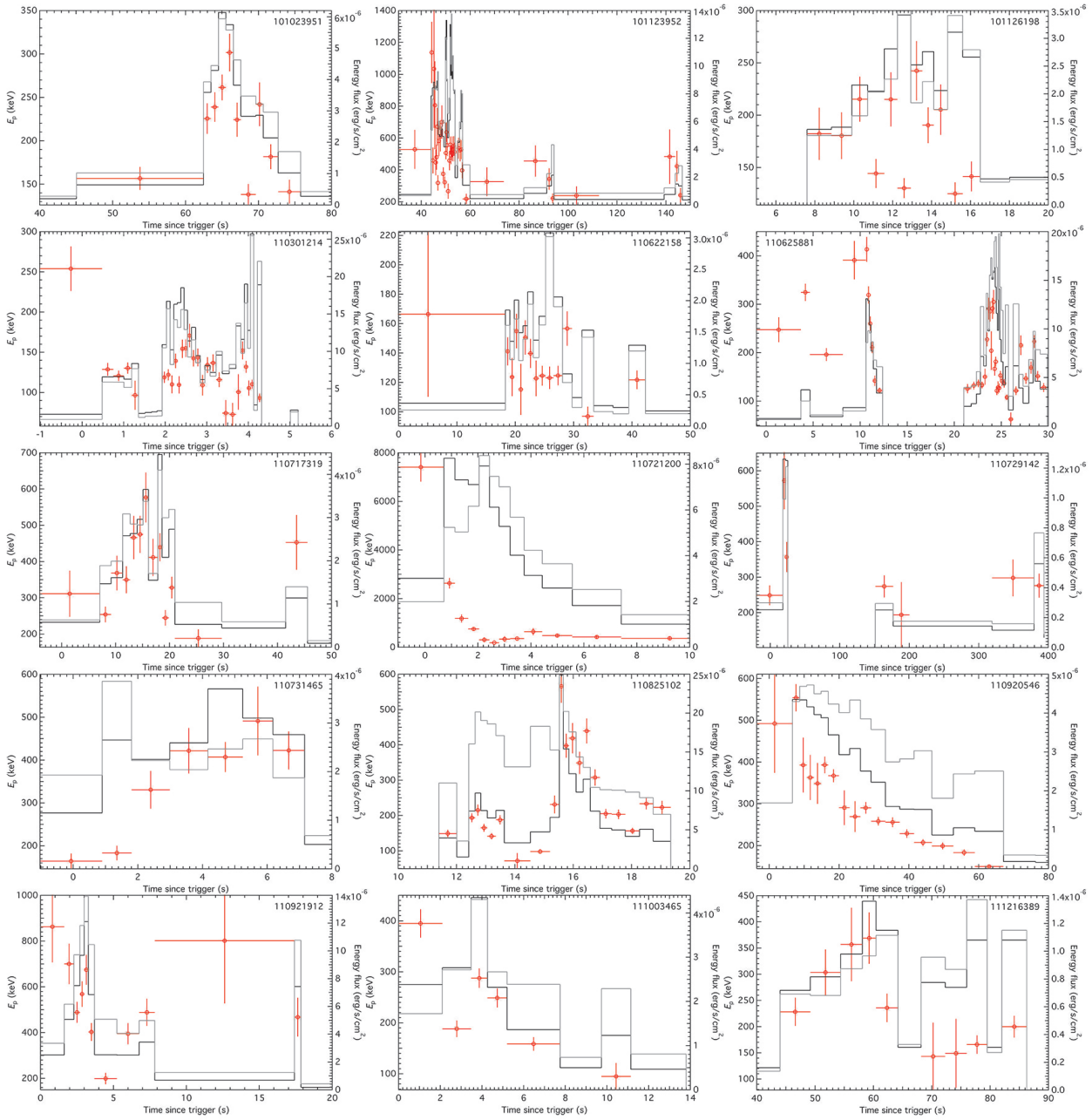

Figure 2.7: Same as Fig. 2.5.

a human would identify its intensity tracking nature by noticing the low $E_{\rm p}$ in the first time bin and the small rise of $E_{\rm p}$ values during the second peak. The case of GRB 111216389 is similar in that the relatively higher value but intensity tracking $E_{\rm p}$ during the first peak to the second peak contributed to a small excess in $\rho_{\rm t}$.

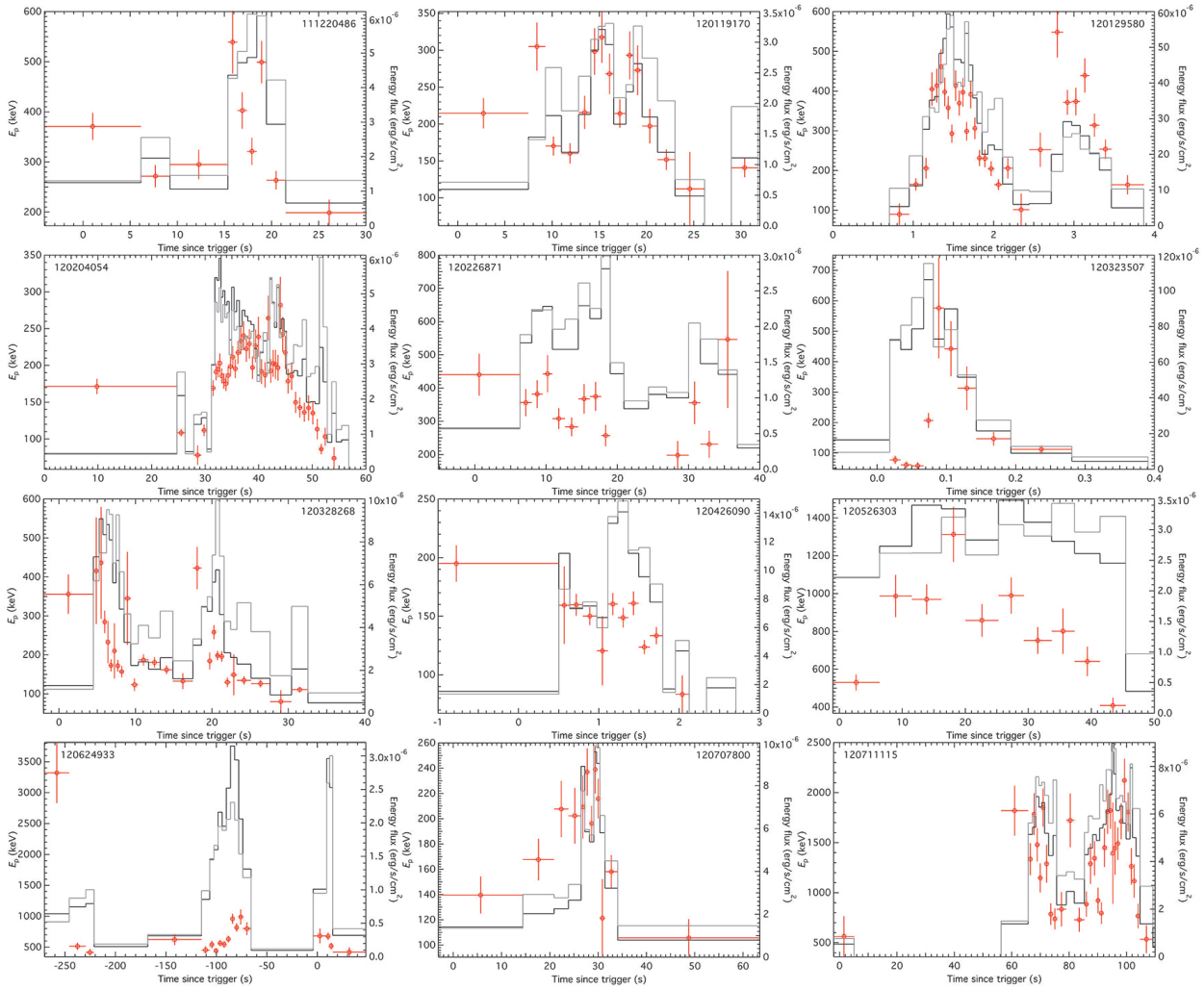

Figure 2.8: Same as Fig. 2.5.

There are 12 GRBs (21%) which show a mix of the two kinds of trends. Some of these bursts are identified by the computer as either one of the two kinds, or as undetermined. Two of them are especially worth mentioning: GRB 090618353 (Fig. 2.5) and GRB 091003191 (Fig. 2.6). They both show an initial hard-to-soft evolution followed by a later intensity tracking behavior, where the computer labeled them as undetermined. The other 10 bursts show a general hard-to-soft decay of $E_{\rm p}$ where the values in between seem to follow the intensity profile. Lu et al. (2012) has shown that intrinsic hard-to-soft evolutions of distinct pulses can overlap and produce such a "h.t.s.+in.track." behavior. They claimed that both "h.t.s." and "in.track." behavior could be intrinsic to a burst or a pulse, which is consistent with our findings that many single pulsed bursts show pure intensity tracking behavior. We also find that the intensity tracking behavior of $E_{\rm p}$ with the energy flux is

more prominent than that with the photon flux in all of the intensity tracking bursts.

A few more bursts are worth of mentioning. GRB 100707032 (Fig. 2.6), GRB 110721200, and GRB 110920546 (both Fig. 2.7) are single pulsed, fast-rise-exponential-decay (FRED) bursts. All of them show pure hard-to-soft behavior. Since the $E_{\rm p}$ evolutions and intensity profiles of these FRED bursts are very similar, $\rho_{\rm en}$ and $\rho_{\rm ph} \approx -\rho_{\rm t} \gtrsim 0.5$, thus the computer cannot determine their evolutionary trends.

In short, we emphasize that even though the process of distinguishing "h.t.s." and "in.track." bursts can be done automatically, the existence of "h.t.s.+in.track." and FRED bursts can be ambiguous to computers. We strongly encourage checking by human eyes after any automated detection process of $E_{\rm p}$ evolutionary trends.

2.3.5 Search for Blackbodies

Many studies have reported evidence for thermal components with $kT \sim 10$ keV in various GRBs (e.g., Mészáros et al. 2002; Ryde 2005; Guiriec et al. 2011; Axelsson et al. 2012; Guiriec et al. 2013; Burgess et al. 2014a,b; Pe'er et al. 2015). Therefore, adding a blackbody component (i.e., a Planck function) to the fit function is a natural way to explore the data in this time-resolved spectral catalog.

We find that except for the single power law, in most of the cases ($\gtrsim 90\%$) it is not possible to obtain converged fits when the blackbody is added to other fitting models (i.e., BAND, COMP, and SBPL). However, we note that the ability of a model to fit the data depends also on the count statistics. Abdo et al. (2009) performed a joint GBM-LAT analysis to GRB 090902B (GBM trigger #090902462, see discussion below) that they can fit a BAND plus PL model to the burst, which is expected because there are more statistics to constrain more parameters. Our results in this chapter indicates the difficulty of fitting a model with 5 or more parameters to the GBM data alone using the S/N = 30 criterion.

The power law plus blackbody model (PLBB) is defined as (see Sect. 1.4)

$$f_{\rm PLBB}(E) = A_{\rm PL}\left(\frac{E}{100\ {\rm keV}}\right)^{\alpha} + A_{\rm BB}\left[\frac{(E/1\ {\rm keV})^2}{\exp(E/kT)-1}\right], \tag{2.1}$$

where $A_{\rm PL}$ and $A_{\rm BB}$ are the normalization factors for the power-law and blackbody component, respectively.

Since PLBB is a not a nested model, it is necessary to perform $\Delta{\rm CSTAT}_{\rm crit}$ simulations for every

pair of competing models, instead of just counting the number of free parameters (see Gruber et al. 2014). However, doing a large number of simulations for every spectrum is obviously impractical. We therefore first identify plausibly significant PLBB spectra by using the same $\Delta\mathrm{CSTAT}_{\mathrm{crit}}$ criteria for a 4-parameters model. Then we generate 10,000 realisations for the identified time intervals for every burst in this subsample and obtain the $\Delta\mathrm{CSTAT}_{\mathrm{crit}}$ for each burst. Then we compare the ΔCSTAT between the BEST model and the PLBB model for each spectrum, i.e., $\Delta\mathrm{CSTAT} = \mathrm{CSTAT(BEST)} - \mathrm{CSTAT(PLBB)}$.

Table 2.3: The 4 bursts with N number of PLBB-identified spectra, and their respective critical ΔCSTAT values.

GRB name	N	$\Delta\mathrm{CSTAT}_{\mathrm{crit}}$
090618353	2	19.55
090902462	32	32.75
110622158	2	12.32
110920546	6	148.37

As a matter of fact, 56 plausibly significant PLBB spectra are identified among 16 bursts, in which 14 bursts have only 1 plausible spectrum identified. Since a blackbody component is likely to be present in multiple spectra within a burst if it is real, we drop these 14 bursts and concentrate on the remaining 4 bursts (42 spectra in total) with multiple PLBB-identified spectra. These bursts are listed in Table 2.3, and their simulated $\Delta\mathrm{CSTAT}_{\mathrm{crit}}$ values are also given.

We find that the spectra of the bursts listed in Table 2.3 have $\Delta\mathrm{CSTAT} > \Delta\mathrm{CSTAT}_{\mathrm{crit}}$, except for GRB 110920546. These 36 PLBB spectral parameters are listed in Table A.3. We note that the 4 PLBB spectra from GRB 090618353 and GRB 110622158 have values of $kT \sim 20$ keV, while the 32 spectra from GRB 090902B show $kT \sim 200$ keV. In GRB 090902B, Abdo et al. (2009) identified an extra power-law component on top of Band functions with hard values of E_{p} using wider time bins and joint GBM-LAT data. Using only the GBM data, we find that most of the BAND plus PL fits of our more resolved time bins in this time interval are either poorly constrained, unconstrained, or even not converged; but, interestingly, our values of the PL indices are very similar to theirs ($\alpha \approx -1.8$). This indicates the ability of a model to fit data depends on (1) how many free parameters (in this case, BB vs. BAND), and (2) the count statistics (GBM alone vs. GBM-LAT). We also note that Pe'er et al. (2012) used a thermal plus non-thermal theoretical model to apply to the spectra of this burst, in which they claimed that the data are consistent with such a hybrid

emission model.

We note that the $\Delta\mathrm{CSTAT}_{\mathrm{crit}}$ can vary much across different bursts. Recently, Burgess et al. (2015) showed that it is very plausible to get false positive for an extra blackbody component in time-integrated spectra due to severe spectral evolution. Therefore, we recommend researchers to perform independent simulations on time-resolved spectra for different bursts in order to reduce the chance of false positives.

2.4 Conclusions

We present the first official gamma-ray burst time-resolved spectral catalog of the brightest subset of bursts observed by the *Fermi* GBM in its first 4 years of mission. We have obtained 1,491 spectra from 81 bursts with high spectral and temporal resolution. We observe a preference of the Comptonized model (i.e., the high-energy cutoff power law) to fit 69% of our spectra sample the best, under our chosen S/N = 30. However, we note that this may be due to poor count statistics at the high energies, as previous catalogs have pointed out (see, e.g., Kaneko et al. 2006; Goldstein et al. 2012). Similarly, Ackermann et al. (2012) showed that for the bursts observed in GBM which happen to be in the field-of-view of the LAT but remain undetected, the upper limits are usually inconsistent with the GBM fit Band function's β, extrapolated to the LAT energy range. This is consistent with the observed fact that COMP dominates the BEST sample, however there is a caveat that the sample selected by Ackermann et al. (2012) may be intrinsically softer in nature.

We have not observed significant deviations of the distributions of fit parameters from those observed in the *Fermi* GBM GRB time-integrated spectral catalogs. In the 4-yr GBM GRB time-integrated spectral catalog (Gruber et al. 2014; von Kienlin et al. 2014), the question of whether there is any time-resolved spectrum with very high value of E_{p} was raised. Down to the level of the temporal resolution of the binned data sets in the current catalog, the answer is "no". The largest value of E_{p} found in this study is $7,400 \pm 600$ keV, in GRB 110721A (GBM trigger #110721200, from -1.024 to 0.711 s relative to GBM trigger time). The time-integrated E_{p} of this burst is 450 ± 30 keV ($T_{90} = 21.822$ s starting from 0.003 s after GBM trigger time, Gruber et al. 2014), which is much lower and indicates severe spectral evolution. However, we note that very high E_{p} on much shorter timescales cannot be excluded. Gruber et al. (2014) discussed the very high $E_{\mathrm{p}} = 15 \pm 2$ MeV observed by Axelsson et al. (2012) in the "higher resolution" first time bin of GRB 110721A. Our aforementioned $E_{\mathrm{p}} = 7,400 \pm 600$ keV is consistent at 2σ level with their "lower

resolution" first time bin of $E_{\rm p} = 5,410^{+410}_{-420}$ keV.

We establish possible logical criteria for automated process of distinguishing between "hard-to-soft" and "intensity tracking" spectral evolutionary trends. With this selection scheme, only 3.5% of bursts would be mis-attributed to the opposite kind. However, we note that inspections using human eyes are often necessary because of the existence of "hard-to-soft + intensity tracking" and FRED bursts.

We also search for plausible blackbody components in the time-resolved spectra by performing simulations on individual bursts. We find that only 3 bursts show extra blackbodies in multiple time bins. We also find that constrained fit results can be obtained only when the Planck function is added to the simple power law, using S/N = 30 binning criterion and GBM data alone.

Finally, we note that the fact that very few blackbodies are found in this catalog does not necessarily imply that thermal components are in general not a dominant component for the prompt emission mechanism. There are many works recently showing that a thermal model can give rise to the observed Band shape (e.g., Pe'er et al. 2006; Giannios 2008; Pe'er & Ryde 2011; Ryde et al. 2011; Vurm et al. 2011; Lazzati et al. 2013). Whether thermal or non-thermal emission dominates the emission mechanism of GRB prompt spectra is a debated topic. Yu et al. (2015b) showed that all standard optically thin synchrotron emission functions are just too smooth to explain the peaks or breaks in the time-resolved spectra, and an independent conclusion is also drawn by Axelsson & Borgonovo (2015) using peak-flux spectra from the GBM GRB time-integrated spectral catalog. Recently, semi-empirical models (Ch. 3, Yu et al. 2015a) and physical models (e.g., Burgess et al. 2011, 2014a; Zhang et al. 2016) are fit to time-resolved spectra of a few GRBs. In the future, direct fitting of serious theoretical models, as oppose to empirical models, is likely the key to resolve these issues.

Chapter 3

Synchrotron Cooling in Energetic *Fermi* GBM GRBs

"An expert is a person who has found out by his own painful experience all the mistakes that one can make in a very narrow field."

- Niels Bohr

Gamma-ray bursts are the most luminous explosions in the Universe known to date. The first GRB was discovered in 1967 (Klebesadel et al. 1973), and after over 45 years of research efforts, it is now believed that GRBs originate from highly relativistic outflows from central compact sources at cosmological distances with bulk Lorentz factors $\Gamma > 100$ (e.g., Lithwick & Sari 2001; Hascoët et al. 2012). This is often understood in terms of the "fireball model" (Goodman 1986; Paczynski 1986; Rees & Meszaros 1992, 1994; Piran 1999), where the GRB itself is produced by dissipation of kinetic energy from the relativistic flow. However, the shape of GRB spectra does not naturally fit the synchrotron spectra predicted by this model. Even after many dedicated missions to explore GRBs, such as *CGRO* (Fishman et al. 1989; Meegan et al. 1992), *BeppoSAX* (Boella et al. 1997), *Swift* (Gehrels et al. 2004), and *Fermi* (Atwood et al. 2009), no single consensus theory has emerged to explain all the features of the prompt emission, although various possibilities in addition to the basic fireball model have been suggested (see, e.g., Zhang 2014, for a recent overview).

To study the physical properties of GRB prompt emission, the observed gamma-ray spectrum is usually fit to a chosen model (either physical or empirical). Then the best-fit parameters can be compared with the physical parameters used in theoretical models and computer simulations. Over the past 20 years, the preferred fitting model has been the empirical Band function (Band et al.

1993), which consists of a smoothly joined broken power law with low-energy power-law index α, high-energy power-law index β, and a characteristic energy $E_{\rm p}$ parameterized as the peak energy in the observed νF_ν spectrum.

Since the observed spectral behavior varies from burst to burst and over time within a single burst, it is crucial to study the fit parameters from a carefully selected sample of GRBs in a systematic way. Well-constrained spectral parameters are also important to distinguish among various theoretical models. However, because of the observed high-energy cutoff nature of the spectrum and the fact that it is harder to detect high-energy gamma-ray photons, the high-energy power-law index is often poorly constrained for most bursts. Thanks to the broad spectral coverage of *Fermi* GBM (Bissaldi et al. 2009; Meegan et al. 2009), we are now able to obtain the spectral indices with good precision.

Motivated by the fact that most catalog studies of large GRB samples do not consider the quality of high-energy photon statistics (e.g., Kaneko et al. 2006; Nava et al. 2011; Goldstein et al. 2012, 2013; Gruber et al. 2014), we present time-resolved spectroscopy for eight energetic GRBs with good high-energy statistics in the GBM GRB zoo (Bissaldi et al. 2011) to obtain an accurate measurement of β. We describe the selection criteria, analysis procedures, and empirical fitting models in Sect. 3.1. The observational results are presented in Sect. 3.3. We present the fit results from the standard Band function in Sect. 3.3.1, and a test synchrotron model in Sect. 3.3.2. In Sect. 3.4 we discuss the theoretical implications of the observed parameter distributions in the context of different models. The conclusion is given in Sect. 3.5.

3.1 Burst, Detector, and Data Selection

Our sample consists of bursts that are among the most energetic bursts observed by *Fermi* GBM until 21 August 2013. They are selected according to two criteria: (1) the total fluence in 1 keV - 1 MeV, $f > 1.0 \times 10^{-4}$ erg cm^{-2}; and (2) the signal-to-noise ratio level, S/N $\geq$ 10.0 above 900 keV. The advantage of analyzing bursts with significant photon statistics above 900 keV is that the high-energy power-law index can be better constrained. Moreover, high fluence provides more statistics for time-resolved spectral analysis. Table 3.1 lists the eight long GRBs that satisfy these selection criteria. There are no short bursts in the sample because they do not satisfy our fluence criterion. GRB 130427A is the brightest burst observed by GBM, which caused a pulse pile-up effect in the detectors in its complex-shaped main pulse after $t = T_0 + 2.4$ s. However, it also has a bright first

Table 3.1: The names, GBM trigger numbers, durations, fluence, detectors used, and optimal S/N for the eight bursts studied in this chapter.

GRB Name	GBM Trigger #	T_{90} (s)	f(1 keV - 1 MeV) (10^{-4}erg/cm^2)	NaI	BGO	S/N
090902B	090902.462	138.2±3.2	2.22±0.003	n0, n1, n9	b0	50
100724B	100724.029	114.7±3.2	2.17±0.006	n0, n1, n2	b0	40
100826A	100826.957	85.0±0.7	1.64±0.010	n7, n8	b1	30
101123A	101123.952	103.9±0.7	1.13±0.001	n9, na	b1	30
120526A	120526.303	43.6±1.0	1.16±0.002	n4	b0	20
130427A	130427.324	138.2±3.2	24.62±0.012	n6, na	b1	20
130504C	130504.978	73.2±2.1	1.29±0.002	n2, n9	b0	30
130606B	130606.497	52.2±0.7	2.01±0.002	n7, n8, nb	b1	40

pulse that is well suited for testing the synchrotron model (Preece et al. 2014) and that satisfies our selection criteria by itself. Therefore, this first pulse ($t < T_0 + 2.4$ s) is included in our analysis.

3.2 Spectral Analysis Method

The light curves are binned using a fixed S/N for each burst (but varying across bursts, see last column of Table 3.1) to avoid artificial binning bias while preserving the general shape of the light curve by avoiding merging peaks and valleys (e.g., Guiriec et al. 2010), resulting in a total of 299 spectra. The binned light curves are shown in Figs. 3.1 and 3.2 with time relative to the GBM trigger time T_0.

Time-resolved spectroscopy is performed with the GBM official spectral analysis software RMFIT[1] v4.3BA and the GBM response matrices v2.0. To account for the change in orientation of the source with respect to the detectors caused by the slew of the spacecraft, RSP2 files containing the detector response matrices (DRM) for every two degrees on the sky are used. For each burst a low-order polynomial (order 2 - 4) is fit to every energy channel according to a user-defined background interval before and after the prompt phase and interpolated across the emission interval.

Bhat (2013) reported that the typical minimum variability timescale (MVT) for short and long GRBs are 24 ms and 0.25 s, respectively. The average temporal resolution of the time bins ($T_{\rm bin}$) used in this work is 2.18 s, which is longer than the MVT. The pulse duration ($T_{\rm pulse}$) ranges from seconds to tens of seconds (see Figs. 3.1 and 3.2), which is, of course, by definition shorter than or equal to the burst duration T_{90}. So we have the typical values of MVT $< T_{\rm bin} < T_{\rm pulse} < T_{90}$.

[1]The public version of the RMFIT software is available at `http://fermi.gsfc.nasa.gov/ssc/data/analysis/rmfit/`

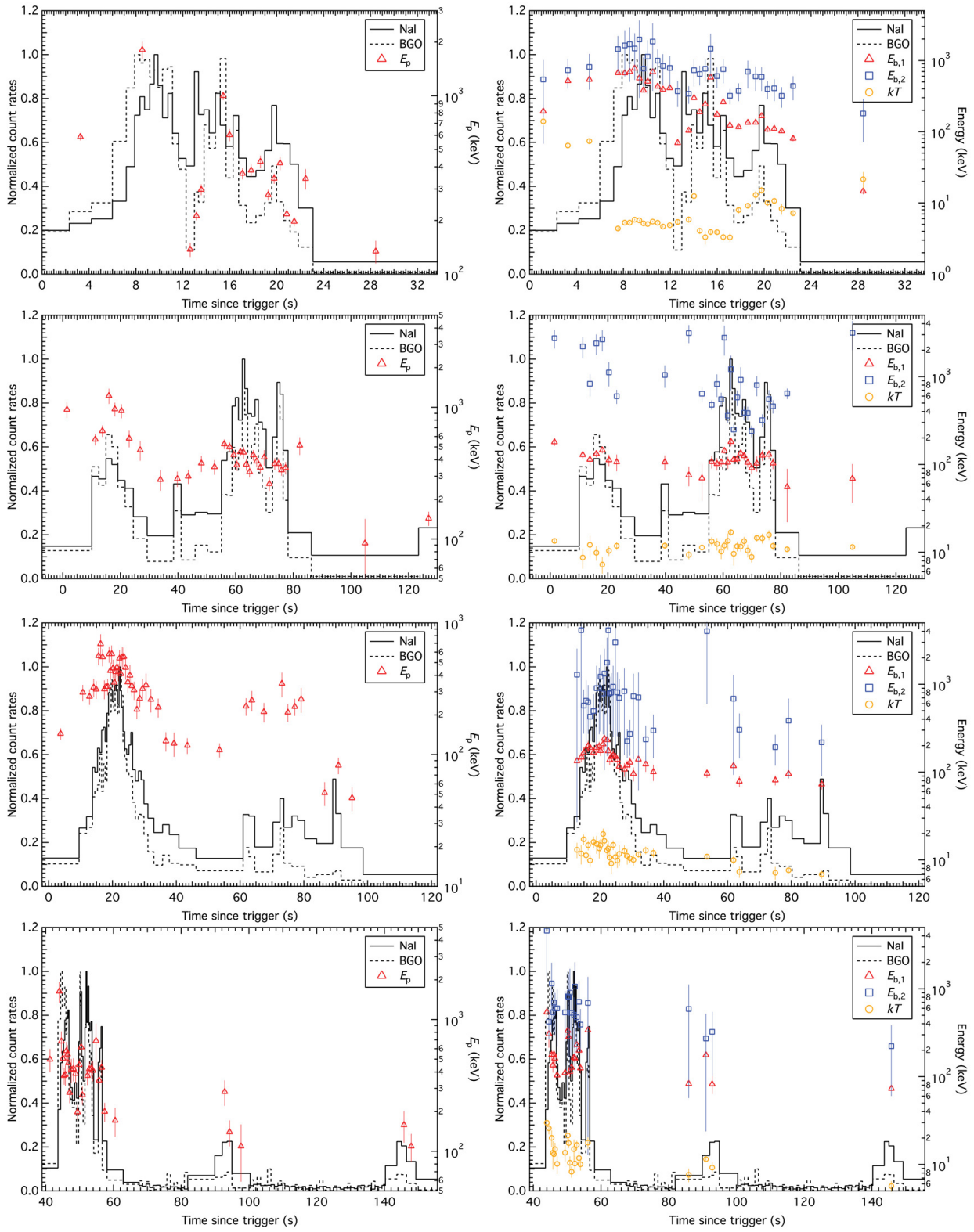

Figure 3.1: Panels from top to bottom: light curves of GRB 090902B, GRB 100724B, GRB 100826A, and GRB 101123A with the evolutions of constrained $E_{\rm p}$, $E_{\rm b,1}$, $E_{\rm b,2}$, and kT overlaid.

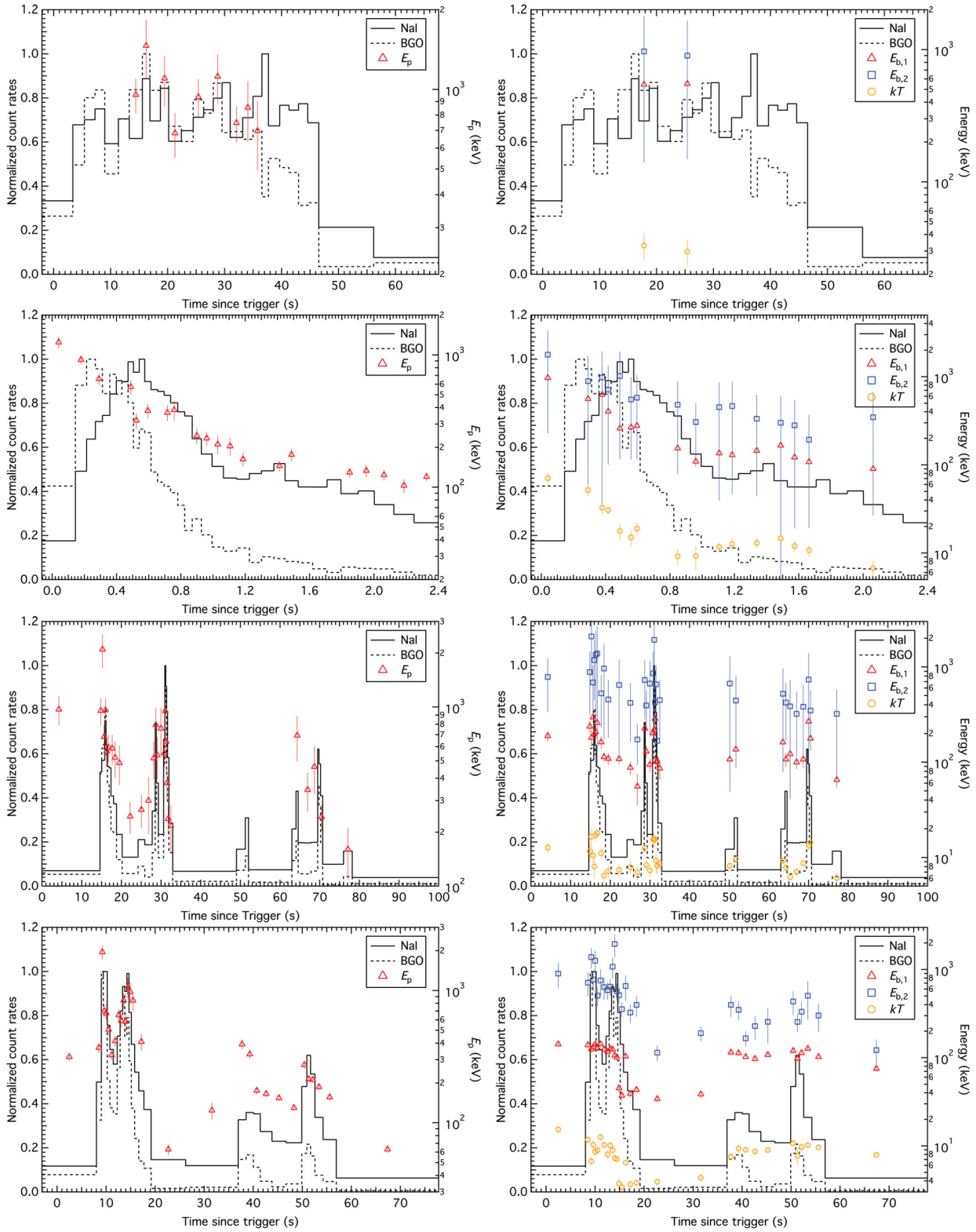

Figure 3.2: Panels from top to bottom: light curves of GRB 120526A, GRB 130427A, GRB 130504C, and GRB 130606B with the evolutions of constrained $E_{\rm p}$, $E_{\rm b,1}$, $E_{\rm b,2}$, and kT overlaid.

The variable temporal S/N binning technique can avoid the resulting statistics being dominated by the brightest few bursts. This is because the optimal S/N for each burst is different, which leads to similar number of bins for every bursts (see Table A.4). GRB 100724B is discussed separately because of its ambiguous parameter distributions. We have checked the statistics contributed by individual bursts and found that our conclusions are not affected if any one burst (even for GRB 100724B, see Sect. 3.3.1) is removed from the overall sample.

In this work, the Band function (BAND) and combinations of a semi-empirical synchrotron function (SYNC) and blackbody (BB) are fit to each spectrum. See Sect. 1.4 for function definitions.

3.3 Time-Resolved Spectral Analysis Results

3.3.1 BAND Fits

The Band function has long been known to provide a good fit to prompt emission spectra (Band et al. 1993), where the typical reduced-$\chi^2 \approx 1$ (there is a caveat that the χ^2 statistics may not be suitable for non-Gaussian data) and the Castor C-statistics values (CSTAT, Cash 1979) are low (often a few hundred to a thousand for GBM fits depending on the data quality of individual burst) among the simplest models (e.g., Goldstein et al. 2012; Gruber et al. 2014). If, in addition to a low CSTAT value corresponding to a low reduced-χ^2 value (≈ 1), all parameters in an individual spectral fit have 1σ relative error $\sigma_{\rm parameter}/(\text{parameter value}) < 1.0$ (for power-law indices we use absolute error $\sigma_{\rm parameter} < 1.0$), we define the fit as a constrained fit. For all these good fits, we verify that the data points are within $\approx 99.73\%$ confidence level to the model curves. Although we find that in some extreme cases the asymmetric errors of β may be unconstrained on the negative side, our selection criteria can filter most of these cases by ensuring the symmetric error (which is the mean of the asymmetric errors) to be well behaved. As a result, 216 of the total 299 spectra ($\approx 72\%$) are constrained. Figure 3.3 shows the distributions of the constrained parameters for the Band model: the low-energy power-law index α, the high-energy power-law index β, the peak energy in the observed νF_ν spectrum $E_{\rm p}$, and the difference between the low- and high-energy power law $\Delta s \equiv \alpha - \beta$.

The distributions of α, β, $E_{\rm p}$, and Δs are clustered around $-0.73^{+0.16}_{-0.21}$, $-2.13^{+0.28}_{-0.56}$, $374.4^{+307.3}_{-187.7}$ keV ($\log_{10} E_{\rm p} = 2.57^{+0.26}_{-0.30}$), and $1.38^{+0.54}_{-0.31}$, respectively. The asymmetric distribution errors are determined by taking the difference between the median values of the cumulative distribution function (CDF) and the 68% quantiles. Note that $\alpha = -0.73^{+0.16}_{-0.21}$ shows that the overall sample distribution

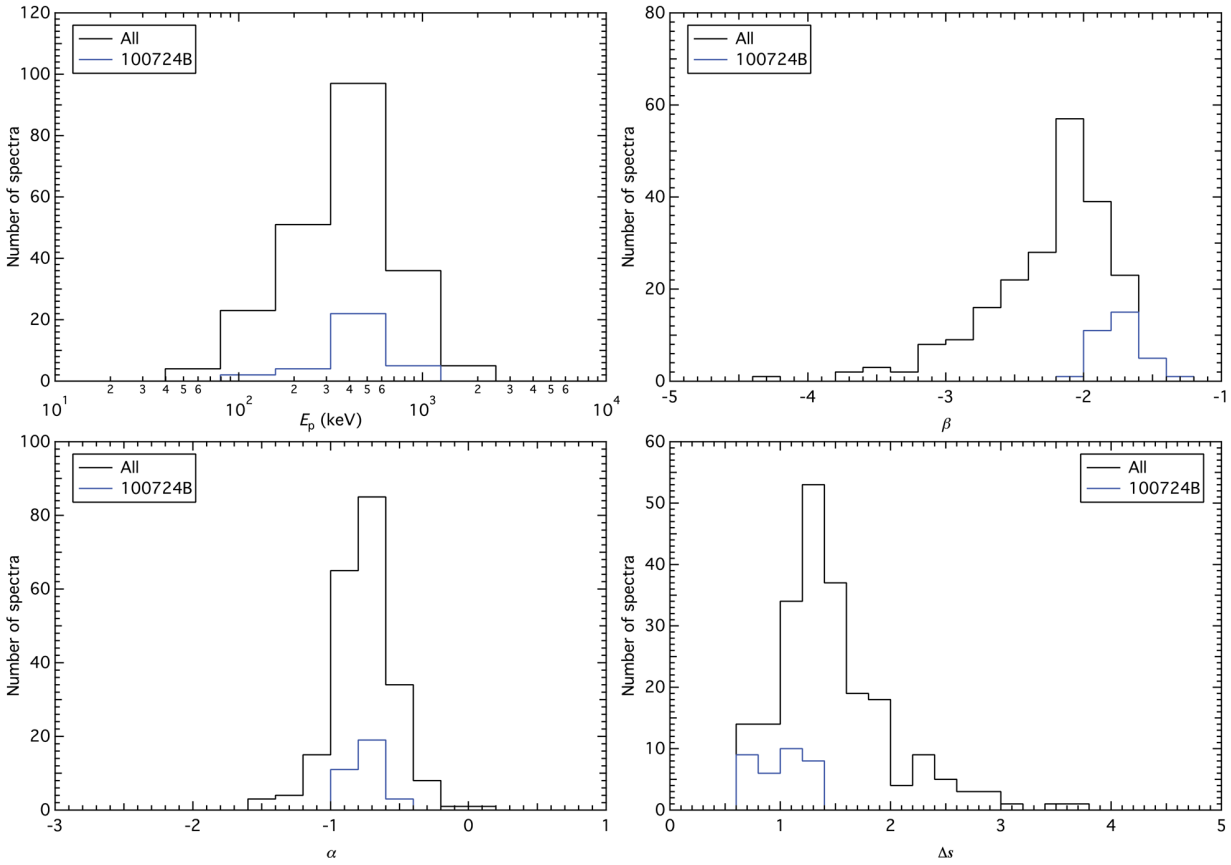

Figure 3.3: Distributions of the constrained parameters obtained from the Band model. The upper left panel shows the distributions of the values of $E_{\rm p}$. The bottom left panel shows the distributions of the values of α. The upper right panel shows the distributions of the values of β. The bottom right panel shows the distributions of the values of $\Delta s = \alpha - \beta$. The blue lines show the distributions of GRB 100724B.

is consistent with the synchrotron line-of-death (see Sect. 1.2.1). About a third of the individual spectra are consistent with the value $\alpha = -2/3$ within 1σ. The slope $\beta = -2.13^{+0.28}_{-0.56}$ is consistent with typically observed values. The average errors of α and β are $\sigma_\alpha \sim 0.1$ and $\sigma_\beta \sim 0.2$. So in Fig. 3.3 a bin width equal to 0.2 was chosen to display the histograms. This implies that the observed dispersions in the power-law index distributions cannot be explained solely by statistical uncertainties. The dispersion is also observed within bursts, indicating that spectral evolution has a non-negligible effect on the parameter distribution. Moreover, it is observed that $\sigma_{E_{\rm p}} \sim 0.1 E_{\rm p}$.

The distribution of $E_{\rm p}$ peaks at $374.4^{+307.3}_{-187.7}$ keV and is only slightly higher than those found in the GBM GRB time-integrated spectral catalogs (Goldstein et al. 2013; Gruber et al. 2014) and the BATSE spectral catalogs (e.g., Kaneko et al. 2006). According to Fig. 3.3, 91% of all

$E_{\rm p} \leq 1$ MeV. The remaining 9% has the highest $E_{\rm p} = 2.1$ MeV (GRB 130504C, see Table A.4). Nava et al. (2011) presented a time-integrated spectral analysis on 44 short GBM GRBs and found that the distribution peaks at $E_{\rm p} = 500^{+260}_{-175}$ keV. This suggests that our long bursts could be as hard as short bursts, which is expected since we selected the bursts with relatively better statistics in the BGO channels. Our bursts lie at the high $E_{\rm p}$-long T_{90} end in the long/soft and short/hard classification of GRBs (Kouveliotou et al. 1993). However, the brightest three short GBM GRBs show an $E_{\rm p}$ as high as 6 MeV (Guiriec et al. 2010). This shows that the $E_{\rm p}$ dispersion within long or short bursts can also be huge. In addition, $E_{\rm p}$ is observed to be decreasing throughout a burst, with intensity-tracking behavior during sub-pulses within a single burst (see Sect. 3.4.1).

As shown in Fig. 3.3, 50% of the hard $\beta > -2$ are from GRB 100724B. We show in Sect. 3.3.2 that this burst is consistent with both the slow- and fast-cooling scenario, and that the general conclusion is not affected because removing this burst will only make the distribution peak narrower.

3.3.2 SYNC Fits

Various studies have shown that a thermal component of about a few times 10 keV may generally exist (e.g., Mészáros et al. 2002; Ryde 2005; Guiriec et al. 2011; Axelsson et al. 2012; Guiriec et al. 2013; Burgess et al. 2014a,b; Pe'er et al. 2015). In addition, Burgess et al. (2014a) showed that a SYNC-type model alone cannot be reconciled with the flatness of α. We find that in most of our spectra adding a blackbody component can greatly improve the fit. Therefore, all the spectra are fit again to include a blackbody component in the SYNC model. The theoretical implications for the SYNC+BB and BAND model are discussed in Sect. 3.4.

Two SYNC+BB models (i.e., SYNC-slow+BB and SYNC-fast+BB) are fit to all spectra using a customized version of RMFIT. We validated that these are good fits to the data by various goodness-of-fit measures: (1) reduced-χ^2 values are close to unity; (2) CSTAT values are comparable to, often lower than, those for the BAND fits (e.g., Gruber et al. 2014; Burgess et al. 2014a); and (3) quantile-quantile plots for the cumulative observed vs. model count rates lie very close to $x = y$, thus confirming that a SYNC+BB model description is consistent with the data. For reference, the CSTAT values for all spectra are listed together with the degree of freedom (DOF) and the fit parameters in Table A.4. We find that both the SYNC-slow+BB and -fast+BB model provide constrained fits in more than 65% of all spectra. We show in Sect. 3.4 that such a test model can provide constraints on various prompt emission mechanism theories. The distributions for the SYNC-slow+BB constrained parameters are plotted in Fig. 3.4. The time-resolved spectral

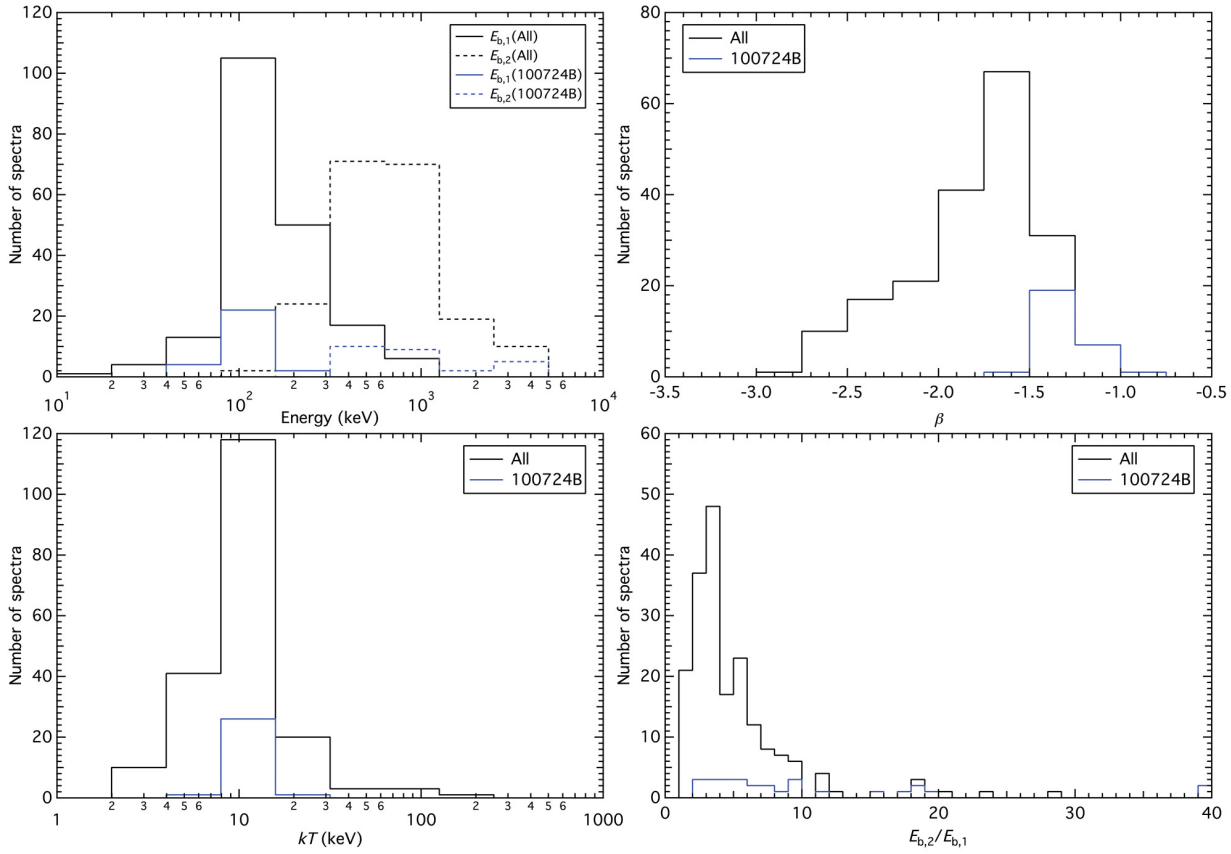

Figure 3.4: Distributions of the constrained parameters obtained from the SYNC+BB model with slow-cooling constraints (i.e., $\alpha = -2/3$ and $\beta - \gamma = 1/2$). The upper left panel shows the break energies $E_{\rm b,1}$ and $E_{\rm b,2}$. The bottom left panel shows the kT distribution. The upper right panel shows the photon indices β of the middle power-law segment. The bottom right panel shows the ratio between the two breaks, $E_{\rm b,2}/E_{\rm b,1}$. The blue lines show the distributions of GRB 100724B. Values that are out of the plotting region are accumulated in the boundary bins.

evolution for GRB 130427A is shown in Fig. 3.5. There is no clear correlation found between the fluxes of the SYNC and BB components.

The upper left panel of Fig. 3.4 shows the distributions of $E_{\rm b,1}$ and $E_{\rm b,2}$. We found that there are two clear peaks for the breaks around $129.6^{+132.2}_{-32.4}$ keV and $631.4^{+582.6}_{-309.6}$ keV for $E_{\rm b,1}$ and $E_{\rm b,2}$, respectively. The asymmetric distribution errors are obtained by the same procedure by constructing CDFs as described in Sect. 3.3.1. Comparing to the BAND fits, it is observed in most of the cases that $E_{\rm b,1} < E_{\rm p} \approx E_{\rm b,2}$. We find that 100% of $E_{\rm b,1} < 1$ MeV and 97% of $E_{\rm b,2} < 3$ MeV.

The bottom left panel shows the kT distribution. The parameter distribution of $kT = 10.4^{+4.9}_{-3.7}$ keV creates a bump at ~ 30 keV. This kT distribution is consistent with most of the sub-dominant ther-

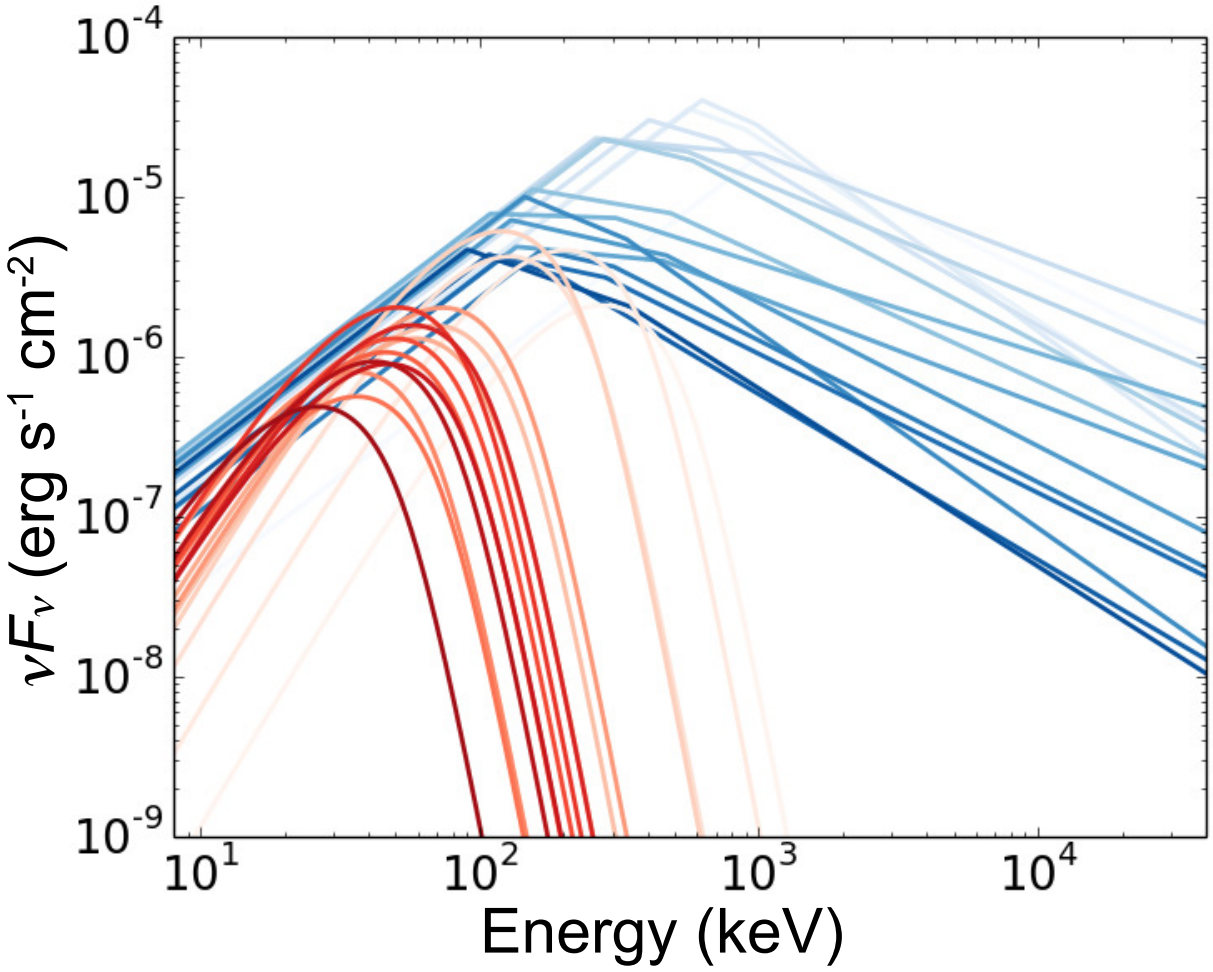

Figure 3.5: νF_ν spectral evolution of the SYNC-slow model for GRB 130427A. The evolution of the SYNC component evolves from cyan to blue, while the BB component evolves from yellow to red. No clear correlation is found between the two components.

mal bursts observed (e.g., Ryde 2005; Guiriec et al. 2011; Axelsson et al. 2012; Guiriec et al. 2013; Burgess et al. 2014a,b; Pe'er et al. 2015). When the BB-to-SYNC flux ratio is high, the Planck function dominates the curvature of the lowest end of the spectrum.

The upper right panel shows the distribution of β, where $\beta - \gamma = 1/2$. The parameter distribution of $\beta = -1.72^{+0.48}_{-0.25}$ translates into the electron distribution index $p = 2.44^{+0.50}_{-0.96}$. A synchrotron spectrum with $p > 2$ (i.e., $\beta < -1.5$) requires no upper cutoff for the total energy of the electrons to remain finite (Sect. 1.2.1). Therefore, the measured high-energy slopes for the SYNC model do not require such a cutoff. In addition, this is also consistent with afterglow-deduced distributions of $p \sim 2.3$ (e.g., Bednarz & Ostrowski 1998; Kirk et al. 2000; Achterberg et al. 2001; Curran et al.

2010; Ryan et al. 2015). GRB 100724B provides most of the cases where $\beta > -1.5$, which matches the fast-cooling index value.

The bottom right panel shows the distribution of the ratio between the two breaks, $E_{\rm b,2}/E_{\rm b,1}$. It is observed that $E_{\rm b,2}$ and $E_{\rm b,1}$ have a peak ratio at $3.77^{+4.01}_{-1.53}$, and over 90% are below 10. If we assume $E_{\rm b,1}$ and $E_{\rm b,2}$ are related to $E_{\rm min} = h\nu_{\rm min}$ and $E_{\rm cool} = h\nu_{\rm cool}$, then a ratio of $E_{\rm b,2}/E_{\rm b,1} < 10$ poses a very tight constraint on the theoretical models (see Sect. 3.4.3).

The parameter distributions for the SYNC-fast model are nearly identical to those of the SYNC-slow model (which is expected because the value of $\beta = -3/2$ is only 0.1 away from the SYNC-slow β distribution peak). The only difference observed is that γ extends to much steeper values (from -1.75 to -4.50 with a peak around -2.0 to -2.5, not a normally distributed population), which reflects the fact that since the power-law segments are no longer connected, γ can go much steeper in the time bins that contain mostly upper limits in the high-energy channels.

In brief, the following features are observed in the SYNC fits: (1) over 90% of $E_{\rm b,2}/E_{\rm b,1} < 10$; (2) a bump or flattening feature at ~ 30 keV; and (3) a general hard-to-soft evolution for the peak or break energy is observed. We discuss the theoretical implications of these observational results in the next section.

3.4 Theoretical Implications

3.4.1 Hard-to-Soft Evolution and Intensity-Tracking Behavior

We show the light curves overlaid on the evolutions of $E_{\rm p}$, $E_{\rm b,1}$, $E_{\rm b,2}$, and kT for every burst in Figs. 3.1 and 3.2. Hard-to-soft evolution over the whole bursting period is observed in every burst with in-pulse intensity-tracking behavior. These two modes of evolutionary trend have been observed in many GRBs (e.g., Ford et al. 1995; Liang & Kargatis 1996; Kaneko et al. 2006; Preece et al. 2000; Guiriec et al. 2010; Lu et al. 2010; Peng et al. 2010; Ghirlanda et al. 2011; Burgess et al. 2014a; Preece et al. 2014). Hard-to-soft evolution is a natural prediction from the SSM (Daigne & Mochkovitch 1998), in which the relative Lorentz factors of the colliding shells become lower and the spectra become softer. For instance, Lu et al. (2012) reported a time-resolved spectral analysis for 62 *Fermi* bursts (51 long + 11 short) with a detailed study of the $E_{\rm p}$ evolution. They found that the two modes for $E_{\rm p}$ evolution are present in different pulses and in different bursts. Despite the complexity of the problem, they suggested that the intensity-tracking behavior could be at least partially attributed to the superposition of hard-to-soft pulses in a highly superimposed

light curve. As all bursts in our sample are multi-pulsed (although for GRB 130427A only the first pulse is analysed, see Sect. 3.1), this possibility cannot be excluded. We also observe that the $E_{\rm p}$ in later pulses is never as high as in the first pulse, even if a later pulse has a higher peak flux. This suggests that the hard-to-soft evolution dominates the intensity-tracking behavior, and that the hard-to-soft evolution is an intrinsic property of GRBs with intensity-tracking behavior added on top.

3.4.2 Synchrotron Emission and Band Function Fits

The values of Δs and β obtained from the BAND fits can be used to compute the electron distribution power-law index p and to distinguish among different cooling scenarios (Preece et al. 2002). Preece et al. (2002) performed time-resolved spectroscopy on 156 BATSE GRBs and found that the results are consistent with the "slow, low", "both", or "fast, high" cases (with "low" and "high" referring to just the lower or higher spectral break).

The relative rate of electron cooling against energy injection into the electron population marks the difference between slow and fast cooling. To obtain the synchrotron cooling and energy injection timescale requires knowledge of the physical parameters of the ejecta, such as magnetic field strength and electron Lorentz factor, as well as precise modeling of the energy output from the central engine. This makes accurate measurements of these timescales difficult. In the internal shock model, the relative Lorentz factors between colliding shells are only mildly relativistic (Daigne & Mochkovitch 1998), and the synchrotron cooling timescale of the relativistic electrons in the ejecta frame is

$$t_{\rm syn} = 6 \left(\frac{\Gamma_{\rm e}}{100} \right)^{-1} \left(\frac{B}{1,000\ {\rm G}} \right)^{-2}\ {\rm s}, \tag{3.1}$$

where $\Gamma_{\rm e}$ is the Lorentz factor of the electrons relative to the ejecta and B is the magnetic field in the shock. One could compare, for instance, $t_{\rm syn}$ with the MVT observed in the light curve (as experienced in the ejecta frame), which is then taken to represent the rate of energy injection into the synchrotron electron population. However, the inferred values of the physical parameters, such as magnetic field strength (see discussion below), vary in a wide range among bursts and sub-pulses within a single bursts. Taken together with the uncertainty in the spatial and temporal profile of the particle acceleration sites (e.g., extended turbulent regions vs. shock acceleration, or intermittent vs. continuous injection), it becomes hard to predict a clear preference for a given cooling regime because of the difficulty of unambiguously interpreting the observable timescales.

We show in the following that a mix of both the slow and fast cooling is implied by the GBM data.

Table 3.2: Electron distribution index p for different cases. [a]Preece et al. (2002), Eqns. (9), (10), and (12). [b]Calculated from the ranges of peak and average values of Δs and β distributions for all eight bursts, given that $1.2 < (\Delta s)_{\rm peak} < 1.4$, $1.4 < (\Delta s)_{\rm average} < 1.6$, $-2.2 < \beta_{\rm peak} < -2.0$, and $-2.4 < \beta_{\rm average} < -2.2$. [c]Calculated from the average values of Δs and β distributions for GRB 100724B alone.

Case[a]	α	$p = f(\Delta s)$	$f(1.2)$ - $f(1.6)$[b]	$f(1.0)$[c]	$p = g(\beta)$	$g(-2.0)$ - $g(-2.4)$[b]	$g(-1.7)$[c]
(1)	(2)	(3)	(4)	(5)	(6)	(7)	(8)
Fast, high	$-3/2$	$2\Delta s + 1$	3.4 - 4.2	3.0	$-2(\beta + 1)$	2.0 - 2.8	1.4
Slow, low	$-2/3$	$2(\Delta s + 1/6)$	2.73 - 3.53	2.33	$-2\beta - 1$	3.0 - 3.8	2.4
Both	$-2/3$	$2(\Delta s - 1/3)$	1.73 - 2.53	1.33	$-2(\beta + 1)$	2.0 - 2.8	1.4

Table 3.2 shows the values of p obtained from the Δs and β distributions (see Eqns. 8 - 12 in Preece et al. 2002). Column 1 shows the three cases where p depends on both Δs and β. Column 2 shows the respective value of α in each case. Columns 3 and 6 show the formulae for p as a function of Δs and β respectively. Columns 4 and 7 give the ranges of possible values of p calculated from the distributions of Δs and β for all eight bursts, and Cols. 5 and 8 give the same for GRB 100724B alone.

The values of p in Col. 4 are inconsistent with the "fast, high" case in Col. 7. The "fast, low" case predicts $\Delta s = 5/6$, which is clearly rejected, as shown in Fig. 3.3. The distribution of fast-cooling $\gamma_{\rm SYNC}$ as mentioned in Sect. 3.3.2 indicates that the electron distribution index above $\gamma_{\rm min}$ can take any value from $p = 1.5$ - 6.0. Theories of electron shock-acceleration typically predict p values between 2 and 3, which makes these very steep values for p suggestive of a cutoff or deviation from a power-law slope in the accelerated particle distribution, rather than a single very steep slope. A steep electron distribution index can also occur when the shock normal is at an angle to the magnetic field, allowing electrons to escape the acceleration region early (Ellison & Double 2004; Baring 2006; Summerlin & Baring 2012; Burgess et al. 2014a). The "slow, high" case, which refers to the higher energy break in the left panel of Fig. 1.3, predicts $\Delta s = 1/2$ and is clearly rejected, as shown in Fig. 3.3. The average values of Δs and β for GRB 100724B are 1.0 and -1.7 respectively, which are also consistent with the "slow, low" and "both" cases (Cols. 5 and 8), at the same time consistent with the "fast, low" case, which predicts $\Delta s = 5/6$.

On the other hand, the BATSE β and Δs distributions suggested that the "slow, low", "fast, low", and "both" cases are all viable processes (see, e.g., Fig. 2 of Preece et al. 2002; Kaneko et al. 2006). Gruber et al. (2014) also showed similar conclusions in the GBM GRB time-integrated spectra. Burgess et al. (2014a) performed a Bayesian time-resolved spectral analysis using physical

synchrotron and thermal models instead of the Band function to several GBM GRBs and found that the slow-cooling scenario better explains the observed data, and their results suggest continuous energy injection is important. Uhm & Zhang (2014) predicted that using a decaying magnetic field as a function of radius, with a decay index b, it is possible for most GRBs to cool via the fast-cooling scenario with $\alpha \sim -1.0$. They predicted that the asymptotic value of the low-energy electron distribution should be $p = (6b-4)/(6b-1)$ instead of $p = 2$ for a constant magnetic field (e.g., Preece et al. 2002), and the spectral index $s = (-p+1)/2 = 3/(12b-2) = \alpha + 1$. We find that in more than 77% of the constrained fits b has values between 0.6 and 2.6. There is no clear evolutionary trend of b. The variability of b within bursts is difficult to reconcile with a large-scale power-law dependence on radius of the magnetic field. However, this can still be the case, but just not as clearly manifested in the data as predicted by Uhm & Zhang (2014).

In brief, our results are consistent with slow cooling with the low-frequency break seen (or in the "both" case, undistinguished between slow and fast cooling). For GRB 100724B, fast cooling is also consistent with the low-frequency break seen. This implies that the second line-of-death, $\alpha = -3/2$, could also be avoided.

3.4.3 Synchrotron Model Fits

The SYNC-slow model is basically a three-segment broken power law, with the middle- and high-energy segment connected (i.e., $\beta_{\rm SYNC} - \gamma_{\rm SYNC} = 1/2$). It is essentially an extended version of the Band model, in which the curvature of BAND is replaced by two breaks and the power-law segment in between. This implies that when we are comparing the results from BAND and SYNC fits, it should be kept in mind that either $\beta_{\rm SYNC}$ or $\gamma_{\rm SYNC}$ could be picking up $\beta_{\rm BAND}$. This is discussed below in this subsection. Moreover, a sharply joined broken power law is intrinsically non-physical. The actual spectrum should always be smooth, so sharp power law fits run the risk of covering a single smooth transition with multiple sharp breaks. However, a smoothly joined triple power law would contain too many parameters, and fitting such a complicated empirical model is statistically unsound. The constrained power-law indices in our SYNC-slow and -fast models mitigate the problem by assuming a synchrotron origin of the observed spectrum a priori, thereby limiting the possible shapes of fit spectra.

Theoretically, the SYNC model has excluded the synchrotron emission from Maxwellian electrons. This is because we wished the synchrotron emission to occur at the correct frequencies (i.e., gamma-rays), which requires the energy per emitting electron to be higher than that obtained by

simply averaging (as demonstrated by Daigne & Mochkovitch 1998). This implies a small subset of electrons at very high energies, far away from the thermal pool from which they were drawn. Alternatively, if the Maxwellian electron distribution peak and the minimum injection Lorentz factor (i.e., $\gamma_{\rm min}$) remain close, the effect of adding the Maxwellian electrons will be a smoothing of the synchrotron function that we could not model with our BAND or SYNC models. Moreover, Burgess et al. (2011) has shown that the Maxwellian electron population is sub-dominant. To avoid further complication of the fit model, we therefore assumed the synchrotron emission is just from the population of shock-accelerated electrons (see Sect. 3.3.2). However, the Maxwellian does not just have to exist as left-over thermal pool from the thermal parts of the jet. It can also be created in the shock region by thermalization of electrons crossing the shock (see, e.g., Spitkovsky 2008).

According to the SYNC-slow fit results, there are two cases to consider: (1) the $\gamma_{\rm SYNC}$ is the high-energy segment in the slow-cooling scenario, that is, $\nu_{\rm min}$ and $\nu_{\rm cool}$ are the predicted break values; or (2) $\gamma_{\rm SYNC}$ is the middle-energy segment in the slow-cooling scenario; in this case, the triple power law is just mimicking the slowly varying Band model. If (1) is true, then we can take $\gamma_{\rm SYNC} = -2.5$ to -2.0, and we will have $p = 2.0$ - 3.0. Table 3.2 shows that the SYNC-slow model is consistent with the "both" case; if (2) is true, then instead of comparing with $\gamma_{\rm SYNC}$, we should compare with $\beta_{\rm SYNC}$ in Eq. 1.22, and we will have $p = 3.0$ - 4.0. Table 3.2 shows that the SYNC-slow model is also consistent with the "slow, low" case.

Burgess et al. (2014a) used a physical non-thermal plus thermal synchrotron kernel to fit a few GBM GRBs and found that slow cooling is physically possible. Since the typically observed value of $\alpha \sim -1.0$, the fast-cooling model has been disfavored because it predicts α should be as steep as $-3/2$ below $\nu_{\rm min}$ (Sari et al. 1998). A blackbody contribution to the lower part of the spectrum would render it even more difficult to reconcile the α slope with the "fast, high" case. On the one hand, our fit results for the SYNC-slow model yield p values closer to the expected range between 2 and 3. On the other hand, a SYNC-fast model, implying that most of the energy of the electrons is radiated away, has the advantage of allowing for a lower efficiency. The total energy in gamma-rays is typically similar to the inferred kinetic energy of the ejecta. Therefore, if the efficiency in converting accelerated electron energies to radiation is low, the efficiency in extracting energy from the ejecta to the non-thermal electron population has to become extremely high to compensate for this (see, e.g., Nousek et al. 2006; Granot et al. 2006, for detailed discussions). The fact that in the SYNC fits, both spectral breaks consistently occur fairly close to one another does alleviate the problem in that it provides essentially a "moderately fast-cooling" scenario, regardless

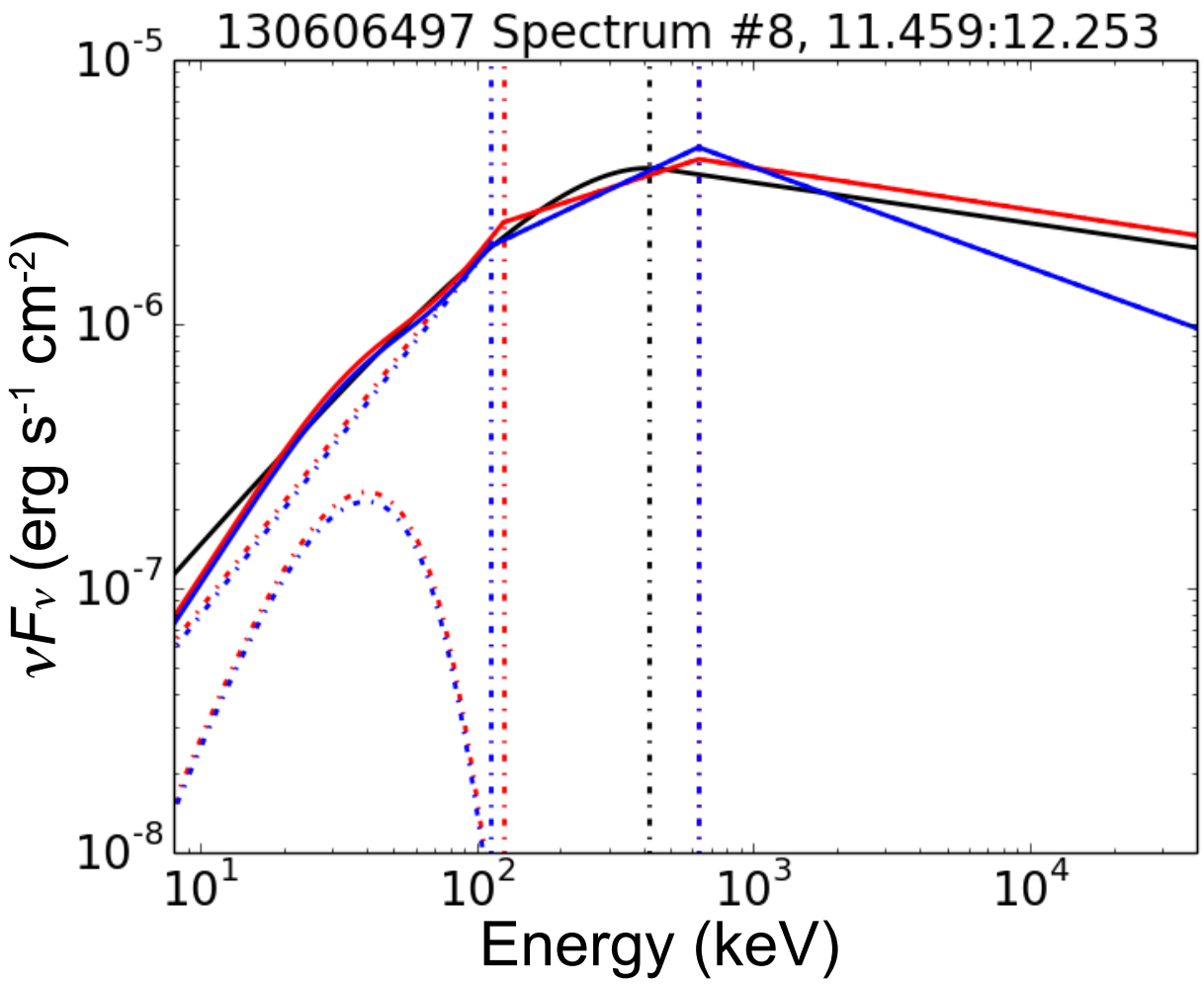

Figure 3.6: Selected spectrum from GRB 130606B plotted in νF_ν space. The black, red, and blue solid curve show the fitted spectrum for the Band, SYNC-slow+BB, and SYNC-fast+BB model, respectively, while the dash-dotted curves show individual SYNC or BB components. The vertical dash-dotted black, red, and blue line show the $E_{\rm p}$ and break energies for the Band, SYNC-slow+BB, and SYNC-fast+BB model, respectively.

of the precise order of the breaks. This, however, raises the question of how the universal break ratio between $\nu_{\rm min}$ and $\nu_{\rm cool}$ inferred from our sample can be understood, as the positions of these breaks are not theoretically expected to be related.

The fast-cooling model with a decaying magnetic field (Uhm & Zhang 2014) predicts a Band function spectral shape with $b \sim 1.0$ - 1.5 (see their Fig. 4), in which the curved Band shape is a summed effect for the emissions of electrons at different times. A decay index $b \lesssim 2.6$ (see Sect. 3.4.2) implies stronger magnetic dissipation, and the electrons at later time could be cooled

by slow cooling, thus the positions of $\nu_{\rm cool}$ and $\nu_{\rm min}$ could reverse and move closer to each other, so that the "both" case is possible. Uhm & Zhang (2014) showed that this is possible on a timescale ~ 1.0 s, consistent with the typical $T_{\rm bin}$ used in this work (see Sect. 3.1). We find that the BAND and SYNC model have very similar shapes (Fig. 3.6) that are consistent with this interpretation and thus provide further support for the "both" case.

3.4.4 Thermal Origin of Prompt Emission

Recently, Beloborodov (2013) suggested that the evolution of $E_{\rm p}$ could be a manifestation of thermal emission. As shown in Fig. 3.3, more than 90% of $E_{\rm p}$ values remain below 1 MeV. The observed clustering of $E_{\rm p} \sim$ few hundred keV, instead of a wide distribution, is hard to explain in the SSM. The observed spectral width in the νF_ν space is $\log(E_1/E_2) \approx 1.0$ - 1.5 decades in photon energy (Beloborodov 2013), where $E_2 - E_1$ is the width at half-maximum. This is narrower than a synchrotron model would predict (Daigne et al. 2011).

Early photospheric models assumed a freely expanding radiation-dominated outflow with no baryonic loading or magnetic field (Goodman 1986; Paczynski 1986). This predicts a sharply defined peak with a Planck spectrum (Beloborodov 2011), which contradicts the observed non-thermal spectra in most GRBs. Detailed radiation transfer simulations have shown that a thermal origin of the Band function is possible (Pe'er et al. 2006; Giannios 2008; Beloborodov 2010; Vurm et al. 2011), and Beloborodov (2013) computed that the maximum $E_{\rm p}$ of a spectrum from thermal plasma is given by $30\Gamma_{\rm P}$ keV under high radiation efficiency, where $\Gamma_{\rm P}$ is the Lorentz factor of the Planckian photospheric shell. With the typical values of the Lorentz factor of GRBs to be ~ 100, $E_{\rm p,max} \sim 3$ MeV in the rest frame. This value is consistent with most of our observed $E_{\rm p} \lesssim 500$ keV, but only when assuming a redshift $z \lesssim 0.83$. Deng & Zhang (2014) also found that $\alpha \sim -1.0$ could be achieved if the radiating photosphere has a constant or increasing luminosity. However, they stated that it is difficult to reproduce the observed hard-to-soft evolution under natural conditions.

3.5 Conclusions

We performed time-resolved spectroscopy for eight energetic, long GRBs observed by *Fermi* GBM during the first five years of its mission. We obtained well-constrained Band spectral parameters and studied their theoretical implications. We showed that even in the bursts with good high-energy statistics above 900 keV, most observed properties can be explained using the synchrotron shock

model. We also tested the observed spectra with a synchrotron plus blackbody model using slow- and fast-cooling parametric constraints, and found that the "both" case is consistent with the data, which requires a narrow distribution of the break ratio $E_{\rm b,2}/E_{\rm b,1} < 10$ with a peak at $3.77^{+4.01}_{-1.53}$. The population of p is found to be 2 - 3, in accordance with the expected range. The picture of a "moderately fast-cooling" scenario can also explain the narrow distribution of the break ratio and relax the efficiency problem for the slow-cooling scenario.

Recently, Frontera et al. (2013) reported the result of the time-resolved spectral analysis of four GRBs observed by BATSE and *BeppoSAX*. They found that a specially devised empirical Comptonized model is the best-fit model to most of their time-resolved spectra. They also found that using a simple power law plus blackbody model (PL + BB) does not give fit results better than the conventional Band function. This is consistent with the results from the *Fermi* GBM GRB time-resolved spectral catalog (Yu et al. submitted) that most of the time-resolved spectra are best fit by the Comptonized model, and only very few spectra are best fit by PL + BB, although they are generally acceptable fits. We showed that the spectral shape $\gtrsim 1$ MeV could be harder than a Comptonized model or simple power law.

Our results confirmed that while most properties of energetic GRBs can be explained in the conventional theoretical models, the radiative process in GRB prompt emission is complicated and cannot be fully explained by a single distribution of electrons (e.g., due to anisotropic distribution of electron energies or continuous acceleration or photospheric emission). The possibility of a decaying magnetic field that modifies the fast-cooling spectrum was also explored, yielding a magnetic field decay index $0.6 < b < 2.6$ for 77% of the constrained fits. However, it is difficult to reconcile the variability of b within bursts with a mechanism where the spectra are shaped by a single large-scale decaying magnetic field. Nevertheless, such a field might still exist, but its impact may be obscured by more local conditions in the flow.

Chapter 4

The Sharpness of GRB Prompt Emission Spectra

"Study hard what interests you the most in the most undisciplined, irreverent and original manner possible."

- Richard Feynman

The prompt emission of gamma-ray bursts (GRBs) is one of the most puzzling observed astronomical phenomena. Since the discovery of GRBs in 1967 (Klebesadel et al. 1973), many emission models have been proposed in order to explain the prompt phase of gamma-ray emission. This phase consists of gamma-rays mainly within tens to a few hundred keV, in some cases as high as a few thousand keV, lasting from a few milliseconds to hundreds of seconds.

Gamma-ray bursts are distributed isotropically (Briggs et al. 1996; Hakkila et al. 1994; Tegmark et al. 1996) and cosmologically (Metzger et al. 1997; Waxman 1997a) over the sky. Despite the last 45 years of research efforts, the dominant emission mechanism of these cosmological sources is still controversial. Synchrotron radiation from a simple electron population is one of the simplest physical phenomena that may be able to produce the observed spectral slopes of the Band function (Band et al. 1993) that is commonly used to describe the photon spectra of GRB prompt emission. The Band function is an empirical mathematical function consisting of two segments of power laws, described by the low- and high-energy photon indices α and β, connected at the peak energy parameterized as $E_{\rm p}$. This peak energy has been observed typically at hundreds of keV (Kaneko et al. 2006; Nava et al. 2011; Goldstein et al. 2012, 2013; Gruber et al. 2014). In what is known as

the fireball model (Goodman 1986; Meszaros et al. 1993; Meszaros & Rees 1993; Rees & Meszaros 1992, 1994; Tavani 1996; Piran 1999), there are ejected shells with different bulk Lorentz factors. When the faster shells catch up with the slower shells, internal shock waves will be produced. The electrons in the shocked region of the shells are accelerated and their energy is radiated via synchrotron emission in the local magnetic field.

The Band function's two power-law indices are usually compared to the slopes of various radiation models, leading to the discovery of the so-called line-of-death problem (Katz 1994a; Crider et al. 1998; Preece et al. 1998a, 2002; Tavani 1995) for the synchrotron theory. When a power-law distribution of electron energies is combined with synchrotron radiation theory, the low-energy power-law photon index is $-2/3$. The fact that a fraction of observed $\alpha > -2/3$ indicates that, at least in some cases, the synchrotron explanation of GRB prompt spectra can be problematic, because the observed spectra rise faster. The observed violations of the line-of-death are typically around 30%. Recently, Burgess et al. (2015) used the Band function to fit a large number of simulated slow-cooling synchrotron spectra (with spectral peak determined by injection energy of the electrons rather than their energy losses, as in the fast-cooling case), concluding that, in practice, the line-of-death may be steeper, $\alpha > -0.8$, than the value of $\alpha > -2/3$. Moreover, they found that the Band function cannot recover the simulated synchrotron peaks and power-law indices. These findings all question the validity of using the synchrotron theories to explain the Band parameters.

Instead of fitting the empirical Band function to the spectra, Burgess et al. (2014a) used a synchrotron function in the fitting process, combining the slow-cooling scenario with thermal emission. Yu et al. (Ch. 3, 2015a) used a double broken power law to fit eight bright GRBs, in which they found that the line-of-death problem could be alleviated in a moderately fast-cooling scenario, in which the fast- and slow-cooling electrons are mixed together, usually with a blackbody component at tens of keV or in a varying magnetic field. However, no single synchrotron model could completely explain all the spectral properties of GRB prompt emission.

In this work we study the sharpness of the synchrotron emission spectrum in comparison to time-resolved spectra of GRBs, a question recently raised by Beloborodov (2013); Vurm & Beloborodov (2015). Our approach focuses on the curvature of the region capturing the peak or break energy in the GRB prompt spectra by re-fitting all the spectra in an energy domain depending on this peak or break, using the burst sample from the *Fermi* GBM GRB time-resolved spectral catalog (Ch. 2, Yu et al. submitted). By comparing the spectral sharpness of the observed spectra to various physical emission models, we are able to directly determine whether a model is capable of

accounting for the peak emission of the observed spectra. By concentrating on the spectral peak or break, we avoid potential issues with interpretation of the asymptotes of the fit functions, which might lie outside the observable domain or be contaminated by additional radiative processes or instrumental effects.

Thanks to the high-quality gamma-ray data obtained by *Fermi* GBM (Meegan et al. 2009), which provides wide energy coverage and fine temporal and spectral resolutions, this is the first time that we can directly compare the curvature of a large number of time-resolved spectra to that of physical models, so that statistically significant conclusions about the prompt emission mechanism can be drawn.

This chapter is structured as follows. In Section 4.1, we describe our analysis method. The results are presented in Section 4.2. In Section 4.3, we check the consistency of our analysis. In Section 4.4, we discuss the theoretical implications. The summary and conclusions are given in Section 4.5.

We note that a recent independent study of the peak-flux GRB spectra (Axelsson & Borgonovo 2015) shows that a synchrotron function could be too wide for the observed Band shape. They measured the full-width-half-maximum in the νF_ν spectra obtained from the 4-years *Fermi* GBM GRB time-integrated spectral catalog (Gruber et al. 2014; von Kienlin et al. 2014) and the BATSE 5B GRB spectral catalog (Goldstein et al. 2013).

4.1 Spectral Sharpness Analysis Method

We take the BEST sample from Ch. 2 (Yu et al. submitted). Only the spectra best fit by the Comptonized model (COMP), the Band function (BAND), and the smoothly broken power law (SBPL) are included in the analysis. The functional forms of these models are given in Sect. 1.4. This is because we are interested in comparing the sharpness around the peak or break energies of theoretical models to the observed spectra. Thus, the 194 spectra best fit by a simple power law or the power law plus blackbody, are excluded. All the 1,297 spectra best fit by either COMP, BAND, or SBPL have convex shape (i.e., $\alpha > -2$ for COMP and $\alpha > \beta$ for BAND and SBPL).

The best-fit model parameters for the 1,297 spectra are obtained from the catalog. Using the catalog values of $E_{\rm p}$, every spectrum is re-fit (using the same best fit function as in the catalog) in a narrower energy domain that covers $E_{\rm p}$ (or the break energy $E_{\rm b}$ if there is no peak in the spectrum). We refer this energy domain as the "data domain", which contains the "triangle domain" (described

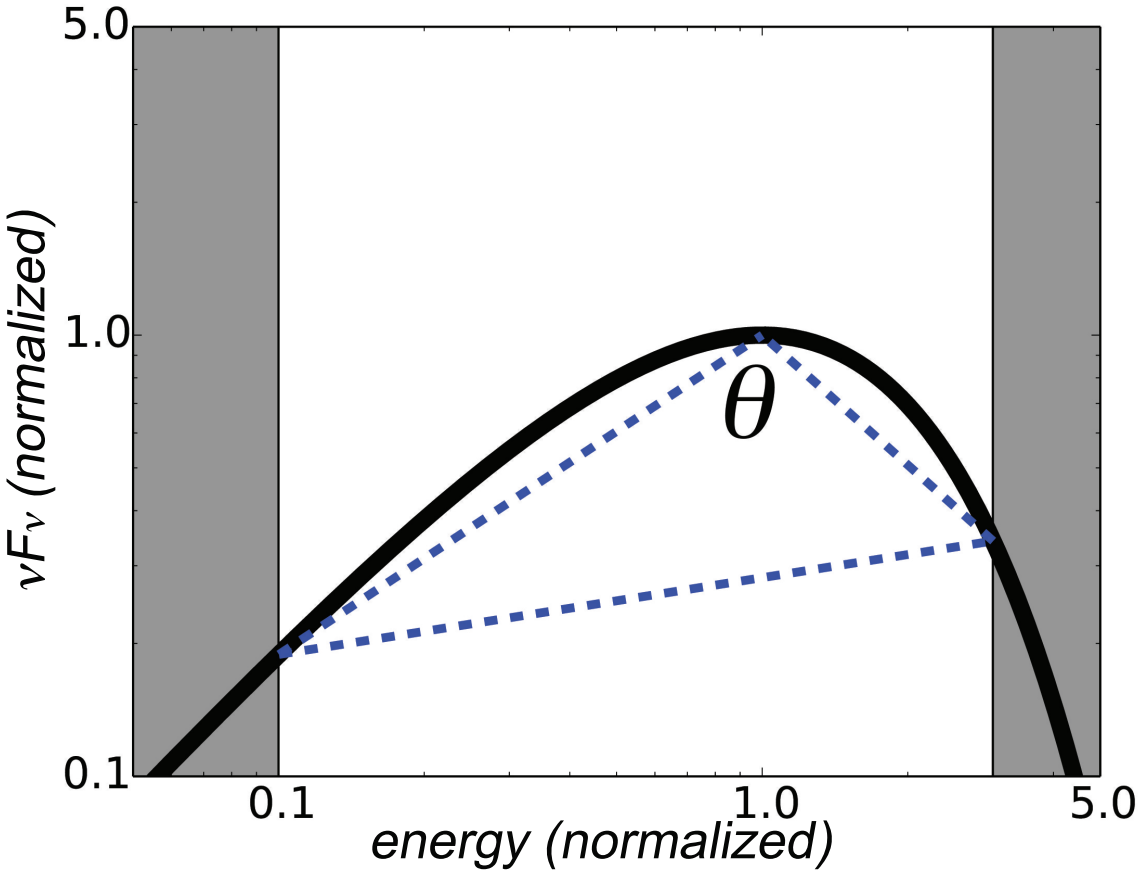

Figure 4.1: Illustration of how the triangle is constructed and the sharpness angle θ is defined. The shaded regions indicate the data domain (see Sect. 4.3.2). The triangle is constructed within the triangle domain (see Sect. 4.3.3), under the best-fit model curve (black). The vertical and horizontal axis are plotted in logarithmic scale in units of normalized νF_ν flux and photon energy, respectively.

below). We find that in the 1,297 spectra, 34 of them have no converged re-fit and are therefore excluded. In the remaining 1,263 spectra, 150 of them have large error bars (according to the criteria from Gruber et al. 2014) and thus are further excluded. In total, 1,113 spectra are used in this work, of which 942 are best fit by COMP, 99 by BAND, and 72 by SBPL.

Motivated by the necessity to model the spectral curvature around E_p and exclude any possible curvature contribution from the low- or high-energy tail, we test the data domain on a few of the brightest bursts (details are discussed in Sect. 4.3.2). As a result, $(E_\mathrm{left}, E_\mathrm{right}) = (0.1E_\mathrm{p}, 3.0E_\mathrm{p})$ is adopted for a good balance between statistics and optimal description of the spectral sharpness. Assuming a typical spectrum with $E_\mathrm{p} \sim 300$ keV, it means that we are covering the range from

~ 30 keV to ~ 900 keV.

The peak energy $E_{\rm p}$ and the peak flux $\nu F_\nu(E_{\rm p})$ are used to normalize the model curve such that the peak coincides with $(x, y) = (E/E_{\rm p}, \nu F_\nu(E)/\nu F_\nu(E_{\rm p})) = (1, 1)$. For the spectra of SBPL fits without a peak, the break energy $E_{\rm b}$ is used instead. For each spectrum, a triangle $\{(1,1), (x_{\rm left}, y_{\rm left}), (x_{\rm right}, y_{\rm right})\}$ below the spectral curve is constructed in dimensionless space as

$$(x, y) = \left\{ \begin{array}{l} (1, 1)\,, \\ (E_{\rm left}/E_{\rm p}, \nu F_\nu(E_{\rm left})/\nu F_\nu(E_{\rm p}))\,, \\ (E_{\rm right}/E_{\rm p}, \nu F_\nu(E_{\rm right})/\nu F_\nu(E_{\rm p})) \end{array} \right\}. \tag{4.1}$$

The sharpness angle θ is computed in logarithmic space, under $(\log 1, \log 1)$ and between $\log x_{\rm left}$ and $\log x_{\rm right}$ (which we refer to as "triangle domain"). Thus, θ is an indication of the spectral sharpness and is independent of the actual position of $E_{\rm p}$ (i.e., also independent of redshift). Figure 4.1 illustrates how such a triangle can be constructed.

Similarly, we also construct the right-angled triangle $\{(1,1), (x_{\rm left}, y_{\rm left}), (1, y_{\rm left})\}$ below the spectral curve between $x_{\rm left}$ and $x = 1$, and compute the left-hand side angle $\theta_{\rm left}$ in logarithmic space, under $(\log 1, \log 1)$ and between $\log x_{\rm left}$ and $\log 1$. Thus, in the limit of small $x_{\rm left}$, $\theta_{\rm left}$ becomes equivalent to a measure of the steepness of the low-energy power-law slope.

In this work, we consider synchrotron radiation without cooling. This is because the ratio between $\nu_{\rm min}$ and $\nu_{\rm cool}$ depends sensitively on assumptions on the shock micro-physics and fluid evolution. Additionally, the sharpness of the cooling break depends intrinsically on the distribution of electrons throughout the shock region, and has no local analog for a single electron population. For the purpose of this paper, it is sufficient to consider the case without cooling: quick evolution of electron energies due to cooling will smoothen the synchrotron spectrum. Therefore, any cooling synchrotron spectrum can never be sharper than Eqn. (1.20).

4.2 Spectral Sharpness Results

Figure 4.2 (left panels) shows the cumulative distribution functions (CDFs) of the sharpness angles θ and the distributions of the errors σ_θ. The dotted, solid, and dashed black vertical lines indicate the values of θ for the normalized blackbody, single-electron synchrotron emission function,[1] and

[1]For a single emission direction, θ and $\theta_{\rm left}$ are 76 and 43 degrees respectively, for the polarization direction perpendicular to the projection of the magnetic field on the sky, and are 67 and 37 degrees respectively, in the parallel case. These values reflect the standard textbook results for single-electron emission prior to convolving with

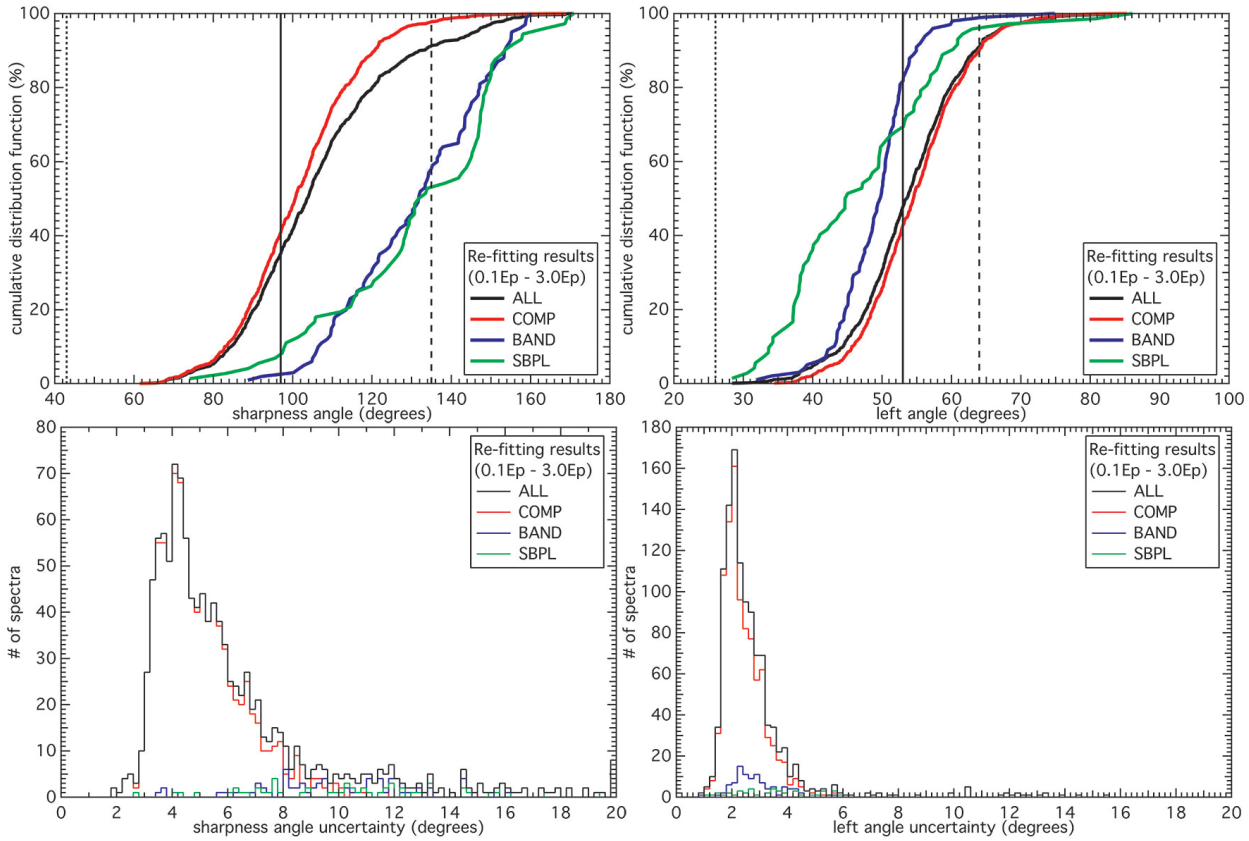

Figure 4.2: Left panels: Cumulative distribution functions of θ and distributions of σ_θ. Right panels: Cumulative distribution functions of $\theta_{\rm left}$ and distributions of $\sigma_{\rm left}$. The limits of the normalized blackbody (dotted line), single-electron synchrotron (solid line), and synchrotron with a Maxwellian distribution function (dashed line) are overlaid. In the above legends, COMP represents the Comptonized model, BAND represents the Band function, SBPL represents the smoothly broken power law, and ALL represents the overall population (COMP + BAND + SBPL).

Table 4.1: Sharpness angle θ and left angle $\theta_{\rm left}$ for various emission models. [a]We note that if $p < 3$, νF_ν keeps on increasing monotonically.

Emission models	θ (degrees)	$\theta_{\rm left}$ (degrees)
Blackbody	43	27
Single-electron synchrotron	97	53
Maxwellian synchrotron	135	64
Synchrotron with $p = 2$[a]	170	40
Synchrotron with $p = 4$	128	56

synchrotron emission function from a Maxwellian electron distribution, from left to right. These values are listed in Table 4.1. It is found that over 35% of the spectra are inconsistent with

an electron distribution function (see Rybicki & Lightman 1979).

single-electron synchrotron emission and 91% are inconsistent with synchrotron emission from a Maxwellian electron distribution. The blackbody spectrum is found to be much sharper than any of the observed spectra.

The synchrotron emission function from a Maxwellian electron distribution produces one of the sharpest (i.e., narrowest) spectra (Sect. 1.2.1). The values of θ for the synchrotron emission function from a power-law electron distribution for $p = 2$ and $p = 4$ are also listed in Table 4.1. The spectrum for $p = 2$ was normalized by the peak position in the F_ν space, because for $p < 3$, νF_ν keeps on increasing monotonically. Notice also that the spectrum for $p = 4$ is of similar sharpness to the spectrum for Maxwellian (for $p \to \infty$, the spectrum would reduce to a single-electron synchrotron spectrum).

In principle, σ_θ should be propagated directly from the errors on the observed photon counts, since the counts are independent of the choice of the fitting models. However, the spectral peak can only be found and the flux can only be normalized when the counts are convolved with a model (COMP, BAND, etc.) and the response matrices, through RMFIT. Therefore, we compute σ_θ by performing Monte-Carlo simulations using the errors of the re-fit model parameters. First, we extract the 1σ errors from the RMFIT results. Because the errors on model fit parameters α and β (see Sect. 1.4) are not necessarily Gaussian, we then randomly draw new values of α and β from a uniform probability function sharing the same 1σ error, and we re-compute θ. This process is repeated 1,000 times for every spectrum. We then take the 1σ width of the resulting θ distribution and average over left and right 1σ values. We note that our method generates the most conservative values of σ_θ, since the uniform probability function has the largest standard deviation.

As shown in the bottom left panel of Fig. 4.2, the resulting distribution of σ_θ has a median around 5 degrees. This is too small to affect our conclusions. However, we note that σ_θ for BAND and SBPL can be systematically larger than those for COMP, because the high-energy tail of COMP is an exponential cutoff with no parameter dependence. Therefore, α has very little effect on the right-hand-side spectrum for COMP fits (see Eqn. 1.38), and σ_θ of COMP may be under-estimated.

Because the fit results for BAND and SBPL fits are distributed over a wide range and have larger angles and errors than COMP, it is of interest to look separately at the low-energy left-hand-side angles $\theta_{\rm left}$. This way we can explore how both sides contribute to the total curvature and shape our results. Also, $\theta_{\rm left}$ is unaffected by the transition from photon counts to upper limits that sometimes already occurs slightly below $3.0E_{\rm p}$ on the right-hand-side. We therefore show, in the right panels of Fig. 4.2, the CDFs of the low-energy left-hand-side angles $\theta_{\rm left}$ (i.e., the angle

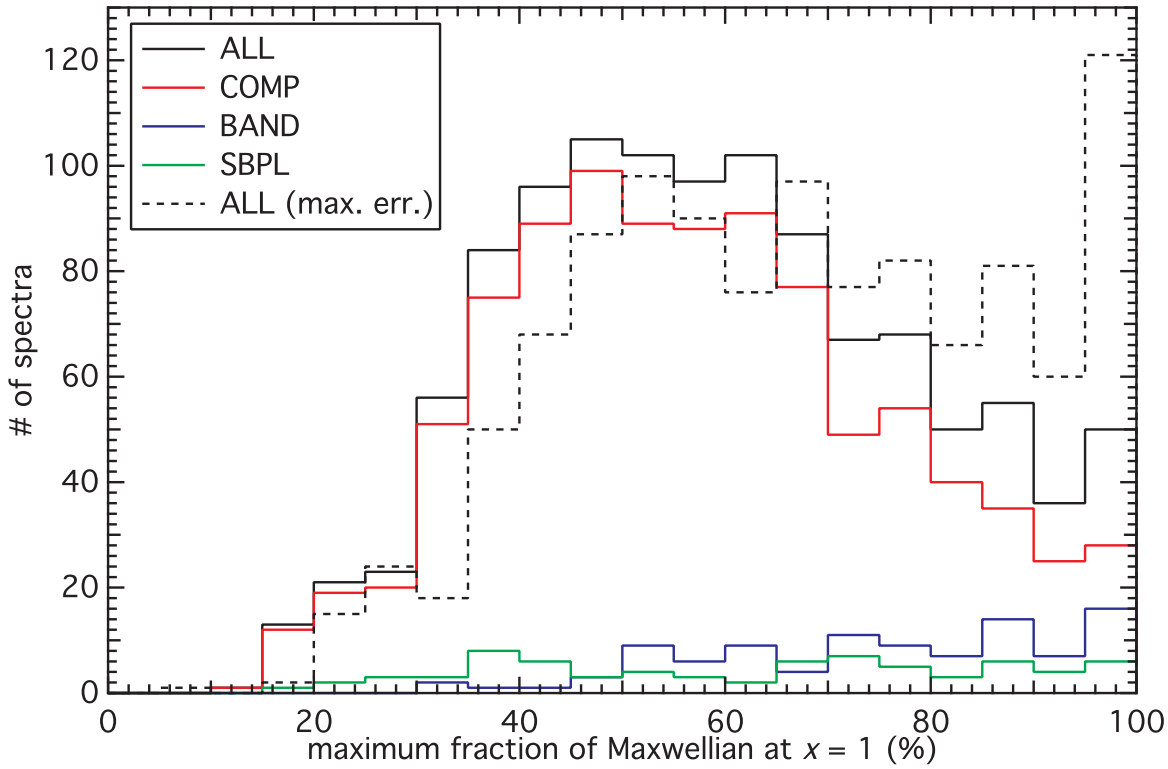

Figure 4.3: Distribution of the maximum fraction contributed from the Maxwellian synchrotron function at $x = 1$. The solid histograms represent the distributions using the best-fit model parameters, while the dashed histogram shows the minimum allowed sharpness by the uncertainties from the best-fit parameters. Spectra with 100% at $x = 1$ are accumulated in the last bin.

under $(\log 1, \log 1)$ and between $\log x_{\rm left}$ and $\log 1$) and the distributions of their errors $\sigma_{\rm left}$.

The top right panel of Fig. 4.2 shows that if one compares $\theta_{\rm left}$ instead of θ, the overall fraction inconsistent with single-electron synchrotron increases to 48%, and the overall fraction inconsistent with Maxwellian synchrotron is also 91%. Therefore, even when only the left-hand-side of the spectral peak (or break) is considered, the same conclusions can be drawn, and the errors remain sufficiently small not to affect the final result. The distributions of the errors on $\theta_{\rm left}$ are similar for the different fit functions, suggesting that their values are not merely driven by the curvature of the fit function itself. In addition, it shows that the low-energy curvature is the main cause of the violation of any synchrotron emission model, and that the upper limits in the high-energy side could harden the high-energy power laws of BAND and SBPL, which make the spectral shape less sharp.

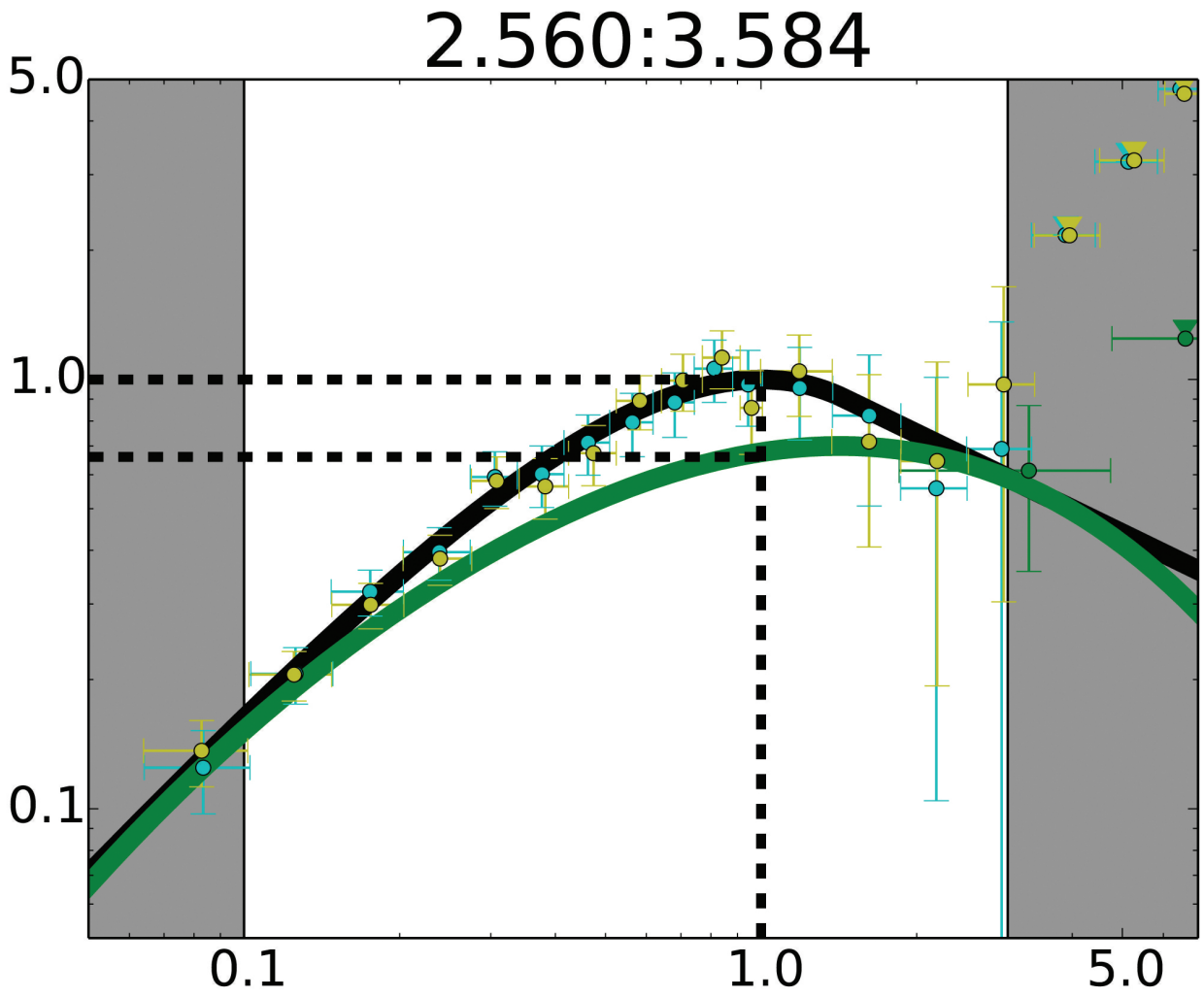

Figure 4.4: Example spectrum taken from GRB 101014.175 (2.560 - 3.584 s), showing the maximum contribution to the best-fit model by the Maxwellian synchrotron function, at $x = 1$. The normalized Maxwellian synchrotron (green curve) and the best-fit model (black curve) overlaid. The black dashed lines show the peak position of the best fit model and the relative normalized flux levels. In this particular spectrum, the Maxwellian fraction is about 65% at $x = 1$. The shaded regions show the boundaries $x_{\rm left} = 0.1$ and $x_{\rm right} = 3.0$. Deep green data points are from the BGO detector and the others are from the NaI detectors. Triangles represent upper limits. For display purpose, the bin size has been increased by a factor of 5 - 10 relative to the standard bin size.

Of our 1,113 spectra, 35% violate the synchrotron line-of-death (i.e., $\alpha > -2/3$), higher than the 20% observed by Gruber et al. (2014) in their peak-flux "P" spectra sample. This implies that a large number of spectra are still consistent with the line-of-death. However, we find that in the 65% of spectra that do not violate the line-of-death, 92% of them violate the Maxwellian limit (i.e., $\theta < 135$ degrees) given in this work. This shows that the sharpness angle method can identify

many more spectra that are consistent with the line-of-death but are still sharper than what the synchrotron theory predicts. By contrast, of the 35% of spectra that violate the line-of-death, only 10% of them do not violate the Maxwellian limit.

Since our results indicate that the synchrotron model alone cannot explain most of the prompt spectra, we can ask the question, if synchrotron emission is still one of the mechanisms that contributes to the observed peak flux, how much at most can it realistically contribute? In Fig. 4.3, we show the distribution of the maximum peak flux contributed from the Maxwellian synchrotron function. For the spectra that do not have a peak, we compute this value at the spectral break. A sample spectrum from GRB 101014.175[2] is plotted in Fig. 4.4. The normalized Maxwellian synchrotron function was shifted vertically and horizontally until the distance between its value at $x = 1$ and the peak of the fit model is minimized. The advantage of evaluating this value at the peak of the fit model is that it is energy domain independent. For the spectra of SBPL without a peak, the break energies $E_{\rm b}$ are used instead. It is found that the Maxwellian can only contribute up to $58^{+23}_{-18}\%$ of the peak flux (solid histogram). Even if the minimum sharpnesses (i.e., the broadest) allowed by the uncertainties in the best-fit parameters are considered, this only slightly increases to $68^{+23}_{-23}\%$ (dashed histogram). Again, we caution that these synchrotron spectra represent a limiting case of high sharpness, relative to that expected from a distribution of temperatures and magnetic field strengths and a rapidly evolving particle population. In that sense, 58% indicates an upper limit.

4.2.1 Spectral Evolution

We now consider the sequence of spectra within bursts. We select and plot in Fig. 4.5 the evolution of θ for 6 example bursts, with the Maxwellian synchrotron limit and the observed light curves overlaid. It can be seen that θ exhibits various evolutionary trends:

(1) In GRB 100414.097 (top left panel), the spectrum becomes less sharp as time evolves. We also plot the spectra of this burst in Fig. 4.6, with the normalized blackbody (red), Maxwellian synchrotron (green), and the best-fit model (black) overlaid. The violation of the Maxwellian synchrotron function is clearly shown in this example, and θ increases with time. In the typical fireball model, θ is expected to increase with time due to, e.g., increasing collision radius and

[2]in this work, the names of the bursts are given according to the *Fermi* GBM trigger designation that is assigned for each new trigger detected. The first 6 digits indicate the year, month, and day of the month, and the last 3 digits indicate the fraction of the day. For more details, please see the online *Fermi* GBM burst catalog at `http://heasarc.gsfc.nasa.gov/W3Browse/fermi/fermigbrst.html`

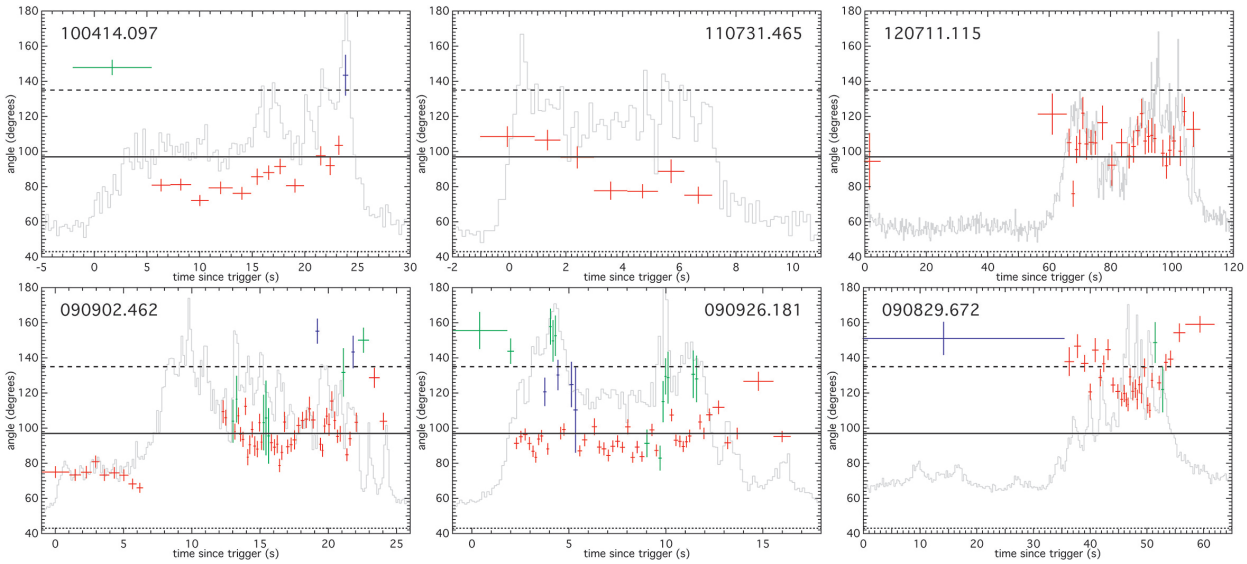

Figure 4.5: Six examples of evolutionary trends of θ. Red, blue, or green color indicates that the best-fit model is COMP, BAND, or SBPL, respectively. The light curves are overlaid in arbitrary units. The limits of the normalized blackbody (dotted line), single-electron synchrotron (solid line), and synchrotron emission from a Maxwellian electron distribution (dashed line) are overlaid.

curvature effects.

(2) In GRB 110731.465 (top central panel), the opposite happens and the spectrum becomes sharper as time evolves.

(3) In GRB 120711.115 (top right panel), θ fluctuates between the limits of single electron and Maxwellian, without clear correlation to the observed light curve. We note that the first time bin at around the trigger time has a small θ.

(4) In GRB 090902.462 (bottom left panel), θ remains approximately constant in the plateau during the first 7 s, and then increases to higher but fluctuating values (11 - 25 s). We note that during 7 - 11 s, the catalog best-fit model is the power law plus blackbody, in accordance with the finding of Abdo et al. (2009). We did not compute the sharpness angle for this period of time because the blackbody is sharper than all synchrotron cases.

(5) In GRB 090926.181 (bottom central panel), the low emission level first time bin gives the largest θ, which is consistent with what Maxwellian synchrotron emission predicts (in contrast to GRB 090902.462), and θ then decreases and fluctuates around the value of the single-electron limit. It increases again in the penultimate time bin to a value marginally consistent with the Maxwellian limit, and then drops again to the single-electron limit.

(6) GRB 090829.672 (bottom right panel) has the largest fraction of spectra consistent with a

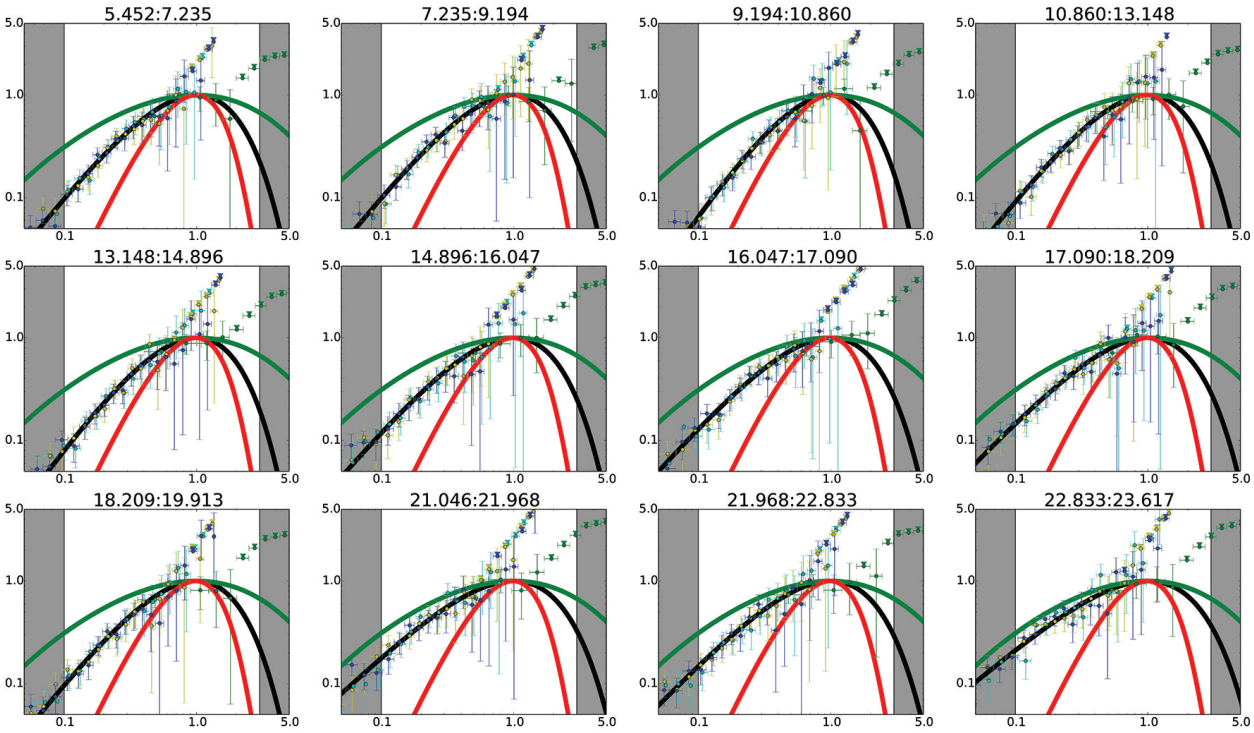

Figure 4.6: Spectral evolution of GRB 100414.097 with the normalized blackbody (red), Maxwellian synchrotron (green), and the best-fit model (black) overlaid. Time evolves from top left to bottom right, and the time since trigger is labeled at the top of each snapshot spectrum, in units of seconds. The peaks of the models are all normalized to $(x, y) = (1, 1)$. Data points and the shaded regions are plotted as described in Fig. 4.4. For display purpose, the bin size has been increased by a factor of 5 relative to the standard bin size.

Maxwellian synchrotron explanation (13 out of 32 spectra, 40%). Similar to GRB 090926.181, it combines a large value of θ with a low emission level. During the main emission pulses between 35 - 55 s, θ decreases below the Maxwellian limit and then increases again to values above the Maxwellian limit.

These bursts are chosen to show the variety of evolutionary trends in θ: gradual increase, gradual decrease, fluctuation between the single-electron and Maxwellian limits, small θ during low emission level and large θ during high emission level, large θ during low emission level and small θ during high emission level, and decrease from above the Maxwellian limit followed by an increase again to above the Maxwellian limit.

4.3 Consistency Checks

4.3.1 Choices of Fit Models

It is observed that over 66% of the time-resolved spectral catalog best-fit models are COMP. This indicates that most of the observed spectra are indeed sharper than BAND or SBPL would predict. The same statistical behavior was also observed in the GBM GRB time-integrated spectral catalogs (Goldstein et al. 2012; Gruber et al. 2014) and the BATSE time-integrated spectral catalogs (Kaneko et al. 2006; Goldstein et al. 2013).

We show in Fig. 4.7 the CDFs of θ and the distributions of σ_θ from the catalog best fits, evaluated using the full data domain of (8 keV, 40 MeV) and triangle domain of $(x_{\rm left}, x_{\rm right}) = (0.1, 3.0)$. It is observed that the catalog best fits produce results similar to the re-fits.

We note that COMP is inherently an exponential cutoff model, while BAND and SBPL are power laws joined by a peak or break energy. This intrinsic difference between the fit functions motivates us to explore the fit results if all spectra are fit using the Band function. Therefore, we further plot in Fig. 4.7 the distributions of θ and σ_θ using the catalog BAND fits ("all BAND"), provided that it is a converged fit with a peak (or break) energy in the νF_ν space, but not necessarily the best fit when compared to other models. We find that it gives larger θ and σ_θ. This indicates that when the Band function is applied to all spectra, the values of θ can be over-estimated due to larger uncertainties. Nevertheless, even in the all-BAND approach, 77% of spectra are sharper than the Maxwellian synchrotron limit.

The models of COMP, BAND, and SBPL have been extensively tested over the years and are found to provide good fits to data (e.g., Kaneko et al. 2006). In Fig. 4.8, we show the comparison of the convolved data points and the respective convolving model curves for an illustrative sample spectrum taken from GRB 100414.097 (see also Fig. 4.6). The red curve and data points are obtained from the COMP fit (CSTAT/dof[3] = 301.66/285), the blue ones are from the BAND fit (CSTAT/dof = 301.61/284), and the orange ones are from the SBPL fit (CSTAT/dof = 301.68/283) with the break scale Δ allowed to vary (see Eqn. 1.36). The fit functions start to diverge when extrapolated outside the data domain, but the data points of different convolving models coincide almost exactly, even when Δ is left as a free parameter. This indicates that these empirical functions provide good descriptions of the observed data, justifying our choices of models to obtain the spectral sharpness angles. However, we note that the fit parameters of SBPL become unconstrained

[3]The modified Cash Statistics (Cash 1979), Caster C-Statistics, per degrees of freedom.

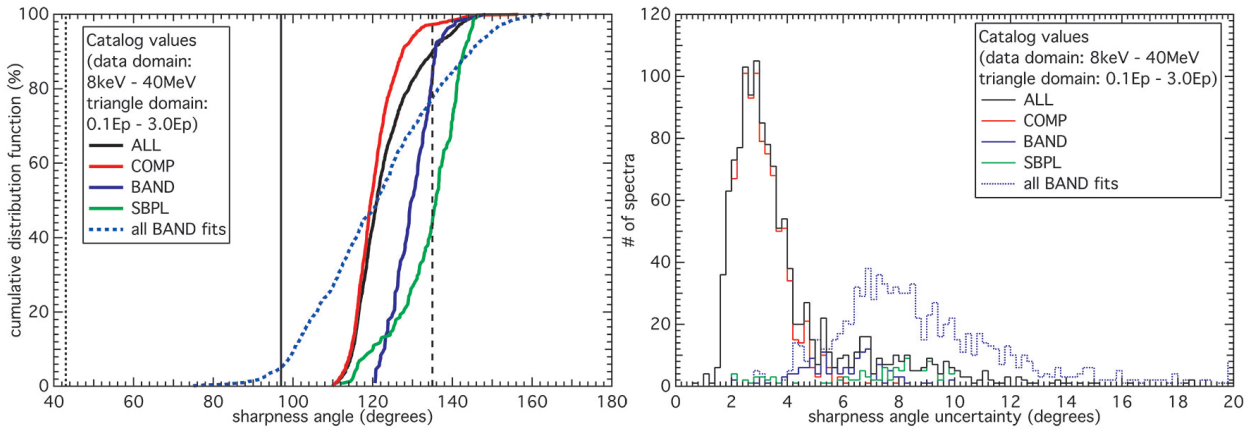

Figure 4.7: Left panel: Cumulative distribution functions of θ for the catalog full energy domain fits. Right panel: Distributions of σ_θ. The limits of the normalized blackbody (dotted line), single-electron synchrotron (solid line), and synchrotron emission from a Maxwellian electron distribution (dashed line) are overlaid. In the above legends, COMP represents the Comptonized model, BAND represents the Band function, SBPL represents the smoothly broken power law, and ALL represents the overall population (COMP + BAND + SBPL). The blue dotted line and histogram show fit results if all spectra are fit using BAND, provided that they are converged fits, but not necessarily the best fit when compared to other models.

for a varying Δ, which indicates degeneracy in the parameter space. Therefore, we follow the catalogs and fix $\Delta = 0.3$.

Figure 4.9 repeats (in grey) the data points convolved with the best fit function (COMP) from Fig. 4.8 and shows a comparison with a SBPL that mimics a Maxwellian synchrotron function (shown in orange, overlaid on the original Maxwellian in green). First we separately fit a SBPL to the Maxwellian synchrotron model in order to obtain a curve that can be used directly in RMFIT. Then we fit this Maxwellian-SBPL function to the data by fixing the fit parameters except for the normalization factor A. This demonstrates how the data points can shift under convolving with a strongly differing fit function. Even though the data points shift, the resulting fit is significantly worse (CSTAT/dof = 558.00/287) than the COMP fit. This is consistent with work by Burgess et al. (2014a), who directly convolved synchrotron emission spectra with photon counts and found CSTAT values differing typically by hundreds relative to best fit curves.

4.3.2 Choice of Data Domain

A key distinction between the current work and others, is that in this work, we want to obtain a mathematical description of the *peak or break curvature* rather than of the whole spectrum. For

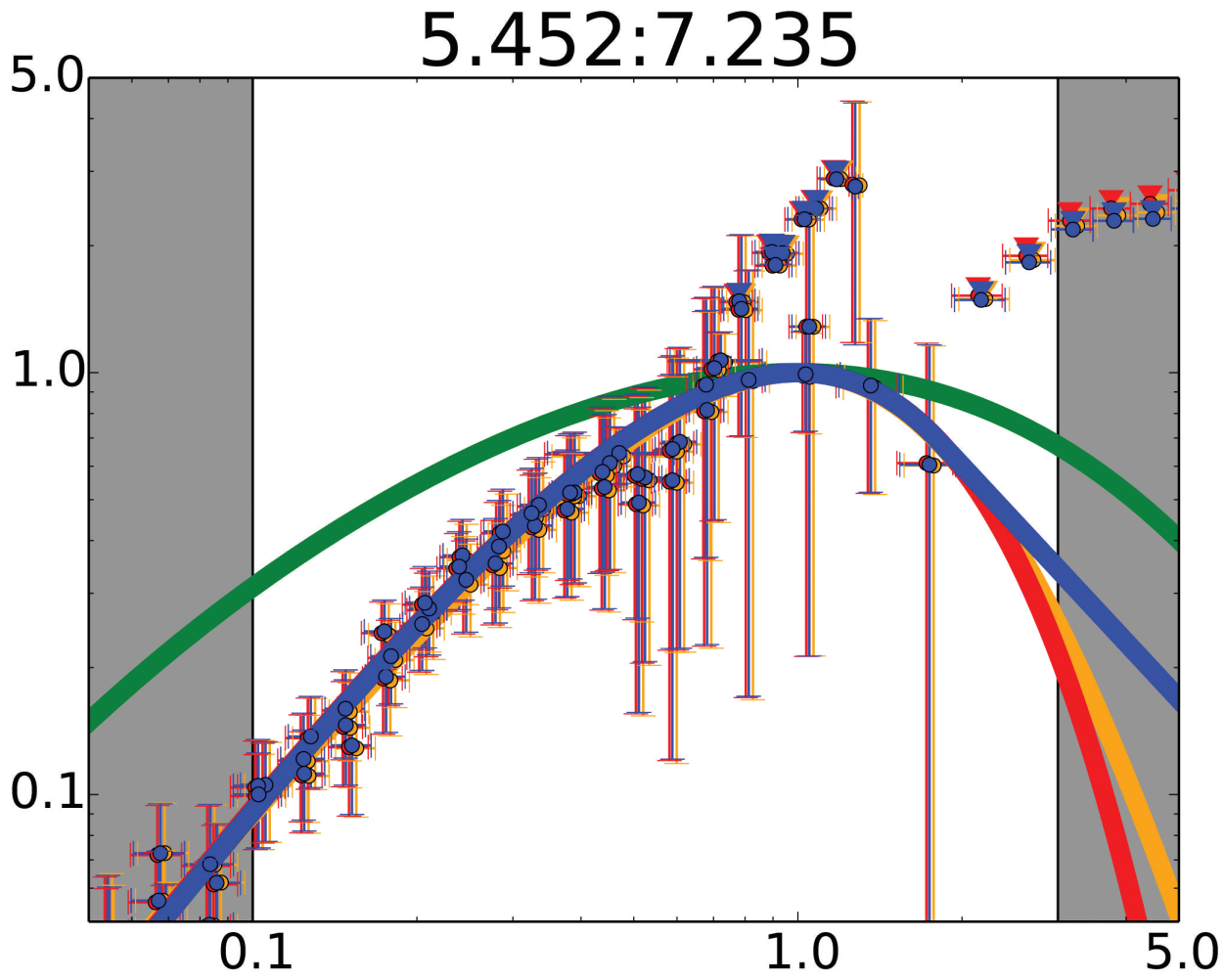

Figure 4.8: Comparison of the convolved data points and the respective convolving model curves for a sample spectrum taken from GRB 100414.097. The red curve and data points are obtained from the COMP fit, the blue ones are from the BAND fit, and the orange ones are from the SBPL fit with the break scale Δ allowed to vary. The Maxwellian synchrotron function is also overlaid (green). For display purpose, the bin size has been increased by a factor of 5 relative to the standard bin size.

this reason, we need to test whether our results hold up under a change in the data domain. The considerations when choosing the data domain size are (1) we want to have as many data points as possible, while (2) we do not want to include data too far away from the spectral peak, which could introduce extra curvature effects on the low-energy end and too many upper limits on the high-energy end that might pull the best fit function away from the data points near the peak or break, or shift the inferred peak or break itself. For smaller data domains, some of the fit parameters can be more weakly constrained than when the full energy domain is used. However, as we show in

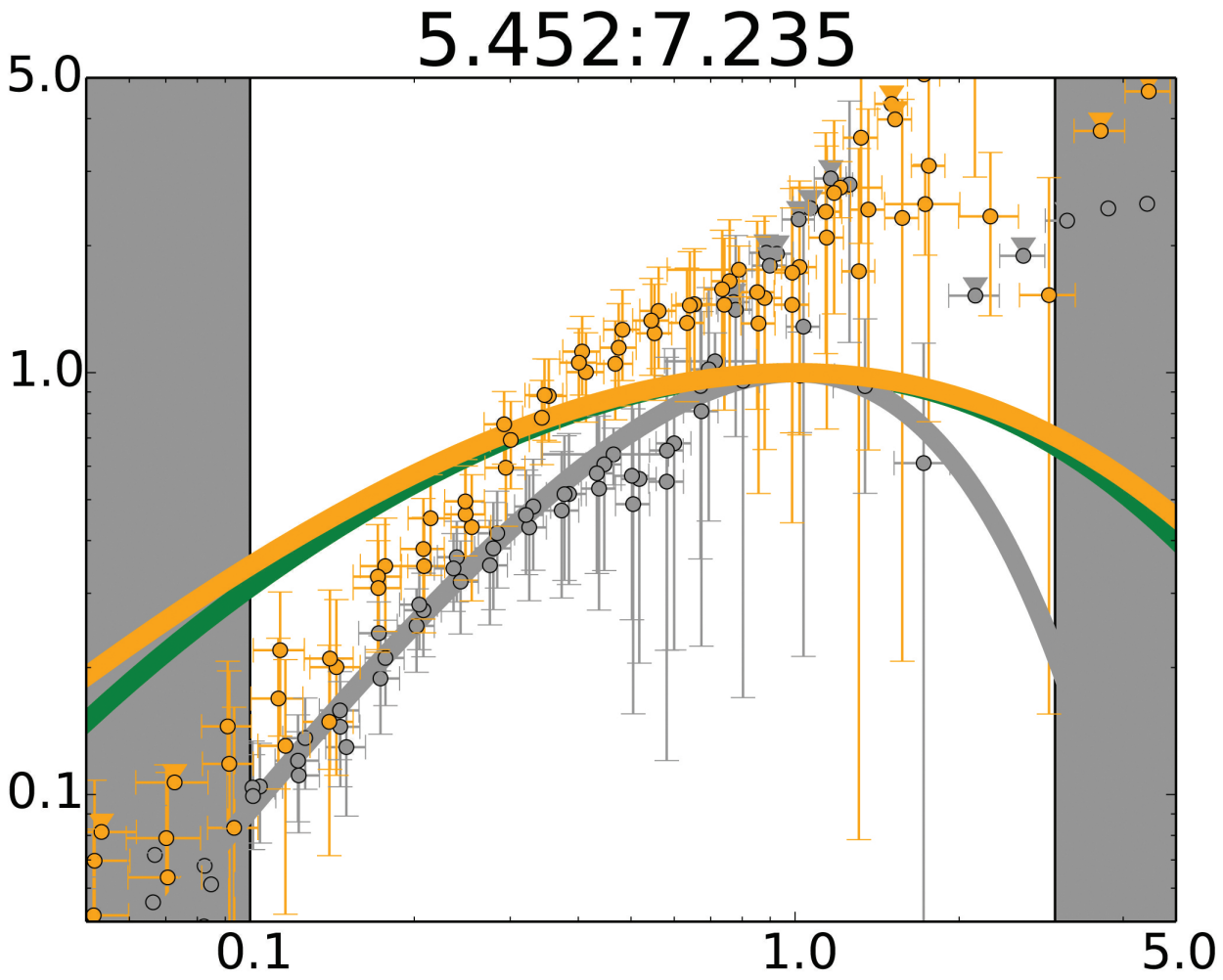

Figure 4.9: Comparison of the convolved data points and the respective convolving model curves for the same spectrum of Fig. 4.8. The orange curve and data points are obtained from the Maxwellian-SBPL fit, and the grey ones are from the COMP fit. The Maxwellian synchrotron function is also overlaid (green). For display purpose, the bin size has been increased by a factor of 5 relative to the standard bin size.

Sect. 4.3.3, the violation of the synchrotron emission model cannot be explained by the errors on the re-fit parameters.

In order to find the optimal data domain size, the re-fitting process is repeated using different values of $E_{\rm right}$, for spectra of the few brightest bursts. We find that the first-upper-limit-data point of the BGO detector is typically at 1.5 - 3.5 times the value of $E_{\rm p}$. Therefore, in order to minimise the effect due to the high-energy upper limits, $E_{\rm right} = 3.0E_{\rm p}$ is adopted. The above checking process is again repeated with different values of $E_{\rm left}$. It is found that data domains smaller than

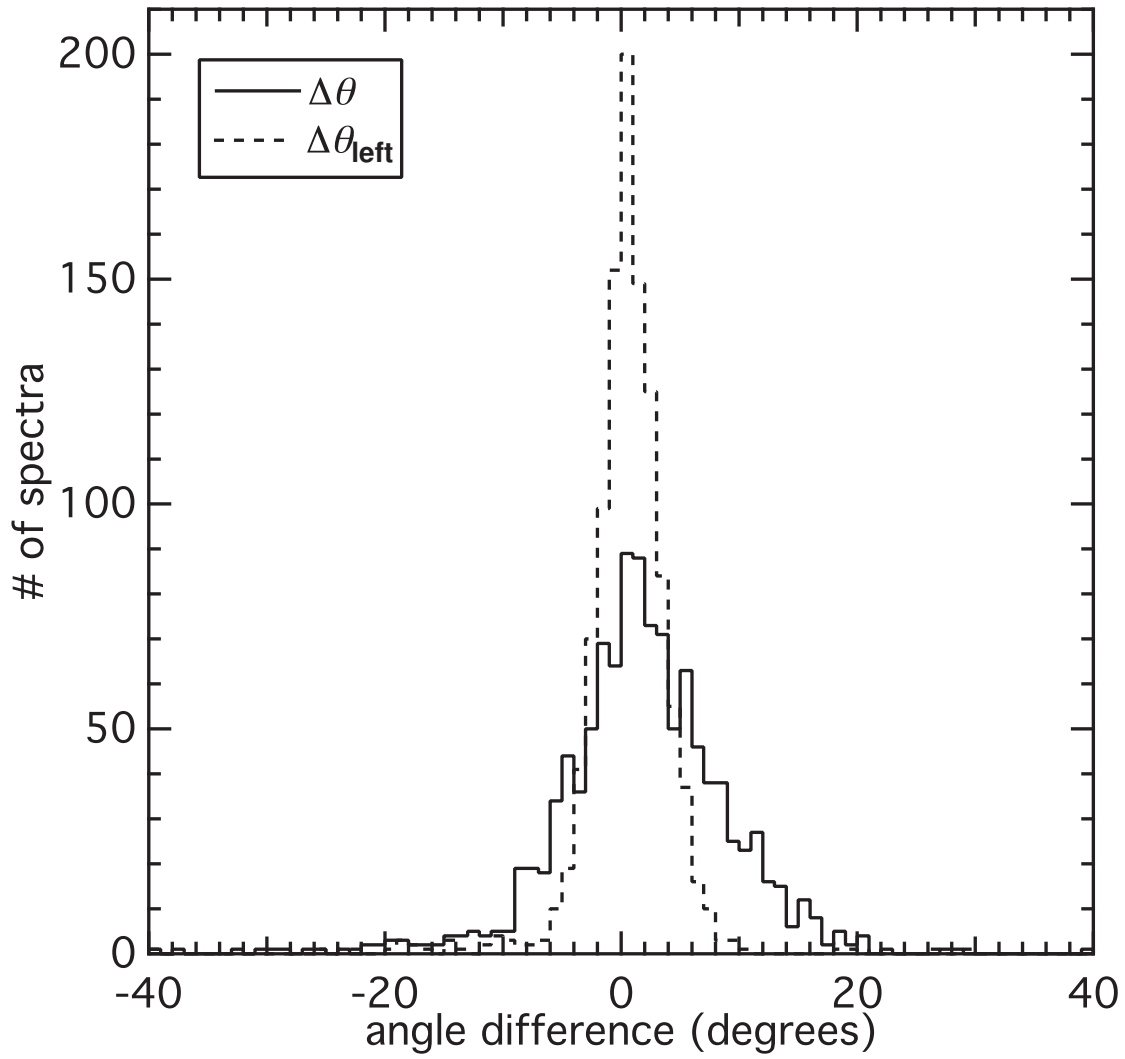

Figure 4.10: Distributions for $\Delta\theta = \theta^{\text{catalog}} - \theta^{\text{re-fit}}$ (solid histogram) and $\Delta\theta_{\text{left}} = \theta^{\text{catalog}}_{\text{left}} - \theta^{\text{re-fit}}_{\text{left}}$ (dashed histogram). The values of $\Delta\theta$ and $\Delta\theta_{\text{left}}$ are normally distributed with medians at 1.7 and 0.6 degrees, respectively.

$(0.1E_{\text{p}}, 3.0E_{\text{p}})$ usually produce large uncertainties in the fits because the data are insufficient to define a definite functional shape.

In Fig. 4.10, we show the differences in θ and θ_{left} between the catalog domain size (i.e., the full GBM energy domain from 8 keV to 40 MeV) and the data domain size mainly used in this work (i.e., $0.1E_{\text{p}}$ to $3.0E_{\text{p}}$), for each spectrum. We find that $\Delta\theta$ and $\Delta\theta_{\text{left}}$ are normally distributed with medians at 1.7 and 0.6 degrees, respectively. This shows that while the extra curvature effects

contributed by the data points on the flanks lead to a change in smoothness, the effect is small, and limiting the data domain size is not strictly necessary (this is also confirmed by Fig. 4.7).

4.3.3 Choice of Triangle Domain

Besides the re-fitting data domain, we also check the validity of the triangle domain used in the computation of θ. There are 3 choices: (1) triangle domain > data domain, (2) triangle domain = data domain, and (3) triangle domain < data domain.

Triangle domain > data domain is obviously not statistically sound, because we have no knowledge of how the data behave outside the data domain. On the other hand, we need to find a balance between staying as close to the peak (or break) as possible and measuring a meaningful amount of curvature. As discussed in Sect. 4.3.2, the choice of $x_{\rm right}$ is already limited by the upper limits, so we concentrate on checking the consistency of $x_{\rm left}$.

In Fig. 4.11, we show the difference between the sharpness angles of the Maxwellian synchrotron function and the fitting models as a function of $x_{\rm left}$ (top left panel) and that between the Maxwellian synchrotron function and the all-BAND fit results (i.e., those described in Sect. 4.3.1 and shown in Fig. 4.7). The same plots for the differences of $\theta_{\rm left}$ are shown in the bottom panels. These plots are produced according to the procedure described below. First, a re-fit spectrum is randomly chosen. Second, we randomly draw new values of α and β from a uniform probability function characterized by the 1σ errors of the spectrum, and a new value of θ is computed. Third, we repeat the first two steps 10,000 times and obtain the distributions for different values of $x_{\rm left}$. We note that the plots have extrapolated below the NaI detector limit of 8 keV$\sim 0.03E_{\rm p}$ for $E_{\rm p} \sim 250$ keV (close to the median $E_{\rm p}$ time-resolved spectral catalog value, Yu et al. submitted), indicated by red vertical lines in Fig. 4.11. The shaded bands show the 1σ region.

For triangle domain choices where the lower boundary of the shaded band lies above 0, the difference between data and synchrotron theory is the clearest. The plot therefore shows how $x_{\rm left} = 0.1$ robustly leads to an unambiguous result. This is true for other choices of $x_{\rm left}$ as well, as long as $x_{\rm left} \gtrsim 0.05$. Fig. 4.11 also shows that, while setting $x_{\rm left} = 0.3$ rather than 0.1 leads to a larger safety margin, the difference in actual angle is negligible. By extrapolating the triangle domain boundary $x_{\rm left}$ to very small values, the long side of the triangle will eventually align with the left power-law asymptote. For any basic synchrotron spectrum, the left angle will then approach $\theta_{\rm left} = \sin^{-1}(3/4) \approx 48.6$ degrees, corresponding to the well-known synchrotron line-of-death slope. Subsequently comparing this angle to one inferred from a best fit, therefore then

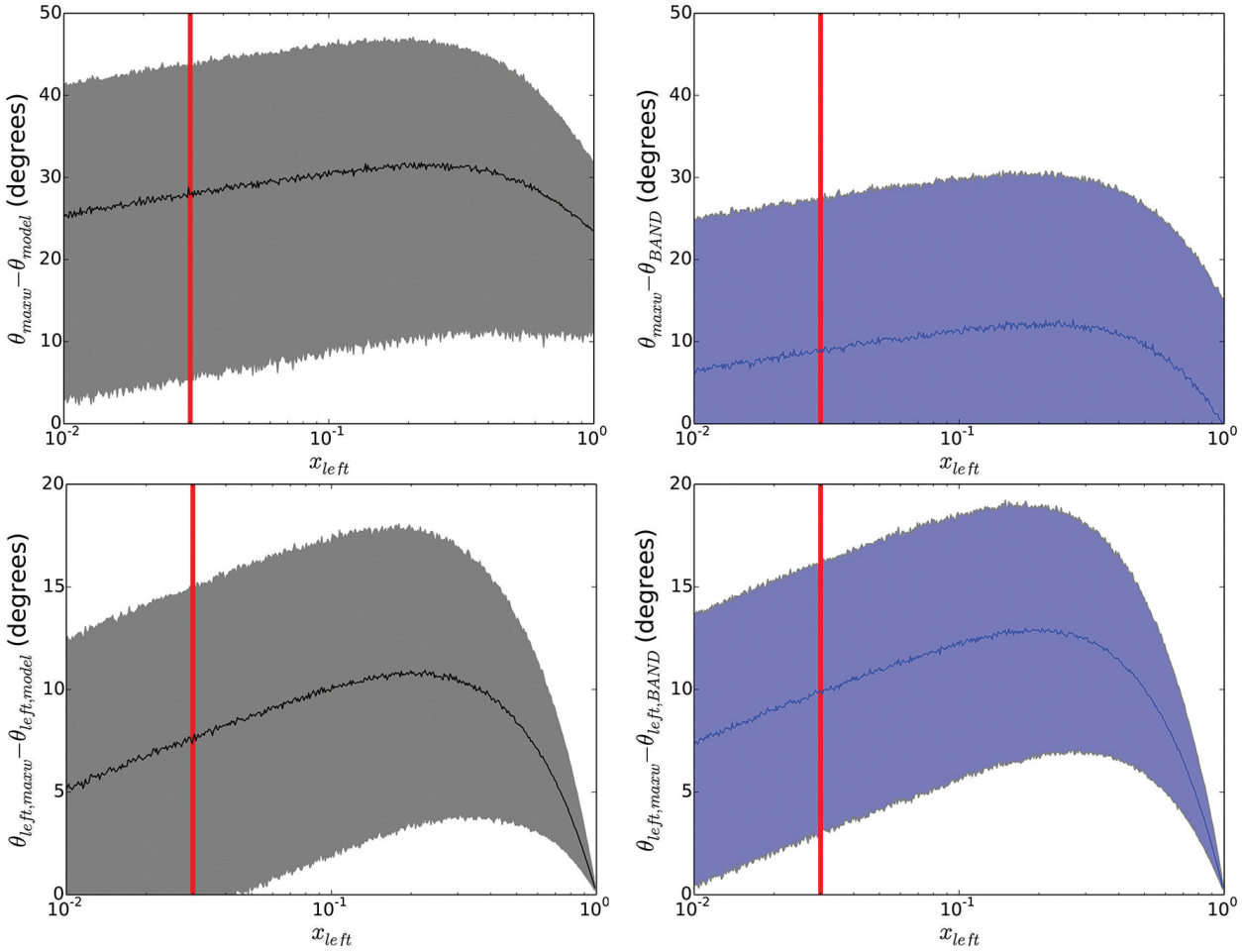

Figure 4.11: Top left panel: Difference between the sharpness angles of the Maxwellian synchrotron function and the re-fitting models, $\theta_{\rm maxw} - \theta_{\rm model}$, as a function of $x_{\rm left}$. Top right panel: Same for $\theta_{\rm maxw} - \theta_{\rm BAND}$. Bottom left panel: Same for $\theta_{\rm left,maxw} - \theta_{\rm left,model}$. Bottom right panel: Same for $\theta_{\rm left,maxw} - \theta_{\rm left,BAND}$. The red vertical lines show the NaI detector limit of 8 keV$\sim 0.03 E_{\rm p}$ for $E_{\rm p} \sim 250$ keV. The shaded regions show the 1σ regions. See main text for details about the plots.

becomes equivalent to testing for violation of the synchrotron line-of-death. We note however, that this analysis indicates a large error margin and extrapolating beyond the data domain.

4.4 Theoretical Implications

Our results show that for most GRB prompt emission spectra, an explanation in terms of synchrotron radiation can be problematic. In the internal shocks of GRBs, a single-electron emission function is obviously non-realistic (as there must be multiple electrons in the outflow) and a Maxwellian population drawn from a single temperature is the limiting case. Even this limiting

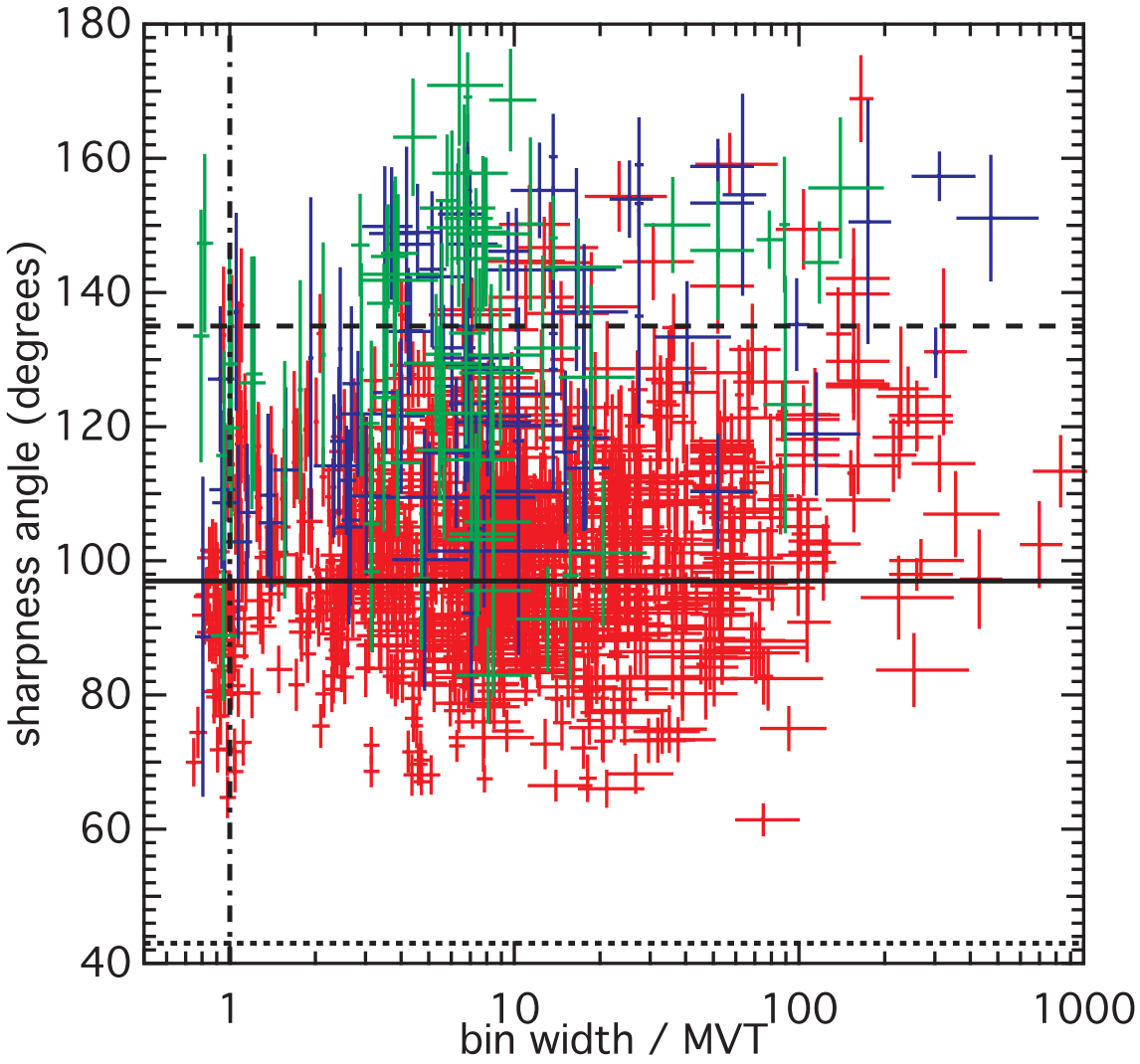

Figure 4.12: Sharpness angles plotted against the temporal bin widths per MVT. Red dat points show spectra best fit by COMP, blue by BAND, and green by SBPL. The vertical dash-dotted line shows where the bin width equals the MVT, only 4.4% of data points are located to the left of the line. The horizontal lines show the limits of the normalized blackbody (dotted), single-electron synchrotron (solid), and synchrotron emission from a Maxwellian electron distribution (dashed).

case is already too wide to fit most GRB time-resolved spectra.

The minimum variability timescale (MVT, e.g., Bhat 2013; Golkhou & Butler 2014) of the light curves is thought to be related to the actual dynamical timescale of the emission process. Therefore, if the temporal bin widths of our spectra are larger than the MVTs, then in the time-resolved spectral catalog we are still looking at averaged time-resolved spectra that are less averaged

than those in the time-integrated spectral catalogs. In Fig. 4.12, we plot θ against temporal bin widths per MVT (for the computational method of the MVT, see Bhat 2013). It is observed that, in 1,064 spectra (49 spectra were excluded because they belong to bursts with no MVT due to bad or not enough GBM data), only 4.4% of the spectra have bin width less than the MVT for the respective burst. This means that the problem for the synchrotron theory may be even more severe, since our spectra are smoothened already. However, this picture is complicated by the possibility that the MVT is time and energy dependent. Golkhou & Butler (2014) use another method to compute the MVT, which is consistent with our method (Golkhou et al. 2015). The uncertainties of the MVT are worthy of independent studies which are beyond the scope of this paper.

For many years, the Band function has been assumed to be the appropriate mathematical description in most of the GRB prompt spectral studies. As already shown in Sect. 4.3.1, the fact that most spectra are best fit by the Comptonized model (both time-integrated and time-resolved) shows that the high-energy tail of the prompt spectrum is actually sharper than a Band function would predict (i.e., maybe somewhere in between BAND and COMP). In a recent study using a subsample of GBM bursts which occurred in the *Fermi* Large Area Telescope[4] (LAT, Atwood et al. 2009) field of view but remained undetected, Ackermann et al. (2012) showed that the Band function's β (as obtained from GBM spectral fits) is too hard to be consistent with the LAT upper limits. All these results are indicating that the Band function can lead to incorrect interpretation of the data. To resolve this problem, there are at least two ways: (1) to invent another empirical mathematical function and then again try to interpret the parameters of this new function by physics; or (2) to fit the observed spectrum directly by physical models.

It is difficult to construct another empirical function which can improve upon the Band function, because it is already very simple in a statistical sense: it has only four parameters, and COMP has three. Yu et al. (Ch. 3, 2015a) have shown that a triple power law with sharp breaks, in which the power-law indices have already been constrained according to the fast- or slow-cooling synchrotron models, could only perform as good as the Band function. They have found that in many cases even an extra blackbody is needed to describe the spectral curvature. Recently, more and more studies are being performed using physical fitting models (e.g., Burgess et al. 2011, 2014a) and simulations under more realistic physical conditions, e.g., varying magnetic fields (e.g., Uhm & Zhang 2014). However, without knowledge of the emission process, it is difficult to formulate a sufficiently well-constrained fit function. Furthermore, there may be multiple emission mechanisms

[4]The *Fermi* Large Area Telescope is a pair production telescope covering the energy range from 20 MeV to 300 GeV.

at work, the sum of which forms the observed prompt spectra.

The fitting results obtained using semi-empirical synchrotron models (e.g., Ch. 3, Yu et al. 2015a) and physical synchrotron models (e.g., Burgess et al. 2011, 2014a) show that extra thermal components are needed to fit the data. The resulting poor CSTAT values and systematic residual trends indicate that a pure non-thermal synchrotron emission function is inconsistent with the data at the peak or break energies, and thus cannot be the dominant process which contributes to the observed flux around this energy range. The distribution of spectral peak sharpness values that we report in this work implies that any model based on standard synchrotron theory without additional radiative mechanisms will systematically struggle to capture the spectral curvature of the prompt emission. This will manifest itself in relatively poor CSTAT values and systematic trends in the fit residuals.

Recently, Axelsson & Borgonovo (2015) have shown that using the full-width-half-maximum measurement of GRB prompt emission spectra taken from the BATSE 5B GRB spectral catalog (Goldstein et al. 2013) and 4-years *Fermi* GBM GRB time-integrated spectral catalog (Gruber et al. 2014), a significant fraction of bursts (78% for long and 85% for short GRBs) could not be explained by a Maxwellian population-based slow-cooling synchrotron function. Our results show that using the time-resolved spectra this violation is actually more severe, with over 91% of spectra obtained from long bursts violating the Maxwellian synchrotron function drawn from a single temperature, which is already a limiting case.

As can be seen from Fig. 4.6, it is obvious that a small number of Planck functions are not enough to reconstruct the observed spectral shape. From the observational point-of-view, fitting many blackbodies (with many parameters) is statistically meaningless, although maybe a sufficiently simple function describing a continuum of temperatures can be formulated. On the theoretical side, simple photospheric models also show difficulties in explaining the observed data. For example, early theoretical studies of a pure thermal origin of GRB prompt emission, such as from freely expanding photospheric outflows with no baryonic matter or magnetic field (Goodman 1986; Paczynski 1986), have shown difficulties in explaining the shape of the prompt emission phase and the two evolutionary trends of $E_{\rm p}$ (i.e.. hard-to-soft evolution and intensity tracking, see, e.g., Ford et al. 1995). Recent studies (e.g., Pe'er et al. 2006; Giannios 2008; Pe'er & Ryde 2011; Ryde et al. 2011; Vurm et al. 2011; Lazzati et al. 2013) suggested that the Band function can be reconstructed from a thermal model. However, Deng & Zhang (2014) claim that the hard-to-soft evolution of $E_{\rm p}$ is difficult to reproduce under natural photospheric conditions.

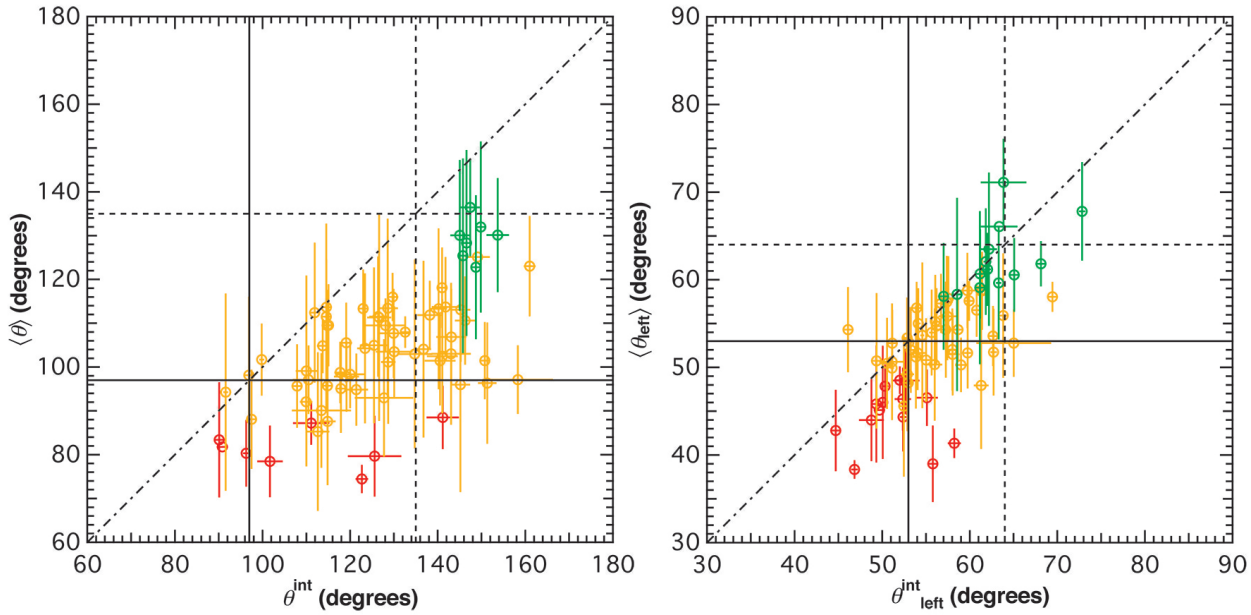

Figure 4.13: Left panel: Comparison between the average sharpness angles, $\langle\theta\rangle$, to the sharpness angles computed using the time-integrated spectral catalog, $\theta^{\rm int}$. Right panel: Comparison between the average left angles, $\langle\theta_{\rm left}\rangle$, to the left angles computed using the time-integrated spectral catalog, $\theta^{\rm int}_{\rm left}$. The dash-dotted line shows $x = y$. The solid and dashed lines show the single-electron synchrotron and Maxwellian synchrotron limit, respectively. We note that the error bars of $\langle\theta\rangle$ and $\langle\theta_{\rm left}\rangle$ represent the spread in θ and $\theta_{\rm left}$. See main text for the color-coding and details about the plots.

A frequently discussed alternative to the baryonic composition of the jets in GRBs is a magnetically, or Poynting flux, dominated jet (Thompson 1994; Drenkhahn & Spruit 2002; Lyutikov & Blandford 2003). In this scenario, the magnetic field dominates the energy density in the emitting region. Thus, the dominant emission mechanism will be synchrotron emission from relativistic electrons, since no cooling mechanism is known which is faster (see, e.g., Beniamini & Piran 2014). Our observational results therefore also pose a challenge to Poynting flux dominated models, although Compton up-scattering from seed photons in the environment of an emerging Baryon-free jet offer a potential means of combining strongly magnetic outflows with a thermalized component or sharp spectrum (see Gill & Thompson 2014, for a recent example). Moreover, Beloborodov (2013) argues that other optically thin emission models share the same problems of the synchrotron emission models, e.g., pitch-angle synchrotron radiation (Lloyd & Petrosian 2000) when the scatter angle in the comoving frame is not isotropic, and jitter radiation in turbulent magnetic fields (Medvedev 2000).

Finally, we compute the average time-resolved sharpness angles and left angles, $\langle\theta\rangle$ and $\langle\theta_{\rm left}\rangle$, weighing each spectrum equally. In Fig. 4.13, we compare $\langle\theta\rangle$ and $\langle\theta_{\rm left}\rangle$ to the sharpness angles and left angles computed using the time-integrated spectral catalog (Gruber et al. 2014), $\theta^{\rm int}$ and $\theta^{\rm int}_{\rm left}$, for every burst in our sample (listed also in Table A.5). In the left panel, green color indicates the 7 bursts (10%) whose average sharpness angles are consistent with the Maxwellian synchrotron limit (individual θ values can still be inconsistent, see, e.g., GRB 090829.672 from Fig. 4.5), orange color indicates the 55 bursts (79%) that are inconsistent with the Maxwellian synchrotron limit but consistent on average with the single-electron synchrotron limit, and red color indicates the 8 bursts (11%) that are inconsistent with the single-electron synchrotron limit. Similarly, in the right panel, green color indicates the 13 bursts (19%) whose average sharpness angles are consistent with the Maxwellian synchrotron limit, orange color indicates the 43 bursts (61%) that are inconsistent with the Maxwellian synchrotron limit but consistent on average with the single-electron synchrotron limit, and red color indicates the 14 bursts (20%) that are inconsistent with the single-electron synchrotron limit. We note that the error bars of $\langle\theta\rangle$ and $\langle\theta_{\rm left}\rangle$ represent the standard deviations $SD = \sqrt{\langle\theta^2\rangle - \langle\theta\rangle^2}$ and $SD_{\rm left} = \sqrt{\langle\theta^2_{\rm left}\rangle - \langle\theta_{\rm left}\rangle^2}$, which indicate the spread of the angle distributions within each burst. The error bars of $\theta^{\rm int}$ and $\theta^{\rm int}_{\rm left}$ are computed using the same procedure as described in Sect. 4.2, and are relatively small because the parameters are better constrained by higher photon counts.

Figure 4.13 shows that the time-integrated angles are systematically larger than the average time-resolved angles for individual bursts, and the data points lie closer to (or sometimes even above) the diagonal in the right panel. One reason for this is that the spectral evolution of $E_{\rm p}$ is corrected for when computing $\langle\theta\rangle$, but not when computing $\theta^{\rm int}$. Another reason is that rotation of the triangle between spectra, where a decrease in $\theta_{\rm left}$ is compensated for by an increase in $\theta_{\rm right} = \theta - \theta_{\rm left}$, or vice versa (i.e., a specific joint change in power-law indices), is also corrected for when computing $\langle\theta\rangle$. This latter compensation is not possible for $\langle\theta_{\rm left}\rangle$, and the the data points in the right panel of Fig. 4.13 therefore lie closer to the diagonal. We also emphasise that different light curve binning methods are used in the time-resolved and time-integrated spectral catalog. In our time-resolved analysis, as mention in Sect. 4.1, the light curves are binned with S/N = 30, and then those spectra without a peak or break are excluded. In the time-integrated spectral catalog (see, e.g., Gruber et al. 2014), all time intervals with $S/N \geq 3.5$ are included. The fact that fewer bursts in the time-integrated spectral analysis are inconsistent with the Maxwellian limit (44 bursts, 62% for $\theta^{\rm int}$, and 62 bursts, 89% for $\theta^{\rm int}_{\rm left}$) underlines the importance of time-resolved analysis.

4.5 Conclusions

We have computed the sharpness angles θ of the observed time-resolved spectra of *Fermi* GRBs, and compared the values to the sharpest cases of the synchrotron radiation theory, namely the single-electron synchrotron and the Maxwellian distributed synchrotron emission function. We find that over 91% of the observed spectra are sharper than the Maxwellian synchrotron model predicts, indicating that synchrotron radiation cannot be responsible for the peaks or breaks of GRB prompt emission spectra. No general evolutionary trend is observed for θ within bursts. Moreover, the Maxwellian synchrotron function can only contribute up to 58^{+23}_{-18}% of the peak flux. We conclude that the underlying prompt emission mechanism in GRBs must produce spectra sharper than a Maxwellian synchrotron function but broader than a blackbody.

It is still possible for synchrotron emission to dominate the spectrum away from the peak or break observed in the GBM energy range (e.g., at the LAT energy range). Also, a sub-dominant synchrotron component can allow for a continuous connection to the afterglow phase, where synchrotron emission is typically dominant (see, e.g., van Eerten 2015, for a recent review). The transition between prompt and afterglow is then marked by the disappearance of the non-synchrotron (likely thermal) component. There are other theoretical possibilities to explain GRB prompt emission, such as the collisional model of electron-positron pairs (e.g., Beloborodov 2010). For recent reviews on GRB prompt emission mechanisms, see, e.g., Zhang (2014) and Pe'er (2015).

A possibly similar inference can be made on the related phenomena of prompt optical emission showing a similar temporal profile as the gamma-ray emission (e.g., Elliott et al. 2014; Greiner et al. 2014) or very early X-ray flares (e.g., Pe'er et al. 2006; see also Hu et al. 2014 for a recent large *Swift* sample study): if the prompt emission is not dominated by synchrotron emission, this is likely the case for this longer wavelength emission as well (see, e.g., Starling et al. 2012; Peng et al. 2014).

We demonstrated in this work a method to quantify the shape of the observed GRB spectra that provides a clear tool for distinguishing between various standard emission functions. Ultimately, the question as to the viability of any particular emission model can only be fully resolved if complete spectral predictions for that model are tested directly against photon counts (see, e.g., Burgess et al. 2014a). Our paper predicts that any model based on standard synchrotron theory without additional radiative mechanisms will systematically struggle to capture the spectral curvature of the prompt emission. This will manifest itself in relatively poor CSTAT values and trends in the fit residuals.

Chapter 5

Summary and Future Directions

"It is scientific only to say what is more likely and what less likely, and not to be proving all the time the possible and impossible."

- Richard Feynman

In this dissertation, I presented time-resolved spectroscopy on GRB prompt emission spectra. The analysis results indicate that optically thin synchrotron emission is very unlikely to be the dominant process in shaping the observed spectral shapes of GRBs, due to the following reasons:

(1) thought some brightest bursts can marginally be explained by a complex empirical model of thermal + non-thermal emission, fine-tuned microphysics parameters and varying magnetic fields are required;
(2) the peaks or breaks of more than 91% of time-resolved prompt spectra is sharper than the sharpest possible pure optically thin synchrotron emission model would predict.

Some possible solutions, however, do exist. For instance a simple enough summation of blackbodies (a "greybody"), absorbed synchrotron (i.e., optically thick), pitch-angle synchrotron, jitter radiation, or collisional processes may be formulated to fit the data. Consequently, the answer to "What is the true emission mechanism of GRB prompt emission?" is still unclear. This is very true in science: falsifying is often easier than validating a hypothesis. Several research directions are foreseeable in the near future. On one hand, "hard science" like to build the next generation of gamma-ray space telescopes with unprecedented precision and resolution is of course necessary to

constraint theoretical models. On the other hand, "soft science" like to analyze existing data using advanced numerical methods can also help to pin-down the true emission mechanism of GRBs, e.g., precise background and spectral fitting techniques using physical models.

Gamma-ray burst prompt emission mechanism is a very important topic because the emission process tells us information of, e.g., the environment of the jet and circum-burst medium, and the nature of the central engine, which can be used to constraint galaxy properties and star formation history. The hope of using GRBs as standard candles also makes them useful in cosmological studies.

While the mission direction of the next generation gamma-ray space telescopes is unclear, the existing data we have in hand are still highly unexplored. The next possible step is to develop an automated time-resolved spectroscopy pipeline to fit these data using advanced Bayesian statistics. This should be able to explain the GRB prompt spectra by fitting physical emission models directly to data, which may lead to a full understanding of these cosmological gamma-ray transients.

Bibliography

Abdo, A. A., Ackermann, M., Ajello, M., et al. 2009, ApJL, 706, L138

Abdo, A. A., Ackermann, M., Ajello, M., et al. 2010, ApJ, 712, 558

Achterberg, A., Gallant, Y. A., Kirk, J. G., & Guthmann, A. W. 2001, MNRAS, 328, 393

Ackermann, M., Ajello, M., Asano, K., et al. 2014, Science, 343, 42

Ackermann, M., Ajello, M., Asano, K., et al. 2013, ApJS, 209, 11

Ackermann, M., Ajello, M., Baldini, L., et al. 2012, ApJ, 754, 121

Akerlof, C., Balsano, R., Barthelmy, S., et al. 2000, ApJL, 532, L25

Amati, L. 2010, arXiv:1002.2232

Amati, L., Frontera, F., Tavani, M., et al. 2002, A&A, 390, 81

Amati, L., Guidorzi, C., Frontera, F., et al. 2008, MNRAS, 391, 577

Atwood, W. B., Abdo, A. A., Ackermann, M., et al. 2009, ApJ, 697, 1071

Axelsson, M., Baldini, L., Barbiellini, G., et al. 2012, ApJL, 757, L31

Axelsson, M. & Borgonovo, L. 2015, MNRAS, 447, 3150

Band, D., Matteson, J., Ford, L., et al. 1993, ApJ, 413, 281

Baring, M. G. 2006, Advances in Space Research, 38, 1281

Baring, M. G. & Braby, M. L. 2004, ApJ, 613, 460

Barthelmy, S. D. 2000, in Society of Photo-Optical Instrumentation Engineers (SPIE) Conference Series, Vol. 4140, X-Ray and Gamma-Ray Instrumentation for Astronomy XI, ed. K. A. Flanagan & O. H. Siegmund, 50–63

Barthelmy, S. D., Barbier, L. M., Cummings, J. R., et al. 2005, Space Sci. Rev., 120, 143

Bednarz, J. & Ostrowski, M. 1998, Physical Review Letters, 80, 3911

Beloborodov, A. M. 2010, MNRAS, 407, 1033

Beloborodov, A. M. 2011, ApJ, 737, 68

Beloborodov, A. M. 2013, ApJ, 764, 157

Beniamini, P. & Piran, T. 2014, MNRAS, 445, 3892

Bhat, P. N. 2013, in "Proc. 7th Huntsville GRB Symp.", Huntsville, Apr. 2013, eConf Proc. C1304143

Bissaldi, E., von Kienlin, A., Kouveliotou, C., et al. 2011, ApJ, 733, 97

Bissaldi, E., von Kienlin, A., Lichti, G., et al. 2009, Experimental Astronomy, 24, 47

Blumenthal, G. R. & Gould, R. J. 1970, Reviews of Modern Physics, 42, 237

Boella, G., Butler, R. C., Perola, G. C., et al. 1997, A&As, 122, 299

Briggs, M. S., Paciesas, W. S., Pendleton, G. N., et al. 1996, ApJ, 459, 40

Burgess, J. M., Preece, R. D., Baring, M. G., et al. 2011, ApJ, 741, 24

Burgess, J. M., Preece, R. D., Connaughton, V., et al. 2014a, ApJ, 784, 17

Burgess, J. M., Preece, R. D., Ryde, F., et al. 2014b, ApJL, 784, L43

Burgess, J. M., Ryde, F., & Yu, H.-F. 2015, MNRAS, 451, 6029

Burrows, D. N., Hill, J. E., Nousek, J. A., et al. 2000, in Society of Photo-Optical Instrumentation Engineers (SPIE) Conference Series, Vol. 4140, X-Ray and Gamma-Ray Instrumentation for Astronomy XI, ed. K. A. Flanagan & O. H. Siegmund, 64–75

Cash, W. 1979, ApJ, 228, 939

Cenko, S. B., Kulkarni, S. R., Horesh, A., et al. 2013, ApJ, 769, 130

Connaughton, V., Briggs, M. S., Goldstein, A., et al. 2015, ApJS, 216, 32

Crider, A., Liang, E. P., Preece, R. D., et al. 1998, in Bulletin of the American Astronomical Society, Vol. 30, American Astronomical Society Meeting Abstracts, 1380

Crusius, A. & Schlickeiser, R. 1986, A&A, 164, L16

Curran, P. A., Evans, P. A., de Pasquale, M., Page, M. J., & van der Horst, A. J. 2010, ApJL, 716, L135

Daigne, F., Bošnjak, Ž., & Dubus, G. 2011, A&A, 526, A110

Daigne, F. & Mochkovitch, R. 1998, MNRAS, 296, 275

Deng, W. & Zhang, B. 2014, ApJ, 785, 112

Dermer, C. D. & Menon, G. 2009, High Energy Radiation from Black Holes: Gamma Rays, Cosmic Rays, and Neutrinos

Drenkhahn, G. & Spruit, H. C. 2002, A&A, 391, 1141

Elliott, J., Yu, H.-F., Schmidl, S., et al. 2014, A&A, 562, A100

Ellison, D. C. & Double, G. P. 2004, Astroparticle Physics, 22, 323

Evans, P. A., Beardmore, A. P., Page, K. L., et al. 2009, MNRAS, 397, 1177

Finke, J. D., Dermer, C. D., & Böttcher, M. 2008, ApJ, 686, 181

Fishman, G. J., Meegan, C. A., Wilson, R. B., et al. 1989, in Bulletin of the American Astronomical Society, Vol. 21, Bulletin of the American Astronomical Society, 860

Ford, L. A., Band, D. L., Matteson, J. L., et al. 1995, ApJ, 439, 307

Frontera, F., Amati, L., Farinelli, R., et al. 2013, ApJ, 779, 175

Frontera, F., Guidorzi, C., Montanari, E., et al. 2009, ApJS, 180, 192

Fynbo, J. U., Jensen, B. L., Gorosabel, J., et al. 2001, A&A, 369, 373

Gehrels, N., Chincarini, G., Giommi, P., et al. 2004, ApJ, 611, 1005

Gendre, B., Stratta, G., Atteia, J. L., et al. 2013, ApJ, 766, 30

Ghirlanda, G., Ghisellini, G., Nava, L., & Burlon, D. 2011, MNRAS, 410, L47

Ghirlanda, G., Nava, L., & Ghisellini, G. 2010, A&A, 511, A43

Ghisellini, G., ed. 2013, Lecture Notes in Physics, Berlin Springer Verlag, Vol. 873, Radiative Processes in High Energy Astrophysics, ed. G. Ghisellini

Giannios, D. 2008, A&A, 480, 305

Giblin, T. W., van Paradijs, J., Kouveliotou, C., et al. 1999, ApJL, 524, L47

Gill, R. & Thompson, C. 2014, ApJ, 796, 81

Goldstein, A., Burgess, J. M., Preece, R. D., et al. 2012, ApJS, 199, 19

Goldstein, A., Preece, R. D., Mallozzi, R. S., et al. 2013, ApJS, 208, 21

Golkhou, V. Z. & Butler, N. R. 2014, ApJ, 787, 90

Golkhou, V. Z., Butler, N. R., & Littlejohns, O. M. 2015, ApJ, 811, 93

González, M. M., Sacahui, J. R., Ramirez, J. L., Patricelli, B., & Kaneko, Y. 2012, ApJ, 755, 140

Goodman, J. 1986, ApJL, 308, L47

Granot, J., Königl, A., & Piran, T. 2006, MNRAS, 370, 1946

Greiner, J., Bornemann, W., Clemens, C., et al. 2008, Publ. Astron. Soc. Pacif., 120, 405

Greiner, J., Krühler, T., Klose, S., et al. 2011, A&A, 526, A30

Greiner, J., Mazzali, P. A., Kann, D. A., et al. 2015, Nature, 523, 189

Greiner, J., Yu, H.-F., Krühler, T., et al. 2014, A&A, 568, A75

Gruber, D., Goldstein, A., von Ahlefeld, V. W., et al. 2014, ApJS, 211, 12

Guiriec, S., Briggs, M. S., Connaugthon, V., et al. 2010, ApJ, 725, 225

Guiriec, S., Connaughton, V., Briggs, M. S., et al. 2011, ApJL, 727, L33

Guiriec, S., Daigne, F., Hascoët, R., et al. 2013, ApJ, 770, 32

Hakkila, J., Meegan, C. A., Pendleton, G. N., et al. 1994, ApJ, 422, 659

Hascoët, R., Daigne, F., Mochkovitch, R., & Vennin, V. 2012, MNRAS, 421, 525

Hill, J. E., Zugger, M. E., Shoemaker, J., et al. 2000, in Society of Photo-Optical Instrumentation Engineers (SPIE) Conference Series, Vol. 4140, X-Ray and Gamma-Ray Instrumentation for Astronomy XI, ed. K. A. Flanagan & O. H. Siegmund, 87–98

Hjorth, J. & Bloom, J. S. 2012, The Gamma-Ray Burst - Supernova Connection, 169–190

Hu, Y.-D., Liang, E.-W., Xi, S.-Q., et al. 2014, ApJ, 789, 145

Huang, Y. F., Dai, Z. G., & Lu, T. 2002, MNRAS, 332, 735

Jones, F. C. 1968, Physical Review, 167, 1159

Kaneko, Y., Preece, R. D., Briggs, M. S., et al. 2006, ApJS, 166, 298

Katz, J. I. 1994a, ApJL, 432, L107

Katz, J. I. 1994b, ApJ, 422, 248

Katz, J. I. & Piran, T. 1997, ApJ, 490, 772

Kirk, J. G., Guthmann, A. W., Gallant, Y. A., & Achterberg, A. 2000, ApJ, 542, 235

Klebesadel, R. W., Strong, I. B., & Olson, R. A. 1973, ApJL, 182, L85

Klein, O. & Nishina, T. 1929, Zeitschrift fur Physik, 52, 853

Kouveliotou, C., Meegan, C. A., Fishman, G. J., et al. 1993, ApJL, 413, L101

Lazzati, D., Covino, S., & Ghisellini, G. 2002, MNRAS, 330, 583

Lazzati, D., Morsony, B. J., Margutti, R., & Begelman, M. C. 2013, ApJ, 765, 103

Levan, A. J., Tanvir, N. R., Starling, R. L. C., et al. 2014, ApJ, 781, 13

Liang, E. & Kargatis, V. 1996, Nature, 381, 49

Lithwick, Y. & Sari, R. 2001, ApJ, 555, 540

Lloyd, N. M. & Petrosian, V. 2000, ApJ, 543, 722

Longair, M. S. 1981, High Energy Astrophysics

Lu, R.-J., Hou, S.-J., & Liang, E.-W. 2010, ApJ, 720, 1146

Lu, R.-J., Wei, J.-J., Liang, E.-W., et al. 2012, ApJ, 756, 112

Lyutikov, M. & Blandford, R. 2003, arXiv:0312347

MacFadyen, A. I. & Woosley, S. E. 1999, ApJ, 524, 262

Medvedev, M. V. 2000, ApJ, 540, 704

Meegan, C., Lichti, G., Bhat, P. N., et al. 2009, ApJ, 702, 791

Meegan, C. A., Fishman, G. J., Wilson, R. B., et al. 1992, Nature, 355, 143

Meszaros, P., Laguna, P., & Rees, M. J. 1993, ApJ, 415, 181

Mészáros, P., Ramirez-Ruiz, E., Rees, M. J., & Zhang, B. 2002, ApJ, 578, 812

Meszaros, P. & Rees, M. J. 1993, ApJL, 418, L59

Mészáros, P., Rees, M. J., & Wijers, R. A. M. J. 1998, ApJ, 499, 301

Metzger, M. R., Djorgovski, S. G., Kulkarni, S. R., et al. 1997, Nature, 387, 878

Nava, L., Ghirlanda, G., Ghisellini, G., & Celotti, A. 2011, A&A, 530, A21

Nousek, J. A., Kouveliotou, C., Grupe, D., et al. 2006, ApJ, 642, 389

Paczynski, B. 1986, ApJL, 308, L43

Paczynski, B. & Rhoads, J. E. 1993, ApJL, 418, L5

Pe'er, A. 2015, Advances in Astronomy, 2015, 22

Pe'er, A., Barlow, H., O'Mahony, S., et al. 2015, ApJ, 813, 127

Pe'er, A., Mészáros, P., & Rees, M. J. 2006, ApJ, 642, 995

Pe'er, A. & Ryde, F. 2011, ApJ, 732, 49

Pe'er, A., Zhang, B.-B., Ryde, F., et al. 2012, MNRAS, 420, 468

Pendleton, G. N., Paciesas, W. S., Briggs, M. S., et al. 1994, ApJ, 431, 416

Peng, F.-K., Liang, E.-W., Wang, X.-Y., et al. 2014, ApJ, 795, 155

Peng, Z. Y., Yin, Y., Bi, X. W., et al. 2010, ApJ, 718, 894

Piran, T. 1999, Phys. Rep., 314, 575

Piran, T. 2004, Reviews of Modern Physics, 76, 1143

Preece, R., Burgess, J. M., von Kienlin, A., et al. 2014, Science, 343, 51

Preece, R. D., Briggs, M. S., Giblin, T. W., et al. 2002, ApJ, 581, 1248

Preece, R. D., Briggs, M. S., Mallozzi, R. S., et al. 1998a, ApJL, 506, L23

Preece, R. D., Briggs, M. S., Mallozzi, R. S., et al. 2000, ApJS, 126, 19

Preece, R. D., Briggs, M. S., Pendleton, G. N., et al. 1996, ApJ, 473, 310

Preece, R. D., Pendleton, G. N., Briggs, M. S., et al. 1998b, ApJ, 496, 849

Racusin, J. L., Karpov, S. V., Sokolowski, M., et al. 2008, Nature, 455, 183

Rees, M. J. & Meszaros, P. 1992, MNRAS, 258, 41P

Rees, M. J. & Meszaros, P. 1994, ApJL, 430, L93

Rhoads, J. E. 1997, ApJL, 487, L1

Ryan, G., van Eerten, H., MacFadyen, A., & Zhang, B.-B. 2015, ApJ, 799, 3

Rybicki, G. B. & Lightman, A. P. 1979, Radiative Processes in Astrophysics

Ryde, F. 1999, Astrophysical Letters and Communications, 39, 281

Ryde, F. 2005, ApJL, 625, L95

Ryde, F., Pe'er, A., Nymark, T., et al. 2011, MNRAS, 415, 3693

Sacahui, J. R., González, M. M., Fraija, N., Ramirez, J. L., & Lee, W. H. 2013, in EAS Publications Series, Vol. 61, EAS Publications Series, ed. A. J. Castro-Tirado, J. Gorosabel, & I. H. Park, 301–305

Sakamoto, T., Barthelmy, S. D., Barbier, L., et al. 2008, ApJS, 175, 179

Sakamoto, T., Barthelmy, S. D., Baumgartner, W. H., et al. 2011, ApJS, 195, 2

Sari, R., Piran, T., & Narayan, R. 1998, ApJL, 497, L17

Spearman, C. 1904, The American Journal of Psychology, 15, 72

Spitkovsky, A. 2008, ApJL, 682, L5

Starling, R. L. C., Page, K. L., Pe'Er, A., Beardmore, A. P., & Osborne, J. P. 2012, MNRAS, 427, 2950

Stratta, G., Gendre, B., Atteia, J. L., et al. 2013, ApJ, 779, 66

Summerlin, E. J. & Baring, M. G. 2012, ApJ, 745, 63

Tanvir, N. R. 2013, arXiv:1307.6156

Tavani, M. 1995, Ap&SS, 231, 181

Tavani, M. 1996, ApJ, 466, 768

Tegmark, M., Hartmann, D. H., Briggs, M. S., & Meegan, C. A. 1996, ApJ, 468, 214

Thompson, C. 1994, MNRAS, 270, 480

Uhm, Z. L. & Zhang, B. 2014, Nature Physics, 10, 351

van den Bergh, S. 1983, Ap. Space Sci., 97, 385

van Eerten, H. J. 2015, Journal of High Energy Astrophysics, 7, 23

van Eerten, H. J. & Wijers, R. A. M. J. 2009, MNRAS, 394, 2164

von Kienlin, A., Meegan, C. A., Paciesas, W. S., et al. 2014, ApJS, 211, 13

Vurm, I. & Beloborodov, A. M. 2015, arXiv:1506.01107

Vurm, I., Beloborodov, A. M., & Poutanen, J. 2011, ApJ, 738, 77

Waxman, E. 1997a, ApJL, 485, L5

Waxman, E. 1997b, ApJL, 489, L33

Wijers, R. A. M. J., Rees, M. J., & Meszaros, P. 1997, MNRAS, 288, L51

Woosley, S. E. 1993, ApJ, 405, 273

Woosley, S. E. 1996, in American Institute of Physics Conference Series, Vol. 384, American Institute of Physics Conference Series, ed. C. Kouveliotou, M. F. Briggs, & G. J. Fishman, 709–718

Yonetoku, D., Murakami, T., Nakamura, T., et al. 2004, ApJ, 609, 935

Yu, H.-F., Greiner, J., van Eerten, H., et al. 2015a, A&A, 573, A81

Yu, H.-F., Preece, R. D., Greiner, J., et al. submitted, A&A

Yu, H.-F., van Eerten, H. J., Greiner, J., et al. 2015b, A&A, 583, A129

Zhang, B. 2014, International Journal of Modern Physics D, 23, 1430002

Zhang, B.-B., Uhm, Z. L., Connaughton, V., Briggs, M. S., & Zhang, B. 2016, ApJ, 816, 72

Acknowledgements

I never believed I would be writing my Ph.D. dissertation here in Garching bei München, Germany. I was an ordinary kid grown up in an old small town, Sai Ying Pun in Hong Kong. I built up my passion for physics only during the last two years in secondary school. I remember that day I randomly read Richard Feynman's book in a book store, when I didn't even know who is this guy. But he changed my life. This guy is so cool, I thought, I wanna be just like him. Of course, I am not a magician nor a genius like him, but I feel happy and touched every time I think about physics, and I know this is what I wanna do.

Time flies. Three years have passed since the day we arrived in Munich. Six years since I graduated from university, and nine years since I left school. I cannot fully describe here the supports I got from many people during this long and sometimes struggling journey. But I am really thankful to my parents, Maria Ma and Barry Yu, who let me study and do whatever I like in my own way, and never stop to show their unlimited loves and supports. I owe them for everything they have sacrificed for me in the past twenty-eight years, for which I have nothing to return but a "Thank You" from the deepest of my heart. I am lucky to have grown up under the loves of my grandparents who will support me whatever happens. They may not understand physics, but that is not the most important thing. Love is, and my family obviously understands love much more than I do in physics.

But physics is important. I wish to express my most sincere gratitude to Priv.-Doz. Dr. Jochen Greiner for his guidance in the past three years. Without his help and encouragements I cannot be writing this dissertation today. He provided me with excellent physical insights about gamma-ray bursts, guided me in my researches and writings, and gave me a lot of freedom to pursue the topics that interest me. He is never parsimonious in providing learning chances for me, like bringing and sending me to international conferences and giving me opportunities to join various research projects. I am glad having him to be my Ph.D. advisor. I hope I did not cause too many troubles

to him.

I would also like to thank Dr. Hendrik van Eerten for explaining the physics of synchrotron radiation theory to me, collaborated with me, corrected my English in our papers, and gave me useful advices for my career with patience. He also drove me to meetings and let me sleep at the backseat. Most importantly, without his initialization, I would not have written my paper on the spectral sharpness of gamma-ray bursts, which leads to an advancement in the understanding of gamma-ray burst prompt emission mechanism.

I must thank everyone from the *Fermi* GBM Team for their supports and professional knowledge in working on the *Fermi* GBM data. Being a part of the team and working as a Burst Advocate have strengthened my experience in collaboration with international research communities and broadened my knowledge on various high-energy astrophysical sources. My work at the Max-Planck-Institut für extraterrestrische Physik (MPE) is supported by the Deutsche Forschungsgemeinschaft (DFG) Cluster of Excellence "Origin and Structure of the Universe" (`http://www.universe-cluster.de`). Especially I would like to thank Kilian Toelge and Dr. Andreas von Kienlin for the translation of Zusammenfassung. My German level is only A2(1) after three years of life in Munich...

I must also give my heartfelt thanks to Prof. Sun Kwok from the University of Hong Kong, who has provided me opportunities to conduct astronomical researches in his research group after my M.Phil. degree, which helped me to stay in the academia before I continued my study in Germany. His advices, both personal and academic, have been very encouraging and helpful, especially during the times when I was confused and frustrated along the path of scientific research.

Special thanks to Prof. Albert Kong and Dr. Thomas Tam from the National Tsing Hua University in Taiwan, Dr. David Hui from the Chungnam National University in Korea, and Prof. K. S. Cheng from the University of Hong Kong. They provided me opportunities to do observational high-energy astrophysics during my M.Phil. study, through the *Fermi* Asian Network, which equipped me with experience and knowledge in gamma-ray astrophysics. I am grateful to Prof. Kong who trusted my ability and recommended me to Priv.-Doz. Dr. Greiner. Without his help and supports I could not have ended up as a professional astrophysicist.

I must take this opportunity to thank my best friends. My bros from the *Star Punch Football Team* (I must spell this brilliant name out in this dissertation, for Nature cannot be fooled) always support me by broken jokes, football games, watching the computer A.I. burning my city center in *Age of Empires*, and the beers and midnight snacks and chats in Hong Kong. Thank you *Physics*

Guys, the crazy times we spent in the Physics Society Room, Room 522, Chemistry and Main Library, and canteens are invaluable. Since this is obviously a serious academic publication, I must specially thank Frank Chan for the good old days we studied together; Fanny Au, Sogo Lau, and Kai-Yan Lee for the unforgettable all-nighters doing revisions for exams; Cyril Lee for his professional guidance in beer selection; *The Three Magi* in Europe for killing time and exchanging academic frustration; MPE/MPA guys for bouldering and climbing with me; everyone in the MPE GRB group for the amazing (research meeting and beer crawling) trips to various European cities; *Dr.* J. Michael Burgess for his bed and the fun time in Stockholm; Joseph Lit, Alex Cheng, Anny Tsoi, Mr. & Mrs. Cheung, Frederick Fung, Keith Ng, Isaac "Kerry" Mok, Eric "Box" Ma, and many others for just being there for me in my life. Sorry I can't list all your names here but I am really proud to have you guys to be my friends.

Finally, Peggy Chan, I love you. We came to Munich together, and I have many things yet to say to you. I will save these words for the moment, but just end by quoting the first lines from the first movie we watched at our home, *Contact*:

"CQ, this is W9GFO. CQ, this is W9GFO here. Come back?"

Appendix A

Long Tables

"I want to know how God created this world. I'm not interested in this or that phenomenon, in the spectrum of this or that element. I want to know His thoughts, the rest are details."

- Albert Einstein

Table A.1: Time-resolved spectral analysis results of the BEST models (Ch. 2). Column (1) lists the GRB names using the *Fermi* GBM trigger designation. Column (2) lists the spectrum numbers within individual burst. Column (3) lists the start times $T_{\rm start}$ and end times $T_{\rm stop}$ for the time bins. Column (4) lists the BEST models. Columns (5) - (9) list the best-fit parameters of the BEST models, if applicable. Column (10) lists the values of CSTAT per degrees of freedom. Columns (11) and (12) list the 10 keV - 1 MeV photon and energy fluxes, respectively.

GRB name	spectrum	$T_{\rm start}$:$T_{\rm stop}$ (s)	BEST model	A (ph s^{-1} cm^{-2} keV^{-1})	α	β	$E_{\rm p}$ (keV)	$E_{\rm b}$ (keV)	CSTAT/dof	photon flux (ph s^{-1} cm^{-2})	energy flux (erg s^{-1} cm^{-2})
(1)	(2)	(3)	(4)	(5)	(6)	(7)	(8)	(9)	(10)	(11)	(12)
080817161	1	-6.144:4.344	COMP	0.0067 ± 0.0010	-0.835 ± 0.060	-	637.80 ± 96.70	-	570.4/480	2.1682±0.24	5.7087E-07±5.5E-08
080817161	2	4.344:5.885	COMP	0.0313 ± 0.0034	-0.829 ± 0.047	-	668.50 ± 79.10	-	492.51/480	10.172±0.82	2.7450E-06±1.8E-07
080817161	3	5.885:7.150	COMP	0.0444 ± 0.0053	-0.827 ± 0.048	-	512.90 ± 53.90	-	529.13/480	13.263±1.1	3.1743E-06±2.2E-07
080817161	4	7.150:8.200	SBPL	0.0439 ± 0.0048	-0.863 ± 0.056	-2.121 ± 0.122	388.69 ± 137.52	191.10 ± 30.90	517.04/479	15.266±1.4	3.3723E-06±2.6E-07
080817161	5	8.200:10.956	COMP	0.0303 ± 0.0049	-0.871 ± 0.057	-	348.20 ± 36.10	-	522.13/480	8.1164±0.93	1.5151E-06±1.4E-07
080817161	6	10.956:12.591	COMP	0.0288 ± 0.0041	-0.865 ± 0.052	-	479.60 ± 56.60	-	497.74/480	8.5970±0.92	1.9294E-06±1.7E-07
080817161	7	12.591:13.934	COMP	0.0380 ± 0.0050	-0.859 ± 0.051	-	482.40 ± 54.60	-	491.33/480	11.319±1.1	2.5594E-06±2.0E-07
080817161	8	13.934:15.019	COMP	0.0407 ± 0.0048	-0.865 ± 0.047	-	591.50 ± 69.80	-	547.03/480	12.969±1.1	3.2167E-06±2.3E-07
080817161	9	15.019:16.156	COMP	0.0427 ± 0.0051	-0.964 ± 0.045	-	570.10 ± 72.90	-	522.31/480	14.229±1.3	3.1806E-06±2.3E-07
080817161	10	16.156:17.397	COMP	0.0469 ± 0.0072	-0.864 ± 0.053	-	373.40 ± 38.30	-	468.44/480	12.804±1.4	2.5037E-06±2.3E-07
080817161	11	17.397:18.589	COMP	0.0405 ± 0.0057	-0.922 ± 0.050	-	453.90 ± 53.10	-	587.4/480	12.337±1.3	2.5707E-06±2.2E-07
080817161	12	18.589:20.151	COMP	0.0340 ± 0.0048	-0.941 ± 0.051	-	452.10 ± 55.00	-	492.46/480	10.475±1.1	2.1464E-06±1.9E-07
080817161	13	20.151:24.341	COMP	0.0181 ± 0.0037	-1.111 ± 0.059	-	342.00 ± 52.90	-	515.34/480	5.9592±0.89	9.3062E-07±1.2E-07
080817161	14	24.341:38.891	COMP	0.0100 ± 0.0035	-1.114 ± 0.086	-	199.20 ± 29.90	-	582.59/480	2.8180±0.73	3.2728E-07±7.6E-08
080817161	15	38.891:54.190	COMP	0.0042 ± 0.0014	-1.248 ± 0.072	-	347.90 ± 87.60	-	552.78/480	1.6091±0.45	2.2790E-07±5.8E-08
080817161	16	54.190:89.088	none	-	-	-	-	-	-	-	-
080825593	1	-1.024:1.603	COMP	0.0398 ± 0.0095	-0.731 ± 0.074	-	255.50 ± 23.70	-	493.97/477	8.2295±1.5	1.3560E-06±2.3E-07
080825593	2	1.603:2.057	SBPL	0.0955 ± 0.0120	-0.690 ± 0.082	-2.064 ± 0.123	306.20 ± 109.70	132.20 ± 21.40	505.72/476	29.878±3.4	6.3902E-06±6.3E-07
080825593	3	2.057:2.803	COMP	0.1215 ± 0.0244	-0.746 ± 0.065	-	245.40 ± 19.60	-	495.88/477	24.921±3.6	3.9609E-06±5.1E-07
080825593	4	2.803:3.274	BAND	0.2632 ± 0.0513	-0.342 ± 0.095	-2.358 ± 0.187	221.50 ± 19.90	138.09 ± 15.75	474.72/476	36.202±4.0	7.2656E-06±6.9E-07
080825593	5	3.274:3.872	COMP	0.1436 ± 0.0301	-0.611 ± 0.071	-	236.50 ± 17.60	-	480.67/477	25.445±3.8	4.1833E-06±5.6E-07
080825593	6	3.872:4.874	COMP	0.0784 ± 0.0213	-0.715 ± 0.073	-	211.90 ± 16.70	-	496.93/477	14.439±3.1	2.0897E-06±4.3E-07
080825593	7	4.874:5.922	COMP	0.1599 ± 0.0400	-0.570 ± 0.076	-	178.60 ± 10.90	-	605.74/477	22.731±4.1	3.0521E-06±5.1E-07
080825593	8	5.922:9.502	COMP	0.0522 ± 0.0193	-0.764 ± 0.088	-	158.30 ± 12.50	-	463.8/477	8.6524±2.6	9.9428E-07±2.8E-07
080825593	9	9.502:11.986	COMP	0.0915 ± 0.0242	-0.626 ± 0.084	-	182.40 ± 13.10	-	507.55/477	14.033±2.6	1.8776E-06±3.1E-07
080825593	10	11.986:14.806	COMP	0.0469 ± 0.0119	-0.765 ± 0.077	-	225.40 ± 20.60	-	498.84/477	9.3886±1.8	1.3910E-06±2.4E-07
080825593	11	14.806:16.323	COMP	0.1046 ± 0.0314	-0.585 ± 0.078	-	168.30 ± 10.30	-	531.15/477	14.535±3.4	1.8539E-06±4.2E-07
080825593	12	16.323:19.254	PL	0.0041 ± 0.0013	-1.491 ± 0.020	-	-	-	728.52/478	2.3032±0.73	3.7496E-07±1.2E-07
080825593	13	19.254:25.254	SBPL	0.0237 ± 0.0086	-1.052 ± 0.099	-2.900 ± 0.504	116.79 ± 37.57	111.30 ± 29.80	489.43/476	9.4644±3.2	9.9675E-07±2.9E-07
080825593	14	25.254:37.888	none	-	-	-	-	-	-	-	-
080916009	1	-1.024:1.524	COMP	0.0247 ± 0.0041	-0.658 ± 0.071	-	501.70 ± 70.20	-	413.71/360	6.7276±0.77	1.8071E-06±1.7E-07
080916009	2	1.524:2.442	COMP	0.0493 ± 0.0081	-0.705 ± 0.066	-	477.10 ± 63.20	-	409.69/360	13.419±1.5	3.3883E-06±3.2E-07
080916009	3	2.442:3.280	COMP	0.0461 ± 0.0069	-0.777 ± 0.059	-	594.40 ± 89.00	-	341.97/360	14.138±1.5	3.7874E-06±3.3E-07
080916009	4	3.280:4.278	COMP	0.0524 ± 0.0077	-0.700 ± 0.062	-	525.50 ± 67.80	-	404.72/360	14.837±1.5	3.9673E-06±3.1E-07

Continued on next page

Table A.1 – continued from previous page

GRB name	spectrum	T_{start}:T_{stop} (s)	BEST model	A (ph s^{-1} cm^{-2} keV^{-1})	α	β	E_p (keV)	E_b (keV)	CSTAT/dof	photon flux (ph s^{-1} cm^{-2})	energy flux (erg s^{-1} cm^{-2})
(1)	(2)	(3)	(4)	(5)	(6)	(7)	(8)	(9)	(10)	(11)	(12)
080916009	5	4.278:5.305	BAND	0.0263 ± 0.0033	−0.914 ± 0.050	−2.025 ± 0.165	1682.00 ± 532.00	861.12 ± 280.14	373.01/359	10.582±1.0	3.3983E-06±2.8E-07
080916009	6	5.305:6.200	COMP	0.0347 ± 0.0036	−1.307 ± 0.029	-	3268.00 ± 777.00	-	383.91/360	16.852±1.8	3.4618E-06±3.1E-07
080916009	7	6.200:7.387	COMP	0.0307 ± 0.0057	−1.151 ± 0.054	-	744.50 ± 224.00	-	380.38/360	12.152±1.7	2.4723E-06±2.9E-07
080916009	8	7.387:9.391	COMP	0.0165 ± 0.0022	−1.264 ± 0.033	-	2538.00 ± 797.00	-	347.08/360	7.7312±1.0	1.6617E-06±1.9E-07
080916009	9	9.391:12.023	COMP	0.0119 ± 0.0016	−1.297 ± 0.030	-	4714.00 ± 1440.00	-	461.84/360	5.7881±0.81	1.2294E-06±1.5E-07
080916009	10	12.023:14.837	COMP	0.0123 ± 0.0027	−1.085 ± 0.062	-	832.30 ± 284.00	-	367.64/360	4.7653±0.82	1.0755E-06±1.6E-07
080916009	11	14.837:17.692	SBPL	0.0158 ± 0.0027	−1.104 ± 0.068	−1.757 ± 0.092	-	189.00 ± 70.30	411.53/359	6.5352±0.96	1.3767E-06±1.7E-07
080916009	12	17.692:20.281	COMP	0.0243 ± 0.0060	−0.987 ± 0.072	-	366.00 ± 70.10	-	406.43/360	7.2882±1.3	1.2921E-06±1.9E-07
080916009	13	20.281:22.466	COMP	0.0276 ± 0.0057	−0.897 ± 0.069	-	439.30 ± 78.60	-	388.05/360	8.1611±1.2	1.7059E-06±2.0E-07
080916009	14	22.466:24.214	COMP	0.0182 ± 0.0041	−1.064 ± 0.062	-	633.60 ± 176.00	-	372.9/360	6.6074±1.2	1.3997E-06±2.1E-07
080916009	15	24.214:26.288	COMP	0.0208 ± 0.0045	−1.007 ± 0.065	-	533.20 ± 123.00	-	363.17/360	7.0274±1.1	1.4694E-06±2.0E-07
080916009	16	26.288:28.948	COMP	0.0198 ± 0.0045	−1.093 ± 0.066	-	507.00 ± 133.00	-	394.55/360	7.0113±1.2	1.3273E-06±1.8E-07
080916009	17	28.948:31.730	COMP	0.0122 ± 0.0025	−1.117 ± 0.057	-	955.20 ± 349.00	-	363.14/360	4.8843±0.82	1.1017E-06±1.6E-07
080916009	18	31.730:35.075	COMP	0.0194 ± 0.0053	−1.060 ± 0.073	-	356.90 ± 77.40	-	414.26/360	6.1631±1.2	1.0221E-06±1.7E-07
080916009	19	35.075:38.517	COMP	0.0151 ± 0.0029	−1.034 ± 0.062	-	690.50 ± 187.00	-	407.55/360	5.4798±0.80	1.2319E-06±1.5E-07
080916009	20	38.517:43.426	COMP	0.0119 ± 0.0024	−1.026 ± 0.065	-	672.50 ± 186.00	-	405.41/360	4.2752±0.66	9.5987E-07±1.2E-07
080916009	21	43.426:47.931	COMP	0.0143 ± 0.0036	−0.840 ± 0.080	-	399.90 ± 74.20	-	424.88/360	3.9500±0.73	8.1782E-07±1.3E-07
080916009	22	47.931:57.730	none	-	-	-	-	-	-	-	-
080916009	23	57.730:64.794	COMP	0.0090 ± 0.0034	−1.048 ± 0.088	-	312.70 ± 74.10	-	409.93/360	2.7108±0.82	4.2255E-07±1.2E-07
080916009	24	64.794:87.040	none	-	-	-	-	-	-	-	-
081009140	1	-1.024:0.792	none	-	-	-	-	-	-	-	-
081009140	2	0.792:1.224	none	-	-	-	-	-	-	-	-
081009140	3	1.224:1.473	none	-	-	-	-	-	-	-	-
081009140	4	1.473:1.666	none	-	-	-	-	-	-	-	-
081009140	5	1.666:1.831	none	-	-	-	-	-	-	-	-
081009140	6	1.831:1.965	none	-	-	-	-	-	-	-	-
081009140	7	1.965:2.076	none	-	-	-	-	-	-	-	-
081009140	8	2.076:2.176	none	-	-	-	-	-	-	-	-
081009140	9	2.176:2.274	none	-	-	-	-	-	-	-	-
081009140	10	2.274:2.372	none	-	-	-	-	-	-	-	-
081009140	11	2.372:2.471	none	-	-	-	-	-	-	-	-
081009140	12	2.471:2.560	none	-	-	-	-	-	-	-	-
081009140	13	2.560:2.657	PL	0.0720 ± 0.0282	−1.839 ± 0.029	-	-	-	547.97/359	57.826±23.0	5.4264E-06±2.1E-06
081009140	14	2.657:2.746	none	-	-	-	-	-	-	-	-
081009140	15	2.746:2.825	none	-	-	-	-	-	-	-	-
081009140	16	2.825:2.906	PL	0.0696 ± 0.0252	−1.747 ± 0.028	-	-	-	512.24/359	50.290±19.0	5.4266E-06±2.0E-06
081009140	17	2.906:2.992	none	-	-	-	-	-	-	-	-
081009140	18	2.992:3.085	none	-	-	-	-	-	-	-	-
081009140	19	3.085:3.182	none	-	-	-	-	-	-	-	-
081009140	20	3.182:3.281	none	-	-	-	-	-	-	-	-
081009140	21	3.281:3.392	none	-	-	-	-	-	-	-	-
081009140	22	3.392:3.507	none	-	-	-	-	-	-	-	-
081009140	23	3.507:3.628	none	-	-	-	-	-	-	-	-

Continued on next page

Table A.1 – continued from previous page

GRB name	spectrum	T_{start}:T_{stop}	BEST	A	α	β	E_p	E_b	CSTAT/dof	photon flux	energy flux
		(s)	model	(ph s^{-1} cm^{-2} keV^{-1})			(keV)	(keV)		(ph s^{-1} cm^{-2})	(erg s^{-1} cm^{-2})
(1)	(2)	(3)	(4)	(5)	(6)	(7)	(8)	(9)	(10)	(11)	(12)
081009140	24	3.628:3.747	none	-	-	-	-	-	-	-	-
081009140	25	3.747:3.864	none	-	-	-	-	-	-	-	-
081009140	26	3.864:3.978	none	-	-	-	-	-	-	-	-
081009140	27	3.978:4.099	none	-	-	-	-	-	-	-	-
081009140	28	4.099:4.223	none	-	-	-	-	-	-	-	-
081009140	29	4.223:4.346	none	-	-	-	-	-	-	-	-
081009140	30	4.346:4.474	none	-	-	-	-	-	-	-	-
081009140	31	4.474:4.595	none	-	-	-	-	-	-	-	-
081009140	32	4.595:4.714	none	-	-	-	-	-	-	-	-
081009140	33	4.714:4.839	none	-	-	-	-	-	-	-	-
081009140	34	4.839:4.979	none	-	-	-	-	-	-	-	-
081009140	35	4.979:5.125	none	-	-	-	-	-	-	-	-
081009140	36	5.125:5.278	none	-	-	-	-	-	-	-	-
081009140	37	5.278:5.444	none	-	-	-	-	-	-	-	-
081009140	38	5.444:5.629	none	-	-	-	-	-	-	-	-
081009140	39	5.629:5.863	none	-	-	-	-	-	-	-	-
081009140	40	5.863:6.106	none	-	-	-	-	-	-	-	-
081009140	41	6.106:6.362	none	-	-	-	-	-	-	-	-
081009140	42	6.362:6.656	none	-	-	-	-	-	-	-	-
081009140	43	6.656:6.993	none	-	-	-	-	-	-	-	-
081009140	44	6.993:7.488	none	-	-	-	-	-	-	-	-
081009140	45	7.488:11.264	none	-	-	-	-	-	-	-	-
081009140	46	32.768:39.934	none	-	-	-	-	-	-	-	-
081009140	47	39.934:40.696	none	-	-	-	-	-	-	-	-
081009140	48	40.696:41.290	none	-	-	-	-	-	-	-	-
081009140	49	41.290:41.769	none	-	-	-	-	-	-	-	-
081009140	50	41.769:42.236	none	-	-	-	-	-	-	-	-
081009140	51	42.236:42.708	none	-	-	-	-	-	-	-	-
081009140	52	42.708:43.272	none	-	-	-	-	-	-	-	-
081009140	53	43.272:43.858	none	-	-	-	-	-	-	-	-
081009140	54	43.858:44.496	none	-	-	-	-	-	-	-	-
081009140	55	44.496:45.512	none	-	-	-	-	-	-	-	-
081009140	56	45.512:47.246	none	-	-	-	-	-	-	-	-
081009140	57	47.246:55.296	none	-	-	-	-	-	-	-	-
081124060	1	-3.072:1.751	none	-	-	-	-	-	-	-	-
081124060	2	1.751:3.787	none	-	-	-	-	-	-	-	-
081124060	3	3.787:6.145	none	-	-	-	-	-	-	-	-
081124060	4	6.145:9.855	none	-	-	-	-	-	-	-	-
081124060	5	9.855:11.601	none	-	-	-	-	-	-	-	-
081124060	6	11.601:12.398	none	-	-	-	-	-	-	-	-
081124060	7	12.398:13.148	none	-	-	-	-	-	-	-	-
081124060	8	13.148:14.081	none	-	-	-	-	-	-	-	-
081124060	9	14.081:15.050	none	-	-	-	-	-	-	-	-

Continued on next page

Table A.1 – continued from previous page

GRB name	spectrum	T_{start}:T_{stop} (s)	BEST model	A (ph s^{-1} cm^{-2} keV^{-1})	α	β	E_p (keV)	E_b (keV)	CSTAT/dof	photon flux (ph s^{-1} cm^{-2})	energy flux (erg s^{-1} cm^{-2})
(1)	(2)	(3)	(4)	(5)	(6)	(7)	(8)	(9)	(10)	(11)	(12)
081124060	10	15.050:16.379	none	-	-	-	-	-	-	-	-
081124060	11	16.379:21.047	none	-	-	-	-	-	-	-	-
081124060	12	21.047:28.672	none	-	-	-	-	-	-	-	-
081125496	1	-1.024:1.766	COMP	0.0365 ± 0.0074	-0.549 ± 0.099	-	362.20 ± 46.00	-	382.4/357	7.9540±1.0	1.8552E-06±1.8E-07
081125496	2	1.766:2.406	COMP	0.1714 ± 0.0363	-0.247 ± 0.102	-	262.60 ± 20.90	-	358.3/357	24.450±3.0	5.0687E-06±4.8E-07
081125496	3	2.406:2.939	COMP	0.3604 ± 0.0862	-0.023 ± 0.114	-	211.20 ± 13.30	-	374.68/357	35.261±4.6	6.4840E-06±6.8E-07
081125496	4	2.939:3.615	COMP	0.3372 ± 0.1270	-0.064 ± 0.132	-	157.10 ± 10.30	-	415.03/357	24.927±5.9	3.4839E-06±7.5E-07
081125496	5	3.615:4.534	PL	0.0069 ± 0.0021	-1.447 ± 0.032	-	-	-	541.67/358	3.7802±1.2	6.5998E-07±2.0E-07
081125496	6	4.534:5.593	PL	0.0103 ± 0.0025	-1.483 ± 0.034	-	-	-	563.57/358	5.7979±1.5	9.5561E-07±2.2E-07
081125496	7	5.593:6.695	none	-	-	-	-	-	-	-	-
081125496	8	6.695:12.288	none	-	-	-	-	-	-	-	-
081207680	1	-5.120:12.357	COMP	0.0142 ± 0.0042	0.098 ± 0.147	-	244.20 ± 20.10	-	597.18/357	1.5019±0.28	3.2644E-07±5.4E-08
081207680	2	12.357:22.424	COMP	0.0124 ± 0.0021	-0.292 ± 0.092	-	401.40 ± 38.00	-	501.84/357	2.5508±0.27	7.3378E-07±6.5E-08
081207680	3	22.424:30.383	BAND	0.0207 ± 0.0040	-0.129 ± 0.123	-2.060 ± 0.128	335.80 ± 40.70	176.02 ± 22.04	380.9/356	3.5702±0.32	1.0782E-06±7.8E-08
081207680	4	30.383:36.765	COMP	0.0108 ± 0.0013	-0.702 ± 0.057	-	848.90 ± 122.00	-	433.38/357	3.6447±0.31	1.2123E-06±8.3E-08
081207680	5	36.765:42.155	COMP	0.0107 ± 0.0013	-0.738 ± 0.058	-	874.30 ± 139.00	-	311.23/357	3.6584±0.34	1.1908E-06±9.1E-08
081207680	6	42.155:48.744	COMP	0.0126 ± 0.0017	-0.624 ± 0.065	-	591.30 ± 73.30	-	382.79/357	3.6544±0.35	1.1021E-06±8.3E-08
081207680	7	48.744:56.238	COMP	0.0099 ± 0.0016	-0.805 ± 0.063	-	615.10 ± 102.00	-	471.89/357	3.1177±0.36	8.3066E-07±7.9E-08
081207680	8	56.238:64.930	COMP	0.0084 ± 0.0014	-0.918 ± 0.060	-	734.70 ± 154.00	-	473.85/357	2.9060±0.35	7.5081E-07±7.4E-08
081207680	9	64.930:80.441	COMP	0.0073 ± 0.0020	-0.878 ± 0.093	-	382.00 ± 80.30	-	447.32/357	2.0242±0.38	3.9800E-07±6.0E-08
081207680	10	80.441:112.640	none	-	-	-	-	-	-	-	-
081215784	1	-3.072:1.414	COMP	0.0136 ± 0.0009	-0.793 ± 0.036	-	1443.00 ± 151.00	-	479.26/477	5.2806±0.31	1.8778E-06±8.7E-08
081215784	2	1.414:1.493	BAND	0.3859 ± 0.0267	-0.365 ± 0.043	-2.629 ± 0.152	942.30 ± 70.00	653.53 ± 59.18	448.68/476	137.17±6.6	6.1365E-05±2.4E-06
081215784	3	1.493:1.574	SBPL	0.3485 ± 0.0245	-0.466 ± 0.043	-2.376 ± 0.100	643.11 ± 80.89	393.90 ± 40.20	458.3/476	138.82±7.2	5.5354E-05±2.2E-06
081215784	4	1.574:1.704	BAND	0.3623 ± 0.0383	-0.400 ± 0.057	-2.240 ± 0.087	499.00 ± 44.30	290.57 ± 26.96	533.15/476	90.636±5.4	2.9221E-05±1.4E-06
081215784	5	1.704:1.926	BAND	0.2672 ± 0.0365	-0.498 ± 0.065	-2.308 ± 0.124	358.30 ± 34.50	219.36 ± 23.25	464.13/476	56.904±4.3	1.4281E-05±8.6E-07
081215784	6	1.926:2.437	BAND	0.2202 ± 0.0382	-0.453 ± 0.086	-2.137 ± 0.097	210.00 ± 19.40	117.90 ± 11.40	552.38/476	32.522±3.0	6.3295E-06±4.9E-07
081215784	7	2.437:3.159	COMP	0.0835 ± 0.0114	-0.874 ± 0.046	-	336.50 ± 27.70	-	542.3/477	22.095±2.2	4.0362E-06±3.4E-07
081215784	8	3.159:3.643	COMP	0.1328 ± 0.0158	-0.648 ± 0.048	-	368.20 ± 25.10	-	539.34/477	31.016±2.5	6.9123E-06±4.5E-07
081215784	9	3.643:3.913	COMP	0.2312 ± 0.0226	-0.571 ± 0.043	-	424.30 ± 25.00	-	527.36/477	55.739±3.8	1.4312E-05±7.6E-07
081215784	10	3.913:4.365	COMP	0.2762 ± 0.0478	-0.515 ± 0.060	-	207.70 ± 10.60	-	525.9/477	41.130±4.7	6.3428E-06±6.3E-07
081215784	11	4.365:4.821	COMP	0.1460 ± 0.0216	-0.670 ± 0.053	-	280.90 ± 18.30	-	526.6/477	30.062±3.1	5.4689E-06±4.8E-07
081215784	12	4.821:5.092	COMP	0.1947 ± 0.0208	-0.515 ± 0.048	-	395.90 ± 23.40	-	477.15/477	43.895±3.3	1.1114E-05±6.8E-07
081215784	13	5.092:5.225	COMP	0.3067 ± 0.0247	-0.551 ± 0.039	-	599.50 ± 36.20	-	522.62/477	87.595±5.2	2.8017E-05±1.3E-06
081215784	14	5.225:5.460	SBPL	0.2346 ± 0.0230	-0.587 ± 0.062	-2.525 ± 0.137	233.15 ± 30.36	164.70 ± 17.90	511.01/476	67.244±5.6	1.4142E-05±9.6E-07
081215784	15	5.460:6.208	COMP	0.1181 ± 0.0200	-0.747 ± 0.055	-	232.30 ± 14.80	-	514.57/477	23.612±2.8	3.6027E-06±3.8E-07
081215784	16	6.208:7.661	BAND	0.1563 ± 0.0363	-0.713 ± 0.101	-2.380 ± 0.165	120.20 ± 11.10	81.39 ± 9.66	510.65/476	21.249±3.6	2.5136E-06±3.6E-07
081215784	17	7.661:12.288	none	-	-	-	-	-	-	-	-
081221681	1	-1.024:5.695	PL	0.0020 ± 0.0007	-1.563 ± 0.026	-	-	-	573.26/361	1.1728±0.43	1.6939E-07±6.0E-08
081221681	2	5.695:15.558	none	-	-	-	-	-	-	-	-
081221681	3	15.558:17.846	none	-	-	-	-	-	-	-	-
081221681	4	17.846:18.544	PL	0.0061 ± 0.0023	-1.557 ± 0.029	-	-	-	646.41/361	3.6137±1.4	5.2670E-07±2.0E-07
081221681	5	18.544:19.124	none	-	-	-	-	-	-	-	-

Continued on next page

Table A.1 – continued from previous page

GRB name	spectrum	T_{start}:T_{stop} (s)	BEST model	A (ph s^{-1} cm^{-2} keV^{-1})	α	β	E_p (keV)	E_b (keV)	CSTAT/dof	photon flux (ph s^{-1} cm^{-2})	energy flux (erg s^{-1} cm^{-2})
(1)	(2)	(3)	(4)	(5)	(6)	(7)	(8)	(9)	(10)	(11)	(12)
081221681	6	19.124:19.688	PL	0.0078 ± 0.0026	−1.541 ± 0.028	-	-	-	638.69/361	4.5712±1.5	6.8362E-07±2.2E-07
081221681	7	19.688:20.248	none	-	-	-	-	-	-	-	-
081221681	8	20.248:20.720	PL	0.0096 ± 0.0027	−1.527 ± 0.028	-	-	-	534.98/361	5.6117±1.6	8.5835E-07±2.4E-07
081221681	9	20.720:21.140	none	-	-	-	-	-	-	-	-
081221681	10	21.140:21.486	PL	0.0094 ± 0.0031	−1.505 ± 0.029	-	-	-	552.35/361	5.3764±1.8	8.5301E-07±2.8E-07
081221681	11	21.486:21.833	PL	0.0080 ± 0.0031	−1.501 ± 0.029	-	-	-	640.99/361	4.5334±1.8	7.2373E-07±2.8E-07
081221681	12	21.833:22.248	PL	0.0088 ± 0.0031	−1.547 ± 0.029	-	-	-	618.8/361	5.1998±1.9	7.7012E-07±2.7E-07
081221681	13	22.248:22.764	none	-	-	-	-	-	-	-	-
081221681	14	22.764:23.309	none	-	-	-	-	-	-	-	-
081221681	15	23.309:23.828	none	-	-	-	-	-	-	-	-
081221681	16	23.828:24.272	PL	0.0085 ± 0.0031	−1.560 ± 0.028	-	-	-	572.69/361	5.0861±1.9	7.3763E-07±2.6E-07
081221681	17	24.272:24.652	none	-	-	-	-	-	-	-	-
081221681	18	24.652:25.150	none	-	-	-	-	-	-	-	-
081221681	19	25.150:25.728	none	-	-	-	-	-	-	-	-
081221681	20	25.728:26.216	none	-	-	-	-	-	-	-	-
081221681	21	26.216:26.689	none	-	-	-	-	-	-	-	-
081221681	22	26.689:27.191	none	-	-	-	-	-	-	-	-
081221681	23	27.191:27.676	none	-	-	-	-	-	-	-	-
081221681	24	27.676:28.206	none	-	-	-	-	-	-	-	-
081221681	25	28.206:28.771	none	-	-	-	-	-	-	-	-
081221681	26	28.771:29.368	none	-	-	-	-	-	-	-	-
081221681	27	29.368:30.074	none	-	-	-	-	-	-	-	-
081221681	28	30.074:30.881	none	-	-	-	-	-	-	-	-
081221681	29	30.881:32.020	none	-	-	-	-	-	-	-	-
081221681	30	32.020:34.288	none	-	-	-	-	-	-	-	-
081221681	31	34.288:54.272	none	-	-	-	-	-	-	-	-
081224887	1	0.000:1.036	COMP	0.0416 ± 0.0033	−0.244 ± 0.064	-	766.00 ± 54.90	-	566.66/478	13.498±0.74	5.9482E-06±2.5E-07
081224887	2	1.036:1.796	COMP	0.0773 ± 0.0067	−0.149 ± 0.062	-	528.90 ± 29.80	-	502.14/478	19.271±1.1	7.2254E-06±3.2E-07
081224887	3	1.796:2.311	COMP	0.1113 ± 0.0128	−0.218 ± 0.065	-	411.80 ± 25.10	-	459.25/478	22.891±1.7	6.9482E-06±4.1E-07
081224887	4	2.311:2.792	COMP	0.1079 ± 0.0126	−0.367 ± 0.060	-	419.80 ± 28.40	-	520.64/478	23.661±1.8	6.7730E-06±4.2E-07
081224887	5	2.792:3.304	COMP	0.1359 ± 0.0164	−0.416 ± 0.059	-	366.60 ± 23.30	-	463.11/478	27.742±2.2	7.0077E-06±4.4E-07
081224887	6	3.304:3.777	COMP	0.1285 ± 0.0200	−0.532 ± 0.063	-	315.70 ± 23.60	-	517.16/478	25.501±2.6	5.4262E-06±4.6E-07
081224887	7	3.777:4.424	COMP	0.1114 ± 0.0170	−0.609 ± 0.059	-	309.90 ± 23.30	-	477.55/478	23.087±2.3	4.6586E-06±3.9E-07
081224887	8	4.424:5.292	COMP	0.1065 ± 0.0201	−0.645 ± 0.066	-	241.30 ± 17.90	-	521.2/478	19.691±2.5	3.2379E-06±3.5E-07
081224887	9	5.292:6.468	COMP	0.0765 ± 0.0179	−0.570 ± 0.074	-	210.40 ± 14.50	-	514.37/478	12.120±2.1	1.8495E-06±2.9E-07
081224887	10	6.468:8.355	COMP	0.0705 ± 0.0194	−0.665 ± 0.079	-	179.40 ± 13.30	-	491.92/478	11.181±2.2	1.4565E-06±2.6E-07
081224887	11	8.355:13.975	COMP	0.0191 ± 0.0073	−0.988 ± 0.077	-	168.30 ± 16.90	-	526.11/478	4.3257±1.4	4.7851E-07±1.4E-07
081224887	12	13.975:35.840	none	-	-	-	-	-	-	-	-
090131090	1	-1.024:3.299	PL	0.0063 ± 0.0015	−1.724 ± 0.033	-	-	-	438.99/359	4.4277±1.1	4.9673E-07±1.2E-07
090131090	2	3.299:3.892	none	-	-	-	-	-	-	-	-
090131090	3	3.892:6.470	PL	0.0060 ± 0.0024	−1.849 ± 0.035	-	-	-	445.6/359	4.8578±2.0	4.5037E-07±1.8E-07
090131090	4	6.470:6.844	PL	0.0224 ± 0.0077	−1.932 ± 0.036	-	-	-	523.1/359	20.096±7.2	1.6534E-06±5.7E-07
090131090	5	6.844:7.015	none	-	-	-	-	-	-	-	-

Continued on next page

Table A.1 – continued from previous page

GRB name	spectrum	T_{start}:T_{stop} (s)	BEST model	A (ph s^{-1} cm^{-2} keV^{-1})	α	β	E_p (keV)	E_b (keV)	CSTAT/dof	photon flux (ph s^{-1} cm^{-2})	energy flux (erg s^{-1} cm^{-2})
(1)	(2)	(3)	(4)	(5)	(6)	(7)	(8)	(9)	(10)	(11)	(12)
090131090	6	7.015:7.221	none	-	-	-	-	-	-	-	-
090131090	7	7.221:7.523	PL	0.0301 ± 0.0107	−2.051 ± 0.040	-	-	-	534.47/359	31.746±12.0	2.2242E-06±7.9E-07
090131090	8	7.523:9.357	none	-	-	-	-	-	-	-	-
090131090	9	21.504:23.114	COMP	0.0379 ± 0.0112	−1.168 ± 0.078	-	229.00 ± 39.00	-	441.43/358	11.906±2.5	1.4591E-06±2.6E-07
090131090	10	23.114:23.422	COMP	0.2461 ± 0.0894	−1.153 ± 0.088	-	126.80 ± 13.00	-	361.29/358	62.590±16.0	5.5391E-06±1.3E-06
090131090	11	23.422:23.898	SBPL	0.0380 ± 0.0118	−1.156 ± 0.237	−2.149 ± 0.139	70.75 ± 34.03	40.02 ± 15.20	368.52/357	24.866±7.5	2.2986E-06±6.3E-07
090131090	12	23.898:26.171	PL	0.0099 ± 0.0024	−1.795 ± 0.033	-	-	-	562.6/359	7.5285±1.9	7.5678E-07±1.8E-07
090131090	13	26.171:29.260	PL	0.0074 ± 0.0018	−1.747 ± 0.033	-	-	-	481.9/359	5.2932±1.4	5.7315E-07±1.4E-07
090131090	14	29.260:32.944	COMP	0.0422 ± 0.0168	−1.328 ± 0.092	-	135.00 ± 21.80	-	549.23/358	14.206±3.9	1.2373E-06±2.9E-07
090131090	15	32.944:37.138	PL	0.0056 ± 0.0020	−1.876 ± 0.037	-	-	-	487.59/359	4.6896±1.7	4.1817E-07±1.5E-07
090131090	16	37.138:41.984	PL	0.0087 ± 0.0024	−1.936 ± 0.082	-	-	-	495.57/359	7.8243±2.6	6.4037E-07±1.7E-07
090328401	1	-3.072:5.936	COMP	0.0115 ± 0.0015	−0.771 ± 0.056	-	530.50 ± 62.10	-	596.68/478	3.3868±0.31	8.6302E-07±6.4E-08
090328401	2	5.936:11.950	COMP	0.0104 ± 0.0011	−0.843 ± 0.046	-	959.50 ± 143.00	-	617.44/478	3.7400±0.30	1.1366E-06±7.5E-08
090328401	3	11.950:15.372	COMP	0.0217 ± 0.0018	−0.798 ± 0.039	-	868.20 ± 91.70	-	559.98/478	7.5307±0.46	2.3145E-06±1.1E-07
090328401	4	15.372:17.243	COMP	0.0379 ± 0.0040	−0.758 ± 0.045	-	537.00 ± 50.10	-	489.1/478	11.102±0.83	2.8761E-06±1.7E-07
090328401	5	17.243:19.788	COMP	0.0222 ± 0.0026	−0.984 ± 0.043	-	681.00 ± 99.00	-	529.7/478	7.8255±0.70	1.8438E-06±1.4E-07
090328401	6	19.788:22.693	COMP	0.0277 ± 0.0035	−1.046 ± 0.042	-	494.40 ± 64.30	-	568.98/478	9.4164±0.87	1.8420E-06±1.4E-07
090328401	7	22.693:24.369	COMP	0.0394 ± 0.0047	−0.907 ± 0.043	-	503.90 ± 54.50	-	568.75/478	12.264±1.0	2.7290E-06±1.9E-07
090328401	8	24.369:29.123	COMP	0.0160 ± 0.0027	−1.171 ± 0.046	-	448.50 ± 76.80	-	530.7/478	5.9003±0.74	9.9116E-07±1.1E-07
090328401	9	29.123:56.570	PL	0.0014 ± 0.0003	−1.501 ± 0.027	-	-	-	777.71/479	0.78280±0.17	1.2533E-07±2.6E-08
090328401	10	56.570:77.824	none	-	-	-	-	-	-	-	-
090424592	1	-1.024:0.472	COMP	0.2516 ± 0.0979	−0.873 ± 0.086	-	97.66 ± 5.58	-	522.52/478	37.029±10.0	2.9769E-06±8.0E-07
090424592	2	0.472:0.614	BAND	0.5241 ± 0.2080	−0.752 ± 0.094	−3.063 ± 0.441	99.76 ± 6.77	96.39 ± 17.81	501.56/477	65.507±25.0	5.9679E-06±2.1E-06
090424592	3	0.614:0.708	COMP	1.0350 ± 0.2650	−0.740 ± 0.067	-	139.20 ± 7.25	-	484.72/478	154.58±29.0	1.6314E-05±2.8E-06
090424592	4	0.708:0.792	COMP	0.9842 ± 0.2560	−0.833 ± 0.067	-	138.90 ± 7.92	-	444.46/478	166.24±31.0	1.7040E-05±3.0E-06
090424592	5	0.792:0.883	COMP	1.0150 ± 0.2540	−0.852 ± 0.065	-	139.80 ± 7.96	-	465.21/478	176.46±32.0	1.8060E-05±3.0E-06
090424592	6	0.883:0.976	COMP	1.0450 ± 0.2720	−0.783 ± 0.068	-	138.00 ± 7.46	-	468.01/478	164.45±31.0	1.7027E-05±3.0E-06
090424592	7	0.976:1.070	COMP	0.4558 ± 0.0781	−0.950 ± 0.052	-	248.50 ± 20.20	-	465.92/478	115.40±14.0	1.6663E-05±1.8E-06
090424592	8	1.070:1.155	COMP	0.6105 ± 0.1270	−0.838 ± 0.059	-	202.70 ± 14.30	-	465.86/478	125.55±19.0	1.6697E-05±2.2E-06
090424592	9	1.155:1.262	COMP	0.5173 ± 0.1040	−0.930 ± 0.057	-	199.20 ± 14.80	-	474.68/478	117.31±17.0	1.4815E-05±1.9E-06
090424592	10	1.262:1.339	COMP	1.0500 ± 0.1860	−0.502 ± 0.060	-	218.70 ± 12.00	-	456.14/478	159.99±19.0	2.5849E-05±2.6E-06
090424592	11	1.339:1.417	COMP	0.5982 ± 0.0948	−0.758 ± 0.051	-	268.70 ± 18.40	-	460.43/478	130.01±15.0	2.1890E-05±2.1E-06
090424592	12	1.417:1.494	COMP	0.8583 ± 0.1310	−0.667 ± 0.052	-	252.60 ± 15.50	-	454.73/478	166.43±17.0	2.8027E-05±2.4E-06
090424592	13	1.494:1.609	COMP	0.9154 ± 0.2480	−0.615 ± 0.071	-	137.10 ± 6.49	-	426.42/478	114.97±23.0	1.2428E-05±2.4E-06
090424592	14	1.609:1.842	SBPL	0.0843 ± 0.0287	−0.996 ± 0.112	−2.606 ± 0.186	77.12 ± 15.37	64.60 ± 11.90	537.68/477	43.806±14.0	3.9651E-06±1.2E-06
090424592	15	1.842:2.076	BAND	0.3913 ± 0.1420	−0.696 ± 0.124	−2.528 ± 0.199	90.45 ± 8.19	67.06 ± 8.32	499.82/477	42.731±13.0	4.1438E-06±1.2E-06
090424592	16	2.076:2.249	COMP	0.7359 ± 0.2020	−0.694 ± 0.071	-	133.70 ± 6.79	-	467.0/478	100.85±20.0	1.0475E-05±2.0E-06
090424592	17	2.249:2.484	SBPL	0.0752 ± 0.0264	−0.538 ± 0.194	−2.564 ± 0.135	61.26 ± 10.17	44.01 ± 6.86	517.0/477	41.970±15.0	3.7099E-06±1.2E-06
090424592	18	2.484:2.713	COMP	0.2802 ± 0.0612	−0.997 ± 0.059	-	182.40 ± 14.10	-	467.38/478	66.371±11.0	7.6965E-06±1.1E-06
090424592	19	2.713:2.880	COMP	0.6703 ± 0.1500	−0.680 ± 0.066	-	160.50 ± 8.61	-	499.66/478	101.08±16.0	1.2053E-05±1.7E-06
090424592	20	2.880:3.035	COMP	0.3853 ± 0.0620	−0.773 ± 0.053	-	265.50 ± 19.80	-	502.84/478	84.361±9.2	1.3979E-05±1.3E-06
090424592	21	3.035:3.212	COMP	0.7130 ± 0.2730	−0.444 ± 0.080	-	116.40 ± 4.69	-	462.4/478	63.008±20.0	6.2773E-06±2.0E-06
090424592	22	3.212:3.705	SBPL	0.0566 ± 0.0223	−1.168 ± 0.118	−2.714 ± 0.225	64.68 ± 14.40	60.94 ± 13.00	534.76/477	36.494±14.0	2.8011E-06±1.0E-06

Continued on next page

Table A.1 – continued from previous page

GRB name	spectrum	T_{start}:T_{stop} (s)	BEST model	A (ph s^{-1} cm^{-2} keV^{-1})	α	β	E_p (keV)	E_b (keV)	CSTAT/dof	photon flux (ph s^{-1} cm^{-2})	energy flux (erg s^{-1} cm^{-2})
(1)	(2)	(3)	(4)	(5)	(6)	(7)	(8)	(9)	(10)	(11)	(12)
090424592	23	3.705:3.868	COMP	0.5904 ± 0.1370	-0.603 ± 0.068	-	167.50 ± 9.22	-	442.82/478	83.576±14.0	1.0554E-05±1.6E-06
090424592	24	3.868:4.032	COMP	0.6368 ± 0.1740	-0.733 ± 0.070	-	134.70 ± 7.01	-	477.0/478	92.351±19.0	9.5375E-06±1.8E-06
090424592	25	4.032:4.141	COMP	0.5341 ± 0.0741	-0.584 ± 0.054	-	299.80 ± 19.00	-	443.53/478	106.64±9.9	2.1256E-05±1.6E-06
090424592	26	4.141:4.218	COMP	0.6336 ± 0.0935	-0.429 ± 0.057	-	289.90 ± 16.40	-	480.36/478	110.76±11.0	2.3152E-05±2.0E-06
090424592	27	4.218:4.318	COMP	1.3210 ± 0.2830	-0.461 ± 0.067	-	162.00 ± 7.40	-	441.39/478	155.02±23.0	1.9941E-05±2.6E-06
090424592	28	4.318:4.430	COMP	0.6891 ± 0.1710	-0.610 ± 0.068	-	163.80 ± 9.03	-	456.67/478	96.890±17.0	1.1997E-05±2.0E-06
090424592	29	4.430:4.552	COMP	2.1640 ± 0.6430	-0.292 ± 0.079	-	118.70 ± 4.32	-	475.89/478	158.49±34.0	1.6586E-05±3.4E-06
090424592	30	4.552:4.678	COMP	0.7635 ± 0.1720	-0.662 ± 0.066	-	166.90 ± 9.34	-	530.52/478	115.54±18.0	1.4263E-05±2.0E-06
090424592	31	4.678:4.790	COMP	1.6110 ± 0.4930	-0.560 ± 0.077	-	116.00 ± 4.85	-	491.44/478	166.74±37.0	1.6145E-05±3.5E-06
090424592	32	4.790:4.928	COMP	0.6978 ± 0.1540	-0.608 ± 0.067	-	177.40 ± 10.30	-	479.07/478	103.13±15.0	1.3583E-05±1.8E-06
090424592	33	4.928:5.294	PL	0.0173 ± 0.0063	-1.802 ± 0.025	-	-	-	806.86/479	13.308±4.9	1.3206E-06±4.8E-07
090424592	34	5.294:8.879	PL	0.0064 ± 0.0024	-1.943 ± 0.028	-	-	-	611.93/479	5.8975±2.2	4.7571E-07±1.8E-07
090424592	35	8.879:19.456	none	-	-	-	-	-	-	-	-
090528516	1	-6.144:8.064	PL	0.0011 ± 0.0004	-1.427 ± 0.023	-	-	-	850.97/479	0.56880±0.23	1.0266E-07±4.0E-08
090528516	2	8.064:10.077	COMP	0.0447 ± 0.0094	-0.887 ± 0.061	-	282.10 ± 29.00	-	492.04/478	11.161±1.8	1.8109E-06±2.6E-07
090528516	3	10.077:12.531	COMP	0.0495 ± 0.0112	-0.843 ± 0.063	-	235.30 ± 20.80	-	534.36/478	10.967±1.9	1.6140E-06±2.5E-07
090528516	4	12.531:16.200	COMP	0.0244 ± 0.0075	-1.049 ± 0.063	-	221.20 ± 24.30	-	544.18/478	6.6171±1.7	8.4484E-07±2.1E-07
090528516	5	16.200:20.575	COMP	0.0347 ± 0.0093	-1.193 ± 0.063	-	201.80 ± 25.50	-	622.36/478	10.849±2.2	1.2246E-06±2.2E-07
090528516	6	20.575:24.849	COMP	0.0401 ± 0.0111	-1.114 ± 0.065	-	184.50 ± 19.70	-	531.31/478	11.033±2.4	1.2270E-06±2.4E-07
090528516	7	24.849:29.068	COMP	0.0408 ± 0.0099	-1.107 ± 0.062	-	212.40 ± 24.30	-	525.94/478	11.650±2.1	1.4112E-06±2.2E-07
090528516	8	29.068:31.354	COMP	0.0749 ± 0.0196	-0.917 ± 0.070	-	181.20 ± 15.60	-	567.18/478	16.040±3.0	1.9135E-06±3.3E-07
090528516	9	31.354:36.595	COMP	0.0273 ± 0.0100	-1.139 ± 0.070	-	159.40 ± 16.60	-	618.16/478	7.3891±2.3	7.4747E-07±2.2E-07
090528516	10	36.595:45.567	PL	0.0027 ± 0.0010	-1.650 ± 0.023	-	-	-	744.97/479	1.7800±0.67	2.2411E-07±8.3E-08
090528516	11	45.567:48.783	COMP	0.0450 ± 0.0164	-0.759 ± 0.080	-	164.10 ± 12.30	-	470.19/478	7.5649±2.3	8.9311E-07±2.6E-07
090528516	12	48.783:85.181	none	-	-	-	-	-	-	-	-
090528516	13	85.181:116.736	none	-	-	-	-	-	-	-	-
090530760	1	-1.024:3.854	COMP	0.0459 ± 0.0090	-0.295 ± 0.090	-	237.60 ± 15.00	-	577.64/481	6.2276±0.75	1.1641E-06±1.2E-07
090530760	2	3.854:5.428	COMP	0.2336 ± 0.0647	-0.078 ± 0.104	-	157.20 ± 7.38	-	545.61/481	17.539±3.1	2.4436E-06±3.9E-07
090530760	3	5.428:7.053	COMP	0.2297 ± 0.0820	-0.040 ± 0.109	-	136.80 ± 5.92	-	580.03/481	14.211±3.7	1.7700E-06±4.4E-07
090530760	4	7.053:8.522	COMP	0.4739 ± 0.1770	0.040 ± 0.114	-	122.90 ± 4.94	-	497.71/481	23.553±6.0	2.7182E-06±6.7E-07
090530760	5	8.522:9.851	PL	0.0049 ± 0.0014	-1.478 ± 0.025	-	-	-	849.71/482	2.7188±0.82	4.5013E-07±1.3E-07
090530760	6	9.851:11.263	PL	0.0042 ± 0.0016	-1.523 ± 0.024	-	-	-	795.83/482	2.4368±0.92	3.7555E-07±1.4E-07
090530760	7	11.263:12.882	PL	0.0050 ± 0.0017	-1.575 ± 0.024	-	-	-	883.27/482	3.0175±1.0	4.2733E-07±1.4E-07
090530760	8	12.882:14.518	none	-	-	-	-	-	-	-	-
090530760	9	14.518:16.206	PL	0.0056 ± 0.0018	-1.606 ± 0.027	-	-	-	854.02/482	3.4698±1.1	4.6730E-07±1.5E-07
090530760	10	16.206:18.105	none	-	-	-	-	-	-	-	-
090530760	11	18.105:20.264	none	-	-	-	-	-	-	-	-
090530760	12	20.264:22.458	SBPL	0.0386 ± 0.0153	-0.591 ± 0.190	-2.997 ± 0.283	65.39 ± 12.80	57.86 ± 10.50	558.14/480	19.693±7.6	1.6448E-06±5.8E-07
090530760	13	22.458:25.182	none	-	-	-	-	-	-	-	-
090530760	14	25.182:27.806	none	-	-	-	-	-	-	-	-
090530760	15	27.806:31.254	none	-	-	-	-	-	-	-	-
090530760	16	31.254:34.506	none	-	-	-	-	-	-	-	-
090530760	17	34.506:38.230	none	-	-	-	-	-	-	-	-

Continued on next page

Table A.1 – continued from previous page

GRB name	spectrum	T_{start}:T_{stop} (s)	BEST model	A (ph s^{-1} cm^{-2} keV^{-1})	α	β	E_p (keV)	E_b (keV)	CSTAT/dof	photon flux (ph s^{-1} cm^{-2})	energy flux (erg s^{-1} cm^{-2})
(1)	(2)	(3)	(4)	(5)	(6)	(7)	(8)	(9)	(10)	(11)	(12)
090530760	18	38.230:41.795	none	-	-	-	-	-	-	-	-
090530760	19	41.795:46.001	none	-	-	-	-	-	-	-	-
090530760	20	46.001:50.922	none	-	-	-	-	-	-	-	-
090530760	21	50.922:55.337	none	-	-	-	-	-	-	-	-
090530760	22	55.337:60.110	none	-	-	-	-	-	-	-	-
090530760	23	60.110:64.928	none	-	-	-	-	-	-	-	-
090530760	24	64.928:68.479	none	-	-	-	-	-	-	-	-
090530760	25	68.479:71.551	none	-	-	-	-	-	-	-	-
090530760	26	71.551:74.654	none	-	-	-	-	-	-	-	-
090530760	27	74.654:77.868	none	-	-	-	-	-	-	-	-
090530760	28	77.868:80.995	none	-	-	-	-	-	-	-	-
090530760	29	80.995:84.364	none	-	-	-	-	-	-	-	-
090530760	30	84.364:88.312	none	-	-	-	-	-	-	-	-
090530760	31	88.312:92.914	none	-	-	-	-	-	-	-	-
090530760	32	92.914:98.808	none	-	-	-	-	-	-	-	-
090530760	33	98.808:105.360	none	-	-	-	-	-	-	-	-
090530760	34	105.360:112.867	none	-	-	-	-	-	-	-	-
090530760	35	112.867:121.936	none	-	-	-	-	-	-	-	-
090530760	36	121.936:132.402	none	-	-	-	-	-	-	-	-
090530760	37	132.402:150.320	none	-	-	-	-	-	-	-	-
090530760	38	150.320:202.752	none	-	-	-	-	-	-	-	-
090618353	1	-1.024:64.342	BAND	0.0539 ± 0.0039	-0.805 ± 0.033	-2.186 ± 0.042	168.10 ± 6.88	101.05 ± 4.52	1488.7/237	10.005±0.41	1.4415E-06±4.9E-08
090618353	2	64.342:64.555	COMP	0.2433 ± 0.0358	-1.068 ± 0.060	-	421.40 ± 56.60	-	260.66/238	80.944±9.1	1.4487E-05±1.1E-06
090618353	3	64.555:64.777	SBPL	0.1731 ± 0.0254	-1.033 ± 0.091	-2.049 ± 0.101	342.94 ± 141.21	150.10 ± 38.30	235.45/237	65.364±8.1	1.1758E-05±1.1E-06
090618353	4	64.777:65.008	COMP	0.2065 ± 0.0315	-0.991 ± 0.063	-	416.10 ± 53.50	-	250.05/238	64.310±7.3	1.2174E-05±9.9E-07
090618353	5	65.008:65.239	COMP	0.2554 ± 0.0417	-1.017 ± 0.065	-	340.10 ± 40.30	-	222.16/238	76.599±9.2	1.2808E-05±1.1E-06
090618353	6	65.239:65.445	COMP	0.1542 ± 0.0248	-1.129 ± 0.060	-	506.60 ± 90.60	-	272.15/238	56.134±7.1	1.0301E-05±9.7E-07
090618353	7	65.445:65.662	COMP	0.2580 ± 0.0464	-1.007 ± 0.068	-	336.00 ± 42.40	-	226.33/238	76.416±9.9	1.2776E-05±1.2E-06
090618353	8	65.662:65.893	COMP	0.2545 ± 0.0494	-1.028 ± 0.069	-	302.60 ± 39.00	-	233.14/238	74.410±10.0	1.1577E-05±1.1E-06
090618353	9	65.893:66.120	COMP	0.2907 ± 0.0526	-0.938 ± 0.071	-	291.60 ± 31.60	-	221.95/238	77.051±9.6	1.2402E-05±1.1E-06
090618353	10	66.120:66.367	BAND	0.2080 ± 0.0460	-1.071 ± 0.085	-2.387 ± 0.165	339.90 ± 73.70	241.16 ± 55.58	256.05/237	65.770±8.7	1.0824E-05±1.0E-06
090618353	11	66.367:66.598	COMP	0.1874 ± 0.0366	-1.150 ± 0.067	-	343.20 ± 55.90	-	223.19/238	63.905±9.1	9.7425E-06±1.0E-06
090618353	12	66.598:66.835	COMP	0.2776 ± 0.0523	-0.984 ± 0.071	-	278.90 ± 31.40	-	253.67/238	75.697±10.0	1.1540E-05±1.1E-06
090618353	13	66.835:67.070	COMP	0.2235 ± 0.0414	-1.110 ± 0.066	-	321.10 ± 44.70	-	231.19/238	72.039±9.7	1.0944E-05±1.1E-06
090618353	14	67.070:67.309	COMP	0.3199 ± 0.0703	-0.981 ± 0.075	-	238.00 ± 26.70	-	256.16/238	82.159±12.0	1.1383E-05±1.3E-06
090618353	15	67.309:67.562	BAND	0.4071 ± 0.1250	-0.888 ± 0.131	-2.331 ± 0.127	180.80 ± 31.10	120.97 ± 21.24	229.18/237	85.545±13.0	1.1813E-05±1.4E-06
090618353	16	67.562:67.807	COMP	0.1938 ± 0.0409	-1.103 ± 0.070	-	308.30 ± 46.20	-	256.39/238	61.350±9.3	9.1741E-06±1.0E-06
090618353	17	67.807:68.041	COMP	0.1487 ± 0.0322	-1.149 ± 0.069	-	342.00 ± 58.90	-	287.45/238	50.634±8.1	7.7107E-06±9.5E-07
090618353	18	68.041:68.262	COMP	0.2450 ± 0.0552	-1.120 ± 0.072	-	265.30 ± 37.80	-	236.41/238	75.798±12.0	1.0344E-05±1.2E-06
090618353	19	68.262:68.495	COMP	0.2102 ± 0.0452	-1.188 ± 0.070	-	283.10 ± 43.50	-	258.64/238	71.257±11.0	9.6353E-06±1.1E-06
090618353	20	68.495:68.740	COMP	0.2670 ± 0.0576	-1.140 ± 0.073	-	244.90 ± 32.20	-	279.82/238	82.565±12.0	1.0666E-05±1.2E-06
090618353	21	68.740:68.968	BAND	0.2602 ± 0.0799	-0.951 ± 0.131	-2.146 ± 0.140	196.40 ± 43.30	114.88 ± 25.71	268.93/237	61.403±9.6	8.9081E-06±1.1E-06
090618353	22	68.968:69.191	BAND	0.6670 ± 0.2090	-0.744 ± 0.139	-2.462 ± 0.183	157.70 ± 21.90	110.88 ± 17.45	256.63/237	109.86±17.0	1.4669E-05±1.8E-06

Continued on next page

Table A.1 – continued from previous page

GRB name	spectrum	T_{start}:T_{stop} (s)	BEST model	A (ph s^{-1} cm^{-2} keV^{-1})	α	β	E_p (keV)	E_b (keV)	CSTAT/dof	photon flux (ph s^{-1} cm^{-2})	energy flux (erg s^{-1} cm^{-2})
(1)	(2)	(3)	(4)	(5)	(6)	(7)	(8)	(9)	(10)	(11)	(12)
090618353	23	69.191:69.411	COMP	0.2255 ± 0.0429	-1.173 ± 0.066	-	316.20 ± 47.40	-	256.46/238	77.209±11.0	1.1131E-05±1.1E-06
090618353	24	69.411:69.649	COMP	0.1536 ± 0.0311	-1.155 ± 0.067	-	351.30 ± 59.00	-	253.25/238	52.934±8.0	8.1283E-06±9.4E-07
090618353	25	69.649:69.879	COMP	0.2648 ± 0.0675	-0.996 ± 0.084	-	214.70 ± 24.90	-	228.48/238	66.535±11.0	8.5768E-06±1.2E-06
090618353	26	69.879:70.116	COMP	0.2626 ± 0.0598	-1.131 ± 0.075	-	233.80 ± 30.30	-	232.81/238	79.260±13.0	1.0033E-05±1.2E-06
090618353	27	70.116:70.389	COMP	0.4628 ± 0.1290	-0.966 ± 0.088	-	172.90 ± 17.30	-	262.04/238	102.83±18.0	1.1695E-05±1.7E-06
090618353	28	70.389:70.636	COMP	0.2575 ± 0.0659	-1.071 ± 0.082	-	213.00 ± 26.50	-	265.52/238	70.368±12.0	8.7084E-06±1.2E-06
090618353	29	70.636:70.909	COMP	0.2438 ± 0.0580	-1.084 ± 0.076	-	230.10 ± 29.20	-	231.1/238	69.417±11.0	8.9292E-06±1.1E-06
090618353	30	70.909:71.160	COMP	0.3129 ± 0.0992	-0.952 ± 0.093	-	174.10 ± 19.00	-	247.62/238	68.530±14.0	7.8724E-06±1.4E-06
090618353	31	71.160:71.430	COMP	0.2645 ± 0.0734	-1.047 ± 0.086	-	188.70 ± 21.70	-	269.36/238	67.268±13.0	7.8251E-06±1.2E-06
090618353	32	71.430:71.706	COMP	0.3940 ± 0.1210	-1.043 ± 0.090	-	160.10 ± 17.30	-	260.37/238	93.735±19.0	9.8682E-06±1.6E-06
090618353	33	71.706:71.977	COMP	0.3201 ± 0.1030	-1.110 ± 0.091	-	165.30 ± 20.30	-	286.42/238	84.164±18.0	8.8132E-06±1.5E-06
090618353	34	71.977:72.290	COMP	0.3209 ± 0.1020	-0.991 ± 0.094	-	164.70 ± 18.00	-	266.57/238	72.160±15.0	7.8790E-06±1.3E-06
090618353	35	72.290:72.655	COMP	0.1558 ± 0.0496	-1.163 ± 0.089	-	182.50 ± 25.30	-	260.32/238	45.389±10.0	4.9256E-06±9.3E-07
090618353	36	72.655:73.097	COMP	0.2439 ± 0.0869	-1.048 ± 0.098	-	147.20 ± 16.50	-	287.95/238	56.472±13.0	5.6373E-06±1.1E-06
090618353	37	73.097:73.618	SBPL	0.0596 ± 0.0136	-1.088 ± 0.204	-2.112 ± 0.064	114.08 ± 39.18	53.85 ± 14.50	274.69/237	31.367±7.0	3.4441E-06±6.8E-07
090618353	38	73.618:74.257	PL	0.0120 ± 0.0042	-1.720 ± 0.036	-	-	-	324.03/239	8.3443±3.0	9.4231E-07±3.3E-07
090618353	39	74.257:75.257	PL	0.0162 ± 0.0034	-1.769 ± 0.034	-	-	-	348.54/239	11.901±2.8	1.2469E-06±2.6E-07
090618353	40	75.257:76.463	PL	0.0088 ± 0.0030	-1.724 ± 0.034	-	-	-	334.58/239	6.1955±2.2	6.9548E-07±2.3E-07
090618353	41	76.463:77.317	SBPL	0.0402 ± 0.0141	-1.223 ± 0.175	-2.379 ± 0.223	81.42 ± 32.64	61.70 ± 21.10	260.8/237	23.540±7.8	2.1247E-06±6.3E-07
090618353	42	77.317:77.945	SBPL	0.0544 ± 0.0118	-1.236 ± 0.187	-2.072 ± 0.061	121.47 ± 51.98	53.71 ± 16.90	254.06/237	31.032±6.6	3.2797E-06±6.1E-07
090618353	43	77.945:78.482	SBPL	0.0707 ± 0.0219	-1.091 ± 0.150	-2.486 ± 0.261	100.30 ± 33.76	79.03 ± 23.20	262.33/237	33.139±9.5	3.3892E-06±8.4E-07
090618353	44	78.482:79.115	SBPL	0.1053 ± 0.0355	-1.294 ± 0.113	-2.920 ± 0.443	93.49 ± 30.57	101.40 ± 30.70	297.14/237	54.690±17.0	4.6635E-06±1.2E-06
090618353	45	79.115:79.706	SBPL	0.0560 ± 0.0122	-0.981 ± 0.349	-2.044 ± 0.061	90.98 ± 41.55	34.68 ± 11.50	271.49/237	34.133±7.4	3.4944E-06±6.6E-07
090618353	46	79.706:80.155	PL	0.0191 ± 0.0044	-1.614 ± 0.035	-	-	-	339.81/239	11.928±2.9	1.5945E-06±3.6E-07
090618353	47	80.155:80.538	SBPL	0.0755 ± 0.0174	-0.779 ± 0.259	-2.118 ± 0.070	107.57 ± 35.03	46.65 ± 10.90	268.21/237	36.585±8.2	4.2529E-06±8.4E-07
090618353	48	80.538:80.874	COMP	0.2180 ± 0.0693	-1.149 ± 0.089	-	169.60 ± 21.90	-	254.86/238	60.928±13.0	6.3788E-06±1.2E-06
090618353	49	80.874:81.227	SBPL	0.0681 ± 0.0171	-0.973 ± 0.252	-2.096 ± 0.070	102.95 ± 41.48	44.56 ± 12.10	273.86/237	37.049±9.1	4.0001E-06±8.7E-07
090618353	50	81.227:81.627	COMP	0.2328 ± 0.0815	-1.117 ± 0.094	-	146.30 ± 16.70	-	239.98/238	59.185±14.0	5.7550E-06±1.2E-06
090618353	51	81.627:82.008	COMP	0.1212 ± 0.0420	-1.285 ± 0.087	-	171.50 ± 27.10	-	234.73/238	40.813±10.0	4.0728E-06±9.0E-07
090618353	52	82.008:82.381	COMP	0.1806 ± 0.0581	-1.148 ± 0.090	-	169.10 ± 22.00	-	271.54/238	50.368±11.0	5.2667E-06±9.9E-07
090618353	53	82.381:82.788	BAND	0.1692 ± 0.0662	-0.871 ± 0.171	-2.100 ± 0.068	126.70 ± 24.30	73.16 ± 13.23	275.82/237	29.921±6.4	3.7820E-06±7.2E-07
090618353	54	82.788:83.219	SBPL	0.0659 ± 0.0150	-0.824 ± 0.285	-2.072 ± 0.072	109.46 ± 44.62	43.57 ± 11.60	270.59/237	33.433±7.4	3.8549E-06±7.5E-07
090618353	55	83.219:83.655	COMP	0.2152 ± 0.0854	-1.022 ± 0.105	-	138.30 ± 15.10	-	291.02/238	46.851±13.0	4.5374E-06±1.1E-06
090618353	56	83.655:84.062	COMP	0.2023 ± 0.0664	-1.202 ± 0.088	-	162.60 ± 21.90	-	250.61/238	59.910±13.0	6.0044E-06±1.1E-06
090618353	57	84.062:84.365	COMP	0.2216 ± 0.0605	-1.124 ± 0.083	-	193.00 ± 24.30	-	275.03/238	62.554±12.0	7.1274E-06±1.1E-06
090618353	58	84.365:84.696	COMP	0.3167 ± 0.0975	-1.085 ± 0.088	-	162.10 ± 18.50	-	281.14/238	80.049±16.0	8.3598E-06±1.4E-06
090618353	59	84.696:84.995	SBPL	0.0960 ± 0.0188	-1.268 ± 0.103	-2.162 ± 0.099	192.89 ± 69.13	110.10 ± 31.80	228.66/237	44.414±8.4	5.5703E-06±8.9E-07
090618353	60	84.995:85.352	SBPL	0.0872 ± 0.0177	-1.237 ± 0.141	-2.162 ± 0.061	130.82 ± 37.14	76.26 ± 20.40	255.93/237	43.899±8.8	4.9122E-06±8.7E-07
090618353	61	85.352:85.746	COMP	0.2790 ± 0.0958	-0.960 ± 0.099	-	151.50 ± 15.50	-	263.56/238	58.067±13.0	6.0743E-06±1.2E-06
090618353	62	85.746:86.166	COMP	0.3232 ± 0.1180	-0.887 ± 0.104	-	140.70 ± 13.30	-	278.96/238	58.939±14.0	6.0098E-06±1.3E-06
090618353	63	86.166:86.604	PL	0.0143 ± 0.0045	-1.662 ± 0.035	-	-	-	291.12/239	9.3577±3.1	1.1592E-06±3.6E-07
090618353	64	86.604:87.021	BAND	0.1464 ± 0.0557	-1.104 ± 0.166	-2.030 ± 0.087	133.60 ± 36.20	72.56 ± 18.58	286.1/237	36.680±7.3	4.3931E-06±7.6E-07
090618353	65	87.021:87.386	COMP	0.2149 ± 0.0709	-1.102 ± 0.093	-	156.40 ± 17.80	-	260.12/238	54.808±12.0	5.5716E-06±1.1E-06

Continued on next page

Table A.1 – continued from previous page

GRB name	spectrum	T_{start}:T_{stop} (s)	BEST model	A (ph s^{-1} cm^{-2} keV^{-1})	α	β	E_p (keV)	E_b (keV)	CSTAT/dof	photon flux (ph s^{-1} cm^{-2})	energy flux (erg s^{-1} cm^{-2})
(1)	(2)	(3)	(4)	(5)	(6)	(7)	(8)	(9)	(10)	(11)	(12)
090618353	66	87.386:87.724	SBPL	0.0925 ± 0.0183	-1.140 ± 0.133	-2.171 ± 0.067	147.44 ± 38.12	83.84 ± 20.20	239.14/237	41.753±8.1	5.1152E-06±8.7E-07
090618353	67	87.724:88.107	COMP	0.1995 ± 0.0631	-1.132 ± 0.088	-	173.30 ± 22.40	-	247.36/238	54.924±12.0	5.8609E-06±1.0E-06
090618353	68	88.107:88.543	SBPL	0.0811 ± 0.0159	-0.965 ± 0.218	-2.097 ± 0.074	123.23 ± 49.50	53.45 ± 13.90	279.29/237	39.686±7.6	4.6379E-06±7.6E-07
090618353	69	88.543:89.004	SBPL	0.0509 ± 0.0124	-1.136 ± 0.172	-2.017 ± 0.074	159.65 ± 65.20	62.02 ± 18.80	264.34/237	25.145±5.9	3.0658E-06±6.4E-07
090618353	70	89.004:89.568	SBPL	0.0481 ± 0.0108	-1.206 ± 0.228	-1.955 ± 0.073	147.98 ± 72.37	46.86 ± 18.70	282.26/237	27.209±5.9	3.0889E-06±5.8E-07
090618353	71	89.568:90.248	SBPL	0.0422 ± 0.0102	-0.836 ± 0.339	-1.994 ± 0.056	123.05 ± 51.59	36.67 ± 10.80	288.8/237	22.867±5.5	2.6246E-06±5.5E-07
090618353	72	90.248:90.969	SBPL	0.1083 ± 0.0388	-1.236 ± 0.086	-3.815 ± 0.977	120.21 ± 39.59	157.90 ± 44.90	238.39/237	46.600±16.0	4.2276E-06±1.3E-06
090618353	73	90.969:91.702	SBPL	0.0375 ± 0.0128	-1.199 ± 0.207	-2.238 ± 0.184	82.07 ± 39.46	53.04 ± 20.30	257.94/237	22.405±7.3	2.1131E-06±6.1E-07
090618353	74	91.702:92.853	PL	0.0107 ± 0.0032	-1.730 ± 0.033	-	-	-	328.17/239	7.5736±2.3	8.4303E-07±2.5E-07
090618353	75	92.853:94.286	PL	0.0110 ± 0.0018	-1.700 ± 0.031	-	-	-	365.83/239	7.4871±1.4	8.7358E-07±1.3E-07
090618353	76	94.286:96.641	SBPL	0.0142 ± 0.0045	-0.909 ± 0.340	-2.065 ± 0.097	75.77 ± 33.85	32.66 ± 10.90	351.67/237	8.8167±2.8	8.8255E-07±2.6E-07
090618353	77	96.641:110.742	PL	0.0048 ± 0.0009	-1.831 ± 0.016	-	-	-	3354.6/239	3.8080±0.73	3.6343E-07±6.7E-08
090618353	78	110.742:112.177	PL	0.0098 ± 0.0031	-1.873 ± 0.035	-	-	-	497.01/239	8.1165±2.7	7.2763E-07±2.3E-07
090618353	79	112.177:113.541	none	-	-	-	-	-	-	-	-
090618353	80	113.541:114.571	PL	0.0110 ± 0.0040	-1.903 ± 0.037	-	-	-	494.77/239	9.4780±3.6	8.1351E-07±3.0E-07
090618353	81	114.571:115.539	PL	0.0172 ± 0.0051	-1.999 ± 0.040	-	-	-	511.27/239	16.848±5.3	1.2665E-06±3.7E-07
090618353	82	115.539:116.865	PL	0.0157 ± 0.0047	-2.030 ± 0.038	-	-	-	457.26/239	16.021±5.1	1.1561E-06±3.5E-07
090618353	83	116.865:118.808	PL	0.0130 ± 0.0030	-1.985 ± 0.035	-	-	-	780.67/239	12.470±3.2	9.5527E-07±2.2E-07
090618353	84	118.808:174.080	SBPL	0.0016 ± 0.0005	-2.077 ± 0.026	-1.053 ± 0.103	-	360.90 ± 94.90	2727.2/237	1.8066±0.50	1.4411E-07±3.9E-08
090626189	1	-4.352:1.792	COMP	0.0204 ± 0.0043	-0.674 ± 0.088	-	319.30 ± 37.80	-	365.6/357	4.5028±0.62	8.9608E-07±1.0E-07
090626189	2	1.792:2.816	BAND	0.2594 ± 0.0427	-0.328 ± 0.082	-2.408 ± 0.119	226.00 ± 16.90	144.22 ± 12.23	386.58/356	35.772±2.8	7.2406E-06±4.4E-07
090626189	3	2.816:3.840	BAND	0.5259 ± 0.1000	-0.253 ± 0.099	-2.378 ± 0.114	131.10 ± 8.46	83.44 ± 6.03	363.75/356	42.342±4.6	6.1955E-06±5.5E-07
090626189	4	3.840:4.864	COMP	0.2759 ± 0.0755	-0.743 ± 0.071	-	130.50 ± 6.80	-	396.19/357	39.790±7.7	4.0074E-06±7.2E-07
090626189	5	4.864:5.888	SBPL	0.0233 ± 0.0081	-0.701 ± 0.267	-2.214 ± 0.128	77.81 ± 26.03	40.69 ± 10.20	343.69/356	12.574±4.3	1.2928E-06±4.1E-07
090626189	6	5.888:8.960	PL	0.0078 ± 0.0023	-1.846 ± 0.034	-	-	-	493.53/358	6.3322±1.9	5.8778E-07±1.7E-07
090626189	7	8.960:16.128	PL	0.0084 ± 0.0014	-1.800 ± 0.027	-	-	-	359.75/358	6.4308±1.2	6.3899E-07±1.1E-07
090626189	8	16.128:17.152	COMP	0.0577 ± 0.0164	-1.294 ± 0.072	-	218.40 ± 37.60	-	371.71/357	20.942±4.3	2.3361E-06±4.1E-07
090626189	9	17.152:18.176	none	-	-	-	-	-	-	-	-
090626189	10	18.176:19.200	COMP	0.1193 ± 0.0286	-1.045 ± 0.069	-	193.10 ± 20.00	-	388.7/357	30.619±4.9	3.6059E-06±4.7E-07
090626189	11	19.200:21.248	COMP	0.0357 ± 0.0091	-1.330 ± 0.067	-	276.50 ± 60.30	-	348.13/357	14.206±2.6	1.7224E-06±2.6E-07
090626189	12	21.248:22.272	COMP	0.1020 ± 0.0107	-0.927 ± 0.039	-	425.60 ± 37.00	-	330.48/357	30.521±2.2	6.1354E-06±3.5E-07
090626189	13	22.272:24.320	COMP	0.0303 ± 0.0065	-1.243 ± 0.061	-	393.50 ± 88.70	-	399.81/357	11.704±1.8	1.7512E-06±2.2E-07
090626189	14	24.320:26.368	PL	0.0052 ± 0.0018	-1.626 ± 0.031	-	-	-	411.08/358	3.3063±1.2	4.3145E-07±1.5E-07
090626189	15	26.368:33.537	none	-	-	-	-	-	-	-	-
090626189	16	33.537:34.561	COMP	0.0799 ± 0.0177	-0.972 ± 0.070	-	254.90 ± 30.10	-	425.56/357	20.898±3.1	3.0297E-06±3.7E-07
090626189	17	34.561:35.585	COMP	0.1229 ± 0.0144	-0.871 ± 0.042	-	331.50 ± 24.50	-	397.3/357	32.255±2.6	5.8489E-06±3.7E-07
090626189	18	35.585:38.657	PL	0.0053 ± 0.0019	-1.731 ± 0.034	-	-	-	385.76/358	3.7535±1.4	4.1495E-07±1.4E-07
090626189	19	38.657:43.777	PL	0.0060 ± 0.0016	-1.791 ± 0.026	-	-	-	461.37/358	4.5546±1.3	4.5900E-07±1.2E-07
090626189	20	43.777:44.801	COMP	0.0269 ± 0.0069	-1.300 ± 0.063	-	458.90 ± 137.00	-	350.07/357	11.255±2.3	1.6913E-06±3.0E-07
090626189	21	44.801:45.825	SBPL	0.0215 ± 0.0080	-1.014 ± 0.206	-2.134 ± 0.164	94.32 ± 43.30	51.02 ± 17.50	400.94/356	11.318±4.0	1.2294E-06±4.0E-07
090626189	22	45.825:47.873	none	-	-	-	-	-	-	-	-
090626189	23	47.873:55.041	none	-	-	-	-	-	-	-	-
090626189	24	55.041:78.593	none	-	-	-	-	-	-	-	-

Continued on next page

Table A.1 – continued from previous page

GRB name	spectrum	T_{start}:T_{stop} (s)	BEST model	A (ph s^{-1} cm^{-2} keV^{-1})	α	β	E_p (keV)	E_b (keV)	CSTAT/dof	photon flux (ph s^{-1} cm^{-2})	energy flux (erg s^{-1} cm^{-2})
(1)	(2)	(3)	(4)	(5)	(6)	(7)	(8)	(9)	(10)	(11)	(12)
090718762	1	-1.024:10.913	none	-	-	-	-	-	-	-	-
090718762	2	10.913:13.869	COMP	0.0346 ± 0.0095	-0.925 ± 0.085	-	236.80 ± 31.50	-	484.89/477	8.3798±1.6	1.1886E-06±1.9E-07
090718762	3	13.869:15.281	COMP	0.1775 ± 0.0705	-0.454 ± 0.104	-	130.20 ± 7.90	-	515.18/477	17.412±5.1	1.8885E-06±5.2E-07
090718762	4	15.281:16.454	none	-	-	-	-	-	-	-	-
090718762	5	16.454:19.694	none	-	-	-	-	-	-	-	-
090718762	6	19.694:20.897	COMP	0.0215 ± 0.0079	-1.419 ± 0.068	-	270.50 ± 72.60	-	511.9/477	9.4872±3.0	1.0735E-06±3.1E-07
090718762	7	20.897:21.439	COMP	0.1017 ± 0.0231	-0.962 ± 0.067	-	239.90 ± 26.40	-	504.39/477	25.748±4.2	3.6133E-06±5.1E-07
090718762	8	21.439:21.855	COMP	0.1810 ± 0.0383	-0.810 ± 0.067	-	225.30 ± 19.70	-	532.95/477	37.989±5.5	5.5079E-06±6.7E-07
090718762	9	21.855:22.265	COMP	0.2008 ± 0.0425	-0.670 ± 0.069	-	213.10 ± 15.50	-	477.07/477	35.435±5.1	5.2453E-06±6.6E-07
090718762	10	22.265:22.700	COMP	0.1194 ± 0.0308	-0.827 ± 0.072	-	212.30 ± 19.60	-	579.85/477	24.806±4.8	3.4237E-06±5.9E-07
090718762	11	22.700:23.400	COMP	0.1207 ± 0.0359	-0.794 ± 0.082	-	177.30 ± 15.60	-	554.15/477	22.064±4.7	2.7176E-06±5.2E-07
090718762	12	23.400:24.924	PL	0.0053 ± 0.0019	-1.554 ± 0.028	-	-	-	618.0/478	3.1711±1.1	4.6510E-07±1.6E-07
090718762	13	24.924:32.768	none	-	-	-	-	-	-	-	-
090719063	1	-1.024:1.071	COMP	0.0380 ± 0.0049	-0.051 ± 0.095	-	432.40 ± 30.70	-	395.65/357	7.8238±0.62	2.6507E-06±1.6E-07
090719063	2	1.071:1.662	COMP	0.2972 ± 0.0623	0.204 ± 0.105	-	221.40 ± 11.00	-	374.23/357	25.936±3.1	5.2921E-06±5.2E-07
090719063	3	1.662:2.168	COMP	0.3133 ± 0.0825	0.174 ± 0.113	-	190.20 ± 9.69	-	389.92/357	23.097±3.8	4.0624E-06±6.0E-07
090719063	4	2.168:2.701	COMP	0.3692 ± 0.1020	0.130 ± 0.112	-	176.10 ± 8.70	-	386.86/357	25.712±4.5	4.1692E-06±6.6E-07
090719063	5	2.701:3.213	COMP	0.2335 ± 0.0508	-0.248 ± 0.088	-	218.50 ± 13.60	-	391.67/357	28.374±3.8	5.0191E-06±5.7E-07
090719063	6	3.213:3.723	COMP	0.1402 ± 0.0256	-0.367 ± 0.078	-	286.70 ± 20.90	-	365.24/357	23.309±2.7	4.9613E-06±4.7E-07
090719063	7	3.723:4.165	COMP	0.1612 ± 0.0244	-0.398 ± 0.071	-	328.40 ± 23.50	-	402.49/357	30.181±2.9	7.0685E-06±5.3E-07
090719063	8	4.165:4.509	COMP	0.1203 ± 0.0177	-0.469 ± 0.068	-	422.30 ± 36.90	-	382.48/357	27.586±2.7	7.4990E-06±5.7E-07
090719063	9	4.509:4.775	COMP	0.1978 ± 0.0284	-0.386 ± 0.068	-	358.50 ± 25.20	-	370.98/357	39.171±3.7	9.8724E-06±7.3E-07
090719063	10	4.775:5.023	COMP	0.3522 ± 0.0592	-0.309 ± 0.075	-	267.60 ± 16.60	-	397.29/357	53.292±5.5	1.0965E-05±9.0E-07
090719063	11	5.023:5.265	COMP	0.3982 ± 0.0740	-0.176 ± 0.083	-	241.20 ± 13.80	-	363.9/357	50.014±5.7	9.8751E-06±9.2E-07
090719063	12	5.265:5.530	COMP	0.3384 ± 0.0618	-0.331 ± 0.075	-	251.90 ± 15.90	-	367.29/357	49.566±5.7	9.6098E-06±8.8E-07
090719063	13	5.530:5.799	COMP	0.2841 ± 0.0564	-0.334 ± 0.080	-	244.70 ± 16.00	-	334.62/357	40.729±5.2	7.6992E-06±8.2E-07
090719063	14	5.799:6.067	COMP	0.2018 ± 0.0474	-0.391 ± 0.085	-	235.90 ± 17.60	-	387.18/357	29.442±4.7	5.2820E-06±7.3E-07
090719063	15	6.067:6.343	COMP	0.3025 ± 0.0628	-0.451 ± 0.079	-	237.50 ± 16.90	-	367.93/357	46.649±6.1	8.2216E-06±8.8E-07
090719063	16	6.343:6.622	COMP	0.3771 ± 0.0918	-0.467 ± 0.083	-	199.40 ± 13.80	-	428.06/357	52.035±8.0	7.9023E-06±1.0E-06
090719063	17	6.622:6.916	COMP	0.2861 ± 0.0766	-0.355 ± 0.090	-	188.80 ± 12.00	-	376.49/357	33.875±6.2	5.1070E-06±8.5E-07
090719063	18	6.916:7.264	COMP	0.1467 ± 0.0439	-0.483 ± 0.090	-	201.50 ± 15.60	-	410.12/357	20.719±4.6	3.1559E-06±6.5E-07
090719063	19	7.264:7.732	COMP	0.3848 ± 0.1270	-0.370 ± 0.100	-	145.80 ± 8.66	-	374.18/357	37.360±8.3	4.5323E-06±9.3E-07
090719063	20	7.732:8.438	SBPL	0.0722 ± 0.0288	-0.918 ± 0.093	-3.566 ± 0.744	114.98 ± 31.58	127.60 ± 30.10	395.97/356	25.110±9.5	2.5901E-06±8.8E-07
090719063	21	8.438:9.249	none	-	-	-	-	-	-	-	-
090719063	22	9.249:10.233	none	-	-	-	-	-	-	-	-
090719063	23	10.233:11.416	none	-	-	-	-	-	-	-	-
090719063	24	11.416:13.505	none	-	-	-	-	-	-	-	-
090719063	25	13.505:29.696	none	-	-	-	-	-	-	-	-
090804940	1	-1.024:1.096	none	-	-	-	-	-	-	-	-
090804940	2	1.096:1.476	SBPL	0.1394 ± 0.0547	-0.764 ± 0.088	-3.871 ± 0.610	101.94 ± 19.40	116.30 ± 19.80	543.32/478	46.013±17.0	4.5398E-06±1.6E-06
090804940	3	1.476:1.794	COMP	0.6706 ± 0.2290	-0.356 ± 0.088	-	125.40 ± 5.60	-	512.46/479	56.142±14.0	6.0501E-06±1.5E-06
090804940	4	1.794:2.106	PL	0.0145 ± 0.0040	-1.532 ± 0.024	-	-	-	913.44/480	8.4587±2.4	1.2856E-06±3.5E-07
090804940	5	2.106:2.493	PL	0.0153 ± 0.0042	-1.611 ± 0.023	-	-	-	787.93/480	9.5645±2.7	1.2792E-06±3.5E-07

Continued on next page

Table A.1 – continued from previous page

GRB name	spectrum	T_{start}:T_{stop} (s)	BEST model	A (ph s^{-1} cm^{-2} keV^{-1})	α	β	E_p (keV)	E_b (keV)	CSTAT/dof	photon flux (ph s^{-1} cm^{-2})	energy flux (erg s^{-1} cm^{-2})
(1)	(2)	(3)	(4)	(5)	(6)	(7)	(8)	(9)	(10)	(11)	(12)
090804940	6	2.493:2.965	PL	0.0117 ± 0.0036	-1.589 ± 0.023	-	-	-	751.95/480	7.1972±2.3	9.9707E-07±3.0E-07
090804940	7	2.965:3.488	PL	0.0104 ± 0.0034	-1.591 ± 0.024	-	-	-	760.61/480	6.3911±2.1	8.8227E-07±2.8E-07
090804940	8	3.488:4.070	PL	0.0112 ± 0.0041	-1.696 ± 0.026	-	-	-	836.02/480	7.6591±2.8	8.9418E-07±3.2E-07
090804940	9	4.070:4.651	none	-	-	-	-	-	-	-	-
090804940	10	4.651:5.569	none	-	-	-	-	-	-	-	-
090804940	11	5.569:7.879	none	-	-	-	-	-	-	-	-
090804940	12	7.879:11.264	none	-	-	-	-	-	-	-	-
090809978	1	-2.048:2.205	COMP	0.0240 ± 0.0043	-0.477 ± 0.086	-	397.60 ± 44.40	-	561.74/479	5.3192±0.62	1.3793E-06±1.4E-07
090809978	2	2.205:2.786	BAND	0.2072 ± 0.0442	-0.242 ± 0.112	-2.138 ± 0.128	229.00 ± 23.80	127.58 ± 13.81	475.67/478	27.466±3.0	6.1689E-06±5.6E-07
090809978	3	2.786:3.267	COMP	0.1164 ± 0.0204	-0.626 ± 0.065	-	331.00 ± 30.20	-	490.58/479	25.327±3.1	5.3084E-06±5.5E-07
090809978	4	3.267:3.764	BAND	0.1970 ± 0.0439	-0.538 ± 0.104	-2.114 ± 0.149	205.90 ± 26.00	114.51 ± 16.04	517.48/478	31.119±4.1	5.7865E-06±6.5E-07
090809978	5	3.764:4.286	COMP	0.1810 ± 0.0404	-0.664 ± 0.072	-	221.30 ± 17.50	-	491.37/479	32.453±4.9	4.9559E-06±6.5E-07
090809978	6	4.286:4.884	COMP	0.2257 ± 0.0659	-0.609 ± 0.083	-	168.90 ± 11.90	-	513.34/479	32.350±6.6	4.1018E-06±7.7E-07
090809978	7	4.884:5.590	COMP	0.1003 ± 0.0306	-0.964 ± 0.074	-	189.90 ± 20.00	-	496.93/479	23.198±5.4	2.7984E-06±5.9E-07
090809978	8	5.590:6.552	COMP	0.1081 ± 0.0408	-0.769 ± 0.085	-	155.40 ± 12.60	-	515.28/479	17.851±5.3	2.0196E-06±5.7E-07
090809978	9	6.552:7.733	SBPL	0.0205 ± 0.0077	-0.944 ± 0.161	-2.113 ± 0.140	108.05 ± 43.84	54.67 ± 14.50	512.04/478	9.8556±3.6	1.1562E-06±4.0E-07
090809978	10	7.733:9.646	none	-	-	-	-	-	-	-	-
090809978	11	9.646:27.648	none	-	-	-	-	-	-	-	-
090820027	1	28.672:30.712	COMP	0.0742 ± 0.0263	-0.723 ± 0.100	-	174.10 ± 17.60	-	369.73/359	12.370±3.0	1.5426E-06±3.3E-07
090820027	2	30.712:31.028	BAND	0.6224 ± 0.1790	0.004 ± 0.157	-2.275 ± 0.150	147.50 ± 13.60	87.60 ± 8.62	397.84/358	42.721±6.5	7.5879E-06±9.5E-07
090820027	3	31.028:31.263	BAND	0.5011 ± 0.1260	-0.195 ± 0.124	-2.371 ± 0.177	179.10 ± 16.50	111.51 ± 12.03	402.66/358	50.554±7.3	9.3144E-06±1.1E-06
090820027	4	31.263:31.434	COMP	0.3474 ± 0.0624	-0.505 ± 0.071	-	263.10 ± 18.40	-	389.38/359	60.155±7.4	1.1251E-05±1.2E-06
090820027	5	31.434:31.575	BAND	0.8441 ± 0.2000	-0.200 ± 0.113	-2.533 ± 0.188	193.40 ± 16.50	128.94 ± 13.43	313.29/358	90.913±12.0	1.7025E-05±1.8E-06
090820027	6	31.575:31.700	BAND	0.9801 ± 0.2370	-0.132 ± 0.113	-2.704 ± 0.216	198.50 ± 16.10	139.91 ± 14.49	356.14/358	101.19±13.0	1.9234E-05±2.0E-06
090820027	7	31.700:31.833	COMP	0.6098 ± 0.1170	-0.340 ± 0.074	-	238.90 ± 14.40	-	354.1/359	86.246±11.0	1.5929E-05±1.7E-06
090820027	8	31.833:31.957	COMP	0.4103 ± 0.0765	-0.608 ± 0.067	-	281.70 ± 22.50	-	322.91/359	80.515±10.0	1.5129E-05±1.6E-06
090820027	9	31.957:32.078	COMP	0.4201 ± 0.0735	-0.600 ± 0.065	-	296.90 ± 23.30	-	366.08/359	84.427±10.0	1.6566E-05±1.6E-06
090820027	10	32.078:32.195	COMP	0.5319 ± 0.0961	-0.454 ± 0.071	-	268.00 ± 18.30	-	371.75/359	89.626±11.0	1.7391E-05±1.7E-06
090820027	11	32.195:32.310	COMP	0.5584 ± 0.0995	-0.541 ± 0.066	-	265.90 ± 18.70	-	365.75/359	100.25±12.0	1.8596E-05±1.8E-06
090820027	12	32.310:32.417	SBPL	0.4421 ± 0.0616	-0.254 ± 0.118	-2.502 ± 0.162	173.04 ± 28.10	111.70 ± 14.30	336.78/358	109.56±14.0	2.1262E-05±2.2E-06
090820027	13	32.417:32.513	BAND	0.9351 ± 0.2180	-0.233 ± 0.109	-2.532 ± 0.191	208.60 ± 18.50	138.86 ± 15.15	315.23/358	110.89±14.0	2.1627E-05±2.2E-06
090820027	14	32.513:32.614	COMP	0.5500 ± 0.0958	-0.512 ± 0.066	-	275.80 ± 19.00	-	340.94/359	98.817±12.0	1.9112E-05±1.9E-06
090820027	15	32.614:32.710	COMP	0.8534 ± 0.1750	-0.364 ± 0.075	-	231.90 ± 14.60	-	296.74/359	120.14±16.0	2.1452E-05±2.3E-06
090820027	16	32.710:32.806	COMP	0.6300 ± 0.1090	-0.523 ± 0.067	-	267.50 ± 18.20	-	390.12/359	111.92±13.0	2.1028E-05±2.0E-06
090820027	17	32.806:32.898	COMP	0.8355 ± 0.1450	-0.512 ± 0.066	-	262.60 ± 17.10	-	319.05/359	145.29±17.0	2.7043E-05±2.4E-06
090820027	18	32.898:32.982	COMP	0.5663 ± 0.1040	-0.545 ± 0.067	-	288.50 ± 21.80	-	379.56/359	107.29±13.0	2.1171E-05±2.1E-06
090820027	19	32.982:33.066	BAND	1.3290 ± 0.3230	-0.239 ± 0.110	-2.648 ± 0.203	189.80 ± 16.00	133.27 ± 13.92	310.34/358	145.13±19.0	2.5902E-05±2.8E-06
090820027	20	33.066:33.148	COMP	0.8781 ± 0.1610	-0.492 ± 0.070	-	243.70 ± 15.80	-	312.45/359	142.84±17.0	2.5267E-05±2.5E-06
090820027	21	33.148:33.231	BAND	0.9817 ± 0.2330	-0.410 ± 0.106	-2.428 ± 0.171	198.50 ± 20.20	129.23 ± 14.80	279.57/358	131.61±17.0	2.3531E-05±2.5E-06
090820027	22	33.231:33.315	COMP	0.7701 ± 0.1440	-0.502 ± 0.068	-	246.50 ± 16.00	-	359.45/359	127.35±16.0	2.2635E-05±2.4E-06
090820027	23	33.315:33.401	BAND	1.3960 ± 0.3390	-0.212 ± 0.110	-2.718 ± 0.220	185.40 ± 14.70	133.37 ± 14.09	361.08/358	145.16±19.0	2.5422E-05±2.8E-06
090820027	24	33.401:33.486	SBPL	0.5732 ± 0.0870	-0.501 ± 0.089	-2.835 ± 0.227	164.34 ± 24.50	133.50 ± 17.40	342.99/358	151.15±21.0	2.5684E-05±2.9E-06
090820027	25	33.486:33.570	COMP	0.7321 ± 0.1460	-0.509 ± 0.072	-	234.60 ± 15.80	-	354.98/359	117.80±16.0	2.0068E-05±2.3E-06

Continued on next page

Table A.1 – continued from previous page

GRB name	spectrum	T_{start}:T_{stop} (s)	BEST model	A (ph s^{-1} cm^{-2} keV^{-1})	α	β	E_p (keV)	E_b (keV)	CSTAT/dof	photon flux (ph s^{-1} cm^{-2})	energy flux (erg s^{-1} cm^{-2})
(1)	(2)	(3)	(4)	(5)	(6)	(7)	(8)	(9)	(10)	(11)	(12)
090820027	26	33.570:33.653	COMP	0.9713 ± 0.2050	-0.441 ± 0.073	-	220.20 ± 14.00	-	358.37/359	140.64±20.0	2.3377E-05±2.7E-06
090820027	27	33.653:33.735	COMP	0.8816 ± 0.1920	-0.425 ± 0.076	-	211.80 ± 13.30	-	355.62/359	122.21±18.0	1.9786E-05±2.5E-06
090820027	28	33.735:33.828	COMP	0.9190 ± 0.2030	-0.450 ± 0.076	-	205.00 ± 12.60	-	307.79/359	127.27±19.0	1.9883E-05±2.5E-06
090820027	29	33.828:33.917	COMP	0.5553 ± 0.1140	-0.517 ± 0.072	-	241.80 ± 16.70	-	353.47/359	91.851±13.0	1.5978E-05±2.0E-06
090820027	30	33.917:33.995	COMP	0.5730 ± 0.1190	-0.569 ± 0.070	-	253.10 ± 19.40	-	333.63/359	102.05±15.0	1.7991E-05±2.2E-06
090820027	31	33.995:34.075	COMP	0.7650 ± 0.1340	-0.699 ± 0.063	-	266.10 ± 20.10	-	349.44/359	157.03±19.0	2.7042E-05±2.6E-06
090820027	32	34.075:34.159	COMP	0.9332 ± 0.1810	-0.580 ± 0.067	-	234.10 ± 16.20	-	320.64/359	159.81±20.0	2.6388E-05±2.7E-06
090820027	33	34.159:34.245	COMP	0.6203 ± 0.1040	-0.560 ± 0.065	-	273.90 ± 18.70	-	330.74/359	115.14±13.0	2.1670E-05±2.1E-06
090820027	34	34.245:34.324	COMP	0.5581 ± 0.0965	-0.591 ± 0.064	-	304.10 ± 23.30	-	334.63/359	112.96±14.0	2.2668E-05±2.2E-06
090820027	35	34.324:34.402	COMP	0.5786 ± 0.0964	-0.640 ± 0.062	-	307.60 ± 23.90	-	345.02/359	122.24±14.0	2.4112E-05±2.3E-06
090820027	36	34.402:34.476	COMP	0.6723 ± 0.1110	-0.543 ± 0.064	-	307.20 ± 22.50	-	315.92/359	132.22±15.0	2.7394E-05±2.4E-06
090820027	37	34.476:34.552	COMP	0.5523 ± 0.0901	-0.560 ± 0.063	-	329.50 ± 25.80	-	333.52/359	114.68±13.0	2.4815E-05±2.2E-06
090820027	38	34.552:34.627	COMP	0.6807 ± 0.1080	-0.572 ± 0.061	-	315.20 ± 22.90	-	361.99/359	138.79±15.0	2.8887E-05±2.5E-06
090820027	39	34.627:34.700	COMP	0.6275 ± 0.1100	-0.592 ± 0.064	-	294.40 ± 22.50	-	314.37/359	124.68±15.0	2.4419E-05±2.4E-06
090820027	40	34.700:34.779	COMP	0.5646 ± 0.0965	-0.665 ± 0.061	-	303.10 ± 24.10	-	363.25/359	120.67±14.0	2.3234E-05±2.2E-06
090820027	41	34.779:34.855	COMP	0.6098 ± 0.0982	-0.678 ± 0.059	-	336.70 ± 28.10	-	328.78/359	138.89±15.0	2.8602E-05±2.5E-06
090820027	42	34.855:34.936	COMP	0.5606 ± 0.0926	-0.669 ± 0.060	-	315.70 ± 25.50	-	405.0/359	122.77±14.0	2.4282E-05±2.2E-06
090820027	43	34.936:35.016	COMP	0.8173 ± 0.1490	-0.486 ± 0.068	-	258.40 ± 17.20	-	408.95/359	137.71±17.0	2.5596E-05±2.5E-06
090820027	44	35.016:35.103	COMP	0.7636 ± 0.1330	-0.604 ± 0.065	-	260.80 ± 18.30	-	379.29/359	142.64±17.0	2.5332E-05±2.4E-06
090820027	45	35.103:35.184	COMP	1.0020 ± 0.1900	-0.486 ± 0.070	-	238.50 ± 15.50	-	298.17/359	159.83±20.0	2.7854E-05±2.8E-06
090820027	46	35.184:35.268	COMP	0.6161 ± 0.1040	-0.531 ± 0.066	-	288.10 ± 20.50	-	336.53/359	115.43±13.0	2.2901E-05±2.1E-06
090820027	47	35.268:35.353	COMP	0.8231 ± 0.1590	-0.468 ± 0.070	-	240.60 ± 15.80	-	352.3/359	130.02±17.0	2.2992E-05±2.4E-06
090820027	48	35.353:35.439	COMP	0.8558 ± 0.1620	-0.451 ± 0.070	-	237.60 ± 15.00	-	391.22/359	132.10±17.0	2.3278E-05±2.4E-06
090820027	49	35.439:35.530	COMP	0.7472 ± 0.1570	-0.445 ± 0.073	-	228.30 ± 14.80	-	294.65/359	111.51±16.0	1.9058E-05±2.3E-06
090820027	50	35.530:35.610	COMP	0.9623 ± 0.1770	-0.490 ± 0.068	-	249.00 ± 16.50	-	327.47/359	158.57±19.0	2.8564E-05±2.7E-06
090820027	51	35.610:35.692	COMP	0.9328 ± 0.2020	-0.506 ± 0.073	-	230.10 ± 16.20	-	320.08/359	147.72±21.0	2.4806E-05±2.8E-06
090820027	52	35.692:35.782	COMP	0.5546 ± 0.1050	-0.612 ± 0.067	-	258.50 ± 19.10	-	320.01/359	103.79±14.0	1.8244E-05±2.0E-06
090820027	53	35.782:35.875	COMP	0.9073 ± 0.1910	-0.483 ± 0.073	-	213.70 ± 13.60	-	348.89/359	133.66±19.0	2.1340E-05±2.5E-06
090820027	54	35.875:35.964	COMP	0.6696 ± 0.1450	-0.577 ± 0.072	-	233.00 ± 17.60	-	311.28/359	114.02±17.0	1.8784E-05±2.3E-06
090820027	55	35.964:36.055	COMP	0.9667 ± 0.2060	-0.435 ± 0.075	-	207.30 ± 12.70	-	400.11/359	133.05±19.0	2.1090E-05±2.5E-06
090820027	56	36.055:36.157	COMP	0.6634 ± 0.1390	-0.639 ± 0.070	-	219.20 ± 15.50	-	350.54/359	115.43±17.0	1.7678E-05±2.1E-06
090820027	57	36.157:36.270	COMP	0.4280 ± 0.0880	-0.742 ± 0.066	-	255.40 ± 22.00	-	331.14/359	89.414±13.0	1.4630E-05±1.7E-06
090820027	58	36.270:36.385	COMP	0.5616 ± 0.1030	-0.695 ± 0.065	-	254.90 ± 19.40	-	362.41/359	112.17±14.0	1.8761E-05±1.9E-06
090820027	59	36.385:36.510	COMP	0.4610 ± 0.0954	-0.714 ± 0.068	-	236.90 ± 19.10	-	398.75/359	90.178±13.0	1.4164E-05±1.7E-06
090820027	60	36.510:36.641	COMP	0.3739 ± 0.0683	-0.811 ± 0.063	-	289.40 ± 26.90	-	375.98/359	88.189±11.0	1.5180E-05±1.6E-06
090820027	61	36.641:36.770	COMP	0.3646 ± 0.0661	-0.826 ± 0.062	-	292.30 ± 27.60	-	340.62/359	87.491±11.0	1.5035E-05±1.5E-06
090820027	62	36.770:36.896	COMP	0.4804 ± 0.1030	-0.727 ± 0.070	-	235.50 ± 19.70	-	362.09/359	94.915±14.0	1.4753E-05±1.8E-06
090820027	63	36.896:37.029	COMP	0.5134 ± 0.1100	-0.754 ± 0.070	-	226.10 ± 19.00	-	358.49/359	101.94±15.0	1.5200E-05±1.8E-06
090820027	64	37.029:37.169	COMP	0.4108 ± 0.0877	-0.800 ± 0.066	-	245.70 ± 22.60	-	378.12/359	89.015±13.0	1.3774E-05±1.6E-06
090820027	65	37.169:37.324	COMP	0.4532 ± 0.0992	-0.751 ± 0.069	-	218.40 ± 17.80	-	350.62/359	88.172±13.0	1.2830E-05±1.6E-06
090820027	66	37.324:37.478	COMP	0.3729 ± 0.0757	-0.692 ± 0.070	-	255.80 ± 22.00	-	285.05/359	74.444±10.0	1.2498E-05±1.4E-06
090820027	67	37.478:37.638	COMP	0.3243 ± 0.0704	-0.766 ± 0.068	-	248.80 ± 23.20	-	360.92/359	68.397±10.0	1.0856E-05±1.3E-06
090820027	68	37.638:37.797	COMP	0.4198 ± 0.0959	-0.586 ± 0.076	-	223.20 ± 17.30	-	406.73/359	70.181±11.0	1.1141E-05±1.4E-06

Continued on next page

Table A.1 – continued from previous page

GRB name	spectrum	T_{start}:T_{stop} (s)	BEST model	A (ph s^{-1} cm^{-2} keV^{-1})	α	β	E_p (keV)	E_b (keV)	CSTAT/dof	photon flux (ph s^{-1} cm^{-2})	energy flux (erg s^{-1} cm^{-2})
(1)	(2)	(3)	(4)	(5)	(6)	(7)	(8)	(9)	(10)	(11)	(12)
090820027	69	37.797:37.965	COMP	0.4341 ± 0.0896	-0.668 ± 0.070	-	232.80 ± 18.20	-	363.26/359	80.497±11.0	1.2737E-05±1.4E-06
090820027	70	37.965:38.135	COMP	0.3783 ± 0.0836	-0.763 ± 0.072	-	229.20 ± 19.90	-	354.82/359	76.340±11.0	1.1443E-05±1.4E-06
090820027	71	38.135:38.339	COMP	0.5124 ± 0.1230	-0.708 ± 0.075	-	189.60 ± 14.50	-	383.35/359	88.100±14.0	1.1768E-05±1.6E-06
090820027	72	38.339:38.550	COMP	0.4096 ± 0.1110	-0.524 ± 0.085	-	187.00 ± 13.20	-	410.79/359	57.226±11.0	8.0851E-06±1.3E-06
090820027	73	38.550:38.782	COMP	0.4367 ± 0.1180	-0.600 ± 0.084	-	177.60 ± 12.90	-	410.78/359	64.038±12.0	8.4636E-06±1.3E-06
090820027	74	38.782:39.058	COMP	0.4182 ± 0.1250	-0.587 ± 0.087	-	164.80 ± 11.90	-	316.14/359	57.505±12.0	7.2071E-06±1.3E-06
090820027	75	39.058:39.340	COMP	0.2841 ± 0.0850	-0.642 ± 0.085	-	174.90 ± 13.60	-	347.58/359	43.263±9.2	5.5703E-06±1.1E-06
090820027	76	39.340:39.671	COMP	0.2567 ± 0.0798	-0.745 ± 0.088	-	171.10 ± 14.90	-	378.62/359	43.489±9.4	5.3106E-06±1.0E-06
090820027	77	39.671:40.060	PL	0.0118 ± 0.0040	-1.529 ± 0.029	-	-	-	629.96/360	6.8645±2.4	1.0461E-06±3.5E-07
090820027	78	40.060:40.455	PL	0.0139 ± 0.0046	-1.594 ± 0.029	-	-	-	498.1/360	8.5915±2.9	1.1799E-06±3.8E-07
090820027	79	40.455:40.774	BAND	0.2291 ± 0.0906	-0.834 ± 0.104	-3.039 ± 0.769	139.00 ± 14.90	133.85 ± 46.26	383.55/358	39.066±12.0	4.2739E-06±1.2E-06
090820027	80	40.774:41.085	COMP	0.1952 ± 0.0697	-0.944 ± 0.083	-	158.30 ± 15.40	-	427.42/359	40.710±11.0	4.3922E-06±1.1E-06
090820027	81	41.085:41.386	COMP	0.1718 ± 0.0615	-0.891 ± 0.085	-	169.50 ± 16.90	-	336.6/359	34.578±9.5	3.9800E-06±1.0E-06
090820027	82	41.386:41.698	SBPL	0.0651 ± 0.0234	-1.136 ± 0.078	-2.836 ± 0.520	146.75 ± 54.31	139.70 ± 41.40	379.19/358	25.969±9.0	2.9922E-06±9.5E-07
090820027	83	41.698:42.019	COMP	0.2447 ± 0.0681	-1.077 ± 0.073	-	173.40 ± 18.70	-	419.24/359	62.948±12.0	6.8448E-06±1.1E-06
090820027	84	42.019:42.318	COMP	0.2195 ± 0.0749	-0.997 ± 0.084	-	156.10 ± 15.90	-	379.23/359	48.839±12.0	5.1251E-06±1.2E-06
090820027	85	42.318:42.654	COMP	0.2359 ± 0.0843	-0.880 ± 0.087	-	146.70 ± 12.70	-	379.24/359	43.650±12.0	4.5731E-06±1.1E-06
090820027	86	42.654:43.029	PL	0.0122 ± 0.0043	-1.568 ± 0.030	-	-	-	473.67/360	7.3645±2.6	1.0545E-06±3.7E-07
090820027	87	43.029:43.506	PL	0.0145 ± 0.0037	-1.544 ± 0.029	-	-	-	456.52/360	8.5427±2.3	1.2721E-06±3.2E-07
090820027	88	43.506:44.156	PL	0.0119 ± 0.0039	-1.644 ± 0.032	-	-	-	461.86/360	7.7420±2.6	9.8068E-07±3.2E-07
090820027	89	44.156:45.602	none	-	-	-	-	-	-	-	-
090820027	90	45.602:51.175	none	-	-	-	-	-	-	-	-
090820027	91	51.175:58.098	none	-	-	-	-	-	-	-	-
090820027	92	58.098:62.464	none	-	-	-	-	-	-	-	-
090829672	1	-7.168:35.466	BAND	0.0126 ± 0.0027	-1.566 ± 0.052	-2.211 ± 0.133	85.26 ± 11.80	66.26 ± 14.42	1559.4/477	5.7176±1.1	4.6019E-07±8.2E-08
090829672	2	35.466:37.152	COMP	0.0284 ± 0.0061	-1.498 ± 0.041	-	375.70 ± 99.90	-	458.8/478	14.330±2.6	1.6936E-06±2.8E-07
090829672	3	37.152:38.361	COMP	0.0530 ± 0.0103	-1.556 ± 0.042	-	303.80 ± 76.30	-	624.43/478	28.134±4.3	2.9960E-06±3.9E-07
090829672	4	38.361:39.681	COMP	0.0456 ± 0.0140	-1.376 ± 0.053	-	168.30 ± 21.20	-	535.03/478	17.395±4.5	1.6559E-06±4.0E-07
090829672	5	39.681:40.315	COMP	0.1115 ± 0.0211	-1.228 ± 0.048	-	239.10 ± 28.00	-	557.01/478	38.026±5.3	4.6090E-06±5.5E-07
090829672	6	40.315:41.466	COMP	0.0421 ± 0.0101	-1.537 ± 0.046	-	258.00 ± 59.40	-	498.44/478	21.412±4.2	2.2073E-06±3.9E-07
090829672	7	41.466:42.091	COMP	0.1100 ± 0.0203	-1.235 ± 0.046	-	249.00 ± 29.60	-	490.81/478	38.142±5.2	4.6993E-06±5.5E-07
090829672	8	42.091:42.688	COMP	0.1086 ± 0.0259	-1.344 ± 0.052	-	178.10 ± 20.80	-	545.09/478	40.101±7.4	3.9719E-06±6.6E-07
090829672	9	42.688:43.611	COMP	0.0434 ± 0.0122	-1.524 ± 0.049	-	211.40 ± 40.80	-	541.54/478	21.141±5.1	2.0594E-06±4.5E-07
090829672	10	43.611:44.442	COMP	0.1250 ± 0.0303	-1.236 ± 0.054	-	158.70 ± 15.10	-	559.4/478	38.567±7.0	3.7617E-06±6.0E-07
090829672	11	44.442:45.316	COMP	0.1843 ± 0.0453	-1.192 ± 0.056	-	137.30 ± 11.00	-	535.02/478	50.999±9.0	4.6665E-06±7.3E-07
090829672	12	45.316:45.814	COMP	0.1679 ± 0.0434	-1.119 ± 0.057	-	152.60 ± 12.20	-	548.55/478	43.502±8.7	4.3273E-06±8.0E-07
090829672	13	45.814:46.198	COMP	0.1473 ± 0.0262	-1.132 ± 0.048	-	261.80 ± 27.90	-	551.96/478	46.073±6.1	6.1938E-06±7.1E-07
090829672	14	46.198:46.546	COMP	0.2009 ± 0.0358	-1.058 ± 0.049	-	233.50 ± 21.20	-	544.2/478	55.851±7.2	7.3402E-06±8.1E-07
090829672	15	46.546:46.799	COMP	0.3221 ± 0.0498	-0.973 ± 0.047	-	250.50 ± 19.90	-	522.69/478	83.675±9.0	1.2011E-05±1.1E-06
090829672	16	46.799:47.235	COMP	0.1206 ± 0.0236	-1.235 ± 0.048	-	244.30 ± 29.10	-	547.85/478	41.646±6.3	5.0835E-06±6.7E-07
090829672	17	47.235:47.790	COMP	0.0972 ± 0.0191	-1.264 ± 0.047	-	265.70 ± 36.50	-	434.21/478	35.425±5.3	4.4197E-06±5.7E-07
090829672	18	47.790:48.154	COMP	0.1776 ± 0.0243	-1.093 ± 0.041	-	352.80 ± 38.50	-	467.96/478	57.788±5.7	9.3117E-06±7.4E-07
090829672	19	48.154:48.421	COMP	0.1640 ± 0.0238	-1.086 ± 0.043	-	379.40 ± 45.20	-	533.21/478	54.023±5.8	9.0678E-06±8.2E-07

Continued on next page

Table A.1 – continued from previous page

GRB name	spectrum	T_{start}:T_{stop} (s)	BEST model	A (ph s^{-1} cm^{-2} keV^{-1})	α	β	E_p (keV)	E_b (keV)	CSTAT/dof	photon flux (ph s^{-1} cm^{-2})	energy flux (erg s^{-1} cm^{-2})
(1)	(2)	(3)	(4)	(5)	(6)	(7)	(8)	(9)	(10)	(11)	(12)
090829672	20	48.421:48.874	COMP	0.1290 ± 0.0258	-1.236 ± 0.049	-	226.50 ± 25.90	-	544.24/478	43.847±6.6	5.1485E-06±6.8E-07
090829672	21	48.874:49.211	COMP	0.1326 ± 0.0177	-1.068 ± 0.041	-	420.20 ± 49.90	-	494.93/478	44.106±4.4	7.8852E-06±6.7E-07
090829672	22	49.211:49.956	COMP	0.0952 ± 0.0201	-1.276 ± 0.049	-	214.80 ± 25.80	-	561.46/478	33.561±5.4	3.7563E-06±5.3E-07
090829672	23	49.956:50.345	COMP	0.1524 ± 0.0267	-1.010 ± 0.049	-	270.20 ± 26.30	-	504.78/478	42.240±5.4	6.2168E-06±6.8E-07
090829672	24	50.345:50.686	COMP	0.1746 ± 0.0352	-1.044 ± 0.051	-	217.80 ± 19.30	-	499.11/478	46.626±7.1	5.9206E-06±8.0E-07
090829672	25	50.686:51.102	COMP	0.1621 ± 0.0342	-1.244 ± 0.051	-	196.60 ± 20.70	-	583.15/478	53.659±8.5	5.8389E-06±8.1E-07
090829672	26	51.102:51.803	SBPL	0.0428 ± 0.0083	-1.017 ± 0.191	-1.953 ± 0.067	130.01 ± 51.19	35.35 ± 9.19	531.46/477	24.940±4.7	2.7792E-06±4.8E-07
090829672	27	51.803:52.537	COMP	0.0714 ± 0.0167	-1.299 ± 0.048	-	209.70 ± 25.20	-	524.46/478	25.765±4.9	2.8175E-06±4.9E-07
090829672	28	52.537:53.030	SBPL	0.1064 ± 0.0205	-1.249 ± 0.062	-2.427 ± 0.203	125.10 ± 32.24	100.80 ± 21.90	519.79/477	50.406±9.0	5.3909E-06±8.3E-07
090829672	29	53.030:53.673	COMP	0.1112 ± 0.0319	-1.463 ± 0.055	-	131.50 ± 15.10	-	545.3/478	45.701±10.0	3.7874E-06±7.8E-07
090829672	30	53.673:54.665	COMP	0.0684 ± 0.0206	-1.465 ± 0.055	-	140.70 ± 17.70	-	490.4/478	28.624±7.0	2.4403E-06±5.5E-07
090829672	31	54.665:56.773	COMP	0.0261 ± 0.0078	-1.606 ± 0.047	-	193.70 ± 41.70	-	507.39/478	14.108±3.6	1.2805E-06±3.0E-07
090829672	32	56.773:61.937	COMP	0.0189 ± 0.0058	-1.722 ± 0.047	-	139.90 ± 31.20	-	518.15/478	11.803±3.1	9.3541E-07±2.2E-07
090829672	33	61.937:115.712	none	-	-	-	-	-	-	-	-
090902462	1	-1.024:1.039	COMP	0.0435 ± 0.0053	-0.301 ± 0.070	-	422.90 ± 30.40	-	546.12/479	9.3811±0.72	2.7903E-06±1.7E-07
090902462	2	1.039:1.882	COMP	0.0622 ± 0.0064	-0.273 ± 0.064	-	528.50 ± 37.20	-	536.67/479	15.678±1.1	5.5143E-06±3.1E-07
090902462	3	1.882:2.667	COMP	0.0563 ± 0.0045	-0.200 ± 0.062	-	733.70 ± 49.10	-	517.95/479	17.877±0.97	7.8971E-06±3.3E-07
090902462	4	2.667:3.240	COMP	0.0950 ± 0.0091	-0.232 ± 0.063	-	532.30 ± 33.70	-	519.86/479	23.966±1.5	8.6530E-06±4.3E-07
090902462	5	3.240:3.956	COMP	0.0649 ± 0.0059	-0.283 ± 0.060	-	625.40 ± 44.40	-	557.52/479	18.382±1.1	7.1204E-06±3.5E-07
090902462	6	3.956:4.698	COMP	0.0872 ± 0.0089	-0.220 ± 0.065	-	478.50 ± 30.30	-	491.65/479	20.220±1.3	6.8388E-06±3.5E-07
090902462	7	4.698:5.362	COMP	0.0683 ± 0.0056	-0.189 ± 0.060	-	666.80 ± 42.40	-	540.26/479	20.321±1.1	8.5860E-06±3.8E-07
090902462	8	5.362:5.960	COMP	0.0836 ± 0.0065	-0.103 ± 0.063	-	653.50 ± 37.00	-	575.91/479	24.769±1.3	1.0813E-05±4.3E-07
090902462	9	5.960:6.433	COMP	0.0828 ± 0.0061	-0.010 ± 0.065	-	738.40 ± 40.20	-	496.82/479	27.615±1.3	1.3468E-05±5.0E-07
090902462	10	6.433:6.851	SBPL	0.0738 ± 0.0044	-0.653 ± 0.034	-4.244 ± 0.861	920.86 ± 183.28	1086.00 ± 183.00	533.83/478	34.228±1.7	1.5363E-05±5.9E-07
090902462	11	6.851:7.218	SBPL	0.0789 ± 0.0049	-0.696 ± 0.033	-3.664 ± 0.552	909.32 ± 163.01	979.30 ± 151.00	570.72/478	35.798±1.9	1.5281E-05±6.2E-07
090902462	12	7.218:7.500	COMP	0.1276 ± 0.0088	-0.647 ± 0.037	-	1120.00 ± 94.80	-	595.69/479	46.651±2.6	1.7814E-05±7.7E-07
090902462	13	7.500:7.774	COMP	0.1411 ± 0.0086	-0.815 ± 0.029	-	1558.00 ± 130.00	-	637.18/479	55.487±3.0	1.9578E-05±8.2E-07
090902462	14	7.774:7.958	COMP	0.1698 ± 0.0113	-0.953 ± 0.027	-	1714.00 ± 180.00	-	553.48/479	68.818±4.2	2.1205E-05±1.0E-06
090902462	15	7.958:8.119	COMP	0.2292 ± 0.0147	-1.135 ± 0.024	-	1919.00 ± 233.00	-	552.72/479	99.364±6.2	2.4792E-05±1.2E-06
090902462	16	8.119:8.280	COMP	0.2152 ± 0.0168	-1.097 ± 0.028	-	1432.00 ± 212.00	-	581.77/479	89.569±6.2	2.2469E-05±1.3E-06
090902462	17	8.280:8.424	COMP	0.2401 ± 0.0170	-1.137 ± 0.026	-	1695.00 ± 248.00	-	670.2/479	103.21±6.8	2.5277E-05±1.4E-06
090902462	18	8.424:8.563	COMP	0.2123 ± 0.0157	-1.097 ± 0.026	-	1668.00 ± 235.00	-	698.57/479	89.590±6.1	2.3052E-05±1.3E-06
090902462	19	8.563:8.706	COMP	0.2387 ± 0.0176	-1.173 ± 0.025	-	1688.00 ± 269.00	-	650.55/479	104.38±7.1	2.4367E-05±1.4E-06
090902462	20	8.706:8.874	COMP	0.1910 ± 0.0138	-1.223 ± 0.024	-	2099.00 ± 341.00	-	652.19/479	86.868±6.1	1.9453E-05±1.1E-06
090902462	21	8.874:9.030	COMP	0.2107 ± 0.0153	-1.111 ± 0.027	-	1612.00 ± 230.00	-	668.22/479	89.175±6.0	2.2418E-05±1.2E-06
090902462	22	9.030:9.184	COMP	0.2681 ± 0.0177	-1.195 ± 0.024	-	1738.00 ± 245.00	-	691.19/479	118.77±7.5	2.7050E-05±1.4E-06
090902462	23	9.184:9.315	COMP	0.2532 ± 0.0184	-1.279 ± 0.024	-	1860.00 ± 305.00	-	591.21/479	118.24±8.5	2.4182E-05±1.4E-06
090902462	24	9.315:9.443	COMP	0.2401 ± 0.0193	-1.278 ± 0.025	-	1729.00 ± 336.00	-	580.99/479	111.65±8.4	2.2688E-05±1.4E-06
090902462	25	9.443:9.595	COMP	0.2588 ± 0.0190	-1.290 ± 0.024	-	1483.00 ± 239.00	-	627.05/479	120.21±8.5	2.3601E-05±1.3E-06
090902462	26	9.595:9.721	COMP	0.2417 ± 0.0201	-1.245 ± 0.026	-	1423.00 ± 255.00	-	574.66/479	108.77±8.3	2.2551E-05±1.4E-06
090902462	27	9.721:9.816	COMP	0.4213 ± 0.0351	-1.062 ± 0.031	-	887.10 ± 110.00	-	637.03/479	162.34±11.0	3.8251E-05±2.1E-06
090902462	28	9.816:9.938	COMP	0.3064 ± 0.0289	-1.235 ± 0.031	-	898.50 ± 154.00	-	622.23/479	131.74±10.0	2.5489E-05±1.6E-06
090902462	29	9.938:10.059	COMP	0.2442 ± 0.0208	-1.076 ± 0.030	-	1195.00 ± 178.00	-	556.83/479	98.708±7.2	2.4557E-05±1.5E-06

Continued on next page

Table A.1 – continued from previous page

GRB name	spectrum	T_{start}:T_{stop} (s)	BEST model	A (ph s^{-1} cm^{-2} keV^{-1})	α	β	E_p (keV)	E_b (keV)	CSTAT/dof	photon flux (ph s^{-1} cm^{-2})	energy flux (erg s^{-1} cm^{-2})
(1)	(2)	(3)	(4)	(5)	(6)	(7)	(8)	(9)	(10)	(11)	(12)
090902462	30	10.059:10.206	COMP	0.2610 ± 0.0200	−1.104 ± 0.029	-	1191.00 ± 163.00	-	630.61/479	106.87±7.1	2.5702E-05±1.4E-06
090902462	31	10.206:10.383	COMP	0.2169 ± 0.0178	−1.136 ± 0.030	-	1139.00 ± 176.00	-	619.63/479	89.813±6.3	2.0600E-05±1.2E-06
090902462	32	10.383:10.561	COMP	0.2391 ± 0.0157	−1.160 ± 0.024	-	1687.00 ± 225.00	-	734.44/479	103.90±6.5	2.4661E-05±1.2E-06
090902462	33	10.561:10.720	COMP	0.2229 ± 0.0153	−1.155 ± 0.025	-	1798.00 ± 245.00	-	671.26/479	97.037±6.4	2.3406E-05±1.2E-06
090902462	34	10.720:10.881	COMP	0.2289 ± 0.0178	−1.270 ± 0.026	-	1508.00 ± 263.00	-	610.08/479	105.05±7.7	2.1232E-05±1.3E-06
090902462	35	10.881:11.011	COMP	0.2249 ± 0.0171	−1.041 ± 0.028	-	1374.00 ± 175.00	-	576.99/479	91.099±6.2	2.4304E-05±1.4E-06
090902462	36	11.011:11.145	COMP	0.2612 ± 0.0199	−1.048 ± 0.029	-	1219.00 ± 151.00	-	596.3/479	104.54±7.0	2.7016E-05±1.4E-06
090902462	37	11.145:11.326	COMP	0.1745 ± 0.0143	−1.097 ± 0.029	-	1289.00 ± 195.00	-	618.35/479	71.818±5.1	1.7685E-05±1.0E-06
090902462	38	11.326:11.521	COMP	0.1277 ± 0.0112	−1.191 ± 0.028	-	1586.00 ± 294.00	-	635.8/479	56.095±4.5	1.2686E-05±8.7E-07
090902462	39	11.521:11.718	COMP	0.1703 ± 0.0139	−0.955 ± 0.032	-	1117.00 ± 140.00	-	569.53/479	65.024±4.4	1.8308E-05±1.0E-06
090902462	40	11.718:11.934	COMP	0.1749 ± 0.0140	−1.103 ± 0.030	-	1212.00 ± 181.00	-	670.33/479	71.709±5.0	1.7320E-05±9.6E-07
090902462	41	11.934:12.204	COMP	0.1156 ± 0.0121	−1.265 ± 0.032	-	1110.00 ± 252.00	-	523.48/479	51.746±4.7	1.0056E-05±7.5E-07
090902462	42	12.204:12.390	COMP	0.1635 ± 0.0241	−1.034 ± 0.047	-	481.80 ± 66.10	-	466.56/479	54.824±6.0	1.0712E-05±9.7E-07
090902462	43	12.390:12.584	COMP	0.2432 ± 0.0583	−1.018 ± 0.061	-	196.00 ± 17.20	-	518.23/479	60.780±11.0	7.3076E-06±1.2E-06
090902462	44	12.584:12.933	BAND	0.3664 ± 0.1300	−0.984 ± 0.124	−2.548 ± 0.219	80.29 ± 8.18	65.35 ± 9.93	535.1/478	59.314±18.0	4.9693E-06±1.4E-06
090902462	45	12.933:13.100	SBPL	0.2300 ± 0.0398	−0.782 ± 0.069	−2.804 ± 0.273	162.80 ± 29.43	139.10 ± 21.60	492.73/478	70.693±11.0	1.0556E-05±1.5E-06
090902462	46	13.100:13.219	COMP	0.3406 ± 0.0475	−0.704 ± 0.052	-	375.10 ± 30.20	-	513.54/479	83.188±8.2	1.8139E-05±1.5E-06
090902462	47	13.219:13.346	SBPL	0.4066 ± 0.0540	−0.650 ± 0.073	−2.627 ± 0.186	176.62 ± 27.12	134.50 ± 17.50	535.81/478	117.27±14.0	1.9931E-05±2.0E-06
090902462	48	13.346:13.477	COMP	0.3232 ± 0.0513	−0.861 ± 0.053	-	322.50 ± 28.90	-	468.28/479	83.237±9.4	1.4925E-05±1.4E-06
090902462	49	13.477:13.663	COMP	0.2878 ± 0.0471	−0.856 ± 0.052	-	293.50 ± 25.10	-	508.65/479	71.033±8.1	1.2033E-05±1.1E-06
090902462	50	13.663:13.845	COMP	0.2375 ± 0.0343	−0.732 ± 0.053	-	368.50 ± 31.70	-	493.74/479	58.617±5.9	1.2416E-05±1.0E-06
090902462	51	13.845:14.032	COMP	0.2479 ± 0.0326	−0.866 ± 0.048	-	400.10 ± 37.10	-	499.4/479	69.514±6.5	1.4137E-05±1.1E-06
090902462	52	14.032:14.171	COMP	0.2420 ± 0.0201	−0.612 ± 0.041	-	778.30 ± 63.20	-	509.25/479	78.181±4.9	2.7021E-05±1.3E-06
090902462	53	14.171:14.336	COMP	0.2140 ± 0.0173	−0.733 ± 0.038	-	896.20 ± 81.70	-	526.68/479	73.770±4.7	2.4295E-05±1.2E-06
090902462	54	14.336:14.512	COMP	0.2518 ± 0.0364	−0.761 ± 0.052	-	359.40 ± 30.90	-	498.97/479	62.724±6.4	1.2834E-05±1.1E-06
090902462	55	14.512:14.712	COMP	0.1837 ± 0.0151	−0.788 ± 0.037	-	905.40 ± 90.00	-	477.29/479	64.165±4.1	2.0150E-05±1.0E-06
090902462	56	14.712:14.889	COMP	0.1903 ± 0.0176	−0.670 ± 0.042	-	710.00 ± 63.50	-	533.06/479	60.009±4.1	1.9033E-05±1.0E-06
090902462	57	14.889:15.040	COMP	0.2245 ± 0.0228	−0.709 ± 0.043	-	635.00 ± 57.40	-	468.23/479	68.649±5.2	2.0047E-05±1.2E-06
090902462	58	15.040:15.181	COMP	0.2359 ± 0.0206	−0.555 ± 0.043	-	713.60 ± 54.50	-	550.25/479	73.050±4.7	2.5366E-05±1.3E-06
090902462	59	15.181:15.345	SBPL	0.1589 ± 0.0109	−0.681 ± 0.034	−3.961 ± 0.762	673.79 ± 137.03	766.30 ± 132.00	480.21/478	67.533±3.8	2.6128E-05±1.2E-06
090902462	60	15.345:15.534	SBPL	0.1401 ± 0.0090	−0.889 ± 0.028	−4.079 ± 0.896	982.90 ± 238.60	1208.00 ± 247.00	507.24/478	62.195±3.7	2.2387E-05±1.0E-06
090902462	61	15.534:15.723	SBPL	0.1323 ± 0.0085	−0.722 ± 0.032	−3.851 ± 0.634	866.99 ± 159.90	973.00 ± 156.00	477.48/478	59.115±3.3	2.4329E-05±1.1E-06
090902462	62	15.723:15.947	COMP	0.1591 ± 0.0195	−0.792 ± 0.047	-	516.10 ± 52.70	-	533.83/479	46.719±4.1	1.1536E-05±8.3E-07
090902462	63	15.947:16.184	COMP	0.1694 ± 0.0246	−0.837 ± 0.051	-	398.10 ± 40.40	-	581.0/479	46.431±4.8	9.6117E-06±8.1E-07
090902462	64	16.184:16.347	COMP	0.1993 ± 0.0198	−0.715 ± 0.043	-	702.90 ± 68.10	-	537.9/479	63.331±4.6	1.9268E-05±1.1E-06
090902462	65	16.347:16.507	COMP	0.2214 ± 0.0207	−0.612 ± 0.044	-	667.60 ± 56.00	-	471.47/479	67.264±4.5	2.1695E-05±1.2E-06
090902462	66	16.507:16.688	COMP	0.2152 ± 0.0207	−0.691 ± 0.043	-	613.30 ± 52.70	-	482.62/479	64.573±4.5	1.8813E-05±1.0E-06
090902462	67	16.688:16.901	COMP	0.1394 ± 0.0134	−0.764 ± 0.042	-	787.60 ± 83.90	-	552.28/479	46.552±3.4	1.4225E-05±8.5E-07
090902462	68	16.901:17.163	COMP	0.2768 ± 0.0488	−0.723 ± 0.060	-	257.50 ± 19.80	-	521.2/479	57.013±6.7	9.4796E-06±9.2E-07
090902462	69	17.163:17.389	COMP	0.1885 ± 0.0230	−0.664 ± 0.051	-	436.90 ± 36.20	-	502.08/479	48.333±4.1	1.1911E-05±8.3E-07
090902462	70	17.389:17.672	COMP	0.1307 ± 0.0157	−0.849 ± 0.047	-	565.80 ± 64.90	-	468.03/479	40.753±3.5	1.0051E-05±7.0E-07
090902462	71	17.672:17.979	COMP	0.1723 ± 0.0244	−0.785 ± 0.053	-	365.80 ± 32.80	-	480.05/479	44.009±4.3	8.9688E-06±7.1E-07
090902462	72	17.979:18.254	COMP	0.1715 ± 0.0301	−0.807 ± 0.057	-	297.40 ± 26.30	-	514.64/479	40.765±5.1	7.1648E-06±7.7E-07

Continued on next page

Table A.1 – continued from previous page

GRB name	spectrum	T_{start}:T_{stop} (s)	BEST model	A (ph s^{-1} cm^{-2} keV^{-1})	α	β	E_p (keV)	E_b (keV)	CSTAT/dof	photon flux (ph s^{-1} cm^{-2})	energy flux (erg s^{-1} cm^{-2})
(1)	(2)	(3)	(4)	(5)	(6)	(7)	(8)	(9)	(10)	(11)	(12)
090902462	73	18.254:18.512	COMP	0.1600 ± 0.0260	-0.868 ± 0.053	-	346.90 ± 34.50	-	469.15/479	42.641±5.0	7.9636E-06±7.8E-07
090902462	74	18.512:18.729	COMP	0.1443 ± 0.0147	-0.852 ± 0.041	-	780.90 ± 92.00	-	511.0/479	49.394±3.9	1.3874E-05±8.7E-07
090902462	75	18.729:19.065	COMP	0.1616 ± 0.0293	-0.928 ± 0.057	-	285.40 ± 28.10	-	500.6/479	42.173±5.4	6.7262E-06±7.2E-07
090902462	76	19.065:19.340	BAND	0.1943 ± 0.0358	-0.744 ± 0.082	-2.000 ± 0.100	299.50 ± 45.70	153.47 ± 24.36	503.1/478	45.031±4.6	9.2753E-06±7.9E-07
090902462	77	19.340:19.507	COMP	0.3402 ± 0.0536	-0.554 ± 0.059	-	292.70 ± 19.60	-	495.4/479	65.441±7.0	1.3005E-05±1.2E-06
090902462	78	19.507:19.650	COMP	0.3707 ± 0.0511	-0.463 ± 0.057	-	336.40 ± 21.40	-	471.79/479	73.293±6.8	1.6942E-05±1.3E-06
090902462	79	19.650:19.809	COMP	0.2749 ± 0.0350	-0.648 ± 0.052	-	411.00 ± 32.10	-	536.24/479	67.838±6.0	1.6251E-05±1.2E-06
090902462	80	19.809:19.958	COMP	0.3039 ± 0.0373	-0.782 ± 0.048	-	428.50 ± 37.00	-	444.05/479	82.645±7.2	1.8567E-05±1.3E-06
090902462	81	19.958:20.148	COMP	0.1656 ± 0.0186	-0.922 ± 0.043	-	655.50 ± 80.80	-	463.67/479	55.879±4.8	1.3752E-05±9.5E-07
090902462	82	20.148:20.383	COMP	0.1498 ± 0.0274	-0.900 ± 0.055	-	325.80 ± 33.40	-	488.98/479	40.043±5.4	7.0490E-06±8.3E-07
090902462	83	20.383:20.567	COMP	0.2171 ± 0.0281	-0.828 ± 0.048	-	435.90 ± 41.50	-	501.08/479	61.211±5.7	1.3426E-05±1.0E-06
090902462	84	20.567:20.787	COMP	0.3871 ± 0.0831	-0.679 ± 0.066	-	202.20 ± 13.30	-	530.14/479	66.895±9.9	9.4846E-06±1.2E-06
090902462	85	20.787:20.964	COMP	0.2084 ± 0.0257	-0.717 ± 0.049	-	460.30 ± 40.40	-	557.93/479	56.233±5.0	1.3790E-05±1.0E-06
090902462	86	20.964:21.246	SBPL	0.1549 ± 0.0295	-0.733 ± 0.121	-2.332 ± 0.143	117.16 ± 25.19	72.96 ± 12.40	456.73/478	58.144±10.0	7.4757E-06±1.1E-06
090902462	87	21.246:21.486	COMP	0.2886 ± 0.0553	-0.588 ± 0.065	-	246.40 ± 17.30	-	543.65/479	51.368±6.6	8.7999E-06±9.6E-07
090902462	88	21.486:21.702	COMP	0.2692 ± 0.0474	-0.616 ± 0.062	-	273.30 ± 19.90	-	466.61/479	52.198±6.3	9.5558E-06±9.7E-07
090902462	89	21.702:21.930	BAND	0.3147 ± 0.0655	-0.645 ± 0.098	-2.052 ± 0.115	199.50 ± 25.80	106.97 ± 14.53	520.94/478	54.381±6.9	9.6158E-06±1.0E-06
090902462	90	21.930:22.174	COMP	0.1363 ± 0.0202	-0.921 ± 0.050	-	444.60 ± 51.80	-	548.96/479	41.195±4.5	8.5059E-06±7.8E-07
090902462	91	22.174:22.982	SBPL	0.0371 ± 0.0084	-1.058 ± 0.215	-2.026 ± 0.093	95.40 ± 40.16	39.38 ± 12.20	531.6/478	21.791±4.8	2.3101E-06±4.5E-07
090902462	92	22.982:23.766	COMP	0.0879 ± 0.0272	-1.276 ± 0.070	-	156.90 ± 18.80	-	537.46/479	28.659±6.7	2.7333E-06±5.8E-07
090902462	93	23.766:24.314	COMP	0.0988 ± 0.0261	-0.979 ± 0.068	-	207.20 ± 21.00	-	564.48/479	24.080±4.8	3.0526E-06±5.5E-07
090902462	94	24.314:33.792	PL	0.0038 ± 0.0013	-1.863 ± 0.030	-	-	-	608.65/480	3.1357±1.1	2.8363E-07±9.9E-08
090926181	1	-1.024:1.826	SBPL	0.0231 ± 0.0027	-0.779 ± 0.067	-2.067 ± 0.127	380.55 ± 130.97	170.70 ± 28.20	565.14/477	7.6793±0.80	1.7547E-06±1.6E-07
090926181	2	1.826:2.168	SBPL	0.1494 ± 0.0139	-0.427 ± 0.068	-2.301 ± 0.115	287.84 ± 46.91	161.00 ± 17.00	512.74/477	41.907±3.3	1.0453E-05±6.9E-07
090926181	3	2.168:2.425	COMP	0.2473 ± 0.0266	-0.488 ± 0.048	-	385.70 ± 22.50	-	504.45/478	54.135±4.0	1.3664E-05±8.2E-07
090926181	4	2.425:2.625	COMP	0.3109 ± 0.0326	-0.525 ± 0.046	-	405.00 ± 24.00	-	526.67/478	71.391±5.2	1.8256E-05±1.0E-06
090926181	5	2.625:2.865	COMP	0.2579 ± 0.0323	-0.543 ± 0.049	-	337.30 ± 20.30	-	523.8/478	53.683±4.7	1.1930E-05±8.6E-07
090926181	6	2.865:3.071	COMP	0.2236 ± 0.0199	-0.592 ± 0.042	-	564.40 ± 39.00	-	512.12/478	62.734±4.0	1.8869E-05±9.7E-07
090926181	7	3.071:3.228	COMP	0.3339 ± 0.0335	-0.399 ± 0.048	-	431.30 ± 24.30	-	470.87/478	75.518±5.2	2.1655E-05±1.2E-06
090926181	8	3.228:3.364	COMP	0.4095 ± 0.0459	-0.398 ± 0.051	-	369.40 ± 20.60	-	455.62/478	83.340±6.3	2.1360E-05±1.3E-06
090926181	9	3.364:3.516	COMP	0.3896 ± 0.0413	-0.531 ± 0.046	-	380.30 ± 21.60	-	445.74/478	86.483±6.4	2.1097E-05±1.3E-06
090926181	10	3.516:3.676	COMP	0.4066 ± 0.0445	-0.515 ± 0.047	-	365.80 ± 20.60	-	543.91/478	87.416±6.5	2.0921E-05±1.3E-06
090926181	11	3.676:3.840	BAND	0.5208 ± 0.0822	-0.358 ± 0.074	-2.368 ± 0.129	259.30 ± 20.80	161.97 ± 14.80	506.96/477	81.753±7.0	1.7978E-05±1.3E-06
090926181	12	3.840:3.980	COMP	0.4374 ± 0.0545	-0.493 ± 0.049	-	328.20 ± 18.50	-	544.67/478	86.748±7.4	1.9382E-05±1.4E-06
090926181	13	3.980:4.116	SBPL	0.3622 ± 0.0341	-0.500 ± 0.068	-2.228 ± 0.088	257.06 ± 41.98	133.80 ± 13.60	475.85/477	102.16±8.5	2.2586E-05±1.6E-06
090926181	14	4.116:4.246	SBPL	0.3771 ± 0.0357	-0.525 ± 0.068	-2.218 ± 0.093	259.63 ± 46.49	133.10 ± 14.00	506.15/477	107.53±9.0	2.3476E-05±1.6E-06
090926181	15	4.246:4.369	SBPL	0.3825 ± 0.0369	-0.508 ± 0.069	-2.262 ± 0.098	245.92 ± 38.72	134.00 ± 14.00	470.62/477	107.66±9.2	2.3322E-05±1.7E-06
090926181	16	4.369:4.507	BAND	0.5403 ± 0.0849	-0.454 ± 0.073	-2.153 ± 0.089	258.50 ± 23.30	145.83 ± 13.65	552.59/477	91.821±7.9	2.0024E-05±1.4E-06
090926181	17	4.507:4.656	COMP	0.3514 ± 0.0432	-0.641 ± 0.046	-	351.00 ± 22.70	-	477.95/478	79.678±6.9	1.7265E-05±1.2E-06
090926181	18	4.656:4.834	COMP	0.3542 ± 0.0427	-0.686 ± 0.044	-	343.60 ± 22.00	-	504.12/478	81.927±6.9	1.7039E-05±1.2E-06
090926181	19	4.834:5.025	SBPL	0.1937 ± 0.0182	-0.791 ± 0.055	-1.938 ± 0.064	734.41 ± 264.88	161.00 ± 21.90	553.73/477	65.659±5.2	1.5394E-05±1.0E-06
090926181	20	5.025:5.236	BAND	0.2446 ± 0.0347	-0.698 ± 0.060	-2.209 ± 0.125	361.20 ± 41.90	212.58 ± 27.30	484.07/477	59.126±5.0	1.3303E-05±9.2E-07
090926181	21	5.236:5.447	BAND	0.2326 ± 0.0319	-0.714 ± 0.057	-2.271 ± 0.143	396.60 ± 46.30	242.62 ± 32.57	491.22/477	59.113±4.9	1.3723E-05±9.3E-07

Continued on next page

Table A.1 – continued from previous page

GRB name	spectrum	T_{start}:T_{stop}	BEST	A	α	β	E_p	E_b	CSTAT/dof	photon flux	energy flux
		(s)	model	(ph s^{-1} cm^{-2} keV^{-1})			(keV)	(keV)		(ph s^{-1} cm^{-2})	(erg s^{-1} cm^{-2})
(1)	(2)	(3)	(4)	(5)	(6)	(7)	(8)	(9)	(10)	(11)	(12)
090926181	22	5.447:5.677	COMP	0.2774 ± 0.0318	-0.599 ± 0.046	-	363.50 ± 23.10	-	536.94/478	62.388±4.9	1.4191E-05±9.1E-07
090926181	23	5.677:5.945	COMP	0.1927 ± 0.0226	-0.733 ± 0.044	-	401.10 ± 30.40	-	521.87/478	49.438±4.1	1.1047E-05±7.7E-07
090926181	24	5.945:6.183	BAND	0.2067 ± 0.0277	-0.823 ± 0.056	-2.140 ± 0.107	425.50 ± 58.10	240.85 ± 34.65	538.67/477	57.969±4.7	1.3003E-05±8.5E-07
090926181	25	6.183:6.450	COMP	0.1772 ± 0.0196	-0.934 ± 0.040	-	495.80 ± 49.90	-	524.37/478	55.826±4.6	1.2046E-05±7.9E-07
090926181	26	6.450:6.686	COMP	0.1961 ± 0.0183	-0.685 ± 0.041	-	547.50 ± 41.90	-	501.82/478	56.100±3.8	1.5514E-05±8.4E-07
090926181	27	6.686:6.925	COMP	0.2002 ± 0.0175	-0.730 ± 0.037	-	598.60 ± 47.40	-	535.05/478	60.368±3.9	1.6874E-05±8.6E-07
090926181	28	6.925:7.143	COMP	0.2215 ± 0.0230	-0.606 ± 0.044	-	460.40 ± 32.70	-	509.57/478	56.613±4.1	1.4984E-05±8.9E-07
090926181	29	7.143:7.386	COMP	0.2413 ± 0.0320	-0.622 ± 0.049	-	322.30 ± 21.10	-	510.0/478	51.582±4.8	1.0636E-05±8.3E-07
090926181	30	7.386:7.633	COMP	0.2298 ± 0.0353	-0.638 ± 0.053	-	280.50 ± 18.40	-	515.89/478	46.081±5.0	8.5081E-06±8.1E-07
090926181	31	7.633:7.897	COMP	0.2920 ± 0.0492	-0.591 ± 0.054	-	233.60 ± 13.30	-	534.23/478	50.429±6.0	8.2798E-06±8.7E-07
090926181	32	7.897:8.177	COMP	0.1597 ± 0.0248	-0.849 ± 0.048	-	327.00 ± 28.10	-	499.64/478	40.961±4.7	7.4677E-06±7.3E-07
090926181	33	8.177:8.402	COMP	0.3155 ± 0.0458	-0.549 ± 0.052	-	276.60 ± 16.40	-	442.3/478	58.400±5.8	1.1137E-05±9.4E-07
090926181	34	8.402:8.642	COMP	0.2433 ± 0.0317	-0.657 ± 0.049	-	326.60 ± 22.10	-	525.31/478	53.734±4.9	1.0967E-05±8.4E-07
090926181	35	8.642:8.891	COMP	0.2812 ± 0.0406	-0.602 ± 0.051	-	278.00 ± 17.10	-	530.35/478	54.459±5.4	1.0164E-05±8.6E-07
090926181	36	8.891:9.158	SBPL	0.2574 ± 0.0349	-0.752 ± 0.056	-3.191 ± 0.306	163.75 ± 22.83	159.70 ± 20.00	484.62/477	75.599±9.5	1.1189E-05±1.2E-06
090926181	37	9.158:9.410	COMP	0.2842 ± 0.0406	-0.751 ± 0.049	-	285.90 ± 19.70	-	506.52/478	63.205±6.2	1.1161E-05±9.1E-07
090926181	38	9.410:9.617	COMP	0.2970 ± 0.0320	-0.625 ± 0.044	-	396.20 ± 25.80	-	525.61/478	71.033±5.3	1.6869E-05±1.0E-06
090926181	39	9.617:9.782	SBPL	0.2889 ± 0.0298	-0.585 ± 0.048	-3.571 ± 0.393	244.98 ± 33.06	253.70 ± 30.50	453.58/477	83.301±7.3	1.7785E-05±1.3E-06
090926181	40	9.782:9.926	SBPL	0.2539 ± 0.0282	-0.938 ± 0.048	-2.319 ± 0.125	277.86 ± 51.03	181.90 ± 25.40	524.87/477	89.091±8.7	1.6717E-05±1.4E-06
090926181	41	9.926:10.034	SBPL	0.4337 ± 0.0503	-1.352 ± 0.037	-2.409 ± 0.156	252.64 ± 58.18	212.30 ± 44.20	489.7/477	205.29±21.0	2.7248E-05±2.3E-06
090926181	42	10.034:10.188	SBPL	0.2543 ± 0.0346	-1.136 ± 0.048	-2.451 ± 0.185	199.78 ± 42.35	156.90 ± 27.20	483.11/477	100.77±13.0	1.4182E-05±1.5E-06
090926181	43	10.188:10.404	COMP	0.3771 ± 0.0954	-0.966 ± 0.059	-	145.20 ± 8.97	-	513.7/478	77.942±15.0	7.8985E-06±1.4E-06
090926181	44	10.404:10.633	COMP	0.3276 ± 0.0637	-0.791 ± 0.055	-	201.40 ± 13.10	-	535.0/478	63.789±9.0	8.6125E-06±1.1E-06
090926181	45	10.633:10.810	COMP	0.4088 ± 0.0736	-0.641 ± 0.057	-	227.90 ± 14.30	-	513.77/478	72.930±9.1	1.1500E-05±1.2E-06
090926181	46	10.810:10.980	COMP	0.4435 ± 0.0753	-0.575 ± 0.056	-	233.30 ± 13.50	-	468.41/478	75.439±8.9	1.2455E-05±1.3E-06
090926181	47	10.980:11.140	COMP	0.4139 ± 0.0560	-0.677 ± 0.048	-	289.90 ± 17.90	-	547.9/478	87.167±8.2	1.6162E-05±1.3E-06
090926181	48	11.140:11.317	COMP	0.3538 ± 0.0477	-0.720 ± 0.046	-	304.60 ± 20.10	-	489.75/478	79.091±7.5	1.4847E-05±1.2E-06
090926181	49	11.317:11.499	SBPL	0.3029 ± 0.0335	-0.812 ± 0.059	-2.398 ± 0.130	192.70 ± 29.81	131.10 ± 16.20	481.48/477	97.547±9.9	1.6257E-05±1.4E-06
090926181	50	11.499:11.668	SBPL	0.2549 ± 0.0360	-0.831 ± 0.069	-2.436 ± 0.154	162.92 ± 28.49	114.70 ± 16.20	454.51/477	84.604±11.0	1.2675E-05±1.4E-06
090926181	51	11.668:11.852	COMP	0.2578 ± 0.0439	-0.947 ± 0.048	-	272.90 ± 23.00	-	492.07/478	67.407±8.5	1.0340E-05±1.1E-06
090926181	52	11.852:12.072	COMP	0.3930 ± 0.0661	-0.817 ± 0.050	-	218.50 ± 13.90	-	506.32/478	81.861±9.7	1.1581E-05±1.2E-06
090926181	53	12.072:12.403	COMP	0.2517 ± 0.0571	-0.925 ± 0.056	-	167.10 ± 10.80	-	517.71/478	52.509±9.0	5.9152E-06±9.4E-07
090926181	54	12.403:13.016	COMP	0.1655 ± 0.0385	-1.098 ± 0.055	-	164.00 ± 12.90	-	525.69/478	42.854±7.4	4.4741E-06±7.0E-07
090926181	55	13.016:13.360	COMP	0.1888 ± 0.0276	-0.754 ± 0.050	-	298.60 ± 22.10	-	560.6/478	42.977±4.4	7.8062E-06±6.7E-07
090926181	56	13.360:13.995	COMP	0.2506 ± 0.0683	-0.765 ± 0.067	-	138.80 ± 7.66	-	461.9/478	38.625±7.9	4.0366E-06±7.8E-07
090926181	57	13.995:15.547	COMP	0.0305 ± 0.0105	-1.305 ± 0.058	-	183.40 ± 23.70	-	563.45/478	10.792±3.2	1.1002E-06±3.1E-07
090926181	58	15.547:16.437	COMP	0.2209 ± 0.0606	-0.700 ± 0.067	-	137.80 ± 7.27	-	533.33/478	31.125±6.4	3.2982E-06±6.4E-07
090926181	59	16.437:23.223	PL	0.0037 ± 0.0013	-1.755 ± 0.025	-	-	-	778.75/479	2.7070±0.95	2.8844E-07±9.9E-08
090926181	60	23.223:43.008	none	-	-	-	-	-	-	-	-
091003191	1	-1.024:1.823	COMP	0.0188 ± 0.0032	-1.065 ± 0.060	-	642.80 ± 144.00	-	377.32/359	6.8681±0.86	1.4608E-06±1.4E-07
091003191	2	1.823:3.909	COMP	0.0296 ± 0.0046	-0.738 ± 0.066	-	472.00 ± 58.70	-	320.58/359	8.1750±0.86	2.0049E-06±1.7E-07
091003191	3	3.909:5.419	COMP	0.0372 ± 0.0068	-0.920 ± 0.064	-	416.30 ± 60.70	-	368.29/359	11.014±1.4	2.1995E-06±2.2E-07
091003191	4	5.419:10.057	COMP	0.0160 ± 0.0058	-1.160 ± 0.089	-	237.20 ± 47.40	-	393.26/359	5.0278±1.3	6.2957E-07±1.5E-07

Continued on next page

Table A.1 – continued from previous page

GRB name	spectrum	T_{start}:T_{stop} (s)	BEST model	A (ph s^{-1} cm^{-2} keV^{-1})	α	β	E_p (keV)	E_b (keV)	CSTAT/dof	photon flux (ph s^{-1} cm^{-2})	energy flux (erg s^{-1} cm^{-2})
(1)	(2)	(3)	(4)	(5)	(6)	(7)	(8)	(9)	(10)	(11)	(12)
091003191	5	10.057:15.252	PL	0.0037 ± 0.0011	-1.645 ± 0.031	-	-	-	378.52/360	2.4007±0.71	3.0427E-07±8.6E-08
091003191	6	15.252:16.912	COMP	0.0368 ± 0.0097	-1.088 ± 0.072	-	274.70 ± 44.30	-	374.5/359	11.141±2.1	1.5767E-06±2.5E-07
091003191	7	16.912:17.813	COMP	0.0677 ± 0.0115	-0.916 ± 0.060	-	375.40 ± 47.00	-	365.87/359	19.300±2.3	3.6525E-06±3.3E-07
091003191	8	17.813:18.406	COMP	0.0917 ± 0.0156	-0.912 ± 0.059	-	361.20 ± 42.40	-	409.34/359	25.700±3.0	4.7715E-06±4.4E-07
091003191	9	18.406:18.849	COMP	0.1579 ± 0.0292	-0.543 ± 0.071	-	281.80 ± 22.20	-	384.48/359	29.453±3.5	5.7138E-06±5.5E-07
091003191	10	18.849:19.049	COMP	0.1651 ± 0.0160	-0.641 ± 0.048	-	679.20 ± 59.50	-	360.59/359	50.858±3.7	1.6191E-05±9.0E-07
091003191	11	19.049:19.327	SBPL	0.1287 ± 0.0158	-0.677 ± 0.075	-2.214 ± 0.133	347.79 ± 106.69	182.40 ± 29.40	406.13/358	40.668±4.0	9.6945E-06±7.5E-07
091003191	12	19.327:20.088	SBPL	0.0471 ± 0.0088	-1.015 ± 0.128	-1.932 ± 0.117	219.18 ± 87.44	75.59 ± 22.30	421.32/358	19.779±3.3	2.9502E-06±4.1E-07
091003191	13	20.088:21.385	COMP	0.0537 ± 0.0138	-1.157 ± 0.069	-	247.70 ± 38.00	-	410.81/359	17.039±3.1	2.1873E-06±3.2E-07
091003191	14	21.385:35.840	none	-	-	-	-	-	-	-	-
091010113	1	-1.024:0.358	COMP	0.0309 ± 0.0097	-1.093 ± 0.078	-	260.60 ± 43.70	-	403.63/360	9.2734±2.2	1.2702E-06±2.7E-07
091010113	2	0.358:2.273	PL	0.0052 ± 0.0020	-1.675 ± 0.028	-	-	-	476.09/361	3.5048±1.4	4.2330E-07±1.6E-07
091010113	3	2.273:2.408	COMP	0.8238 ± 0.2350	-0.187 ± 0.093	-	170.90 ± 9.38	-	335.71/360	75.391±14.0	1.0981E-05±1.9E-06
091010113	4	2.408:2.527	COMP	0.8453 ± 0.2740	-0.473 ± 0.087	-	147.70 ± 8.58	-	343.65/360	93.787±22.0	1.1171E-05±2.4E-06
091010113	5	2.527:2.680	COMP	0.7353 ± 0.2840	-0.557 ± 0.094	-	125.30 ± 7.16	-	366.16/360	80.222±23.0	8.2314E-06±2.3E-06
091010113	6	2.680:3.049	PL	0.0150 ± 0.0054	-1.727 ± 0.029	-	-	-	510.54/361	10.595±3.9	1.1790E-06±4.2E-07
091010113	7	3.049:5.265	none	-	-	-	-	-	-	-	-
091010113	8	5.265:7.076	none	-	-	-	-	-	-	-	-
091010113	9	7.076:13.312	none	-	-	-	-	-	-	-	-
091120191	1	-1.024:1.815	COMP	0.0466 ± 0.0113	-0.569 ± 0.083	-	227.50 ± 18.30	-	542.28/479	7.7522±1.3	1.2585E-06±1.9E-07
091120191	2	1.815:3.450	COMP	0.0388 ± 0.0092	-0.985 ± 0.067	-	275.50 ± 34.60	-	601.05/479	10.566±1.9	1.5954E-06±2.5E-07
091120191	3	3.450:9.470	none	-	-	-	-	-	-	-	-
091120191	4	9.470:11.651	COMP	0.0377 ± 0.0121	-0.920 ± 0.076	-	194.30 ± 19.20	-	539.49/479	8.3442±2.1	1.0414E-06±2.5E-07
091120191	5	11.651:13.534	COMP	0.0365 ± 0.0106	-0.964 ± 0.071	-	216.70 ± 23.20	-	528.41/479	8.9041±2.0	1.1701E-06±2.5E-07
091120191	6	13.534:18.287	none	-	-	-	-	-	-	-	-
091120191	7	18.287:25.283	none	-	-	-	-	-	-	-	-
091120191	8	25.283:26.523	PL	0.0073 ± 0.0024	-1.622 ± 0.023	-	-	-	609.51/480	4.6481±1.5	6.1142E-07±2.0E-07
091120191	9	26.523:27.117	COMP	0.1690 ± 0.0529	-0.808 ± 0.075	-	152.00 ± 10.70	-	584.08/479	28.976±6.9	3.1875E-06±7.1E-07
091120191	10	27.117:28.652	none	-	-	-	-	-	-	-	-
091120191	11	28.652:33.046	none	-	-	-	-	-	-	-	-
091120191	12	33.046:35.583	none	-	-	-	-	-	-	-	-
091120191	13	35.583:40.960	none	-	-	-	-	-	-	-	-
091120191	14	47.104:51.479	none	-	-	-	-	-	-	-	-
091120191	15	51.479:56.320	none	-	-	-	-	-	-	-	-
091127976	1	-1.024:0.310	SBPL	0.0284 ± 0.0070	-0.697 ± 0.193	-2.238 ± 0.113	78.93 ± 19.14	43.51 ± 8.43	540.91/477	14.715±3.5	1.5395E-06±3.3E-07
091127976	2	0.310:0.414	SBPL	0.1855 ± 0.0390	-0.310 ± 0.275	-2.359 ± 0.086	55.08 ± 9.26	32.21 ± 5.02	445.46/477	113.79±24.0	1.0190E-05±2.0E-06
091127976	3	0.414:0.523	COMP	0.6217 ± 0.1980	-1.297 ± 0.065	-	99.29 ± 6.54	-	473.37/478	182.72±45.0	1.3691E-05±3.2E-06
091127976	4	0.523:0.657	SBPL	0.1324 ± 0.0312	-0.722 ± 0.244	-2.344 ± 0.091	50.74 ± 10.04	32.36 ± 6.08	441.39/477	93.622±22.0	7.6654E-06±1.7E-06
091127976	5	0.657:0.794	SBPL	0.1758 ± 0.0608	-1.210 ± 0.098	-2.920 ± 0.266	68.56 ± 14.39	71.98 ± 14.30	483.07/477	108.82±36.0	8.1590E-06±2.5E-06
091127976	6	0.794:1.028	SBPL	0.1042 ± 0.0331	-1.089 ± 0.155	-2.654 ± 0.161	49.62 ± 10.24	44.30 ± 8.75	473.72/477	82.776±26.0	5.7688E-06±1.7E-06
091127976	7	1.028:1.274	COMP	0.4599 ± 0.1690	-1.245 ± 0.073	-	85.23 ± 5.23	-	518.26/478	117.15±33.0	8.1854E-06±2.2E-06
091127976	8	1.274:1.416	COMP	0.2702 ± 0.0637	-1.255 ± 0.055	-	190.60 ± 20.40	-	487.05/478	90.303±16.0	9.5921E-06±1.5E-06
091127976	9	1.416:1.530	COMP	0.3573 ± 0.0657	-1.211 ± 0.048	-	239.60 ± 25.30	-	482.38/478	119.82±16.0	1.4641E-05±1.7E-06

Continued on next page

Table A.1 – continued from previous page

GRB name	spectrum	T_{start}:T_{stop} (s)	BEST model	A (ph s^{-1} cm^{-2} keV^{-1})	α	β	E_p (keV)	E_b (keV)	CSTAT/dof	photon flux (ph s^{-1} cm^{-2})	energy flux (erg s^{-1} cm^{-2})
(1)	(2)	(3)	(4)	(5)	(6)	(7)	(8)	(9)	(10)	(11)	(12)
091127976	10	1.530:1.722	COMP	0.1331 ± 0.0342	−1.435 ± 0.054	-	205.30 ± 32.00	-	501.05/478	57.471±12.0	5.7824E-06±1.0E-06
091127976	11	1.722:2.245	COMP	0.0756 ± 0.0212	−1.513 ± 0.056	-	166.20 ± 26.70	-	508.15/478	35.168±7.8	3.1423E-06±6.2E-07
091127976	12	2.245:3.619	SBPL	0.0221 ± 0.0078	−1.274 ± 0.154	−2.367 ± 0.156	57.39 ± 17.50	44.99 ± 12.80	545.53/477	16.390±5.7	1.2763E-06±4.1E-07
091127976	13	3.619:4.534	none	-	-	-	-	-	-	-	-
091127976	14	4.534:5.815	none	-	-	-	-	-	-	-	-
091127976	15	5.815:6.730	none	-	-	-	-	-	-	-	-
091127976	16	6.730:6.984	none	-	-	-	-	-	-	-	-
091127976	17	6.984:7.276	none	-	-	-	-	-	-	-	-
091127976	18	7.276:7.695	none	-	-	-	-	-	-	-	-
091127976	19	7.695:8.503	none	-	-	-	-	-	-	-	-
091127976	20	8.503:15.360	none	-	-	-	-	-	-	-	-
091128285	1	-41.217:0.003	none	-	-	-	-	-	-	-	-
091128285	2	0.003:5.888	COMP	0.0222 ± 0.0066	−0.848 ± 0.079	-	236.30 ± 29.60	-	422.03/358	4.9626±1.1	7.3022E-07±1.4E-07
091128285	3	5.888:7.936	COMP	0.0519 ± 0.0100	−0.478 ± 0.076	-	306.90 ± 27.40	-	381.47/358	9.7459±1.2	2.0837E-06±2.1E-07
091128285	4	7.936:11.008	COMP	0.0377 ± 0.0088	−0.549 ± 0.074	-	255.60 ± 22.00	-	385.54/358	6.6393±1.1	1.1904E-06±1.8E-07
091128285	5	11.008:14.080	COMP	0.0295 ± 0.0075	−0.675 ± 0.074	-	267.10 ± 27.50	-	405.8/358	5.9453±1.1	1.0392E-06±1.8E-07
091128285	6	14.080:16.128	COMP	0.0262 ± 0.0079	−0.683 ± 0.080	-	272.30 ± 30.90	-	374.3/358	5.3733±1.3	9.4899E-07±2.1E-07
091128285	7	16.128:20.224	none	-	-	-	-	-	-	-	-
091128285	8	20.224:26.368	PL	0.0022 ± 0.0008	−1.486 ± 0.029	-	-	-	475.06/359	1.2176±0.48	1.9933E-07±7.7E-08
091128285	9	26.368:32.513	none	-	-	-	-	-	-	-	-
091128285	10	32.513:38.657	none	-	-	-	-	-	-	-	-
091128285	11	38.657:48.897	none	-	-	-	-	-	-	-	-
091128285	12	48.897:109.314	none	-	-	-	-	-	-	-	-
100122616	1	-4.096:20.213	none	-	-	-	-	-	-	-	-
100122616	2	20.213:20.697	none	-	-	-	-	-	-	-	-
100122616	3	20.697:21.080	none	-	-	-	-	-	-	-	-
100122616	4	21.080:21.471	SBPL	0.0890 ± 0.0281	−1.269 ± 0.164	−2.529 ± 0.195	58.86 ± 18.06	52.41 ± 15.00	367.96/357	64.532±20.0	4.8492E-06±1.3E-06
100122616	5	21.471:21.887	none	-	-	-	-	-	-	-	-
100122616	6	21.887:22.412	SBPL	0.0391 ± 0.0149	−1.086 ± 0.292	−2.341 ± 0.130	48.04 ± 16.21	34.40 ± 10.80	372.79/357	30.907±12.0	2.3523E-06±8.5E-07
100122616	7	22.412:23.200	PL	0.0247 ± 0.0058	−1.902 ± 0.030	-	-	-	420.46/359	21.471±5.3	1.8353E-06±4.3E-07
100122616	8	23.200:24.909	PL	0.0128 ± 0.0042	−1.975 ± 0.033	-	-	-	420.62/359	12.247±4.1	9.4436E-07±3.1E-07
100122616	9	24.909:37.888	none	-	-	-	-	-	-	-	-
100322045	1	-1.024:1.310	COMP	0.0621 ± 0.0163	−0.569 ± 0.082	-	194.60 ± 13.90	-	513.2/478	9.3515±1.7	1.3415E-06±2.3E-07
100322045	2	1.310:2.025	COMP	0.2062 ± 0.0509	−0.399 ± 0.080	-	173.60 ± 9.31	-	543.72/478	23.882±4.1	3.3100E-06±5.2E-07
100322045	3	2.025:4.613	COMP	0.0996 ± 0.0397	−0.526 ± 0.098	-	132.90 ± 8.03	-	585.84/478	10.910±3.3	1.1792E-06±3.4E-07
100322045	4	4.613:5.445	COMP	0.1390 ± 0.0392	−0.588 ± 0.081	-	172.50 ± 11.30	-	507.71/478	19.730±4.0	2.5598E-06±4.8E-07
100322045	5	5.445:6.617	COMP	0.1500 ± 0.0528	−0.739 ± 0.085	-	132.50 ± 8.54	-	571.15/478	21.742±5.7	2.2140E-06±5.5E-07
100322045	6	6.617:7.446	SBPL	0.0746 ± 0.0264	−0.732 ± 0.111	−3.179 ± 0.374	92.55 ± 17.60	89.88 ± 15.50	511.54/477	27.305±9.1	2.7280E-06±8.3E-07
100322045	7	7.446:8.748	COMP	0.1139 ± 0.0338	−0.673 ± 0.083	-	159.20 ± 10.80	-	520.68/478	16.962±3.6	2.0136E-06±4.0E-07
100322045	8	8.748:10.811	PL	0.0050 ± 0.0020	−1.709 ± 0.026	-	-	-	633.37/479	3.5002±1.4	3.9997E-07±1.6E-07
100322045	9	10.811:19.941	PL	0.0030 ± 0.0008	−1.629 ± 0.028	-	-	-	743.71/479	1.9440±0.52	2.5226E-07±6.4E-08
100322045	10	19.941:22.483	COMP	0.0334 ± 0.0083	−0.988 ± 0.070	-	238.50 ± 28.20	-	538.27/478	8.6842±1.6	1.1967E-06±1.9E-07
100322045	11	22.483:26.449	SBPL	0.0120 ± 0.0024	−0.785 ± 0.206	−1.791 ± 0.086	-	55.10 ± 16.20	670.54/477	4.9023±0.89	8.1437E-07±1.3E-07

Continued on next page

Table A.1 – continued from previous page

GRB name	spectrum	T_{start}:T_{stop} (s)	BEST model	A (ph s^{-1} cm^{-2} keV^{-1})	α	β	E_p (keV)	E_b (keV)	CSTAT/dof	photon flux (ph s^{-1} cm^{-2})	energy flux (erg s^{-1} cm^{-2})
(1)	(2)	(3)	(4)	(5)	(6)	(7)	(8)	(9)	(10)	(11)	(12)
100322045	12	26.449:28.506	COMP	0.0306 ± 0.0037	−0.706 ± 0.057	-	534.90 ± 56.30	-	546.61/478	8.7507±0.76	2.3505E-06±1.7E-07
100322045	13	28.506:29.803	COMP	0.0293 ± 0.0034	−0.751 ± 0.055	-	739.10 ± 97.10	-	498.19/478	9.5699±0.84	2.8841E-06±2.1E-07
100322045	14	29.803:31.290	COMP	0.0320 ± 0.0031	−0.897 ± 0.044	-	930.30 ± 133.00	-	491.49/478	11.609±0.89	3.3043E-06±2.1E-07
100322045	15	31.290:32.307	COMP	0.0491 ± 0.0040	−0.712 ± 0.045	-	855.70 ± 85.10	-	519.02/478	16.646±1.1	5.4921E-06±2.7E-07
100322045	16	32.307:33.125	COMP	0.0587 ± 0.0053	−0.696 ± 0.048	-	718.10 ± 69.50	-	485.2/478	18.691±1.3	5.8302E-06±3.1E-07
100322045	17	33.125:34.013	COMP	0.0545 ± 0.0057	−0.663 ± 0.052	-	601.70 ± 57.40	-	512.38/478	16.077±1.2	4.7432E-06±2.9E-07
100322045	18	34.013:34.908	COMP	0.0454 ± 0.0051	−0.864 ± 0.048	-	736.10 ± 98.20	-	549.45/478	15.373±1.3	4.1776E-06±2.9E-07
100322045	19	34.908:35.798	BAND	0.0428 ± 0.0050	−0.906 ± 0.053	−1.981 ± 0.106	853.10 ± 178.00	418.56 ± 90.17	524.26/477	15.292±1.2	4.2003E-06±2.8E-07
100322045	20	35.798:36.765	COMP	0.0496 ± 0.0052	−0.954 ± 0.044	-	753.20 ± 105.00	-	519.85/478	17.564±1.4	4.4116E-06±2.8E-07
100322045	21	36.765:37.793	COMP	0.0469 ± 0.0057	−0.886 ± 0.050	-	582.20 ± 72.90	-	575.45/478	15.067±1.4	3.6453E-06±2.7E-07
100322045	22	37.793:39.936	COMP	0.0262 ± 0.0047	−0.984 ± 0.062	-	437.90 ± 69.70	-	587.47/478	8.2626±1.1	1.6088E-06±1.7E-07
100324172	1	-2.048:1.576	COMP	0.0285 ± 0.0024	0.224 ± 0.085	-	516.90 ± 26.90	-	504.94/478	6.9951±0.36	3.0068E-06±1.3E-07
100324172	2	1.576:2.253	COMP	0.1086 ± 0.0098	0.098 ± 0.067	-	457.80 ± 21.70	-	487.92/478	23.268±1.3	8.7312E-06±4.0E-07
100324172	3	2.253:3.030	COMP	0.0951 ± 0.0085	−0.147 ± 0.057	-	483.50 ± 25.70	-	491.37/478	22.010±1.3	7.7682E-06±3.7E-07
100324172	4	3.030:3.777	COMP	0.1191 ± 0.0130	−0.262 ± 0.058	-	393.20 ± 22.50	-	470.17/478	23.948±1.7	6.8733E-06±3.9E-07
100324172	5	3.777:4.686	COMP	0.1323 ± 0.0190	−0.283 ± 0.063	-	282.10 ± 15.20	-	542.11/478	20.541±1.9	4.4638E-06±3.6E-07
100324172	6	4.686:5.109	COMP	0.1854 ± 0.0222	−0.403 ± 0.052	-	355.70 ± 20.90	-	519.89/478	36.843±2.9	9.1516E-06±6.0E-07
100324172	7	5.109:5.622	COMP	0.1857 ± 0.0252	−0.326 ± 0.059	-	307.80 ± 17.30	-	534.34/478	31.781±2.8	7.2954E-06±5.3E-07
100324172	8	5.622:6.838	COMP	0.0884 ± 0.0134	−0.583 ± 0.056	-	292.00 ± 20.00	-	484.05/478	17.363±1.8	3.3955E-06±3.0E-07
100324172	9	6.838:14.377	COMP	0.0266 ± 0.0074	−0.976 ± 0.066	-	189.50 ± 18.50	-	565.47/478	6.2384±1.3	7.4743E-07±1.5E-07
100324172	10	14.377:29.696	none	-	-	-	-	-	-	-	-
100414097	1	-2.048:5.452	SBPL	0.0144 ± 0.0009	−0.548 ± 0.047	−2.307 ± 0.124	561.48 ± 97.43	326.70 ± 36.00	834.78/476	5.2792±0.27	1.8323E-06±7.4E-08
100414097	2	5.452:7.235	COMP	0.0367 ± 0.0028	−0.325 ± 0.055	-	685.20 ± 44.40	-	604.34/477	11.017±0.58	4.3785E-06±1.8E-07
100414097	3	7.235:9.194	COMP	0.0385 ± 0.0033	−0.300 ± 0.058	-	549.20 ± 34.10	-	582.81/477	10.018±0.58	3.5615E-06±1.7E-07
100414097	4	9.194:10.860	COMP	0.0387 ± 0.0031	−0.226 ± 0.061	-	608.70 ± 37.50	-	634.89/477	10.757±0.59	4.2355E-06±1.8E-07
100414097	5	10.860:13.148	COMP	0.0303 ± 0.0023	−0.373 ± 0.053	-	696.60 ± 46.90	-	540.83/477	9.1799±0.49	3.5720E-06±1.5E-07
100414097	6	13.148:14.896	COMP	0.0386 ± 0.0030	−0.412 ± 0.053	-	655.30 ± 45.30	-	610.65/477	11.303±0.63	4.1579E-06±1.8E-07
100414097	7	14.896:16.047	COMP	0.0428 ± 0.0040	−0.639 ± 0.048	-	686.40 ± 63.30	-	551.83/477	13.232±0.90	4.2390E-06±2.3E-07
100414097	8	16.047:17.090	COMP	0.0562 ± 0.0060	−0.579 ± 0.053	-	513.80 ± 41.60	-	535.66/477	15.002±1.1	4.3150E-06±2.6E-07
100414097	9	17.090:18.209	COMP	0.0529 ± 0.0049	−0.583 ± 0.049	-	593.10 ± 47.40	-	531.47/477	15.171±1.0	4.7133E-06±2.5E-07
100414097	10	18.209:19.913	COMP	0.0358 ± 0.0028	−0.518 ± 0.049	-	737.10 ± 57.60	-	606.28/477	11.213±0.64	4.0637E-06±1.8E-07
100414097	11	19.913:21.046	SBPL	0.0436 ± 0.0042	−0.608 ± 0.066	−2.046 ± 0.091	522.27 ± 182.03	200.10 ± 26.80	595.19/476	14.245±1.1	3.9992E-06±2.5E-07
100414097	12	21.046:21.968	COMP	0.0495 ± 0.0052	−0.722 ± 0.048	-	626.00 ± 63.10	-	564.32/477	15.138±1.2	4.3476E-06±2.7E-07
100414097	13	21.968:22.833	COMP	0.0537 ± 0.0048	−0.782 ± 0.043	-	774.80 ± 81.90	-	534.69/477	17.936±1.2	5.3622E-06±2.9E-07
100414097	14	22.833:23.617	COMP	0.0696 ± 0.0071	−0.778 ± 0.046	-	567.30 ± 54.20	-	555.47/477	21.025±1.6	5.5039E-06±3.2E-07
100414097	15	23.617:24.107	BAND	0.1240 ± 0.0175	−0.554 ± 0.070	−2.272 ± 0.143	400.10 ± 45.70	240.44 ± 30.15	523.97/476	28.955±2.3	7.5020E-06±4.6E-07
100414097	16	24.107:63.488	PL	0.0028 ± 0.0003	−1.390 ± 0.022	-	-	-	3036.0/478	1.4477±0.16	2.7688E-07±2.4E-08
100511035	1	-1.024:11.065	none	-	-	-	-	-	-	-	-
100511035	2	11.065:19.223	none	-	-	-	-	-	-	-	-
100511035	3	19.223:24.113	PL	0.0029 ± 0.0006	−1.379 ± 0.029	-	-	-	666.38/479	1.4975±0.35	2.9172E-07±6.1E-08
100511035	4	24.113:25.195	COMP	0.0427 ± 0.0056	−0.876 ± 0.052	-	669.20 ± 98.20	-	537.88/478	14.171±1.4	3.6731E-06±2.9E-07
100511035	5	25.195:26.713	COMP	0.0331 ± 0.0053	−0.975 ± 0.056	-	566.90 ± 96.30	-	498.84/478	11.091±1.3	2.4513E-06±2.4E-07
100511035	6	26.713:30.139	COMP	0.0113 ± 0.0031	−1.203 ± 0.069	-	553.70 ± 178.00	-	596.5/478	4.4477±0.99	7.8200E-07±1.5E-07

Continued on next page

Table A.1 – continued from previous page

GRB name	spectrum	T_{start}:T_{stop} (s)	BEST model	A (ph s^{-1} cm^{-2} keV^{-1})	α	β	E_p (keV)	E_b (keV)	CSTAT/dof	photon flux (ph s^{-1} cm^{-2})	energy flux (erg s^{-1} cm^{-2})
(1)	(2)	(3)	(4)	(5)	(6)	(7)	(8)	(9)	(10)	(11)	(12)
100511035	7	30.139:39.936	none	-	-	-	-	-	-	-	-
100612726	1	-1.024:2.358	COMP	0.0505 ± 0.0115	-0.614 ± 0.062	-	230.10 ± 15.30	-	569.04/480	8.8269±1.6	1.4190E-06±2.4E-07
100612726	2	2.358:3.324	BAND	0.3890 ± 0.1230	-0.166 ± 0.108	-2.721 ± 0.228	116.40 ± 6.75	85.01 ± 7.99	547.34/479	24.484±6.9	3.0897E-06±8.0E-07
100612726	3	3.324:3.944	BAND	0.4545 ± 0.1360	-0.246 ± 0.113	-2.517 ± 0.174	114.30 ± 7.53	77.84 ± 6.77	544.32/479	31.545±7.9	4.0479E-06±9.4E-07
100612726	4	3.944:4.532	COMP	0.4298 ± 0.1500	-0.555 ± 0.072	-	126.50 ± 5.61	-	531.64/480	47.112±14.0	4.8722E-06±1.4E-06
100612726	5	4.532:5.233	PL	0.0117 ± 0.0039	-1.607 ± 0.021	-	-	-	896.77/481	7.2790±2.5	9.8152E-07±3.3E-07
100612726	6	5.233:6.895	PL	0.0092 ± 0.0034	-1.742 ± 0.022	-	-	-	750.92/481	6.6147±2.5	7.2009E-07±2.6E-07
100612726	7	6.895:20.480	none	-	-	-	-	-	-	-	-
100707032	1	-1.024:0.784	BAND	0.0280 ± 0.0030	0.481 ± 0.142	-2.324 ± 0.123	611.10 ± 51.40	349.75 ± 29.87	419.06/356	9.0092±0.50	4.7659E-06±2.1E-07
100707032	2	0.784:1.085	SBPL	0.0883 ± 0.0088	0.248 ± 0.122	-2.476 ± 0.128	495.33 ± 64.75	287.80 ± 31.00	394.55/356	36.922±2.2	1.7207E-05±7.8E-07
100707032	3	1.085:1.321	SBPL	0.1365 ± 0.0139	0.260 ± 0.130	-2.355 ± 0.103	444.31 ± 58.79	232.30 ± 24.10	430.97/356	48.126±3.1	2.0259E-05±9.8E-07
100707032	4	1.321:1.517	SBPL	0.1067 ± 0.0119	0.249 ± 0.129	-2.319 ± 0.107	498.99 ± 75.11	252.60 ± 28.10	383.28/356	41.056±2.9	1.8347E-05±1.0E-06
100707032	5	1.517:1.702	COMP	0.1833 ± 0.0188	0.051 ± 0.078	-	566.10 ± 34.20	-	373.54/357	48.783±3.2	2.0929E-05±1.1E-06
100707032	6	1.702:1.897	SBPL	0.2064 ± 0.0230	0.336 ± 0.144	-2.433 ± 0.124	324.20 ± 43.27	179.90 ± 18.80	426.0/356	57.324±4.4	2.0312E-05±1.2E-06
100707032	7	1.897:2.099	SBPL	0.1959 ± 0.0219	0.501 ± 0.174	-2.349 ± 0.119	305.59 ± 45.76	153.90 ± 16.00	369.48/356	50.001±4.1	1.7190E-05±1.1E-06
100707032	8	2.099:2.298	BAND	0.2678 ± 0.0508	0.243 ± 0.127	-2.400 ± 0.168	353.50 ± 33.20	211.55 ± 21.46	382.13/356	42.708±3.8	1.4684E-05±1.0E-06
100707032	9	2.298:2.516	COMP	0.2396 ± 0.0324	-0.024 ± 0.083	-	389.00 ± 23.90	-	372.05/357	44.251±3.7	1.3934E-05±9.5E-07
100707032	10	2.516:2.740	COMP	0.2067 ± 0.0346	0.146 ± 0.096	-	339.10 ± 20.50	-	364.98/357	31.286±3.3	9.2988E-06±8.4E-07
100707032	11	2.740:2.990	SBPL	0.1467 ± 0.0194	-0.042 ± 0.124	-2.400 ± 0.164	259.23 ± 46.75	148.00 ± 18.60	367.05/356	36.431±4.0	9.9235E-06±9.2E-07
100707032	12	2.990:3.233	COMP	0.5019 ± 0.1130	0.205 ± 0.106	-	231.20 ± 12.70	-	397.34/357	46.259±6.1	9.8339E-06±1.1E-06
100707032	13	3.233:3.480	SBPL	0.1784 ± 0.0296	0.063 ± 0.158	-2.473 ± 0.191	180.42 ± 33.93	107.30 ± 14.60	330.39/356	40.137±6.0	8.7272E-06±1.1E-06
100707032	14	3.480:3.737	COMP	0.4756 ± 0.1170	0.005 ± 0.101	-	209.30 ± 12.00	-	363.65/357	45.042±6.9	8.2797E-06±1.1E-06
100707032	15	3.737:3.995	COMP	0.7737 ± 0.2040	0.121 ± 0.109	-	187.10 ± 9.78	-	406.82/357	58.443±9.1	9.9964E-06±1.4E-06
100707032	16	3.995:4.271	COMP	0.4646 ± 0.1280	-0.070 ± 0.103	-	187.30 ± 10.70	-	355.67/357	41.634±7.6	6.7839E-06±1.1E-06
100707032	17	4.271:4.556	BAND	1.0310 ± 0.3440	0.399 ± 0.191	-2.385 ± 0.174	133.40 ± 10.90	81.33 ± 7.28	361.75/356	40.689±7.5	7.2323E-06±1.1E-06
100707032	18	4.556:4.852	COMP	0.4672 ± 0.1610	-0.178 ± 0.106	-	158.50 ± 9.09	-	366.21/357	39.363±9.7	5.3864E-06±1.2E-06
100707032	19	4.852:5.189	BAND	0.5867 ± 0.2270	0.195 ± 0.201	-2.263 ± 0.162	118.60 ± 11.50	70.29 ± 7.08	387.67/356	25.104±6.0	4.0715E-06±8.7E-07
100707032	20	5.189:5.613	COMP	0.4259 ± 0.1410	-0.280 ± 0.104	-	157.20 ± 9.54	-	413.59/357	39.806±8.9	5.2616E-06±1.1E-06
100707032	21	5.613:6.078	COMP	0.2871 ± 0.0967	-0.344 ± 0.103	-	167.10 ± 11.20	-	410.16/357	30.348±7.1	4.1476E-06±9.0E-07
100707032	22	6.078:6.689	COMP	0.1890 ± 0.0730	-0.279 ± 0.106	-	163.70 ± 10.50	-	382.08/357	18.306±5.5	2.5052E-06±7.1E-07
100707032	23	6.689:7.358	COMP	0.2207 ± 0.0876	-0.350 ± 0.106	-	153.20 ± 10.20	-	403.09/357	21.819±6.5	2.7694E-06±7.8E-07
100707032	24	7.358:8.001	SBPL	0.0809 ± 0.0321	-0.741 ± 0.093	-3.934 ± 0.990	134.47 ± 38.79	152.20 ± 35.80	395.2/356	23.332±8.9	2.8134E-06±9.7E-07
100707032	25	8.001:8.749	PL	0.0058 ± 0.0017	-1.375 ± 0.027	-	-	-	619.86/358	2.9860±0.92	5.8665E-07±1.7E-07
100707032	26	8.749:9.496	SBPL	0.0369 ± 0.0135	-0.387 ± 0.203	-2.339 ± 0.196	113.65 ± 33.33	65.11 ± 13.20	370.99/356	12.413±4.3	1.7197E-06±5.5E-07
100707032	27	9.496:10.332	PL	0.0067 ± 0.0019	-1.424 ± 0.027	-	-	-	481.85/358	3.5711±1.1	6.4793E-07±1.8E-07
100707032	28	10.332:11.232	PL	0.0050 ± 0.0019	-1.452 ± 0.028	-	-	-	574.19/358	2.7292±1.1	4.7292E-07±1.8E-07
100707032	29	11.232:12.226	none	-	-	-	-	-	-	-	-
100707032	30	12.226:13.348	PL	0.0064 ± 0.0024	-1.561 ± 0.030	-	-	-	533.38/358	3.8384±1.5	5.5754E-07±2.1E-07
100707032	31	13.348:14.669	none	-	-	-	-	-	-	-	-
100707032	32	14.669:16.372	none	-	-	-	-	-	-	-	-
100707032	33	16.372:18.635	none	-	-	-	-	-	-	-	-
100707032	34	18.635:21.239	PL	0.0116 ± 0.0034	-1.893 ± 0.036	-	-	-	484.17/358	9.9428±3.1	8.6263E-07±2.5E-07
100707032	35	21.239:25.985	none	-	-	-	-	-	-	-	-

Continued on next page

Table A.1 – continued from previous page

GRB name	spectrum	T_{start}:T_{stop} (s)	BEST model	A (ph s^{-1} cm^{-2} keV^{-1})	α	β	E_p (keV)	E_b (keV)	CSTAT/dof	photon flux (ph s^{-1} cm^{-2})	energy flux (erg s^{-1} cm^{-2})
(1)	(2)	(3)	(4)	(5)	(6)	(7)	(8)	(9)	(10)	(11)	(12)
100707032	36	25.985:36.370	none	-	-	-	-	-	-	-	-
100707032	37	36.370:52.131	none	-	-	-	-	-	-	-	-
100707032	38	52.131:69.442	PL	0.0026 ± 0.0009	-1.704 ± 0.041	-	-	-	567.53/358	1.8103±0.63	2.0911E-07±6.9E-08
100707032	39	69.442:93.238	none	-	-	-	-	-	-	-	-
100707032	40	93.238:97.280	none	-	-	-	-	-	-	-	-
100719989	1	-4.096:2.131	SBPL	0.0200 ± 0.0021	-0.290 ± 0.128	-2.158 ± 0.103	365.27 ± 117.22	158.00 ± 20.80	524.51/358	5.5903±0.46	1.5746E-06±9.9E-08
100719989	2	2.131:2.396	COMP	0.1869 ± 0.0168	-0.401 ± 0.056	-	529.90 ± 32.00	-	327.54/359	48.261±3.2	1.5832E-05±7.8E-07
100719989	3	2.396:2.563	COMP	0.2391 ± 0.0183	-0.703 ± 0.042	-	789.20 ± 58.90	-	393.79/359	78.822±5.0	2.5428E-05±1.2E-06
100719989	4	2.563:2.753	SBPL	0.2742 ± 0.0292	-0.555 ± 0.081	-2.253 ± 0.095	303.80 ± 51.45	164.60 ± 20.60	426.43/358	80.945±6.8	1.9379E-05±1.3E-06
100719989	5	2.753:3.092	COMP	0.2058 ± 0.0283	-0.664 ± 0.059	-	339.70 ± 25.70	-	426.22/359	46.621±4.4	9.7395E-06±7.0E-07
100719989	6	3.092:3.560	COMP	0.2252 ± 0.0333	-0.355 ± 0.070	-	280.20 ± 16.20	-	361.77/359	36.495±3.4	7.6587E-06±5.7E-07
100719989	7	3.560:3.917	SBPL	0.1620 ± 0.0203	-0.401 ± 0.101	-2.531 ± 0.169	193.65 ± 30.29	131.70 ± 16.90	395.92/358	42.099±4.7	8.4455E-06±7.7E-07
100719989	8	3.917:4.211	SBPL	0.1827 ± 0.0222	-0.513 ± 0.087	-2.557 ± 0.172	212.13 ± 33.78	150.30 ± 19.70	414.64/358	49.997±5.3	1.0213E-05±8.7E-07
100719989	9	4.211:4.417	SBPL	0.2495 ± 0.0260	-0.366 ± 0.112	-2.140 ± 0.085	277.54 ± 76.16	117.40 ± 14.40	387.81/358	67.611±6.0	1.5476E-05±1.1E-06
100719989	10	4.417:4.614	COMP	0.3163 ± 0.0466	-0.531 ± 0.062	-	307.80 ± 20.20	-	378.18/359	61.755±6.2	1.2895E-05±1.0E-06
100719989	11	4.614:4.909	COMP	0.2774 ± 0.0505	-0.540 ± 0.071	-	244.70 ± 16.30	-	436.49/359	47.177±5.7	8.2068E-06±8.1E-07
100719989	12	4.909:5.475	COMP	0.2691 ± 0.0682	-0.563 ± 0.085	-	170.10 ± 10.70	-	413.77/359	36.745±6.1	4.7585E-06±7.0E-07
100719989	13	5.475:6.634	COMP	0.0728 ± 0.0259	-0.912 ± 0.085	-	157.30 ± 14.00	-	423.41/359	14.537±4.0	1.5799E-06±4.1E-07
100719989	14	6.634:20.507	none	-	-	-	-	-	-	-	-
100719989	15	20.507:22.686	BAND	0.0391 ± 0.0087	-0.933 ± 0.098	-1.955 ± 0.111	277.40 ± 59.80	135.76 ± 29.90	461.13/358	10.396±1.3	1.8491E-06±1.9E-07
100719989	16	22.686:34.816	PL	0.0038 ± 0.0008	-1.655 ± 0.040	-	-	-	931.81/360	2.4605±0.58	3.0675E-07±6.3E-08
100722096	1	-2.048:0.500	none	-	-	-	-	-	-	-	-
100722096	2	0.500:1.073	none	-	-	-	-	-	-	-	-
100722096	3	1.073:1.729	PL	0.0118 ± 0.0042	-1.777 ± 0.024	-	-	-	692.16/480	8.8441±3.2	9.1026E-07±3.2E-07
100722096	4	1.729:2.093	PL	0.0156 ± 0.0045	-1.659 ± 0.022	-	-	-	676.43/480	10.262±3.0	1.2701E-06±3.6E-07
100722096	5	2.093:2.957	PL	0.0109 ± 0.0036	-1.791 ± 0.023	-	-	-	628.84/480	8.3307±2.8	8.3873E-07±2.8E-07
100722096	6	2.957:3.397	BAND	0.1809 ± 0.0703	-0.702 ± 0.110	-2.576 ± 0.236	102.00 ± 8.75	77.15 ± 10.39	521.54/478	21.584±7.8	2.2086E-06±7.5E-07
100722096	7	3.397:6.197	none	-	-	-	-	-	-	-	-
100722096	8	6.197:12.288	none	-	-	-	-	-	-	-	-
100724029	1	-37.889:4.096	BAND	0.0048 ± 0.0014	-0.654 ± 0.152	-1.624 ± 0.079	238.50 ± 63.60	88.98 ± 23.24	563.08/477	0.95837±0.16	2.1635E-07±3.0E-08
100724029	2	4.096:8.192	BAND	0.0198 ± 0.0022	-0.784 ± 0.053	-1.883 ± 0.081	653.60 ± 108.00	298.30 ± 49.39	490.79/477	6.2907±0.45	1.7724E-06±1.0E-07
100724029	3	8.192:10.240	SBPL	0.0321 ± 0.0029	-0.682 ± 0.061	-1.821 ± 0.058	-	159.40 ± 20.90	472.97/477	10.659±0.79	2.8408E-06±1.7E-07
100724029	4	10.240:11.264	SBPL	0.0345 ± 0.0037	-0.714 ± 0.064	-1.853 ± 0.079	-	192.60 ± 31.80	534.26/477	11.906±1.1	3.3137E-06±2.4E-07
100724029	5	11.264:13.312	SBPL	0.0318 ± 0.0027	-0.742 ± 0.049	-1.840 ± 0.059	-	183.10 ± 23.30	506.95/477	10.987±0.75	2.9541E-06±1.7E-07
100724029	6	13.312:14.336	BAND	0.0465 ± 0.0075	-0.613 ± 0.076	-2.046 ± 0.130	439.70 ± 66.40	229.77 ± 36.83	500.0/477	11.787±1.1	3.1556E-06±2.4E-07
100724029	7	14.336:15.360	BAND	0.0448 ± 0.0056	-0.765 ± 0.057	-1.843 ± 0.074	613.50 ± 107.00	270.57 ± 46.79	480.82/477	13.880±1.1	3.8943E-06±2.4E-07
100724029	8	15.360:16.384	SBPL	0.0450 ± 0.0043	-0.725 ± 0.057	-1.843 ± 0.061	-	186.90 ± 26.80	495.47/477	15.507±1.2	4.2507E-06±2.6E-07
100724029	9	16.384:17.408	SBPL	0.0401 ± 0.0039	-0.763 ± 0.056	-1.774 ± 0.058	-	199.30 ± 31.90	554.07/477	14.350±1.1	4.0483E-06±2.5E-07
100724029	10	17.408:18.432	SBPL	0.0428 ± 0.0042	-0.716 ± 0.058	-1.887 ± 0.070	-	198.80 ± 29.30	481.03/477	14.771±1.1	4.1001E-06±2.6E-07
100724029	11	18.432:19.456	SBPL	0.0329 ± 0.0036	-0.844 ± 0.053	-1.863 ± 0.080	-	250.00 ± 47.40	438.31/477	12.348±1.1	3.4333E-06±2.4E-07
100724029	12	19.456:20.480	SBPL	0.0331 ± 0.0037	-0.870 ± 0.051	-1.967 ± 0.102	764.11 ± 266.93	266.40 ± 51.50	483.84/477	12.485±1.1	3.3545E-06±2.4E-07
100724029	13	20.480:22.528	BAND	0.0462 ± 0.0065	-0.650 ± 0.066	-1.785 ± 0.057	337.20 ± 44.20	145.44 ± 18.67	473.51/477	10.711±0.83	2.6016E-06±1.7E-07
100724029	14	22.528:24.576	BAND	0.0479 ± 0.0066	-0.755 ± 0.058	-2.056 ± 0.102	383.30 ± 49.30	203.93 ± 27.72	471.26/477	12.372±0.98	2.8091E-06±1.8E-07

Continued on next page

Table A.1 – continued from previous page

GRB name	spectrum	T_{start}:T_{stop} (s)	BEST model	A (ph s^{-1} cm^{-2} keV^{-1})	α	β	E_p (keV)	E_b (keV)	CSTAT/dof	photon flux (ph s^{-1} cm^{-2})	energy flux (erg s^{-1} cm^{-2})
(1)	(2)	(3)	(4)	(5)	(6)	(7)	(8)	(9)	(10)	(11)	(12)
100724029	15	24.576:26.624	BAND	0.0466 ± 0.0075	−0.660 ± 0.071	−1.984 ± 0.093	330.80 ± 43.30	167.28 ± 22.33	480.83/477	10.627±0.95	2.4293E-06±1.8E-07
100724029	16	26.624:30.720	BAND	0.0221 ± 0.0034	−0.900 ± 0.059	−1.935 ± 0.107	407.00 ± 70.30	193.86 ± 34.88	506.05/477	6.4584±0.63	1.3723E-06±1.1E-07
100724029	17	30.720:34.817	BAND	0.0224 ± 0.0054	−0.755 ± 0.115	−1.735 ± 0.084	208.40 ± 43.30	85.58 ± 17.22	456.31/477	4.5620±0.69	8.8105E-07±1.2E-07
100724029	18	34.817:38.913	COMP	0.0222 ± 0.0032	−0.938 ± 0.047	-	414.00 ± 48.40	-	436.74/478	6.6253±0.70	1.3022E-06±1.1E-07
100724029	19	38.913:39.937	BAND	0.0830 ± 0.0158	−0.634 ± 0.083	−2.167 ± 0.141	284.00 ± 36.70	162.39 ± 22.85	461.24/477	17.056±1.8	3.5444E-06±3.0E-07
100724029	20	39.937:41.985	SBPL	0.0272 ± 0.0032	−0.805 ± 0.062	−2.005 ± 0.110	362.42 ± 127.97	141.00 ± 22.10	434.0/477	9.0772±0.97	1.9193E-06±1.8E-07
100724029	21	41.985:45.057	COMP	0.0384 ± 0.0067	−0.829 ± 0.055	-	278.30 ± 24.90	-	504.23/478	9.0373±1.1	1.5017E-06±1.5E-07
100724029	22	45.057:47.105	COMP	0.0333 ± 0.0049	−0.797 ± 0.050	-	383.50 ± 37.30	-	556.26/478	8.7331±0.94	1.8189E-06±1.7E-07
100724029	23	47.105:49.153	COMP	0.0363 ± 0.0057	−0.894 ± 0.051	-	378.30 ± 42.70	-	491.69/478	10.191±1.1	1.9689E-06±1.8E-07
100724029	24	49.153:53.249	BAND	0.0258 ± 0.0054	−0.724 ± 0.095	−1.801 ± 0.086	199.70 ± 31.40	87.73 ± 13.66	514.81/477	4.9519±0.71	9.2690E-07±1.2E-07
100724029	25	53.249:55.297	COMP	0.0371 ± 0.0046	−0.845 ± 0.043	-	452.80 ± 44.10	-	463.06/478	10.713±0.95	2.3725E-06±1.7E-07
100724029	26	55.297:56.321	COMP	0.0761 ± 0.0099	−0.657 ± 0.051	-	361.00 ± 27.70	-	493.07/478	17.695±1.6	3.8716E-06±2.7E-07
100724029	27	56.321:57.345	COMP	0.0463 ± 0.0053	−0.823 ± 0.043	-	565.90 ± 60.60	-	506.71/478	14.253±1.2	3.5939E-06±2.5E-07
100724029	28	57.345:58.369	COMP	0.0490 ± 0.0066	−0.765 ± 0.050	-	445.40 ± 44.30	-	493.78/478	13.390±1.3	3.1155E-06±2.5E-07
100724029	29	58.369:59.393	COMP	0.0693 ± 0.0067	−0.736 ± 0.037	-	486.10 ± 36.20	-	526.12/478	19.303±1.3	4.8185E-06±2.7E-07
100724029	30	59.393:60.417	SBPL	0.0642 ± 0.0057	−0.797 ± 0.042	−2.259 ± 0.122	342.56 ± 71.22	199.60 ± 24.20	535.94/477	21.423±1.6	4.8267E-06±3.0E-07
100724029	31	60.417:61.441	BAND	0.1114 ± 0.0150	−0.562 ± 0.059	−2.198 ± 0.106	302.10 ± 26.80	175.38 ± 17.32	467.44/477	22.448±1.7	5.0011E-06±3.1E-07
100724029	32	61.441:62.465	SBPL	0.0743 ± 0.0060	−0.715 ± 0.047	−2.088 ± 0.078	416.06 ± 140.47	171.70 ± 18.50	503.19/477	24.029±1.6	5.7076E-06±3.1E-07
100724029	33	62.465:63.489	SBPL	0.0800 ± 0.0055	−0.738 ± 0.039	−1.977 ± 0.056	687.44 ± 221.21	186.20 ± 18.10	474.83/477	26.948±1.5	6.8841E-06±3.1E-07
100724029	34	63.489:64.513	BAND	0.1128 ± 0.0140	−0.557 ± 0.056	−2.082 ± 0.079	328.00 ± 29.90	177.27 ± 16.65	467.91/477	23.837±1.6	5.6749E-06±3.1E-07
100724029	35	64.513:65.537	BAND	0.0839 ± 0.0113	−0.652 ± 0.057	−2.121 ± 0.107	344.80 ± 36.50	190.94 ± 21.87	478.39/477	19.303±1.5	4.4211E-06±2.8E-07
100724029	36	65.537:66.561	BAND	0.0784 ± 0.0092	−0.697 ± 0.050	−2.195 ± 0.122	429.40 ± 46.30	249.11 ± 29.93	508.5/477	20.415±1.4	5.0252E-06±2.8E-07
100724029	37	66.561:67.585	COMP	0.0767 ± 0.0066	−0.764 ± 0.034	-	532.90 ± 38.70	-	538.78/478	22.468±1.4	5.7674E-06±2.9E-07
100724029	38	67.585:68.609	COMP	0.0702 ± 0.0078	−0.744 ± 0.041	-	417.70 ± 31.90	-	496.43/478	18.443±1.5	4.1937E-06±2.7E-07
100724029	39	68.609:69.633	COMP	0.0671 ± 0.0071	−0.772 ± 0.039	-	464.60 ± 37.20	-	513.37/478	18.735±1.4	4.4414E-06±2.7E-07
100724029	40	69.633:70.657	COMP	0.0602 ± 0.0069	−0.852 ± 0.040	-	475.30 ± 44.60	-	538.34/478	17.762±1.5	4.0123E-06±2.7E-07
100724029	41	70.657:71.681	SBPL	0.0505 ± 0.0057	−0.773 ± 0.064	−2.078 ± 0.110	332.87 ± 115.55	147.00 ± 21.70	537.22/477	16.447±1.6	3.4920E-06±2.9E-07
100724029	42	71.681:72.705	BAND	0.0619 ± 0.0131	−0.607 ± 0.091	−2.047 ± 0.141	252.20 ± 34.40	133.27 ± 20.08	454.75/477	11.759±1.5	2.3931E-06±2.7E-07
100724029	43	72.705:73.729	BAND	0.0850 ± 0.0138	−0.590 ± 0.074	−2.014 ± 0.090	312.50 ± 38.20	161.11 ± 20.04	462.41/477	17.929±1.6	4.1366E-06±2.9E-07
100724029	44	73.729:74.753	BAND	0.0870 ± 0.0104	−0.603 ± 0.052	−2.183 ± 0.110	381.50 ± 36.40	219.03 ± 22.98	565.76/477	20.378±1.4	5.0358E-06±2.8E-07
100724029	45	74.753:75.777	SBPL	0.0840 ± 0.0060	−0.714 ± 0.041	−2.081 ± 0.066	461.03 ± 154.41	182.20 ± 17.20	458.38/477	27.448±1.6	6.7421E-06±3.2E-07
100724029	46	75.777:76.801	BAND	0.1059 ± 0.0148	−0.639 ± 0.058	−2.246 ± 0.124	312.80 ± 30.50	187.95 ± 21.02	482.15/477	22.910±1.8	4.9358E-06±3.1E-07
100724029	47	76.801:77.825	COMP	0.0661 ± 0.0082	−0.826 ± 0.044	-	414.30 ± 37.70	-	512.14/478	18.243±1.6	3.8973E-06±2.7E-07
100724029	48	77.825:79.873	BAND	0.0486 ± 0.0081	−0.709 ± 0.067	−2.057 ± 0.120	269.20 ± 31.50	143.69 ± 18.93	467.39/477	10.398±1.1	2.0572E-06±1.8E-07
100724029	49	79.873:83.969	BAND	0.0278 ± 0.0063	−0.822 ± 0.100	−1.862 ± 0.103	213.50 ± 39.50	97.58 ± 18.02	496.53/477	6.0252±0.86	1.0697E-06±1.3E-07
100724029	50	83.969:92.161	COMP	0.0111 ± 0.0024	−0.865 ± 0.063	-	342.80 ± 44.00	-	539.78/478	2.9317±0.47	5.4516E-07±7.6E-08
100724029	51	92.161:105.474	SBPL	0.0079 ± 0.0013	−0.930 ± 0.089	−1.900 ± 0.113	342.43 ± 124.18	99.92 ± 22.50	490.55/477	2.9344±0.43	5.2493E-07±6.6E-08
100724029	52	105.474:114.690	COMP	0.0093 ± 0.0021	−1.107 ± 0.057	-	373.40 ± 67.90	-	523.51/478	3.1263±0.54	5.1192E-07±7.6E-08
100724029	53	114.690:120.834	PL	0.0017 ± 0.0006	−1.497 ± 0.024	-	-	-	597.7/479	0.98552±0.37	1.5879E-07±5.9E-08
100724029	54	120.834:125.954	COMP	0.0236 ± 0.0081	−0.953 ± 0.072	-	171.60 ± 16.90	-	522.49/478	5.1559±1.4	5.8542E-07±1.5E-07
100724029	55	125.954:129.026	COMP	0.0272 ± 0.0086	−1.033 ± 0.062	-	181.20 ± 17.80	-	497.19/478	6.7096±1.7	7.6437E-07±1.9E-07
100724029	56	129.026:132.098	PL	0.0031 ± 0.0009	−1.493 ± 0.021	-	-	-	569.88/479	1.7571±0.53	2.8480E-07±8.4E-08
100724029	57	132.098:137.218	PL	0.0031 ± 0.0010	−1.615 ± 0.030	-	-	-	510.96/479	1.9579±0.63	2.6070E-07±8.0E-08

Continued on next page

Table A.1 – continued from previous page

GRB name	spectrum	T_{start}:T_{stop} (s)	BEST model	A (ph s^{-1} cm^{-2} keV^{-1})	α	β	E_p (keV)	E_b (keV)	CSTAT/dof	photon flux (ph s^{-1} cm^{-2})	energy flux (erg s^{-1} cm^{-2})
(1)	(2)	(3)	(4)	(5)	(6)	(7)	(8)	(9)	(10)	(11)	(12)
100724029	58	137.218:203.779	PL	0.0010 ± 0.0002	−1.541 ± 0.028	-	-	-	627.77/479	0.58728±0.14	8.8066E-08±2.0E-08
100724029	59	203.779:231.428	none	-	-	-	-	-	-	-	-
100728095	1	-4.096:19.456	COMP	0.0077 ± 0.0015	−0.556 ± 0.092	-	387.20 ± 47.30	-	392.87/359	1.7386±0.22	4.2381E-07±4.2E-08
100728095	2	19.456:46.081	COMP	0.0109 ± 0.0039	−0.396 ± 0.122	-	207.70 ± 19.90	-	466.01/359	1.4514±0.36	2.3390E-07±5.3E-08
100728095	3	46.081:54.273	COMP	0.0166 ± 0.0028	−0.514 ± 0.077	-	371.30 ± 35.80	-	365.91/359	3.5939±0.38	8.7075E-07±7.5E-08
100728095	4	54.273:58.369	COMP	0.0317 ± 0.0051	−0.501 ± 0.074	-	344.00 ± 29.90	-	361.98/359	6.5000±0.65	1.4994E-06±1.2E-07
100728095	5	58.369:63.489	COMP	0.0176 ± 0.0032	−0.560 ± 0.081	-	384.70 ± 42.80	-	340.52/359	4.0030±0.48	9.6908E-07±9.6E-08
100728095	6	63.489:68.609	COMP	0.0210 ± 0.0032	−0.550 ± 0.075	-	416.70 ± 43.00	-	356.65/359	4.9538±0.49	1.2741E-06±9.8E-08
100728095	7	68.609:72.705	COMP	0.0255 ± 0.0034	−0.523 ± 0.070	-	451.90 ± 43.20	-	364.86/359	6.2348±0.54	1.7195E-06±1.1E-07
100728095	8	72.705:76.801	COMP	0.0233 ± 0.0028	−0.525 ± 0.065	-	505.20 ± 47.20	-	369.04/359	6.0486±0.48	1.7862E-06±1.1E-07
100728095	9	76.801:79.873	COMP	0.0380 ± 0.0046	−0.460 ± 0.062	-	407.00 ± 30.60	-	382.13/359	8.4714±0.66	2.2580E-06±1.4E-07
100728095	10	79.873:81.921	COMP	0.0408 ± 0.0050	−0.526 ± 0.061	-	451.90 ± 38.30	-	405.57/359	9.9638±0.81	2.7421E-06±1.7E-07
100728095	11	81.921:83.969	COMP	0.0459 ± 0.0053	−0.538 ± 0.058	-	443.30 ± 35.50	-	376.36/359	11.147±0.85	3.0089E-06±1.7E-07
100728095	12	83.969:86.017	COMP	0.0515 ± 0.0074	−0.390 ± 0.071	-	353.90 ± 26.40	-	337.97/359	10.112±0.90	2.5207E-06±1.7E-07
100728095	13	86.017:89.089	COMP	0.0381 ± 0.0050	−0.582 ± 0.058	-	391.70 ± 32.30	-	387.62/359	8.8332±0.75	2.1384E-06±1.4E-07
100728095	14	89.089:92.161	COMP	0.0403 ± 0.0070	−0.602 ± 0.071	-	312.70 ± 28.40	-	392.21/359	8.3321±0.92	1.7000E-06±1.5E-07
100728095	15	92.161:96.257	COMP	0.0405 ± 0.0082	−0.444 ± 0.080	-	254.80 ± 19.50	-	375.48/359	6.5287±0.84	1.2226E-06±1.3E-07
100728095	16	96.257:103.425	COMP	0.0380 ± 0.0114	−0.444 ± 0.097	-	184.80 ± 13.80	-	372.04/359	4.8398±0.98	6.9716E-07±1.3E-07
100728095	17	103.425:111.618	COMP	0.0204 ± 0.0045	−0.734 ± 0.075	-	266.70 ± 27.50	-	399.21/359	4.3198±0.64	7.3346E-07±9.2E-08
100728095	18	111.618:123.906	SBPL	0.0099 ± 0.0037	−0.848 ± 0.084	−3.567 ± 0.978	150.62 ± 53.94	161.50 ± 43.20	428.29/358	3.0687±1.1	3.9044E-07±1.2E-07
100728095	19	123.906:128.002	COMP	0.0407 ± 0.0101	−0.364 ± 0.090	-	222.90 ± 16.50	-	388.1/359	5.5476±0.91	9.5931E-07±1.4E-07
100728095	20	128.002:135.170	COMP	0.0360 ± 0.0085	−0.535 ± 0.083	-	216.60 ± 17.10	-	386.68/359	5.6247±0.85	8.9100E-07±1.1E-07
100728095	21	135.170:143.362	none	-	-	-	-	-	-	-	-
100728095	22	143.362:168.962	none	-	-	-	-	-	-	-	-
100728095	23	168.962:178.179	PL	0.0016 ± 0.0006	−1.543 ± 0.026	-	-	-	482.58/360	0.95701±0.38	1.4346E-07±5.5E-08
100728095	24	178.179:184.323	COMP	0.0290 ± 0.0090	−0.607 ± 0.093	-	200.00 ± 18.60	-	365.5/359	4.6204±0.98	6.6867E-07±1.3E-07
100728095	25	184.323:283.652	none	-	-	-	-	-	-	-	-
100826957	1	0.000:17.448	BAND	0.0457 ± 0.0032	−0.587 ± 0.034	−1.983 ± 0.037	307.10 ± 16.10	155.70 ± 8.25	786.28/356	9.5481±0.35	2.2017E-06±6.6E-08
100826957	2	17.448:18.143	BAND	0.1129 ± 0.0221	−0.481 ± 0.099	−1.929 ± 0.078	276.00 ± 37.20	135.58 ± 18.03	386.53/356	20.713±2.0	4.8688E-06±3.9E-07
100826957	3	18.143:18.677	SBPL	0.0835 ± 0.0094	−0.691 ± 0.070	−2.065 ± 0.096	430.66 ± 148.88	177.40 ± 26.50	442.96/356	27.019±2.4	6.6972E-06±4.8E-07
100826957	4	18.677:19.127	COMP	0.0847 ± 0.0093	−0.750 ± 0.048	-	665.00 ± 74.90	-	400.62/357	26.685±2.1	7.7003E-06±4.8E-07
100826957	5	19.127:19.558	BAND	0.1173 ± 0.0181	−0.628 ± 0.074	−2.063 ± 0.099	436.80 ± 64.40	231.39 ± 34.21	359.52/356	29.793±2.5	7.8530E-06±5.1E-07
100826957	6	19.558:19.975	SBPL	0.0848 ± 0.0092	−0.764 ± 0.056	−2.123 ± 0.107	577.95 ± 202.87	269.40 ± 45.70	345.56/356	30.516±2.5	8.5720E-06±5.4E-07
100826957	7	19.975:20.469	BAND	0.1270 ± 0.0203	−0.655 ± 0.074	−2.074 ± 0.097	408.60 ± 60.30	218.31 ± 32.54	349.41/356	31.716±2.7	7.9365E-06±5.1E-07
100826957	8	20.469:20.901	SBPL	0.1016 ± 0.0111	−0.712 ± 0.062	−2.207 ± 0.113	420.35 ± 106.09	220.40 ± 33.10	378.45/356	33.903±2.8	8.7391E-06±5.6E-07
100826957	9	20.901:21.312	COMP	0.0977 ± 0.0104	−0.739 ± 0.049	-	654.90 ± 70.40	-	391.26/357	30.487±2.4	8.8203E-06±5.3E-07
100826957	10	21.312:21.758	BAND	0.1569 ± 0.0266	−0.592 ± 0.082	−2.101 ± 0.098	363.70 ± 50.40	198.61 ± 27.55	417.12/356	35.732±3.1	8.7577E-06±5.7E-07
100826957	11	21.758:22.218	COMP	0.0823 ± 0.0085	−0.785 ± 0.046	-	714.60 ± 82.40	-	332.85/357	26.836±2.1	7.7484E-06±4.8E-07
100826957	12	22.218:22.605	BAND	0.1493 ± 0.0238	−0.597 ± 0.079	−1.959 ± 0.073	431.80 ± 67.00	213.55 ± 32.82	354.01/356	37.307±3.0	1.0111E-05±6.0E-07
100826957	13	22.605:23.088	BAND	0.1308 ± 0.0209	−0.622 ± 0.077	−1.990 ± 0.076	412.20 ± 62.10	207.26 ± 31.01	361.28/356	32.327±2.6	8.3947E-06±5.2E-07
100826957	14	23.088:23.685	COMP	0.0547 ± 0.0056	−0.939 ± 0.040	-	1070.00 ± 171.00	-	459.64/357	20.598±1.7	5.8416E-06±3.9E-07
100826957	15	23.685:24.359	BAND	0.0833 ± 0.0149	−0.680 ± 0.083	−1.910 ± 0.084	369.40 ± 62.00	175.04 ± 29.07	372.66/356	20.338±2.0	4.8928E-06±3.8E-07
100826957	16	24.359:25.236	BAND	0.0843 ± 0.0145	−0.639 ± 0.081	−1.928 ± 0.077	351.70 ± 53.40	170.23 ± 25.26	451.19/356	19.584±1.7	4.7196E-06±3.3E-07

Continued on next page

Table A.1 – continued from previous page

GRB name	spectrum	T_{start}:T_{stop} (s)	BEST model	A (ph s^{-1} cm^{-2} keV^{-1})	α	β	E_p (keV)	E_b (keV)	CSTAT/dof	photon flux (ph s^{-1} cm^{-2})	energy flux (erg s^{-1} cm^{-2})
(1)	(2)	(3)	(4)	(5)	(6)	(7)	(8)	(9)	(10)	(11)	(12)
100826957	17	25.236:25.890	SBPL	0.0592 ± 0.0067	-0.848 ± 0.061	-1.919 ± 0.082	794.83 ± 294.45	191.30 ± 34.70	358.42/356	21.078±1.9	5.1441E-06±3.9E-07
100826957	18	25.890:26.700	COMP	0.0542 ± 0.0071	-0.877 ± 0.048	-	578.20 ± 76.00	-	451.97/357	17.246±1.7	4.1945E-06±3.3E-07
100826957	19	26.700:28.004	BAND	0.0838 ± 0.0148	-0.697 ± 0.081	-1.994 ± 0.090	276.70 ± 37.70	141.79 ± 19.70	411.48/356	18.026±1.7	3.6939E-06±2.8E-07
100826957	20	28.004:29.063	BAND	0.1039 ± 0.0197	-0.589 ± 0.088	-2.037 ± 0.093	254.40 ± 31.80	134.29 ± 17.09	420.26/356	19.543±1.9	4.0453E-06±3.2E-07
100826957	21	29.063:30.680	COMP	0.0433 ± 0.0058	-0.968 ± 0.046	-	478.30 ± 60.60	-	456.64/357	13.801±1.3	2.8463E-06±2.3E-07
100826957	22	30.680:122.880	SBPL	0.0116 ± 0.0005	-0.775 ± 0.051	-1.781 ± 0.017	-	44.96 ± 2.90	1320.6/356	5.0894±0.21	7.9565E-07±2.9E-08
100829876	1	-1.024:0.472	none	-	-	-	-	-	-	-	-
100829876	2	0.472:0.688	COMP	0.4196 ± 0.1230	-0.409 ± 0.103	-	231.20 ± 22.50	-	253.05/240	61.202±11.0	1.0727E-05±1.6E-06
100829876	3	0.688:0.846	COMP	0.3570 ± 0.0659	-0.440 ± 0.081	-	365.30 ± 34.60	-	246.86/240	73.576±8.8	1.8315E-05±1.6E-06
100829876	4	0.846:1.030	COMP	0.3845 ± 0.0880	-0.517 ± 0.088	-	280.90 ± 27.60	-	248.7/240	70.080±10.0	1.3737E-05±1.6E-06
100829876	5	1.030:1.588	SBPL	0.0760 ± 0.0267	-0.294 ± 0.270	-2.321 ± 0.216	105.12 ± 40.18	57.43 ± 13.60	273.39/239	26.823±8.7	3.5839E-06±1.0E-06
100829876	6	1.588:1.755	COMP	0.5242 ± 0.1310	-0.083 ± 0.110	-	252.10 ± 19.60	-	238.72/240	64.398±9.6	1.3639E-05±1.7E-06
100829876	7	1.755:6.714	none	-	-	-	-	-	-	-	-
100829876	8	6.714:12.838	none	-	-	-	-	-	-	-	-
100829876	9	12.838:16.384	none	-	-	-	-	-	-	-	-
100910818	1	-1.024:5.293	COMP	0.0119 ± 0.0031	-1.229 ± 0.056	-	283.20 ± 45.90	-	549.87/478	4.2365±0.88	5.5759E-07±1.1E-07
100910818	2	5.293:8.805	COMP	0.0430 ± 0.0114	-0.834 ± 0.071	-	182.90 ± 14.70	-	540.68/478	8.3555±1.6	1.0380E-06±1.8E-07
100910818	3	8.805:9.239	COMP	0.4331 ± 0.0953	-0.448 ± 0.067	-	161.20 ± 7.27	-	461.68/478	49.852±7.5	6.4199E-06±8.8E-07
100910818	4	9.239:11.728	COMP	0.0640 ± 0.0236	-0.981 ± 0.071	-	123.50 ± 8.21	-	483.76/478	12.494±3.8	1.1402E-06±3.3E-07
100910818	5	11.728:13.343	COMP	0.1046 ± 0.0289	-0.844 ± 0.066	-	145.90 ± 9.11	-	462.38/478	18.357±3.8	1.9435E-06±3.8E-07
100910818	6	13.343:21.504	none	-	-	-	-	-	-	-	-
100918863	1	-1.024:26.551	COMP	0.0200 ± 0.0021	-0.424 ± 0.056	-	326.70 ± 17.80	-	779.76/358	3.7774±0.24	8.7057E-07±4.2E-08
100918863	2	26.551:30.596	COMP	0.0351 ± 0.0054	-0.476 ± 0.077	-	334.70 ± 27.80	-	377.98/358	6.9675±0.67	1.5945E-06±1.2E-07
100918863	3	30.596:35.293	COMP	0.0205 ± 0.0033	-0.661 ± 0.072	-	402.70 ± 44.10	-	443.68/358	5.0507±0.54	1.1862E-06±1.0E-07
100918863	4	35.293:41.547	COMP	0.0217 ± 0.0034	-0.629 ± 0.072	-	368.40 ± 36.50	-	465.11/358	4.9947±0.51	1.1277E-06±9.2E-08
100918863	5	41.547:47.578	COMP	0.0228 ± 0.0035	-0.663 ± 0.070	-	376.90 ± 37.90	-	425.51/358	5.4432±0.54	1.2222E-06±9.5E-08
100918863	6	47.578:53.579	COMP	0.0199 ± 0.0030	-0.727 ± 0.067	-	427.60 ± 48.80	-	357.45/358	5.2173±0.52	1.2176E-06±9.4E-08
100918863	7	53.579:58.077	COMP	0.0172 ± 0.0020	-0.764 ± 0.060	-	699.80 ± 94.60	-	393.0/358	5.5385±0.47	1.6165E-06±1.0E-07
100918863	8	58.077:59.618	COMP	0.0272 ± 0.0025	-0.886 ± 0.044	-	1222.00 ± 180.00	-	335.69/358	10.365±0.82	3.2205E-06±2.0E-07
100918863	9	59.618:61.043	COMP	0.0354 ± 0.0038	-0.796 ± 0.055	-	764.70 ± 102.00	-	396.1/358	11.832±0.96	3.4775E-06±2.1E-07
100918863	10	61.043:62.294	COMP	0.0418 ± 0.0048	-0.740 ± 0.059	-	628.30 ± 75.20	-	339.58/358	12.856±1.1	3.6506E-06±2.3E-07
100918863	11	62.294:63.378	COMP	0.0314 ± 0.0032	-0.869 ± 0.048	-	1132.00 ± 176.00	-	395.47/358	11.733±0.99	3.6415E-06±2.4E-07
100918863	12	63.378:64.752	COMP	0.0368 ± 0.0042	-0.766 ± 0.057	-	700.20 ± 89.50	-	344.51/358	11.840±0.99	3.4491E-06±2.2E-07
100918863	13	64.752:66.287	COMP	0.0322 ± 0.0039	-0.765 ± 0.059	-	655.90 ± 86.40	-	352.15/358	10.153±0.90	2.8796E-06±2.0E-07
100918863	14	66.287:67.868	COMP	0.0295 ± 0.0030	-0.922 ± 0.049	-	977.50 ± 157.00	-	435.83/358	10.871±0.91	3.0684E-06±2.0E-07
100918863	15	67.868:69.882	COMP	0.0306 ± 0.0040	-0.816 ± 0.061	-	573.60 ± 77.70	-	416.0/358	9.4284±0.89	2.4081E-06±1.7E-07
100918863	16	69.882:72.241	COMP	0.0268 ± 0.0034	-0.889 ± 0.057	-	643.20 ± 96.40	-	290.13/358	8.8443±0.82	2.2308E-06±1.6E-07
100918863	17	72.241:79.309	COMP	0.0248 ± 0.0046	-0.728 ± 0.073	-	298.50 ± 30.50	-	440.8/358	5.5269±0.66	1.0192E-06±9.7E-08
100918863	18	79.309:88.104	COMP	0.0134 ± 0.0020	-0.935 ± 0.060	-	506.10 ± 78.30	-	435.89/358	4.2529±0.46	9.2662E-07±7.8E-08
100918863	19	88.104:91.588	COMP	0.0218 ± 0.0025	-0.816 ± 0.058	-	684.60 ± 93.90	-	409.16/358	7.0823±0.61	1.9567E-06±1.2E-07
100918863	20	91.588:93.962	COMP	0.0267 ± 0.0031	-0.851 ± 0.056	-	714.80 ± 102.00	-	329.34/358	8.9021±0.76	2.4261E-06±1.6E-07
100918863	21	93.962:96.147	COMP	0.0243 ± 0.0027	-0.780 ± 0.057	-	822.20 ± 115.00	-	363.03/358	8.2575±0.68	2.5306E-06±1.6E-07
100918863	22	96.147:98.247	COMP	0.0258 ± 0.0030	-0.898 ± 0.054	-	791.60 ± 127.00	-	381.29/358	9.0237±0.81	2.4421E-06±1.7E-07

Continued on next page

Table A.1 – continued from previous page

GRB name	spectrum	T_{start}:T_{stop} (s)	BEST model	A (ph s^{-1} cm^{-2} keV^{-1})	α	β	E_p (keV)	E_b (keV)	CSTAT/dof	photon flux (ph s^{-1} cm^{-2})	energy flux (erg s^{-1} cm^{-2})
(1)	(2)	(3)	(4)	(5)	(6)	(7)	(8)	(9)	(10)	(11)	(12)
100918863	23	98.247:100.619	COMP	0.0303 ± 0.0043	−0.762 ± 0.067	-	494.50 ± 62.60	-	425.64/358	8.6110±0.85	2.1304E-06±1.6E-07
100918863	24	100.619:103.859	COMP	0.0210 ± 0.0030	−0.860 ± 0.062	-	580.70 ± 88.10	-	356.29/358	6.6399±0.67	1.6439E-06±1.3E-07
100918863	25	103.859:108.385	COMP	0.0223 ± 0.0036	−0.877 ± 0.067	-	431.20 ± 60.70	-	392.7/358	6.4663±0.72	1.3616E-06±1.1E-07
100918863	26	108.385:119.808	COMP	0.0149 ± 0.0044	−0.841 ± 0.097	-	239.80 ± 33.30	-	397.32/358	3.3108±0.67	4.9462E-07±8.3E-08
101014175	1	-3.584:1.536	COMP	0.0414 ± 0.0021	−0.704 ± 0.028	-	347.00 ± 15.00	-	521.36/256	9.7443±0.30	2.0208E-06±5.8E-08
101014175	2	1.536:2.560	COMP	0.1459 ± 0.0070	−0.782 ± 0.025	-	348.00 ± 14.50	-	455.54/256	36.347±1.1	7.2023E-06±1.9E-07
101014175	3	2.560:3.584	BAND	0.1676 ± 0.0231	−0.748 ± 0.062	−2.351 ± 0.113	130.70 ± 8.71	87.42 ± 7.41	334.86/255	25.109±1.5	3.1003E-06±1.7E-07
101014175	4	3.584:4.608	COMP	0.0745 ± 0.0075	−1.053 ± 0.043	-	220.50 ± 16.80	-	395.53/256	20.191±1.3	2.5733E-06±1.4E-07
101014175	5	4.608:5.632	COMP	0.0690 ± 0.0105	−1.097 ± 0.055	-	123.10 ± 7.64	-	282.75/256	15.975±1.6	1.4105E-06±1.3E-07
101014175	6	5.632:6.656	COMP	0.0730 ± 0.0080	−1.157 ± 0.042	-	176.70 ± 12.70	-	314.76/256	20.887±1.5	2.2297E-06±1.4E-07
101014175	7	6.656:7.680	COMP	0.1024 ± 0.0074	−0.849 ± 0.033	-	268.30 ± 14.40	-	393.08/256	24.157±1.1	3.8784E-06±1.5E-07
101014175	8	7.680:8.704	COMP	0.1350 ± 0.0180	−0.725 ± 0.051	-	119.80 ± 4.53	-	351.83/256	17.961±1.5	1.7137E-06±1.3E-07
101014175	9	8.704:9.728	COMP	0.1164 ± 0.0172	−1.067 ± 0.051	-	101.00 ± 4.70	-	352.86/256	23.604±2.1	1.8701E-06±1.5E-07
101014175	10	9.728:10.752	COMP	0.0495 ± 0.0095	−1.148 ± 0.063	-	109.80 ± 7.68	-	281.49/256	11.817±1.6	9.6544E-07±1.2E-07
101014175	11	10.752:13.824	COMP	0.0132 ± 0.0047	−1.538 ± 0.093	-	58.71 ± 5.87	-	281.84/256	5.0733±1.3	2.9852E-07±7.2E-08
101014175	12	13.824:19.968	SBPL	0.0024 ± 0.0009	−1.540 ± 0.143	−2.832 ± 0.313	36.67 ± 12.57	45.24 ± 14.50	272.61/255	2.8666±1.2	1.5757E-07±6.1E-08
101014175	13	19.968:20.992	COMP	0.0243 ± 0.0041	−1.604 ± 0.052	-	213.80 ± 57.30	-	341.78/256	13.270±1.6	1.2424E-06±1.3E-07
101014175	14	20.992:23.040	COMP	0.0181 ± 0.0027	−1.543 ± 0.049	-	210.20 ± 44.40	-	343.65/256	9.0620±0.99	8.7241E-07±8.6E-08
101014175	15	23.040:24.064	COMP	0.0285 ± 0.0037	−1.306 ± 0.050	-	372.00 ± 80.20	-	305.05/256	11.587±1.1	1.6139E-06±1.3E-07
101014175	16	24.064:26.112	COMP	0.0390 ± 0.0042	−1.270 ± 0.040	-	203.90 ± 19.70	-	342.97/256	13.447±0.94	1.4726E-06±8.9E-08
101014175	17	26.112:27.136	COMP	0.0766 ± 0.0057	−1.004 ± 0.034	-	338.50 ± 26.40	-	388.81/256	22.695±1.1	3.8174E-06±1.6E-07
101014175	18	27.136:28.160	COMP	0.0778 ± 0.0053	−1.007 ± 0.031	-	369.30 ± 27.90	-	397.56/256	23.736±1.1	4.1764E-06±1.6E-07
101014175	19	28.160:31.232	SBPL	0.0050 ± 0.0013	−1.054 ± 0.349	−2.459 ± 0.136	31.44 ± 10.24	25.10 ± 7.54	287.76/255	5.3945±1.4	3.3477E-07±8.3E-08
101014175	20	31.232:33.280	PL	0.0040 ± 0.0012	−2.034 ± 0.035	-	-	-	283.54/257	4.0806±1.2	2.9265E-07±8.7E-08
101014175	21	33.280:34.305	COMP	0.0392 ± 0.0060	−1.317 ± 0.053	-	174.70 ± 20.90	-	320.86/256	13.871±1.4	1.3773E-06±1.3E-07
101014175	22	34.305:35.329	COMP	0.0835 ± 0.0121	−1.097 ± 0.051	-	118.20 ± 6.78	-	374.72/256	19.000±1.7	1.6388E-06±1.3E-07
101014175	23	35.329:36.353	COMP	0.0645 ± 0.0136	−1.213 ± 0.063	-	80.90 ± 4.35	-	352.27/256	15.154±2.2	1.0386E-06±1.4E-07
101014175	24	36.353:49.665	PL	0.0014 ± 0.0004	−2.069 ± 0.052	-	-	-	314.5/257	1.5220±0.49	1.0435E-07±3.2E-08
101014175	25	95.745:101.890	COMP	0.0361 ± 0.0098	−1.047 ± 0.059	-	154.00 ± 13.80	-	402.65/356	8.5161±1.7	8.7339E-07±1.5E-07
101014175	26	101.890:102.914	COMP	0.1351 ± 0.0463	−1.158 ± 0.055	-	96.09 ± 5.17	-	389.73/356	31.037±9.0	2.3502E-06±6.6E-07
101014175	27	102.914:103.938	SBPL	0.0181 ± 0.0069	−1.026 ± 0.164	−2.291 ± 0.102	55.36 ± 12.51	36.17 ± 7.38	370.44/355	12.897±4.9	1.0656E-06±3.9E-07
101014175	28	103.938:105.986	BAND	0.0466 ± 0.0180	−1.176 ± 0.087	−2.429 ± 0.223	84.72 ± 9.12	67.95 ± 12.59	385.8/355	10.697±3.9	9.0399E-07±3.1E-07
101014175	29	105.986:111.106	COMP	0.0402 ± 0.0136	−1.227 ± 0.060	-	114.30 ± 9.99	-	377.53/356	11.032±2.9	9.0533E-07±2.2E-07
101014175	30	111.106:163.331	BAND	0.0091 ± 0.0017	−1.172 ± 0.057	−2.064 ± 0.131	159.70 ± 22.20	88.82 ± 15.61	544.76/355	2.6591±0.40	3.2261E-07±4.1E-08
101014175	31	163.331:203.267	COMP	0.0063 ± 0.0007	−1.325 ± 0.025	-	697.90 ± 142.00	-	528.7/356	2.8274±0.25	4.6659E-07±3.5E-08
101014175	32	203.267:209.411	BAND	0.0601 ± 0.0055	−0.856 ± 0.035	−2.025 ± 0.052	297.50 ± 23.90	155.70 ± 12.89	433.62/355	15.204±0.78	2.8919E-06±1.2E-07
101014175	33	209.411:210.435	BAND	0.1668 ± 0.0102	−0.937 ± 0.023	−2.209 ± 0.069	585.20 ± 46.20	353.19 ± 30.24	390.76/355	55.084±2.2	1.2848E-05±3.9E-07
101014175	34	210.435:211.459	BAND	0.1046 ± 0.0153	−1.026 ± 0.052	−2.052 ± 0.085	297.40 ± 43.90	159.83 ± 24.19	413.36/355	30.797±2.6	5.1698E-06±3.4E-07
101014175	35	211.459:212.483	COMP	0.0728 ± 0.0085	−1.119 ± 0.035	-	455.10 ± 53.70	-	411.55/356	25.762±2.2	4.5698E-06±3.1E-07
101014175	36	212.483:214.531	COMP	0.0538 ± 0.0049	−1.161 ± 0.027	-	529.30 ± 57.80	-	404.88/356	20.271±1.4	3.6704E-06±2.0E-07
101014175	37	214.531:217.603	COMP	0.0431 ± 0.0059	−1.168 ± 0.036	-	308.60 ± 32.90	-	413.36/356	14.607±1.5	2.0889E-06±1.7E-07
101014175	38	217.603:272.900	SBPL	0.0043 ± 0.0007	−1.369 ± 0.039	−2.082 ± 0.167	206.64 ± 83.13	125.40 ± 34.80	656.5/355	2.1262±0.34	2.6823E-07±3.7E-08
101014175	39	414.215:430.599	COMP	0.0137 ± 0.0035	−1.071 ± 0.061	-	225.30 ± 31.40	-	433.65/356	3.8133±0.69	4.8750E-07±7.1E-08

Continued on next page

Table A.1 – continued from previous page

GRB name	spectrum	T_{start}:T_{stop} (s)	BEST model	A (ph s^{-1} cm^{-2} keV^{-1})	α	β	E_p (keV)	E_b (keV)	CSTAT/dof	photon flux (ph s^{-1} cm^{-2})	energy flux (erg s^{-1} cm^{-2})
(1)	(2)	(3)	(4)	(5)	(6)	(7)	(8)	(9)	(10)	(11)	(12)
101014175	40	430.599:435.719	COMP	0.0252 ± 0.0083	-1.173 ± 0.063	-	158.10 ± 18.60	-	362.9/356	7.1142±1.8	7.0900E-07±1.6E-07
101014175	41	435.719:438.791	COMP	0.0272 ± 0.0085	-1.208 ± 0.060	-	179.40 ± 23.20	-	367.66/356	8.3698±2.1	8.8196E-07±2.0E-07
101014175	42	438.791:440.839	COMP	0.0667 ± 0.0169	-1.007 ± 0.059	-	171.20 ± 15.30	-	394.01/356	15.558±2.9	1.7296E-06±2.8E-07
101014175	43	440.839:442.887	COMP	0.0817 ± 0.0226	-1.222 ± 0.059	-	136.30 ± 13.30	-	367.91/356	23.563±4.7	2.1286E-06±3.7E-07
101014175	44	442.887:444.935	COMP	0.0820 ± 0.0251	-1.160 ± 0.063	-	128.30 ± 11.60	-	424.26/356	21.139±4.7	1.8801E-06±3.8E-07
101014175	45	444.935:446.983	PL	0.0055 ± 0.0018	-1.701 ± 0.024	-	-	-	440.32/357	3.7601±1.3	4.3815E-07±1.4E-07
101014175	46	446.983:450.055	COMP	0.0398 ± 0.0132	-1.469 ± 0.062	-	124.90 ± 18.10	-	362.7/356	16.318±4.1	1.3215E-06±2.9E-07
101014175	47	450.055:454.151	PL	0.0041 ± 0.0015	-1.789 ± 0.027	-	-	-	381.06/357	3.0563±1.2	3.1050E-07±1.2E-07
101014175	48	454.151:461.319	none	-	-	-	-	-	-	-	-
101014175	49	461.319:474.631	PL	0.0035 ± 0.0010	-1.895 ± 0.034	-	-	-	411.48/357	3.0149±0.92	2.6162E-07±7.6E-08
101014175	50	474.631:519.688	none	-	-	-	-	-	-	-	-
101023951	1	-2.048:19.456	PL	0.0025 ± 0.0006	-1.732 ± 0.029	-	-	-	631.6/362	1.8079±0.46	1.9953E-07±4.8E-08
101023951	2	45.057:62.465	COMP	0.0219 ± 0.0051	-1.217 ± 0.060	-	156.60 ± 13.20	-	595.06/361	6.5858±1.1	6.4060E-07±9.9E-08
101023951	3	62.465:63.489	COMP	0.1145 ± 0.0213	-0.860 ± 0.066	-	225.60 ± 17.60	-	383.59/361	25.335±3.2	3.5921E-06±3.7E-07
101023951	4	63.489:64.513	COMP	0.1303 ± 0.0214	-0.830 ± 0.059	-	238.80 ± 17.00	-	405.16/361	28.676±3.1	4.2886E-06±3.8E-07
101023951	5	64.513:65.537	COMP	0.1691 ± 0.0202	-0.818 ± 0.046	-	261.40 ± 14.80	-	385.8/361	38.320±3.1	6.1354E-06±3.9E-07
101023951	6	65.537:66.561	COMP	0.1286 ± 0.0150	-0.980 ± 0.043	-	301.60 ± 21.60	-	401.52/361	35.981±2.9	5.7460E-06±3.7E-07
101023951	7	66.561:67.585	COMP	0.1083 ± 0.0195	-1.060 ± 0.058	-	224.20 ± 19.60	-	369.72/361	29.840±3.7	3.8177E-06±4.0E-07
101023951	8	67.585:69.633	BAND	0.1562 ± 0.0343	-0.693 ± 0.102	-2.463 ± 0.179	138.10 ± 12.10	96.89 ± 11.58	443.26/360	22.411±3.3	2.8256E-06±3.4E-07
101023951	9	69.633:70.657	COMP	0.0780 ± 0.0162	-1.007 ± 0.069	-	242.00 ± 25.20	-	453.49/361	20.802±3.0	2.8646E-06±3.5E-07
101023951	10	70.657:72.705	COMP	0.0729 ± 0.0154	-1.078 ± 0.060	-	181.60 ± 14.30	-	423.18/361	19.101±2.9	2.1353E-06±2.9E-07
101023951	11	72.705:75.777	COMP	0.0403 ± 0.0142	-1.172 ± 0.082	-	141.30 ± 13.80	-	501.36/361	10.983±3.0	1.0247E-06±2.6E-07
101023951	12	75.777:81.921	PL	0.0036 ± 0.0013	-1.796 ± 0.028	-	-	-	476.4/362	2.7556±1.0	2.7561E-07±9.9E-08
101023951	13	81.921:101.378	none	-	-	-	-	-	-	-	-
101123952	1	30.720:44.019	BAND	0.0092 ± 0.0018	-0.603 ± 0.105	-1.858 ± 0.091	529.00 ± 122.00	241.19 ± 54.93	539.33/356	2.5308±0.26	7.5670E-07±6.0E-08
101123952	2	44.019:44.560	BAND	0.0543 ± 0.0053	-0.619 ± 0.056	-1.916 ± 0.082	1137.00 ± 192.00	537.14 ± 91.92	314.52/356	19.988±1.4	7.8587E-06±4.2E-07
101123952	3	44.560:45.006	BAND	0.1117 ± 0.0187	-0.536 ± 0.086	-1.780 ± 0.053	459.20 ± 80.70	199.20 ± 34.29	345.92/356	28.305±2.3	8.4267E-06±5.2E-07
101123952	4	45.006:45.389	SBPL	0.0893 ± 0.0102	-0.710 ± 0.064	-1.918 ± 0.074	1034.24 ± 370.45	214.50 ± 36.30	422.72/356	31.139±2.7	8.8501E-06±5.9E-07
101123952	5	45.389:45.754	SBPL	0.0925 ± 0.0107	-0.671 ± 0.070	-1.925 ± 0.078	805.70 ± 275.82	184.50 ± 29.80	373.38/356	30.802±2.8	8.3873E-06±6.0E-07
101123952	6	45.754:46.091	BAND	0.1216 ± 0.0212	-0.655 ± 0.079	-1.912 ± 0.083	447.00 ± 80.70	211.51 ± 37.91	351.56/356	31.825±3.0	8.4630E-06±6.2E-07
101123952	7	46.091:46.374	BAND	0.1156 ± 0.0186	-0.649 ± 0.073	-2.060 ± 0.125	480.30 ± 78.90	253.41 ± 42.48	394.56/356	30.983±3.0	8.4173E-06±6.4E-07
101123952	8	46.374:46.668	BAND	0.0971 ± 0.0135	-0.749 ± 0.060	-2.139 ± 0.153	671.30 ± 119.00	372.17 ± 70.96	364.95/356	30.726±2.8	8.9285E-06±6.4E-07
101123952	9	46.668:46.967	BAND	0.1732 ± 0.0354	-0.535 ± 0.094	-2.006 ± 0.100	318.70 ± 48.20	162.97 ± 24.45	323.23/356	35.698±3.7	8.5933E-06±7.1E-07
101123952	10	46.967:47.477	COMP	0.0670 ± 0.0100	-0.960 ± 0.052	-	581.70 ± 95.80	-	386.33/357	22.419±2.5	5.0729E-06±4.5E-07
101123952	11	47.477:48.123	COMP	0.0616 ± 0.0084	-0.901 ± 0.053	-	611.20 ± 95.10	-	348.38/357	20.208±2.0	4.9254E-06±3.9E-07
101123952	12	48.123:48.727	COMP	0.0620 ± 0.0077	-0.884 ± 0.049	-	700.30 ± 105.00	-	375.43/357	20.909±2.0	5.4713E-06±4.1E-07
101123952	13	48.727:49.266	COMP	0.0927 ± 0.0156	-0.704 ± 0.063	-	375.00 ± 41.00	-	389.2/357	22.647±2.6	4.9359E-06±4.5E-07
101123952	14	49.266:49.898	COMP	0.0923 ± 0.0177	-0.764 ± 0.067	-	322.90 ± 36.50	-	371.81/357	21.964±2.8	4.1821E-06±4.3E-07
101123952	15	49.898:50.172	COMP	0.1525 ± 0.0167	-0.438 ± 0.057	-	506.50 ± 39.20	-	340.89/357	38.660±2.9	1.2055E-05±7.2E-07
101123952	16	50.172:50.441	COMP	0.1459 ± 0.0150	-0.670 ± 0.049	-	636.50 ± 61.10	-	371.82/357	44.134±3.3	1.3306E-05±7.6E-07
101123952	17	50.441:50.707	COMP	0.1139 ± 0.0155	-0.749 ± 0.053	-	555.00 ± 67.10	-	343.51/357	33.676±3.3	8.9207E-06±7.0E-07
101123952	18	50.707:51.270	BAND	0.1114 ± 0.0251	-0.736 ± 0.096	-1.954 ± 0.102	266.70 ± 47.50	132.45 ± 23.70	389.02/356	24.434±3.0	4.8533E-06±4.8E-07
101123952	19	51.270:51.748	COMP	0.0949 ± 0.0142	-0.900 ± 0.054	-	458.70 ± 61.20	-	392.27/357	28.581±3.0	6.0950E-06±5.0E-07

Continued on next page

Table A.1 – continued from previous page

GRB name	spectrum	T_{start}:T_{stop} (s)	BEST model	A (ph s^{-1} cm^{-2} keV^{-1})	α	β	E_p (keV)	E_b (keV)	CSTAT/dof	photon flux (ph s^{-1} cm^{-2})	energy flux (erg s^{-1} cm^{-2})
(1)	(2)	(3)	(4)	(5)	(6)	(7)	(8)	(9)	(10)	(11)	(12)
101123952	20	51.748:51.986	COMP	0.1585 ± 0.0176	-0.636 ± 0.051	-	558.50 ± 51.30	-	342.14/357	44.915±3.6	1.3007E-05±8.1E-07
101123952	21	51.986:52.260	COMP	0.1336 ± 0.0181	-0.750 ± 0.054	-	489.90 ± 54.10	-	384.67/357	37.645±3.6	9.3345E-06±7.1E-07
101123952	22	52.260:52.531	COMP	0.1834 ± 0.0211	-0.699 ± 0.050	-	507.80 ± 47.70	-	390.23/357	51.152±4.1	1.3431E-05±8.0E-07
101123952	23	52.531:52.826	COMP	0.1196 ± 0.0155	-0.794 ± 0.053	-	545.00 ± 65.10	-	381.81/357	35.835±3.4	9.0798E-06±6.7E-07
101123952	24	52.826:53.146	COMP	0.1456 ± 0.0171	-0.674 ± 0.052	-	501.30 ± 47.70	-	355.23/357	39.939±3.3	1.0602E-05±6.7E-07
101123952	25	53.146:53.484	COMP	0.1054 ± 0.0133	-0.714 ± 0.053	-	550.00 ± 61.30	-	419.4/357	30.559±2.8	8.2845E-06±5.9E-07
101123952	26	53.484:53.824	COMP	0.1091 ± 0.0150	-0.717 ± 0.054	-	512.80 ± 58.00	-	365.1/357	30.798±3.0	8.0240E-06±6.1E-07
101123952	27	53.824:54.813	SBPL	0.0273 ± 0.0053	-0.770 ± 0.170	-1.721 ± 0.083	-	61.28 ± 17.30	383.21/356	10.574±1.9	1.9610E-06±3.0E-07
101123952	28	54.813:55.650	COMP	0.0592 ± 0.0078	-0.739 ± 0.057	-	536.00 ± 65.10	-	390.06/357	17.179±1.6	4.5079E-06±3.3E-07
101123952	29	55.650:56.160	COMP	0.0750 ± 0.0110	-0.800 ± 0.056	-	523.30 ± 69.60	-	377.91/357	22.223±2.3	5.4881E-06±4.5E-07
101123952	30	56.160:56.512	COMP	0.1067 ± 0.0137	-0.732 ± 0.054	-	527.10 ± 59.10	-	361.24/357	30.682±2.8	8.0188E-06±5.8E-07
101123952	31	56.512:56.913	COMP	0.1055 ± 0.0176	-0.877 ± 0.057	-	397.40 ± 50.20	-	404.5/357	29.769±3.5	5.9797E-06±5.6E-07
101123952	32	56.913:59.919	COMP	0.0440 ± 0.0132	-0.963 ± 0.085	-	218.30 ± 32.10	-	488.01/357	10.745±2.1	1.4183E-06±2.2E-07
101123952	33	59.919:73.728	COMP	0.0096 ± 0.0034	-0.993 ± 0.115	-	325.70 ± 89.90	-	596.86/357	2.7765±0.64	4.5935E-07±7.7E-08
101123952	34	81.920:91.338	COMP	0.0133 ± 0.0026	-1.088 ± 0.060	-	455.80 ± 98.00	-	478.7/357	4.6122±0.64	8.3841E-07±9.0E-08
101123952	35	91.338:93.217	COMP	0.0270 ± 0.0069	-1.048 ± 0.071	-	342.70 ± 66.90	-	417.94/357	8.3767±1.6	1.3709E-06±2.2E-07
101123952	36	93.217:94.240	COMP	0.0659 ± 0.0198	-0.959 ± 0.080	-	221.50 ± 30.20	-	389.72/357	16.117±3.4	2.1521E-06±3.9E-07
101123952	37	94.240:112.640	COMP	0.0100 ± 0.0038	-1.163 ± 0.094	-	238.80 ± 58.20	-	544.85/357	3.1729±0.83	3.9781E-07±8.2E-08
101123952	38	139.264:143.859	COMP	0.0117 ± 0.0034	-1.212 ± 0.072	-	483.20 ± 171.00	-	404.01/357	4.5567±0.99	7.5713E-07±1.4E-07
101123952	39	143.859:145.151	COMP	0.0253 ± 0.0065	-1.071 ± 0.068	-	423.40 ± 96.20	-	381.93/357	8.4633±1.7	1.5109E-06±2.6E-07
101123952	40	145.151:146.702	COMP	0.0353 ± 0.0119	-1.106 ± 0.080	-	241.40 ± 45.40	-	356.48/357	10.504±2.6	1.3679E-06±2.9E-07
101123952	41	146.702:150.041	PL	0.0040 ± 0.0012	-1.510 ± 0.032	-	-	-	423.7/358	2.3124±0.70	3.6417E-07±1.0E-07
101123952	42	150.041:156.672	none	-	-	-	-	-	-	-	-
101126198	1	-10.240:4.500	none	-	-	-	-	-	-	-	-
101126198	2	4.500:7.600	none	-	-	-	-	-	-	-	-
101126198	3	7.600:8.853	COMP	0.0407 ± 0.0131	-1.226 ± 0.068	-	182.20 ± 24.90	-	490.94/477	12.867±3.2	1.3575E-06±3.1E-07
101126198	4	8.853:9.900	COMP	0.0454 ± 0.0147	-1.147 ± 0.070	-	180.40 ± 22.30	-	567.86/477	12.914±3.3	1.4014E-06±3.3E-07
101126198	5	9.900:10.713	COMP	0.0678 ± 0.0165	-0.968 ± 0.063	-	215.30 ± 21.50	-	547.69/477	16.517±3.0	2.1615E-06±3.5E-07
101126198	6	10.713:11.571	COMP	0.0845 ± 0.0275	-1.109 ± 0.072	-	144.30 ± 13.90	-	654.62/477	21.126±5.3	2.0418E-06±4.7E-07
101126198	7	11.571:12.247	COMP	0.0787 ± 0.0188	-1.135 ± 0.061	-	215.10 ± 25.90	-	489.0/477	23.293±4.1	2.8079E-06±4.2E-07
101126198	8	12.247:12.934	COMP	0.1871 ± 0.0582	-0.952 ± 0.073	-	130.30 ± 9.49	-	532.57/477	35.950±8.1	3.4217E-06±7.1E-07
101126198	9	12.934:13.529	COMP	0.0661 ± 0.0153	-1.073 ± 0.059	-	242.40 ± 28.40	-	508.81/477	18.906±3.4	2.5203E-06±4.0E-07
101126198	10	13.529:14.117	COMP	0.0985 ± 0.0254	-0.966 ± 0.063	-	190.40 ± 17.10	-	561.95/477	22.819±4.4	2.7606E-06±4.8E-07
101126198	11	14.117:14.820	COMP	0.0591 ± 0.0158	-1.155 ± 0.060	-	205.30 ± 24.10	-	585.07/477	17.678±3.7	2.0557E-06±3.9E-07
101126198	12	14.820:15.604	COMP	0.1459 ± 0.0473	-1.119 ± 0.074	-	125.00 ± 10.80	-	556.04/477	35.077±8.2	3.1078E-06±6.6E-07
101126198	13	15.604:16.500	COMP	0.0992 ± 0.0290	-1.217 ± 0.067	-	141.50 ± 14.30	-	550.05/477	28.748±6.2	2.6554E-06±5.1E-07
101126198	14	16.500:18.011	PL	0.0060 ± 0.0022	-1.732 ± 0.027	-	-	-	629.68/478	4.2407±1.6	4.7103E-07±1.7E-07
101126198	15	18.011:20.287	PL	0.0064 ± 0.0020	-1.765 ± 0.029	-	-	-	596.44/478	4.7090±1.5	4.9687E-07±1.5E-07
101126198	16	20.287:24.754	none	-	-	-	-	-	-	-	-
101126198	17	24.754:33.327	none	-	-	-	-	-	-	-	-
101126198	18	33.327:67.584	none	-	-	-	-	-	-	-	-
101231067	1	-1.024:1.957	COMP	0.0184 ± 0.0040	-0.858 ± 0.076	-	479.00 ± 89.10	-	471.38/357	5.4501±0.89	1.2296E-06±1.7E-07
101231067	2	1.957:4.859	COMP	0.0247 ± 0.0082	-0.599 ± 0.097	-	256.80 ± 29.50	-	450.77/357	4.5515±1.2	8.0128E-07±1.9E-07

Continued on next page

Table A.1 – continued from previous page

GRB name	spectrum	T_{start}:T_{stop} (s)	BEST model	A (ph s^{-1} cm^{-2} keV^{-1})	α	β	E_p (keV)	E_b (keV)	CSTAT/dof	photon flux (ph s^{-1} cm^{-2})	energy flux (erg s^{-1} cm^{-2})
(1)	(2)	(3)	(4)	(5)	(6)	(7)	(8)	(9)	(10)	(11)	(12)
101231067	3	4.859:6.441	COMP	0.0931 ± 0.0210	-0.172 ± 0.101	-	255.10 ± 19.10	-	409.63/357	12.289±1.7	2.5530E-06±2.9E-07
101231067	4	6.441:8.155	COMP	0.0392 ± 0.0147	-0.426 ± 0.104	-	223.80 ± 21.20	-	447.02/357	5.6582±1.7	9.5886E-07±2.8E-07
101231067	5	8.155:20.542	none	-	-	-	-	-	-	-	-
101231067	6	20.542:21.644	none	-	-	-	-	-	-	-	-
101231067	7	21.644:23.054	none	-	-	-	-	-	-	-	-
101231067	8	23.054:25.600	none	-	-	-	-	-	-	-	-
110213220	1	-4.096:15.776	none	-	-	-	-	-	-	-	-
110213220	2	15.776:18.235	none	-	-	-	-	-	-	-	-
110213220	3	18.235:19.032	none	-	-	-	-	-	-	-	-
110213220	4	19.032:20.162	none	-	-	-	-	-	-	-	-
110213220	5	20.162:23.604	none	-	-	-	-	-	-	-	-
110213220	6	23.604:35.392	none	-	-	-	-	-	-	-	-
110213220	7	35.392:39.936	none	-	-	-	-	-	-	-	-
110301214	1	-1.024:0.480	COMP	0.0455 ± 0.0113	-0.795 ± 0.078	-	253.90 ± 27.70	-	504.18/477	9.9546±1.8	1.5825E-06±2.5E-07
110301214	2	0.480:0.751	COMP	0.4640 ± 0.1590	-0.737 ± 0.087	-	128.70 ± 8.11	-	441.47/477	65.727±16.0	6.5694E-06±1.5E-06
110301214	3	0.751:1.005	COMP	0.6507 ± 0.2490	-0.521 ± 0.095	-	120.60 ± 6.53	-	501.1/477	65.680±19.0	6.6091E-06±1.8E-06
110301214	4	1.005:1.191	COMP	0.6058 ± 0.2300	-0.429 ± 0.095	-	130.20 ± 6.96	-	442.45/477	57.532±17.0	6.2798E-06±1.7E-06
110301214	5	1.191:1.355	SBPL	0.2525 ± 0.0939	-0.732 ± 0.103	-3.681 ± 0.512	96.53 ± 17.96	105.70 ± 17.90	483.87/476	85.666±30.0	8.3735E-06±2.7E-06
110301214	6	1.355:1.515	PL	0.0205 ± 0.0072	-1.621 ± 0.029	-	-	-	718.54/478	12.952±4.6	1.7076E-06±6.0E-07
110301214	7	1.515:1.671	PL	0.0223 ± 0.0079	-1.660 ± 0.029	-	-	-	750.45/478	14.682±5.3	1.8193E-06±6.4E-07
110301214	8	1.671:1.803	PL	0.0230 ± 0.0081	-1.632 ± 0.029	-	-	-	649.42/478	14.699±5.3	1.9061E-06±6.7E-07
110301214	9	1.803:1.925	PL	0.0243 ± 0.0085	-1.609 ± 0.029	-	-	-	642.58/478	15.198±5.4	2.0436E-06±7.1E-07
110301214	10	1.925:2.029	COMP	0.8167 ± 0.3020	-0.778 ± 0.086	-	118.80 ± 7.06	-	446.88/477	116.69±33.0	1.0921E-05±3.0E-06
110301214	11	2.029:2.117	COMP	1.2360 ± 0.4170	-0.760 ± 0.082	-	121.90 ± 6.94	-	445.72/477	174.96±43.0	1.6738E-05±3.9E-06
110301214	12	2.117:2.208	BAND	0.7850 ± 0.2540	-0.651 ± 0.129	-2.484 ± 0.192	110.00 ± 11.10	78.12 ± 9.80	506.8/476	91.838±22.0	1.0243E-05±2.2E-06
110301214	13	2.208:2.289	COMP	0.9454 ± 0.2790	-0.829 ± 0.078	-	139.20 ± 8.99	-	479.54/477	158.75±34.0	1.6331E-05±3.2E-06
110301214	14	2.289:2.374	BAND	1.2860 ± 0.3750	-0.637 ± 0.128	-2.467 ± 0.175	109.40 ± 10.80	77.17 ± 9.19	421.25/476	147.01±29.0	1.6499E-05±2.9E-06
110301214	15	2.374:2.452	COMP	0.8467 ± 0.2310	-0.942 ± 0.072	-	154.30 ± 11.40	-	402.68/477	173.79±34.0	1.8486E-05±3.2E-06
110301214	16	2.452:2.535	COMP	0.7238 ± 0.2000	-0.916 ± 0.072	-	154.90 ± 11.00	-	480.89/477	143.92±29.0	1.5479E-05±2.9E-06
110301214	17	2.535:2.629	COMP	0.4422 ± 0.1200	-1.007 ± 0.071	-	170.70 ± 14.50	-	482.56/477	103.15±21.0	1.1436E-05±2.1E-06
110301214	18	2.629:2.730	COMP	0.6953 ± 0.2170	-0.891 ± 0.078	-	142.50 ± 10.20	-	463.03/477	128.57±29.0	1.3189E-05±2.7E-06
110301214	19	2.730:2.840	COMP	0.4449 ± 0.1430	-0.990 ± 0.076	-	143.50 ± 11.10	-	415.7/477	94.374±23.0	9.4290E-06±2.2E-06
110301214	20	2.840:2.954	BAND	0.3562 ± 0.1420	-0.960 ± 0.116	-2.643 ± 0.344	109.00 ± 12.80	91.93 ± 19.58	483.41/476	64.571±23.0	6.2238E-06±2.0E-06
110301214	21	2.954:3.078	COMP	0.4316 ± 0.1480	-0.948 ± 0.077	-	134.10 ± 9.78	-	450.47/477	83.707±23.0	8.1146E-06±2.1E-06
110301214	22	3.078:3.224	COMP	0.3490 ± 0.1180	-1.011 ± 0.077	-	136.70 ± 10.70	-	503.07/477	74.621±20.0	7.1843E-06±1.8E-06
110301214	23	3.224:3.372	COMP	0.4984 ± 0.1840	-1.090 ± 0.083	-	115.90 ± 9.10	-	513.21/477	111.49±31.0	9.5101E-06±2.4E-06
110301214	24	3.372:3.540	SBPL	0.1580 ± 0.0544	-0.984 ± 0.132	-2.814 ± 0.256	74.29 ± 16.17	68.77 ± 14.00	506.12/476	82.027±27.0	7.0152E-06±2.1E-06
110301214	25	3.540:3.703	SBPL	0.1770 ± 0.0603	-0.950 ± 0.130	-2.902 ± 0.257	72.53 ± 14.42	68.85 ± 12.90	496.81/476	91.885±30.0	7.6994E-06±2.3E-06
110301214	26	3.703:3.820	SBPL	0.3760 ± 0.1330	-1.074 ± 0.083	-3.833 ± 0.661	100.57 ± 22.10	125.50 ± 25.30	467.13/476	153.43±52.0	1.3435E-05±4.2E-06
110301214	27	3.820:3.908	COMP	0.5673 ± 0.1690	-0.894 ± 0.074	-	152.20 ± 11.10	-	487.02/477	108.65±25.0	1.1639E-05±2.4E-06
110301214	28	3.908:3.980	COMP	1.4110 ± 0.4370	-0.662 ± 0.084	-	131.90 ± 7.42	-	510.2/477	183.47±41.0	1.9046E-05±3.9E-06
110301214	29	3.980:4.050	BAND	1.2590 ± 0.4280	-0.509 ± 0.136	-2.594 ± 0.217	105.40 ± 9.52	77.36 ± 9.31	421.76/476	115.95±30.0	1.2791E-05±3.0E-06
110301214	30	4.050:4.129	COMP	2.3740 ± 0.8230	-0.687 ± 0.088	-	110.20 ± 5.71	-	416.36/477	283.76±68.0	2.5740E-05±5.8E-06

Continued on next page

Table A.1 – continued from previous page

GRB name	spectrum	T_{start}:T_{stop} (s)	BEST model	A (ph s^{-1} cm^{-2} keV^{-1})	α	β	E_p (keV)	E_b (keV)	CSTAT/dof	photon flux (ph s^{-1} cm^{-2})	energy flux (erg s^{-1} cm^{-2})
(1)	(2)	(3)	(4)	(5)	(6)	(7)	(8)	(9)	(10)	(11)	(12)
110301214	31	4.129:4.219	PL	0.0351 ± 0.0117	−1.674 ± 0.029	-	-	-	606.18/478	23.390±8.0	2.8356E-06±9.4E-07
110301214	32	4.219:4.320	COMP	1.5050 ± 0.5990	−0.956 ± 0.089	-	93.27 ± 5.27	-	464.64/477	245.80±72.0	1.8934E-05±5.3E-06
110301214	33	4.320:4.439	none	-	-	-	-	-	-	-	-
110301214	34	4.439:4.604	none	-	-	-	-	-	-	-	-
110301214	35	4.604:4.815	none	-	-	-	-	-	-	-	-
110301214	36	4.815:5.011	none	-	-	-	-	-	-	-	-
110301214	37	5.011:5.199	PL	0.0278 ± 0.0093	−1.793 ± 0.031	-	-	-	522.15/478	21.106±7.2	2.1273E-06±7.1E-07
110301214	38	5.199:5.444	none	-	-	-	-	-	-	-	-
110301214	39	5.444:5.860	none	-	-	-	-	-	-	-	-
110301214	40	5.860:6.582	none	-	-	-	-	-	-	-	-
110301214	41	6.582:7.850	none	-	-	-	-	-	-	-	-
110301214	42	7.850:16.384	none	-	-	-	-	-	-	-	-
110407998	1	-9.472:2.816	COMP	0.0080 ± 0.0013	−0.963 ± 0.056	-	812.20 ± 173.00	-	590.8/476	2.8890±0.36	7.3908E-07±8.1E-08
110407998	2	2.816:3.840	COMP	0.0596 ± 0.0075	−0.732 ± 0.051	-	539.50 ± 56.10	-	467.84/476	17.260±1.6	4.5758E-06±3.6E-07
110407998	3	3.840:4.864	COMP	0.0566 ± 0.0069	−0.810 ± 0.046	-	608.60 ± 70.30	-	486.58/476	17.708±1.6	4.6734E-06±3.5E-07
110407998	4	4.864:5.888	COMP	0.0471 ± 0.0064	−0.841 ± 0.053	-	662.40 ± 96.20	-	544.49/476	15.333±1.5	4.0883E-06±3.4E-07
110407998	5	5.888:7.936	COMP	0.0476 ± 0.0074	−0.939 ± 0.050	-	393.90 ± 44.10	-	548.53/476	14.012±1.6	2.6831E-06±2.6E-07
110407998	6	7.936:12.032	none	-	-	-	-	-	-	-	-
110407998	7	12.032:19.200	none	-	-	-	-	-	-	-	-
110428388	1	-1.280:3.840	COMP	0.0338 ± 0.0059	−0.722 ± 0.054	-	242.30 ± 16.70	-	440.21/360	6.7351±0.83	1.0727E-06±1.2E-07
110428388	2	3.840:4.864	COMP	0.1345 ± 0.0205	−0.328 ± 0.062	-	252.00 ± 13.10	-	437.3/360	19.642±1.9	3.8158E-06±3.1E-07
110428388	3	4.864:5.888	COMP	0.1857 ± 0.0544	−0.276 ± 0.089	-	158.80 ± 8.46	-	389.64/360	17.416±3.5	2.3254E-06±4.4E-07
110428388	4	5.888:6.912	COMP	0.3327 ± 0.0481	0.066 ± 0.061	-	202.40 ± 6.40	-	371.59/360	28.879±2.6	5.2355E-06±4.0E-07
110428388	5	6.912:7.936	SBPL	0.2021 ± 0.0274	−0.417 ± 0.053	−4.372 ± 0.433	141.59 ± 13.96	162.30 ± 14.20	354.05/359	47.184±6.0	6.6639E-06±7.5E-07
110428388	6	7.936:8.960	PL	0.0078 ± 0.0021	−1.600 ± 0.024	-	-	-	779.04/361	4.8388±1.3	6.6050E-07±1.7E-07
110428388	7	8.960:11.008	none	-	-	-	-	-	-	-	-
110622158	1	-8.192:18.304	SBPL	0.0061 ± 0.0009	−0.662 ± 0.111	−1.992 ± 0.045	166.39 ± 56.18	44.05 ± 4.97	992.76/478	2.7961±0.39	3.6745E-07±4.9E-08
110622158	2	18.304:19.070	COMP	0.1106 ± 0.0406	−0.783 ± 0.081	-	141.10 ± 9.57	-	500.22/479	17.610±5.2	1.8524E-06±5.2E-07
110622158	3	19.070:19.822	BAND	0.0836 ± 0.0322	−0.721 ± 0.111	−2.486 ± 0.283	123.60 ± 13.00	88.47 ± 15.00	538.67/478	11.636±4.2	1.3530E-06±4.5E-07
110622158	4	19.822:20.573	COMP	0.0942 ± 0.0304	−0.915 ± 0.072	-	154.90 ± 11.70	-	540.77/479	18.720±4.8	2.0119E-06±4.9E-07
110622158	5	20.573:21.315	BAND	0.0848 ± 0.0296	−0.708 ± 0.146	−2.075 ± 0.131	115.20 ± 17.40	64.49 ± 9.91	520.07/478	11.446±3.0	1.4931E-06±3.6E-07
110622158	6	21.315:22.133	COMP	0.0775 ± 0.0284	−0.916 ± 0.076	-	150.50 ± 11.70	-	526.52/479	15.214±4.6	1.6042E-06±4.6E-07
110622158	7	22.133:23.068	COMP	0.1134 ± 0.0368	−0.910 ± 0.075	-	139.70 ± 9.88	-	531.61/479	21.313±5.3	2.1431E-06±5.0E-07
110622158	8	23.068:24.054	BAND	0.0894 ± 0.0323	−0.700 ± 0.110	−2.572 ± 0.318	122.70 ± 12.10	91.49 ± 16.06	551.87/478	11.974±4.0	1.3688E-06±4.1E-07
110622158	9	24.054:25.194	COMP	0.1362 ± 0.0517	−0.687 ± 0.081	-	124.50 ± 6.75	-	510.22/479	17.675±5.4	1.7471E-06±5.2E-07
110622158	10	25.194:26.547	COMP	0.1932 ± 0.0585	−0.890 ± 0.075	-	123.10 ± 7.62	-	476.63/479	33.145±7.0	3.0835E-06±6.0E-07
110622158	11	26.547:28.077	COMP	0.1590 ± 0.0528	−0.695 ± 0.079	-	124.60 ± 6.66	-	571.25/479	20.872±5.2	2.0595E-06±4.9E-07
110622158	12	28.077:29.726	COMP	0.0396 ± 0.0157	−0.884 ± 0.072	-	156.60 ± 11.70	-	526.4/479	7.6082±2.6	8.3251E-07±2.8E-07
110622158	13	29.726:31.428	PL	0.0053 ± 0.0015	−1.588 ± 0.022	-	-	-	712.94/480	3.2764±0.94	4.5455E-07±1.3E-07
110622158	14	31.428:33.430	BAND	0.1880 ± 0.0696	−0.489 ± 0.120	−2.893 ± 0.363	96.85 ± 6.63	80.58 ± 12.00	580.32/478	15.538±5.3	1.5258E-06±4.7E-07
110622158	15	33.430:36.752	PL	0.0040 ± 0.0012	−1.635 ± 0.020	-	-	-	677.27/480	2.5406±0.77	3.2729E-07±9.7E-08
110622158	16	36.752:39.430	PL	0.0035 ± 0.0012	−1.591 ± 0.021	-	-	-	721.63/480	2.1546±0.74	2.9775E-07±1.0E-07
110622158	17	39.430:42.282	COMP	0.1066 ± 0.0382	−0.661 ± 0.080	-	121.70 ± 6.34	-	536.98/479	13.135±3.7	1.2860E-06±3.5E-07

Continued on next page

Table A.1 – continued from previous page

GRB name	spectrum	T_{start}:T_{stop} (s)	BEST model	A (ph s^{-1} cm^{-2} keV^{-1})	α	β	E_p (keV)	E_b (keV)	CSTAT/dof	photon flux (ph s^{-1} cm^{-2})	energy flux (erg s^{-1} cm^{-2})
(1)	(2)	(3)	(4)	(5)	(6)	(7)	(8)	(9)	(10)	(11)	(12)
110622158	18	42.282:51.555	PL	0.0031 ± 0.0009	−1.736 ± 0.017	-	-	-	852.35/480	2.1998±0.63	2.4155E-07±6.9E-08
110622158	19	51.555:108.544	none	-	-	-	-	-	-	-	-
110625881	1	-1.024:3.698	COMP	0.0215 ± 0.0054	−0.749 ± 0.087	-	247.40 ± 25.70	-	511.55/477	4.4586±0.81	7.1103E-07±1.1E-07
110625881	2	3.698:4.656	COMP	0.0892 ± 0.0121	−0.099 ± 0.079	-	324.60 ± 17.90	-	525.94/477	14.180±1.2	3.7285E-06±2.6E-07
110625881	3	4.656:8.158	COMP	0.0506 ± 0.0134	−0.377 ± 0.101	-	196.10 ± 13.40	-	491.79/477	6.3075±1.1	9.7433E-07±1.6E-07
110625881	4	8.158:10.611	COMP	0.0340 ± 0.0050	−0.718 ± 0.067	-	391.10 ± 39.60	-	501.08/477	8.5531±0.84	1.8992E-06±1.5E-07
110625881	5	10.611:10.801	COMP	0.2142 ± 0.0240	−0.403 ± 0.057	-	413.40 ± 25.70	-	473.59/477	47.172±3.7	1.3102E-05±8.5E-07
110625881	6	10.801:10.974	COMP	0.3125 ± 0.0425	−0.290 ± 0.065	-	319.10 ± 17.80	-	452.53/477	53.869±4.8	1.2934E-05±9.6E-07
110625881	7	10.974:11.155	COMP	0.3429 ± 0.0558	−0.361 ± 0.068	-	260.00 ± 14.80	-	495.29/477	52.659±5.7	1.0362E-05±9.5E-07
110625881	8	11.155:11.399	COMP	0.3488 ± 0.0694	−0.413 ± 0.073	-	210.90 ± 11.80	-	519.72/477	47.655±6.3	7.7247E-06±8.9E-07
110625881	9	11.399:11.729	BAND	0.5238 ± 0.1330	−0.088 ± 0.130	−2.494 ± 0.182	141.90 ± 10.70	92.93 ± 8.79	510.16/476	37.394±5.8	5.8918E-06±7.9E-07
110625881	10	11.729:12.385	COMP	0.3332 ± 0.1150	−0.514 ± 0.091	-	121.70 ± 6.01	-	511.22/477	33.576±8.5	3.4042E-06±8.3E-07
110625881	11	12.385:13.568	none	-	-	-	-	-	-	-	-
110625881	12	13.568:15.366	none	-	-	-	-	-	-	-	-
110625881	13	15.366:21.016	none	-	-	-	-	-	-	-	-
110625881	14	21.016:21.806	COMP	0.1166 ± 0.0452	−0.944 ± 0.087	-	125.70 ± 9.36	-	520.8/477	21.825±6.7	2.0279E-06±5.9E-07
110625881	15	21.806:22.347	COMP	0.1576 ± 0.0597	−0.738 ± 0.086	-	132.00 ± 8.08	-	519.07/477	22.732±7.0	2.3106E-06±6.9E-07
110625881	16	22.347:22.776	COMP	0.2395 ± 0.0799	−0.637 ± 0.087	-	136.40 ± 7.86	-	437.95/477	30.835±7.8	3.2994E-06±8.0E-07
110625881	17	22.776:23.133	COMP	0.5550 ± 0.1540	−0.607 ± 0.082	-	133.10 ± 6.91	-	514.62/477	67.617±13.0	7.1635E-06±1.2E-06
110625881	18	23.133:23.396	BAND	0.3330 ± 0.0833	−0.493 ± 0.123	−2.220 ± 0.145	150.10 ± 16.60	89.50 ± 10.73	483.99/476	40.224±6.1	6.1837E-06±8.0E-07
110625881	19	23.396:23.564	COMP	0.4407 ± 0.0798	−0.594 ± 0.066	-	227.40 ± 14.30	-	513.67/477	75.086±9.0	1.2054E-05±1.2E-06
110625881	20	23.564:23.746	COMP	0.2441 ± 0.0394	−0.753 ± 0.058	-	290.80 ± 22.60	-	491.25/477	54.882±6.3	9.7905E-06±9.4E-07
110625881	21	23.746:23.874	COMP	0.4013 ± 0.0644	−0.700 ± 0.059	-	285.30 ± 20.90	-	438.46/477	85.450±9.4	1.5476E-05±1.4E-06
110625881	22	23.874:24.008	SBPL	0.3155 ± 0.0365	−0.660 ± 0.086	−2.285 ± 0.123	204.08 ± 39.98	117.80 ± 16.60	478.47/476	95.240±9.9	1.7325E-05±1.5E-06
110625881	23	24.008:24.130	COMP	0.3754 ± 0.0592	−0.752 ± 0.055	-	291.50 ± 21.70	-	506.92/477	84.430±9.4	1.5093E-05±1.4E-06
110625881	24	24.130:24.243	COMP	0.3695 ± 0.0602	−0.794 ± 0.054	-	304.90 ± 24.70	-	500.55/477	87.855±10.0	1.5826E-05±1.5E-06
110625881	25	24.243:24.356	BAND	0.9011 ± 0.2030	−0.405 ± 0.103	−2.544 ± 0.186	166.60 ± 14.00	115.39 ± 12.19	449.98/476	104.58±14.0	1.6317E-05±1.8E-06
110625881	26	24.356:24.467	COMP	0.7107 ± 0.1510	−0.614 ± 0.068	-	181.30 ± 10.20	-	495.37/477	107.18±16.0	1.4324E-05±1.9E-06
110625881	27	24.467:24.587	BAND	1.2240 ± 0.3320	−0.252 ± 0.124	−2.659 ± 0.207	121.30 ± 8.85	87.21 ± 8.59	459.49/476	89.823±17.0	1.1558E-05±1.9E-06
110625881	28	24.587:24.712	BAND	0.6972 ± 0.1870	−0.461 ± 0.128	−2.302 ± 0.151	128.00 ± 12.90	80.41 ± 8.92	470.81/476	71.472±13.0	9.8508E-06±1.5E-06
110625881	29	24.712:24.836	BAND	1.2880 ± 0.3350	−0.330 ± 0.118	−2.660 ± 0.210	126.90 ± 9.39	92.03 ± 9.42	429.01/476	108.80±19.0	1.4111E-05±2.1E-06
110625881	30	24.836:24.986	COMP	0.5040 ± 0.1370	−0.731 ± 0.074	-	152.90 ± 9.28	-	508.62/477	78.636±15.0	8.8972E-06±1.6E-06
110625881	31	24.986:25.186	COMP	0.3441 ± 0.1070	−0.914 ± 0.077	-	141.30 ± 10.10	-	489.08/477	65.410±15.0	6.6152E-06±1.4E-06
110625881	32	25.186:25.424	COMP	0.2651 ± 0.0963	−0.774 ± 0.082	-	136.60 ± 8.64	-	510.59/477	41.006±12.0	4.2266E-06±1.2E-06
110625881	33	25.424:25.760	COMP	0.5747 ± 0.2100	−0.695 ± 0.090	-	107.80 ± 5.53	-	528.56/477	68.549±18.0	6.1074E-06±1.6E-06
110625881	34	25.760:26.267	SBPL	0.0303 ± 0.0110	−0.300 ± 0.341	−2.297 ± 0.109	62.34 ± 14.09	34.04 ± 6.74	556.44/476	16.917±6.1	1.6492E-06±5.7E-07
110625881	35	26.267:26.866	COMP	0.3498 ± 0.1070	−0.992 ± 0.082	-	121.30 ± 8.75	-	507.96/477	69.103±14.0	6.2000E-06±1.1E-06
110625881	36	26.866:27.315	COMP	0.1270 ± 0.0291	−0.916 ± 0.070	-	215.20 ± 20.20	-	550.38/477	29.279±4.7	3.9168E-06±5.5E-07
110625881	37	27.315:27.926	COMP	0.1221 ± 0.0406	−0.878 ± 0.081	-	146.70 ± 11.20	-	535.97/477	22.535±5.8	2.3630E-06±5.7E-07
110625881	38	27.926:28.394	COMP	0.2054 ± 0.0521	−0.818 ± 0.075	-	169.10 ± 12.50	-	523.0/477	37.711±6.6	4.4519E-06±6.9E-07
110625881	39	28.394:28.615	COMP	0.3650 ± 0.0683	−0.448 ± 0.070	-	223.00 ± 13.10	-	461.08/477	53.674±6.5	8.9929E-06±9.4E-07
110625881	40	28.615:29.140	COMP	0.2273 ± 0.0597	−0.889 ± 0.075	-	151.40 ± 10.70	-	503.49/477	43.216±7.8	4.6130E-06±7.4E-07
110625881	41	29.140:29.906	COMP	0.2114 ± 0.0651	−0.957 ± 0.082	-	127.90 ± 9.24	-	602.81/477	40.708±8.6	3.8116E-06±7.3E-07

Continued on next page

Table A.1 – continued from previous page

GRB name	spectrum	T_{start}:T_{stop} (s)	BEST model	A (ph s^{-1} cm^{-2} keV^{-1})	α	β	E_p (keV)	E_b (keV)	CSTAT/dof	photon flux (ph s^{-1} cm^{-2})	energy flux (erg s^{-1} cm^{-2})
(1)	(2)	(3)	(4)	(5)	(6)	(7)	(8)	(9)	(10)	(11)	(12)
110625881	42	29.906:38.793	none	-	-	-	-	-	-	-	-
110625881	43	38.793:61.440	none	-	-	-	-	-	-	-	-
110717319	1	-4.096:7.051	BAND	0.0118 ± 0.0028	-0.760 ± 0.117	-2.048 ± 0.174	311.00 ± 63.80	162.85 ± 36.07	639.73/476	2.8109±0.36	5.7790E-07±6.1E-08
110717319	2	7.051:9.156	COMP	0.0462 ± 0.0097	-0.590 ± 0.083	-	253.90 ± 21.70	-	498.89/477	8.3897±1.1	1.4695E-06±1.7E-07
110717319	3	9.156:11.290	COMP	0.0302 ± 0.0051	-0.957 ± 0.063	-	368.00 ± 47.70	-	504.57/477	8.8498±1.1	1.6082E-06±1.6E-07
110717319	4	11.290:12.697	COMP	0.0515 ± 0.0080	-0.862 ± 0.061	-	349.60 ± 37.10	-	546.81/477	13.706±1.4	2.5830E-06±2.1E-07
110717319	5	12.697:13.986	COMP	0.0406 ± 0.0056	-0.946 ± 0.055	-	465.90 ± 59.70	-	536.27/477	12.675±1.3	2.6270E-06±2.1E-07
110717319	6	13.986:15.084	COMP	0.0440 ± 0.0057	-0.800 ± 0.057	-	474.80 ± 51.10	-	559.24/477	12.575±1.2	2.9553E-06±2.2E-07
110717319	7	15.084:16.078	COMP	0.0471 ± 0.0054	-0.877 ± 0.051	-	576.60 ± 68.80	-	534.5/477	15.007±1.3	3.6474E-06±2.5E-07
110717319	8	16.078:17.817	COMP	0.0264 ± 0.0044	-0.885 ± 0.061	-	411.30 ± 51.20	-	488.91/477	7.5872±0.94	1.5457E-06±1.7E-07
110717319	9	17.817:18.602	COMP	0.0703 ± 0.0085	-0.679 ± 0.058	-	439.40 ± 38.70	-	529.08/477	18.215±1.5	4.4611E-06±2.9E-07
110717319	10	18.602:19.853	COMP	0.0630 ± 0.0128	-0.779 ± 0.071	-	244.40 ± 21.40	-	529.92/477	13.316±1.9	2.0750E-06±2.5E-07
110717319	11	19.853:20.977	COMP	0.0593 ± 0.0094	-0.759 ± 0.063	-	327.90 ± 29.80	-	576.23/477	14.177±1.5	2.7349E-06±2.4E-07
110717319	12	20.977:29.680	COMP	0.0175 ± 0.0055	-1.071 ± 0.089	-	188.20 ± 24.70	-	594.25/477	4.6082±1.0	5.2807E-07±1.0E-07
110717319	13	29.680:41.524	SBPL	0.0067 ± 0.0013	-0.740 ± 0.236	-1.810 ± 0.095	-	58.01 ± 17.90	576.8/476	2.6236±0.45	4.4546E-07±6.5E-08
110717319	14	41.524:45.569	COMP	0.0181 ± 0.0030	-1.080 ± 0.059	-	452.70 ± 75.50	-	550.4/477	6.2209±0.74	1.1367E-06±1.1E-07
110717319	15	45.569:88.612	PL	0.0011 ± 0.0003	-1.617 ± 0.045	-	-	-	1156.2/478	0.67934±0.21	9.0078E-08±2.6E-08
110717319	16	88.612:104.448	none	-	-	-	-	-	-	-	-
110721200	1	-1.024:0.711	COMP	0.0198 ± 0.0011	-0.980 ± 0.020	-	7409.00 ± 597.00	-	554.56/478	8.8715±0.50	3.0120E-06±1.3E-07
110721200	2	0.711:1.132	COMP	0.0556 ± 0.0034	-0.889 ± 0.024	-	2632.00 ± 216.00	-	585.61/478	23.424±1.4	8.2636E-06±4.0E-07
110721200	3	1.132:1.633	BAND	0.0601 ± 0.0050	-0.834 ± 0.036	-2.388 ± 0.206	1182.00 ± 165.00	782.80 ± 138.22	550.21/477	22.521±1.5	7.3227E-06±3.9E-07
110721200	4	1.633:2.043	COMP	0.0788 ± 0.0076	-0.926 ± 0.037	-	749.40 ± 85.90	-	533.31/478	27.548±2.1	7.1061E-06±4.5E-07
110721200	5	2.043:2.434	SBPL	0.1219 ± 0.0118	-0.662 ± 0.067	-2.104 ± 0.091	305.63 ± 102.84	130.80 ± 16.30	537.44/477	37.445±3.2	7.9245E-06±5.6E-07
110721200	6	2.434:2.798	BAND	0.2111 ± 0.0422	-0.588 ± 0.098	-1.925 ± 0.078	184.70 ± 23.00	91.30 ± 10.98	508.08/477	33.377±3.7	6.1246E-06±5.7E-07
110721200	7	2.798:3.213	SBPL	0.0826 ± 0.0101	-0.947 ± 0.081	-1.933 ± 0.085	331.13 ± 120.61	93.68 ± 18.00	530.44/477	31.348±3.5	5.2842E-06±5.0E-07
110721200	8	3.213:3.745	COMP	0.0761 ± 0.0119	-1.118 ± 0.044	-	354.00 ± 42.70	-	476.65/478	25.417±3.0	4.0182E-06±4.1E-07
110721200	9	3.745:4.430	COMP	0.0434 ± 0.0064	-1.299 ± 0.039	-	640.50 ± 144.00	-	458.65/478	18.940±2.3	3.1388E-06±3.2E-07
110721200	10	4.430:5.561	COMP	0.0403 ± 0.0060	-1.256 ± 0.041	-	479.60 ± 86.40	-	528.2/478	16.302±1.9	2.5908E-06±2.5E-07
110721200	11	5.561:7.413	COMP	0.0305 ± 0.0049	-1.183 ± 0.045	-	419.20 ± 67.30	-	587.07/478	11.265±1.4	1.8202E-06±1.8E-07
110721200	12	7.413:11.074	COMP	0.0187 ± 0.0034	-1.128 ± 0.051	-	366.70 ± 56.10	-	596.45/478	6.3621±0.88	1.0149E-06±1.2E-07
110721200	13	11.074:39.936	PL	0.0010 ± 0.0002	-1.381 ± 0.026	-	-	-	1349.2/479	0.50612±0.11	9.8288E-08±1.9E-08
110729142	1	-19.808:18.080	COMP	0.0074 ± 0.0019	-0.804 ± 0.081	-	248.90 ± 27.90	-	683.33/477	1.6165±0.29	2.5214E-07±3.9E-08
110729142	2	18.080:22.176	COMP	0.0165 ± 0.0022	-0.913 ± 0.050	-	572.40 ± 80.70	-	550.82/477	5.3451±0.53	1.2552E-06±1.0E-07
110729142	3	22.176:25.248	COMP	0.0246 ± 0.0044	-0.848 ± 0.063	-	356.90 ± 42.30	-	503.12/477	6.5114±0.82	1.2547E-06±1.3E-07
110729142	4	25.248:40.609	none	-	-	-	-	-	-	-	-
110729142	5	40.609:75.425	none	-	-	-	-	-	-	-	-
110729142	6	151.202:176.803	COMP	0.0064 ± 0.0015	-0.899 ± 0.067	-	274.10 ± 31.20	-	737.05/477	1.5881±0.30	2.5120E-07±4.4E-08
110729142	7	176.803:200.355	SBPL	0.0027 ± 0.0010	-0.998 ± 0.085	-2.845 ± 0.877	193.89 ± 92.28	186.70 ± 74.00	585.77/476	0.95079±0.36	1.4367E-07±4.9E-08
110729142	8	319.141:379.558	COMP	0.0024 ± 0.0007	-1.226 ± 0.057	-	298.00 ± 51.90	-	890.21/477	0.86170±0.23	1.1611E-07±2.9E-08
110729142	9	379.558:393.894	COMP	0.0126 ± 0.0023	-1.160 ± 0.049	-	276.20 ± 33.90	-	562.4/477	4.1238±0.57	5.5992E-07±6.6E-08
110729142	10	393.894:459.431	PL	0.0008 ± 0.0002	-1.597 ± 0.025	-	-	-	839.68/478	0.47959±0.14	6.5753E-08±1.9E-08
110731465	1	-1.024:0.897	COMP	0.0475 ± 0.0177	-0.985 ± 0.093	-	164.10 ± 17.90	-	401.07/360	10.608±3.0	1.1549E-06±3.0E-07
110731465	2	0.897:1.807	COMP	0.1114 ± 0.0331	-0.815 ± 0.091	-	183.00 ± 17.10	-	423.65/360	21.220±4.2	2.6510E-06±4.6E-07

Continued on next page

Table A.1 – continued from previous page

GRB name	spectrum	T_{start}:T_{stop} (s)	BEST model	A (ph s^{-1} cm^{-2} keV^{-1})	α	β	E_p (keV)	E_b (keV)	CSTAT/dof	photon flux (ph s^{-1} cm^{-2})	energy flux (erg s^{-1} cm^{-2})
(1)	(2)	(3)	(4)	(5)	(6)	(7)	(8)	(9)	(10)	(11)	(12)
110731465	3	1.807:2.989	COMP	0.0477 ± 0.0101	-0.847 ± 0.078	-	330.60 ± 44.00	-	412.92/360	12.261±1.7	2.2526E-06±2.6E-07
110731465	4	2.989:4.167	COMP	0.0428 ± 0.0073	-0.729 ± 0.074	-	421.80 ± 53.00	-	413.74/360	11.214±1.3	2.5880E-06±2.4E-07
110731465	5	4.167:5.246	COMP	0.0619 ± 0.0089	-0.416 ± 0.078	-	407.10 ± 35.10	-	359.82/360	13.562±1.2	3.6964E-06±2.6E-07
110731465	6	5.246:6.177	COMP	0.0461 ± 0.0077	-0.954 ± 0.064	-	491.10 ± 80.30	-	384.03/360	14.694±1.7	3.0997E-06±2.9E-07
110731465	7	6.177:7.159	COMP	0.0444 ± 0.0073	-0.494 ± 0.082	-	422.50 ± 44.30	-	423.05/360	10.297±1.1	2.7589E-06±2.5E-07
110731465	8	7.159:10.240	PL	0.0060 ± 0.0016	-1.614 ± 0.060	-	-	-	469.7/361	3.7676±1.2	5.0112E-07±1.2E-07
110817191	1	0.000:0.982	BAND	0.0750 ± 0.0126	-0.342 ± 0.096	-2.127 ± 0.097	314.00 ± 32.90	172.87 ± 18.40	603.61/474	13.549±1.2	3.5173E-06±2.7E-07
110817191	2	0.982:1.458	BAND	0.2240 ± 0.0448	-0.341 ± 0.101	-2.217 ± 0.058	208.50 ± 18.10	121.76 ± 10.30	514.45/474	29.667±3.1	5.9182E-06±5.3E-07
110817191	3	1.458:1.936	COMP	0.3277 ± 0.0743	-0.284 ± 0.080	-	174.80 ± 8.24	-	496.11/475	33.841±5.2	4.8859E-06±6.8E-07
110817191	4	1.936:2.593	COMP	0.1261 ± 0.0317	-0.657 ± 0.069	-	177.80 ± 10.40	-	597.18/475	19.743±3.9	2.5597E-06±4.8E-07
110817191	5	2.593:3.570	PL	0.0141 ± 0.0020	-1.592 ± 0.021	-	-	-	834.52/476	8.7021±1.3	1.2000E-06±1.6E-07
110817191	6	3.570:6.214	PL	0.0066 ± 0.0015	-1.702 ± 0.020	-	-	-	2966.4/476	4.5429±1.1	5.2579E-07±1.2E-07
110817191	7	6.214:10.240	PL	0.0030 ± 0.0006	-1.798 ± 0.030	-	-	-	10505.0/476	2.3146±0.54	2.3085E-07±4.6E-08
110825102	1	-1.024:11.395	none	-	-	-	-	-	-	-	-
110825102	2	11.395:12.007	COMP	0.1996 ± 0.0587	-0.885 ± 0.070	-	148.90 ± 10.30	-	496.62/478	37.423±8.4	3.9588E-06±8.3E-07
110825102	3	12.007:12.420	PL	0.0184 ± 0.0055	-1.658 ± 0.022	-	-	-	825.48/479	12.087±3.7	1.5027E-06±4.5E-07
110825102	4	12.420:12.635	COMP	0.3171 ± 0.0746	-0.698 ± 0.066	-	193.40 ± 12.60	-	483.3/478	54.536±9.7	7.4224E-06±1.2E-06
110825102	5	12.635:12.829	COMP	0.3425 ± 0.0711	-0.786 ± 0.063	-	215.10 ± 15.60	-	509.75/478	68.495±10.0	9.7192E-06±1.3E-06
110825102	6	12.829:13.053	COMP	0.3495 ± 0.0927	-0.836 ± 0.068	-	165.00 ± 11.10	-	486.08/478	64.762±13.0	7.4731E-06±1.4E-06
110825102	7	13.053:13.348	COMP	0.3594 ± 0.1080	-0.857 ± 0.072	-	141.20 ± 8.97	-	481.51/478	63.234±14.0	6.5110E-06±1.4E-06
110825102	8	13.348:13.637	COMP	0.3137 ± 0.0723	-0.780 ± 0.067	-	187.60 ± 13.10	-	553.22/478	58.137±9.6	7.4966E-06±1.1E-06
110825102	9	13.637:14.530	SBPL	0.0663 ± 0.0249	-1.414 ± 0.096	-2.722 ± 0.308	71.53 ± 22.06	75.99 ± 21.50	528.93/477	44.499±16.0	3.3225E-06±1.1E-06
110825102	10	14.530:15.202	COMP	0.2580 ± 0.1030	-1.181 ± 0.079	-	97.85 ± 6.86	-	533.39/478	62.188±19.0	4.7266E-06±1.4E-06
110825102	11	15.202:15.522	COMP	0.1766 ± 0.0389	-1.108 ± 0.058	-	231.20 ± 25.30	-	469.93/478	51.890±8.5	6.5939E-06±9.5E-07
110825102	12	15.522:15.662	COMP	0.2978 ± 0.0300	-0.625 ± 0.047	-	565.70 ± 46.50	-	450.64/478	84.528±6.1	2.4879E-05±1.4E-06
110825102	13	15.662:15.851	COMP	0.2702 ± 0.0358	-0.726 ± 0.051	-	397.50 ± 34.00	-	463.06/478	68.755±6.3	1.5350E-05±1.2E-06
110825102	14	15.851:16.096	COMP	0.2052 ± 0.0275	-0.897 ± 0.048	-	418.70 ± 43.00	-	500.98/478	59.777±5.7	1.2194E-05±9.6E-07
110825102	15	16.096:16.338	COMP	0.1994 ± 0.0311	-0.756 ± 0.056	-	348.90 ± 31.60	-	460.37/478	48.868±5.4	9.8443E-06±9.2E-07
110825102	16	16.338:16.584	COMP	0.1791 ± 0.0222	-0.587 ± 0.053	-	439.30 ± 35.40	-	550.5/478	44.294±3.9	1.1527E-05±8.5E-07
110825102	17	16.584:16.911	COMP	0.1813 ± 0.0298	-0.538 ± 0.063	-	307.50 ± 22.90	-	508.23/478	35.538±4.0	7.3921E-06±7.2E-07
110825102	18	16.911:17.317	COMP	0.2232 ± 0.0513	-0.563 ± 0.071	-	204.80 ± 13.50	-	516.07/478	34.506±5.7	5.1701E-06±7.7E-07
110825102	19	17.317:17.784	COMP	0.2085 ± 0.0467	-0.629 ± 0.069	-	203.30 ± 13.40	-	506.9/478	34.311±5.5	4.9824E-06±7.3E-07
110825102	20	17.784:18.272	COMP	0.2792 ± 0.0819	-0.502 ± 0.077	-	156.40 ± 8.34	-	530.48/478	33.463±7.5	4.1353E-06±8.9E-07
110825102	21	18.272:18.739	COMP	0.1786 ± 0.0354	-0.599 ± 0.067	-	233.30 ± 15.90	-	513.74/478	31.028±4.4	5.0746E-06±6.4E-07
110825102	22	18.739:19.340	COMP	0.1204 ± 0.0285	-0.755 ± 0.069	-	223.00 ± 18.40	-	533.3/478	23.744±4.2	3.5059E-06±5.6E-07
110825102	23	19.340:27.648	none	-	-	-	-	-	-	-	-
110825102	24	70.656:80.669	PL	0.0037 ± 0.0014	-1.794 ± 0.032	-	-	-	562.3/479	2.7837±1.1	2.7986E-07±1.0E-07
110825102	25	80.669:82.944	none	-	-	-	-	-	-	-	-
110903009	1	-7.168:0.692	none	-	-	-	-	-	-	-	-
110903009	2	0.692:3.221	none	-	-	-	-	-	-	-	-
110903009	3	3.221:3.897	none	-	-	-	-	-	-	-	-
110903009	4	3.897:4.197	none	-	-	-	-	-	-	-	-
110903009	5	4.197:4.513	none	-	-	-	-	-	-	-	-

Continued on next page

Table A.1 – continued from previous page

GRB name	spectrum	T_{start}:T_{stop}	BEST	A	α	β	E_p	E_b	CSTAT/dof	photon flux	energy flux
		(s)	model	(ph s^{-1} cm^{-2} keV^{-1})			(keV)	(keV)		(ph s^{-1} cm^{-2})	(erg s^{-1} cm^{-2})
(1)	(2)	(3)	(4)	(5)	(6)	(7)	(8)	(9)	(10)	(11)	(12)
110903009	6	4.513:4.979	none	-	-	-	-	-	-	-	-
110903009	7	4.979:5.469	none	-	-	-	-	-	-	-	-
110903009	8	5.469:6.328	none	-	-	-	-	-	-	-	-
110903009	9	6.328:20.954	none	-	-	-	-	-	-	-	-
110903009	10	20.954:22.134	COMP	0.1074 ± 0.0413	-1.122 ± 0.087	-	131.40 ± 13.90	-	450.88/359	26.530±7.4	2.4108E-06±6.1E-07
110903009	11	22.134:23.851	SBPL	0.0249 ± 0.0086	-1.228 ± 0.238	-2.292 ± 0.155	53.73 ± 21.48	37.98 ± 13.60	434.84/358	19.105±6.6	1.4993E-06±4.7E-07
110903009	12	23.851:28.672	none	-	-	-	-	-	-	-	-
110920546	1	-3.584:6.656	SBPL	0.0123 ± 0.0008	-0.536 ± 0.041	-3.584 ± 0.760	492.19 ± 118.14	496.50 ± 91.70	529.63/477	4.7317±0.24	1.6924E-06±7.1E-08
110920546	2	6.656:8.704	COMP	0.0461 ± 0.0037	-0.279 ± 0.050	-	553.90 ± 32.40	-	523.44/478	12.031±0.64	4.3515E-06±1.9E-07
110920546	3	8.704:10.752	SBPL	0.0380 ± 0.0027	-0.415 ± 0.046	-3.483 ± 0.499	392.83 ± 65.72	379.60 ± 52.40	532.4/477	13.126±0.72	4.3394E-06±2.0E-07
110920546	4	10.752:12.800	SBPL	0.0405 ± 0.0031	-0.394 ± 0.050	-3.019 ± 0.315	363.09 ± 53.90	306.80 ± 36.70	541.8/477	13.225±0.77	4.1616E-06±2.0E-07
110920546	5	12.800:14.848	SBPL	0.0402 ± 0.0031	-0.316 ± 0.057	-2.776 ± 0.237	348.74 ± 48.86	263.80 ± 29.00	537.65/477	12.590±0.77	3.9646E-06±2.0E-07
110920546	6	14.848:16.896	COMP	0.0663 ± 0.0066	-0.135 ± 0.058	-	393.10 ± 19.80	-	560.9/478	12.769±0.78	3.8793E-06±2.0E-07
110920546	7	16.896:19.968	COMP	0.0659 ± 0.0060	-0.114 ± 0.051	-	367.30 ± 15.50	-	526.55/478	11.851±0.66	3.4377E-06±1.6E-07
110920546	8	19.968:23.040	SBPL	0.0379 ± 0.0031	-0.457 ± 0.047	-3.166 ± 0.344	290.63 ± 41.47	261.60 ± 30.20	539.52/477	11.237±0.75	2.9304E-06±1.7E-07
110920546	9	23.040:26.112	SBPL	0.0431 ± 0.0036	-0.365 ± 0.052	-3.597 ± 0.432	269.38 ± 36.87	265.60 ± 30.00	535.3/477	12.143±0.82	3.0936E-06±1.8E-07
110920546	10	26.112:29.184	COMP	0.0726 ± 0.0093	-0.172 ± 0.063	-	290.40 ± 14.00	-	575.44/478	10.785±0.85	2.5080E-06±1.7E-07
110920546	11	29.184:33.281	COMP	0.0835 ± 0.0107	-0.006 ± 0.063	-	258.40 ± 10.20	-	509.07/478	10.010±0.78	2.2213E-06±1.5E-07
110920546	12	33.281:37.377	COMP	0.0578 ± 0.0085	-0.180 ± 0.063	-	256.00 ± 11.70	-	488.86/478	7.6851±0.76	1.5971E-06±1.4E-07
110920546	13	37.377:41.473	COMP	0.0705 ± 0.0120	-0.091 ± 0.071	-	228.90 ± 10.20	-	550.36/478	7.9026±0.89	1.5318E-06±1.5E-07
110920546	14	41.473:46.593	COMP	0.0864 ± 0.0147	-0.054 ± 0.069	-	207.30 ± 8.06	-	583.78/478	8.4921±0.94	1.5223E-06±1.5E-07
110920546	15	46.593:52.737	COMP	0.0513 ± 0.0110	-0.109 ± 0.070	-	199.20 ± 8.18	-	535.6/478	5.0693±0.83	8.6340E-07±1.3E-07
110920546	16	52.737:58.881	COMP	0.0687 ± 0.0150	-0.203 ± 0.072	-	183.30 ± 7.94	-	589.38/478	6.8202±1.1	1.0509E-06±1.6E-07
110920546	17	58.881:67.073	COMP	0.1102 ± 0.0293	0.025 ± 0.080	-	149.90 ± 5.09	-	559.4/478	7.0315±1.4	9.6271E-07±1.8E-07
110920546	18	67.073:76.289	PL	0.0019 ± 0.0005	-1.408 ± 0.016	-	-	-	1165.8/479	0.98380±0.25	1.8329E-07±4.6E-08
110920546	19	76.289:87.553	PL	0.0017 ± 0.0005	-1.463 ± 0.017	-	-	-	1249.7/479	0.95122±0.28	1.6222E-07±4.7E-08
110920546	20	87.553:102.914	PL	0.0017 ± 0.0005	-1.529 ± 0.017	-	-	-	1345.1/479	0.99382±0.31	1.5228E-07±4.6E-08
110920546	21	102.914:131.586	none	-	-	-	-	-	-	-	-
110920546	22	131.586:235.012	none	-	-	-	-	-	-	-	-
110921912	1	0.000:1.627	COMP	0.0269 ± 0.0031	-1.007 ± 0.045	-	862.70 ± 156.00	-	357.2/359	10.049±0.91	2.4969E-06±1.8E-07
110921912	2	1.627:2.290	COMP	0.0559 ± 0.0062	-0.837 ± 0.048	-	700.10 ± 88.40	-	414.77/359	18.486±1.5	5.0550E-06±3.2E-07
110921912	3	2.290:2.705	COMP	0.1063 ± 0.0128	-0.698 ± 0.054	-	488.50 ± 45.70	-	388.95/359	29.153±2.4	7.5033E-06±4.8E-07
110921912	4	2.705:3.001	COMP	0.1201 ± 0.0136	-0.728 ± 0.049	-	568.30 ± 55.80	-	335.01/359	35.471±2.9	9.6799E-06±6.1E-07
110921912	5	3.001:3.280	COMP	0.1317 ± 0.0129	-0.756 ± 0.044	-	674.50 ± 65.50	-	364.25/359	41.803±3.1	1.2079E-05±6.7E-07
110921912	6	3.280:3.697	COMP	0.1192 ± 0.0168	-0.769 ± 0.055	-	402.60 ± 39.20	-	427.09/359	31.350±3.0	6.8525E-06±5.0E-07
110921912	7	3.697:5.237	BAND	0.0900 ± 0.0216	-0.642 ± 0.104	-2.298 ± 0.194	198.90 ± 25.00	123.79 ± 18.81	380.23/358	15.234±2.0	2.5208E-06±2.7E-07
110921912	8	5.237:6.762	COMP	0.0442 ± 0.0069	-0.848 ± 0.059	-	394.90 ± 46.40	-	374.99/359	12.179±1.3	2.4913E-06±2.0E-07
110921912	9	6.762:7.831	COMP	0.0503 ± 0.0069	-0.851 ± 0.053	-	488.50 ± 59.60	-	418.23/359	14.964±1.4	3.4295E-06±2.5E-07
110921912	10	7.831:17.409	COMP	0.0086 ± 0.0015	-1.262 ± 0.054	-	801.50 ± 274.00	-	418.28/359	3.7473±0.50	6.8473E-07±7.2E-08
110921912	11	17.409:17.853	BAND	0.1100 ± 0.0178	-0.844 ± 0.068	-2.137 ± 0.135	467.60 ± 84.90	263.44 ± 50.12	375.44/358	32.282±3.0	7.4305E-06±5.0E-07
110921912	12	17.853:24.576	PL	0.0021 ± 0.0007	-1.569 ± 0.039	-	-	-	418.52/360	1.2644±0.46	1.8122E-07±6.2E-08
111003465	1	0.000:2.102	COMP	0.0416 ± 0.0055	-0.431 ± 0.059	-	394.80 ± 27.80	-	533.81/479	8.9955±0.84	2.3829E-06±1.9E-07
111003465	2	2.102:3.479	BAND	0.1274 ± 0.0269	-0.242 ± 0.105	-2.228 ± 0.145	188.20 ± 16.30	109.98 ± 10.95	541.97/478	14.185±1.9	2.7591E-06±3.2E-07

Continued on next page

Table A.1 – continued from previous page

GRB name	spectrum	T_{start}:T_{stop} (s)	BEST model	A (ph s^{-1} cm^{-2} keV^{-1})	α	β	E_p (keV)	E_b (keV)	CSTAT/dof	photon flux (ph s^{-1} cm^{-2})	energy flux (erg s^{-1} cm^{-2})
(1)	(2)	(3)	(4)	(5)	(6)	(7)	(8)	(9)	(10)	(11)	(12)
111003465	3	3.479:4.262	COMP	0.1156 ± 0.0181	-0.585 ± 0.056	-	287.50 ± 19.10	-	537.38/479	22.514±2.5	4.3506E-06±4.1E-07
111003465	4	4.262:5.205	COMP	0.0724 ± 0.0157	-0.671 ± 0.063	-	248.80 ± 18.80	-	500.88/479	13.953±2.4	2.3208E-06±3.6E-07
111003465	5	5.205:7.749	COMP	0.0619 ± 0.0201	-0.917 ± 0.074	-	158.50 ± 13.40	-	565.49/479	12.465±3.1	1.3610E-06±3.2E-07
111003465	6	7.749:9.731	PL	0.0060 ± 0.0020	-1.627 ± 0.022	-	-	-	681.54/480	3.8297±1.3	5.0049E-07±1.6E-07
111003465	7	9.731:11.142	SBPL	0.0239 ± 0.0087	-1.072 ± 0.112	-2.336 ± 0.170	94.89 ± 26.26	65.75 ± 14.70	483.57/478	11.955±4.2	1.2293E-06±4.1E-07
111003465	8	11.142:13.798	PL	0.0059 ± 0.0022	-1.739 ± 0.024	-	-	-	637.07/480	4.2367±1.6	4.6402E-07±1.7E-07
111003465	9	13.798:31.744	none	-	-	-	-	-	-	-	-
111127810	1	-1.024:5.883	none	-	-	-	-	-	-	-	-
111127810	2	5.883:7.122	none	-	-	-	-	-	-	-	-
111127810	3	7.122:7.892	PL	0.0117 ± 0.0039	-1.824 ± 0.027	-	-	-	568.7/479	9.1861±3.1	8.8214E-07±2.9E-07
111127810	4	7.892:8.632	PL	0.0113 ± 0.0039	-1.831 ± 0.027	-	-	-	686.3/479	8.9889±3.2	8.5450E-07±3.0E-07
111127810	5	8.632:9.611	PL	0.0108 ± 0.0040	-1.914 ± 0.030	-	-	-	590.47/479	9.5460±3.5	8.0379E-07±2.9E-07
111127810	6	9.611:10.890	none	-	-	-	-	-	-	-	-
111127810	7	10.890:13.352	none	-	-	-	-	-	-	-	-
111127810	8	13.352:18.432	none	-	-	-	-	-	-	-	-
111216389	1	-11.264:7.344	PL	0.0013 ± 0.0004	-1.467 ± 0.040	-	-	-	675.54/358	0.71569±0.25	1.2087E-07±3.8E-08
111216389	2	7.344:21.909	none	-	-	-	-	-	-	-	-
111216389	3	21.909:36.494	PL	0.0029 ± 0.0007	-1.576 ± 0.037	-	-	-	545.73/358	1.7560±0.45	2.4855E-07±5.8E-08
111216389	4	36.494:44.000	PL	0.0017 ± 0.0007	-1.481 ± 0.029	-	-	-	549.55/358	0.97295±0.39	1.6066E-07±6.3E-08
111216389	5	44.000:49.185	COMP	0.0231 ± 0.0073	-0.823 ± 0.087	-	228.20 ± 26.90	-	468.28/357	4.9383±1.2	7.1791E-07±1.6E-07
111216389	6	49.185:54.372	COMP	0.0186 ± 0.0049	-0.908 ± 0.078	-	303.50 ± 43.70	-	376.87/357	4.8674±0.95	8.1590E-07±1.4E-07
111216389	7	54.372:58.106	COMP	0.0184 ± 0.0047	-1.131 ± 0.067	-	356.70 ± 70.10	-	386.99/357	6.2439±1.2	9.8008E-07±1.7E-07
111216389	8	58.106:60.443	COMP	0.0258 ± 0.0056	-0.844 ± 0.069	-	368.90 ± 49.00	-	393.73/357	6.9046±1.1	1.3595E-06±2.0E-07
111216389	9	60.443:64.215	COMP	0.0347 ± 0.0094	-0.874 ± 0.079	-	235.80 ± 27.20	-	419.74/357	7.9594±1.6	1.1544E-06±2.0E-07
111216389	10	64.215:68.167	PL	0.0037 ± 0.0014	-1.622 ± 0.028	-	-	-	487.39/358	2.3431±0.93	3.0763E-07±1.2E-07
111216389	11	68.167:72.299	SBPL	0.0158 ± 0.0060	-1.211 ± 0.086	-2.589 ± 0.477	143.17 ± 64.32	126.80 ± 44.20	377.07/356	6.8363±2.5	7.7516E-07±2.5E-07
111216389	12	72.299:75.994	SBPL	0.0150 ± 0.0058	-1.170 ± 0.085	-2.587 ± 0.483	148.95 ± 65.98	131.60 ± 45.00	431.06/356	6.2090±2.3	7.4017E-07±2.5E-07
111216389	13	75.994:79.492	COMP	0.0451 ± 0.0165	-0.958 ± 0.086	-	165.80 ± 17.60	-	442.65/357	9.7919±2.7	1.0831E-06±2.8E-07
111216389	14	79.492:82.001	PL	0.0034 ± 0.0013	-1.503 ± 0.026	-	-	-	408.57/358	1.9302±0.77	3.0752E-07±1.2E-07
111216389	15	82.001:86.266	COMP	0.0403 ± 0.0123	-0.837 ± 0.084	-	199.90 ± 20.90	-	368.18/357	8.2182±1.8	1.0824E-06±2.1E-07
111216389	16	86.266:98.304	none	-	-	-	-	-	-	-	-
111220486	1	-4.096:6.144	COMP	0.0236 ± 0.0026	-0.839 ± 0.036	-	370.90 ± 27.20	-	681.14/470	6.2973±0.50	1.2496E-06±8.5E-08
111220486	2	6.144:9.216	COMP	0.0504 ± 0.0079	-0.884 ± 0.046	-	271.60 ± 22.30	-	515.52/470	12.368±1.4	1.9616E-06±1.9E-07
111220486	3	9.216:15.360	COMP	0.0237 ± 0.0040	-1.051 ± 0.042	-	294.90 ± 29.50	-	508.91/470	7.0443±0.92	1.0623E-06±1.2E-07
111220486	4	15.360:16.384	COMP	0.0613 ± 0.0069	-1.003 ± 0.035	-	538.90 ± 62.80	-	512.78/470	20.644±1.8	4.3567E-06±3.2E-07
111220486	5	16.384:17.408	COMP	0.0822 ± 0.0096	-0.941 ± 0.037	-	402.60 ± 36.40	-	522.98/470	24.411±2.1	4.7192E-06±3.4E-07
111220486	6	17.408:18.432	COMP	0.1025 ± 0.0131	-0.995 ± 0.038	-	321.20 ± 27.20	-	497.98/470	29.653±2.7	4.8701E-06±3.7E-07
111220486	7	18.432:19.456	COMP	0.0912 ± 0.0082	-0.967 ± 0.029	-	499.20 ± 42.40	-	485.05/470	29.413±2.0	6.1976E-06±3.5E-07
111220486	8	19.456:21.504	COMP	0.0732 ± 0.0096	-1.024 ± 0.034	-	263.50 ± 18.50	-	512.3/470	20.421±2.0	2.9352E-06±2.6E-07
111220486	9	21.504:30.721	COMP	0.0165 ± 0.0042	-1.357 ± 0.045	-	198.80 ± 26.10	-	580.71/470	6.3537±1.4	6.5759E-07±1.3E-07
111220486	10	30.721:53.249	none	-	-	-	-	-	-	-	-
111228657	1	-62.721:-34.049	none	-	-	-	-	-	-	-	-
111228657	2	-13.568:1.792	none	-	-	-	-	-	-	-	-

Continued on next page

Table A.1 – continued from previous page

GRB name	spectrum	T_{start}:T_{stop} (s)	BEST model	A (ph s^{-1} cm^{-2} keV^{-1})	α	β	E_p (keV)	E_b (keV)	CSTAT/dof	photon flux (ph s^{-1} cm^{-2})	energy flux (erg s^{-1} cm^{-2})
(1)	(2)	(3)	(4)	(5)	(6)	(7)	(8)	(9)	(10)	(11)	(12)
111228657	3	1.792:3.840	PL	0.0081 ± 0.0029	-1.928 ± 0.033	-	-	-	523.54/476	7.3065±2.7	6.0155E-07±2.2E-07
111228657	4	3.840:4.864	PL	0.0091 ± 0.0034	-1.809 ± 0.026	-	-	-	515.36/476	7.1001±2.7	6.9596E-07±2.6E-07
111228657	5	4.864:6.912	none	-	-	-	-	-	-	-	-
111228657	6	6.912:7.936	SBPL	0.0174 ± 0.0063	-1.166 ± 0.221	-2.128 ± 0.096	64.07 ± 28.04	32.86 ± 10.20	548.88/474	12.532±4.5	1.0948E-06±3.8E-07
111228657	7	7.936:9.984	none	-	-	-	-	-	-	-	-
111228657	8	9.984:16.128	none	-	-	-	-	-	-	-	-
111228657	9	41.729:47.873	none	-	-	-	-	-	-	-	-
111228657	10	47.873:48.897	none	-	-	-	-	-	-	-	-
111228657	11	48.897:52.993	none	-	-	-	-	-	-	-	-
111228657	12	52.993:61.185	none	-	-	-	-	-	-	-	-
120119170	1	-2.048:7.492	COMP	0.0220 ± 0.0056	-0.710 ± 0.091	-	214.60 ± 20.50	-	624.78/477	4.0608±0.68	5.9409E-07±8.5E-08
120119170	2	7.492:9.296	COMP	0.0338 ± 0.0067	-0.795 ± 0.070	-	304.90 ± 32.60	-	561.94/477	8.0496±1.1	1.4482E-06±1.8E-07
120119170	3	9.296:10.980	COMP	0.0884 ± 0.0232	-0.736 ± 0.082	-	170.30 ± 12.70	-	512.87/477	14.769±2.6	1.8038E-06±2.8E-07
120119170	4	10.980:12.804	COMP	0.0558 ± 0.0180	-0.876 ± 0.082	-	160.30 ± 13.80	-	543.6/477	10.730±2.6	1.1953E-06±2.7E-07
120119170	5	12.804:14.094	COMP	0.0568 ± 0.0136	-0.972 ± 0.070	-	215.80 ± 22.40	-	560.03/477	13.961±2.4	1.8214E-06±2.7E-07
120119170	6	14.094:14.898	COMP	0.0661 ± 0.0120	-0.920 ± 0.060	-	298.20 ± 31.60	-	558.45/477	17.412±2.3	2.8653E-06±3.1E-07
120119170	7	14.898:15.635	COMP	0.0697 ± 0.0124	-0.910 ± 0.060	-	317.60 ± 34.70	-	534.72/477	18.630±2.3	3.2080E-06±3.4E-07
120119170	8	15.635:16.517	COMP	0.0768 ± 0.0148	-0.891 ± 0.066	-	268.00 ± 27.40	-	551.6/477	18.900±2.5	2.9558E-06±3.2E-07
120119170	9	16.517:17.824	COMP	0.0568 ± 0.0139	-0.835 ± 0.072	-	214.30 ± 19.30	-	509.5/477	11.962±2.1	1.6553E-06±2.6E-07
120119170	10	17.824:18.605	COMP	0.0520 ± 0.0110	-0.885 ± 0.066	-	293.10 ± 32.50	-	501.99/477	13.177±2.1	2.1912E-06±3.0E-07
120119170	11	18.605:19.534	COMP	0.0624 ± 0.0125	-1.077 ± 0.061	-	272.90 ± 33.70	-	551.72/477	18.657±2.7	2.6472E-06±3.2E-07
120119170	12	19.534:21.166	COMP	0.0532 ± 0.0134	-1.148 ± 0.069	-	197.30 ± 23.40	-	523.48/477	15.647±2.8	1.7795E-06±2.7E-07
120119170	13	21.166:23.026	COMP	0.0528 ± 0.0178	-1.001 ± 0.081	-	151.90 ± 14.00	-	529.78/477	11.665±3.0	1.2017E-06±2.9E-07
120119170	14	23.026:26.149	SBPL	0.0090 ± 0.0036	-1.079 ± 0.146	-2.198 ± 0.196	112.22 ± 49.94	67.06 ± 21.40	538.53/476	4.3070±1.6	4.8634E-07±1.7E-07
120119170	15	26.149:28.980	none	-	-	-	-	-	-	-	-
120119170	16	28.980:31.807	COMP	0.0550 ± 0.0195	-0.961 ± 0.089	-	140.90 ± 12.90	-	500.29/477	11.132±2.8	1.1074E-06±2.6E-07
120119170	17	31.807:37.481	none	-	-	-	-	-	-	-	-
120119170	18	37.481:58.368	none	-	-	-	-	-	-	-	-
120129580	1	-1.024:0.704	none	-	-	-	-	-	-	-	-
120129580	2	0.704:0.951	SBPL	0.1168 ± 0.0406	-0.655 ± 0.207	-2.469 ± 0.247	89.69 ± 27.24	60.86 ± 15.20	272.0/237	49.000±16.0	5.3954E-06±1.5E-06
120129580	3	0.951:1.117	COMP	0.6106 ± 0.2190	-0.661 ± 0.108	-	165.00 ± 15.60	-	212.02/238	91.457±21.0	1.1214E-05±2.2E-06
120129580	4	1.117:1.201	BAND	1.1070 ± 0.3340	-0.338 ± 0.137	-2.437 ± 0.171	205.90 ± 26.10	133.54 ± 17.90	248.51/237	142.72±20.0	2.6956E-05±3.0E-06
120129580	5	1.201:1.266	COMP	0.6069 ± 0.0972	-0.713 ± 0.066	-	404.90 ± 41.80	-	249.45/238	154.26±17.0	3.5193E-05±2.9E-06
120129580	6	1.266:1.321	COMP	0.6062 ± 0.0993	-0.632 ± 0.069	-	413.60 ± 42.50	-	196.5/238	148.59±17.0	3.6189E-05±3.0E-06
120129580	7	1.321:1.371	COMP	0.7190 ± 0.1020	-0.650 ± 0.064	-	461.20 ± 44.00	-	224.03/238	187.61±19.0	4.8325E-05±3.6E-06
120129580	8	1.371:1.414	COMP	0.9166 ± 0.1460	-0.553 ± 0.068	-	397.80 ± 36.00	-	221.48/238	211.02±23.0	5.2522E-05±4.1E-06
120129580	9	1.414:1.457	COMP	1.1840 ± 0.1810	-0.557 ± 0.069	-	358.10 ± 28.60	-	213.16/238	257.27±27.0	5.9353E-05±4.5E-06
120129580	10	1.457:1.504	COMP	1.4700 ± 0.2670	-0.517 ± 0.076	-	292.90 ± 23.10	-	183.34/238	275.02±32.0	5.5736E-05±4.7E-06
120129580	11	1.504:1.551	COMP	0.7755 ± 0.1230	-0.566 ± 0.069	-	413.50 ± 38.50	-	228.01/238	183.69±20.0	4.6572E-05±3.7E-06
120129580	12	1.551:1.595	COMP	0.8922 ± 0.1500	-0.464 ± 0.073	-	369.80 ± 31.40	-	246.45/238	187.67±21.0	4.6593E-05±3.9E-06
120129580	13	1.595:1.641	COMP	0.7989 ± 0.1290	-0.539 ± 0.071	-	397.00 ± 36.20	-	219.25/238	182.45±20.0	4.5716E-05±3.7E-06
120129580	14	1.641:1.690	COMP	1.3710 ± 0.2410	-0.553 ± 0.073	-	298.80 ± 23.50	-	200.0/238	266.73±31.0	5.3924E-05±4.6E-06
120129580	15	1.690:1.741	COMP	0.8032 ± 0.1230	-0.606 ± 0.068	-	391.50 ± 35.20	-	271.58/238	188.71±20.0	4.5021E-05±3.5E-06

Continued on next page

Table A.1 – continued from previous page

GRB name	spectrum	T_{start}:T_{stop} (s)	BEST model	A (ph s^{-1} cm^{-2} keV^{-1})	α	β	E_p (keV)	E_b (keV)	CSTAT/dof	photon flux (ph s^{-1} cm^{-2})	energy flux (erg s^{-1} cm^{-2})
(1)	(2)	(3)	(4)	(5)	(6)	(7)	(8)	(9)	(10)	(11)	(12)
120129580	16	1.741:1.793	COMP	0.8879 ± 0.1780	−0.514 ± 0.079	-	306.20 ± 27.20	-	185.39/238	170.61±22.0	3.5817E-05±3.5E-06
120129580	17	1.793:1.855	COMP	1.0330 ± 0.2500	−0.578 ± 0.087	-	231.50 ± 20.20	-	233.28/238	174.96±27.0	2.8724E-05±3.6E-06
120129580	18	1.855:1.929	COMP	0.7265 ± 0.1960	−0.577 ± 0.092	-	230.30 ± 22.10	-	217.66/238	122.58±21.0	2.0049E-05±2.8E-06
120129580	19	1.929:2.010	COMP	0.9580 ± 0.2660	−0.592 ± 0.092	-	204.60 ± 18.50	-	200.36/238	152.19±27.0	2.2560E-05±3.2E-06
120129580	20	2.010:2.112	COMP	1.2990 ± 0.4340	−0.530 ± 0.106	-	164.50 ± 13.70	-	205.07/238	166.63±34.0	2.1273E-05±3.7E-06
120129580	21	2.112:2.242	COMP	0.3958 ± 0.1230	−0.921 ± 0.091	-	205.80 ± 25.90	-	243.35/238	89.757±19.0	1.1657E-05±2.0E-06
120129580	22	2.242:2.444	SBPL	0.1066 ± 0.0271	−0.395 ± 0.335	−2.077 ± 0.129	101.50 ± 40.55	41.68 ± 11.00	280.39/237	46.567±11.0	6.0034E-06±1.2E-06
120129580	23	2.444:2.718	COMP	0.1605 ± 0.0486	−1.038 ± 0.086	-	252.20 ± 43.20	-	222.84/238	44.744±9.2	6.2268E-06±1.0E-06
120129580	24	2.718:2.865	COMP	0.2504 ± 0.0351	−0.663 ± 0.064	-	548.30 ± 63.90	-	210.6/238	71.016±6.9	2.0008E-05±1.4E-06
120129580	25	2.865:2.971	COMP	0.5548 ± 0.0880	−0.448 ± 0.073	-	371.60 ± 31.30	-	225.89/238	116.07±12.0	2.9169E-05±2.1E-06
120129580	26	2.971:3.076	COMP	0.5313 ± 0.0860	−0.589 ± 0.070	-	373.60 ± 34.70	-	214.76/238	120.48±13.0	2.8132E-05±2.1E-06
120129580	27	3.076:3.193	COMP	0.3947 ± 0.0566	−0.642 ± 0.068	-	439.20 ± 43.00	-	230.32/238	100.17±10.0	2.5188E-05±1.8E-06
120129580	28	3.193:3.316	COMP	0.4800 ± 0.0898	−0.543 ± 0.080	-	314.00 ± 28.90	-	228.98/238	95.548±11.0	2.0162E-05±1.8E-06
120129580	29	3.316:3.466	COMP	0.4916 ± 0.1150	−0.586 ± 0.087	-	253.70 ± 24.50	-	220.93/238	88.817±13.0	1.5597E-05±1.7E-06
120129580	30	3.466:3.869	COMP	0.1860 ± 0.0723	−1.097 ± 0.100	-	164.30 ± 24.20	-	230.7/238	47.988±13.0	5.0301E-06±1.1E-06
120129580	31	3.869:7.168	none	-	-	-	-	-	-	-	-
120204054	1	-5.120:24.750	COMP	0.0181 ± 0.0037	−0.922 ± 0.053	-	171.40 ± 10.40	-	672.98/479	3.8180±0.59	4.3764E-07±6.2E-08
120204054	2	24.750:26.292	COMP	0.2117 ± 0.0816	−0.633 ± 0.081	-	108.40 ± 4.89	-	558.32/479	23.149±7.1	2.0982E-06±6.3E-07
120204054	3	26.292:27.880	PL	0.0060 ± 0.0017	−1.600 ± 0.020	-	-	-	751.73/480	3.7000±1.1	5.0414E-07±1.4E-07
120204054	4	27.880:29.310	SBPL	0.0288 ± 0.0097	−0.682 ± 0.137	−2.639 ± 0.173	77.98 ± 13.21	60.45 ± 9.27	537.81/478	13.035±4.3	1.2805E-06±4.0E-07
120204054	5	29.310:30.319	BAND	0.1450 ± 0.0578	−0.496 ± 0.109	−2.902 ± 0.408	111.80 ± 7.84	93.24 ± 15.79	489.6/478	13.598±5.1	1.4665E-06±5.1E-07
120204054	6	30.319:31.170	PL	0.0067 ± 0.0023	−1.586 ± 0.021	-	-	-	805.93/480	4.1230±1.4	5.7448E-07±2.0E-07
120204054	7	31.170:31.825	COMP	0.1387 ± 0.0350	−0.802 ± 0.064	-	169.10 ± 10.70	-	499.94/479	25.012±4.8	2.9686E-06±5.3E-07
120204054	8	31.825:32.244	COMP	0.2445 ± 0.0502	−0.653 ± 0.064	-	191.30 ± 11.50	-	474.19/479	39.788±5.6	5.4612E-06±6.8E-07
120204054	9	32.244:32.594	COMP	0.2480 ± 0.0526	−0.571 ± 0.066	-	194.90 ± 11.20	-	493.57/479	37.445±5.6	5.3760E-06±7.2E-07
120204054	10	32.594:32.943	COMP	0.2344 ± 0.0472	−0.738 ± 0.061	-	203.10 ± 13.30	-	510.84/479	43.264±6.1	6.0061E-06±7.4E-07
120204054	11	32.943:33.311	COMP	0.2487 ± 0.0563	−0.535 ± 0.068	-	185.80 ± 10.30	-	567.78/479	34.998±5.7	4.9013E-06±7.2E-07
120204054	12	33.311:33.686	COMP	0.2466 ± 0.0559	−0.668 ± 0.066	-	178.90 ± 10.50	-	512.8/479	39.196±6.3	5.0865E-06±7.5E-07
120204054	13	33.686:34.094	COMP	0.2418 ± 0.0562	−0.624 ± 0.067	-	175.20 ± 9.96	-	535.98/479	36.103±6.0	4.6842E-06±7.1E-07
120204054	14	34.094:34.494	COMP	0.2010 ± 0.0438	−0.783 ± 0.064	-	186.40 ± 12.30	-	530.93/479	37.285±5.8	4.7762E-06±6.7E-07
120204054	15	34.494:34.948	COMP	0.1467 ± 0.0331	−0.755 ± 0.062	-	198.50 ± 13.50	-	468.08/479	27.238±4.6	3.6931E-06±5.6E-07
120204054	16	34.948:35.400	COMP	0.1814 ± 0.0353	−0.831 ± 0.059	-	211.30 ± 15.00	-	489.47/479	37.788±5.1	5.1859E-06±6.1E-07
120204054	17	35.400:35.878	COMP	0.1847 ± 0.0397	−0.730 ± 0.063	-	195.60 ± 12.80	-	510.83/479	33.135±5.0	4.4896E-06±6.0E-07
120204054	18	35.878:36.391	COMP	0.1647 ± 0.0316	−0.809 ± 0.058	-	217.60 ± 15.40	-	519.39/479	33.972±4.5	4.8075E-06±5.6E-07
120204054	19	36.391:36.914	COMP	0.1234 ± 0.0236	−0.882 ± 0.055	-	233.40 ± 18.30	-	502.18/479	28.392±3.9	4.0732E-06±5.0E-07
120204054	20	36.914:37.434	COMP	0.1329 ± 0.0249	−0.882 ± 0.056	-	240.40 ± 19.50	-	516.86/479	30.939±4.1	4.5287E-06±5.1E-07
120204054	21	37.434:37.972	COMP	0.1373 ± 0.0269	−0.905 ± 0.057	-	222.60 ± 17.70	-	567.11/479	31.724±4.4	4.3617E-06±5.2E-07
120204054	22	37.972:38.562	COMP	0.1234 ± 0.0238	−0.977 ± 0.055	-	229.20 ± 19.80	-	538.81/479	31.194±4.3	4.2194E-06±5.0E-07
120204054	23	38.562:39.127	COMP	0.1463 ± 0.0317	−0.925 ± 0.060	-	197.00 ± 15.30	-	493.44/479	32.845±5.1	4.1235E-06±5.6E-07
120204054	24	39.127:39.692	COMP	0.0981 ± 0.0211	−1.037 ± 0.057	-	226.50 ± 22.20	-	523.5/479	26.414±4.2	3.4391E-06±4.8E-07
120204054	25	39.692:40.229	COMP	0.0693 ± 0.0165	−1.121 ± 0.057	-	239.00 ± 27.10	-	473.32/479	20.907±3.9	2.6844E-06±4.5E-07
120204054	26	40.229:40.841	COMP	0.1131 ± 0.0269	−1.018 ± 0.062	-	191.60 ± 16.80	-	501.31/479	28.056±4.9	3.3244E-06±5.2E-07
120204054	27	40.841:41.521	COMP	0.1185 ± 0.0268	−1.108 ± 0.058	-	187.10 ± 17.00	-	518.25/479	32.582±5.3	3.6582E-06±5.2E-07

Continued on next page

Table A.1 – continued from previous page

GRB name	spectrum	T_{start}:T_{stop} (s)	BEST model	A (ph s^{-1} cm^{-2} keV^{-1})	α	β	E_p (keV)	E_b (keV)	CSTAT/dof	photon flux (ph s^{-1} cm^{-2})	energy flux (erg s^{-1} cm^{-2})
(1)	(2)	(3)	(4)	(5)	(6)	(7)	(8)	(9)	(10)	(11)	(12)
120204054	28	41.521:42.064	COMP	0.0710 ± 0.0148	-1.154 ± 0.050	-	264.30 ± 30.40	-	465.44/479	22.848±3.7	3.0393E-06±4.4E-07
120204054	29	42.064:42.483	COMP	0.1826 ± 0.0397	-1.025 ± 0.059	-	192.50 ± 16.20	-	522.82/479	45.708±7.0	5.4162E-06±7.2E-07
120204054	30	42.483:42.921	COMP	0.1496 ± 0.0322	-1.051 ± 0.057	-	202.70 ± 18.20	-	500.66/479	39.407±6.1	4.7629E-06±6.4E-07
120204054	31	42.921:43.379	COMP	0.1190 ± 0.0268	-1.145 ± 0.056	-	201.50 ± 19.80	-	472.86/479	35.078±5.9	4.0432E-06±6.0E-07
120204054	32	43.379:43.831	COMP	0.1650 ± 0.0361	-1.069 ± 0.057	-	196.80 ± 17.50	-	489.61/479	43.983±6.9	5.1783E-06±7.0E-07
120204054	33	43.831:44.239	COMP	0.0843 ± 0.0169	-1.267 ± 0.048	-	282.10 ± 38.50	-	541.93/479	31.338±4.9	3.9995E-06±5.5E-07
120204054	34	44.239:44.721	COMP	0.1113 ± 0.0215	-1.093 ± 0.051	-	242.30 ± 23.70	-	545.86/479	32.626±4.7	4.2895E-06±5.4E-07
120204054	35	44.721:45.197	COMP	0.1086 ± 0.0235	-1.139 ± 0.056	-	217.60 ± 22.50	-	545.14/479	32.525±5.3	3.9263E-06±5.6E-07
120204054	36	45.197:45.784	COMP	0.0896 ± 0.0239	-1.132 ± 0.059	-	178.70 ± 16.70	-	484.59/479	25.003±5.2	2.7060E-06±5.2E-07
120204054	37	45.784:46.518	COMP	0.0850 ± 0.0209	-1.169 ± 0.058	-	185.50 ± 18.60	-	548.58/479	25.188±4.7	2.7408E-06±4.6E-07
120204054	38	46.518:47.264	COMP	0.0997 ± 0.0282	-1.220 ± 0.063	-	149.70 ± 14.20	-	467.0/479	29.660±6.4	2.8111E-06±5.5E-07
120204054	39	47.264:48.128	COMP	0.0926 ± 0.0267	-1.272 ± 0.062	-	142.70 ± 13.70	-	435.4/479	29.279±6.4	2.6588E-06±5.3E-07
120204054	40	48.128:48.904	COMP	0.1114 ± 0.0313	-1.289 ± 0.062	-	136.30 ± 12.80	-	560.85/479	35.604±7.5	3.1425E-06±6.0E-07
120204054	41	48.904:49.693	COMP	0.0565 ± 0.0194	-1.416 ± 0.061	-	142.20 ± 17.10	-	516.77/479	22.074±6.3	1.9121E-06±5.1E-07
120204054	42	49.693:50.510	COMP	0.0588 ± 0.0201	-1.419 ± 0.061	-	135.20 ± 15.50	-	502.18/479	22.818±6.4	1.9311E-06±5.1E-07
120204054	43	50.510:51.325	COMP	0.0541 ± 0.0207	-1.539 ± 0.063	-	113.40 ± 13.80	-	535.69/479	24.488±7.8	1.8706E-06±5.7E-07
120204054	44	51.325:52.033	COMP	0.1402 ± 0.0556	-1.442 ± 0.070	-	86.17 ± 7.11	-	553.21/479	50.497±16.0	3.4743E-06±1.0E-06
120204054	45	52.033:52.791	COMP	0.0740 ± 0.0272	-1.558 ± 0.066	-	103.10 ± 12.30	-	561.73/479	33.908±9.9	2.4870E-06±6.7E-07
120204054	46	52.791:53.653	PL	0.0102 ± 0.0037	-1.850 ± 0.023	-	-	-	580.88/480	8.3396±3.1	7.6916E-07±2.8E-07
120204054	47	53.653:54.450	BAND	0.0524 ± 0.0209	-1.511 ± 0.117	-2.282 ± 0.202	73.81 ± 15.10	60.45 ± 18.57	447.04/478	20.852±7.5	1.5993E-06±5.3E-07
120204054	48	54.450:55.497	PL	0.0105 ± 0.0039	-1.927 ± 0.024	-	-	-	562.58/480	9.4565±3.6	7.8024E-07±2.9E-07
120204054	49	55.497:56.823	PL	0.0114 ± 0.0036	-1.945 ± 0.025	-	-	-	542.85/480	10.438±3.3	8.3888E-07±2.6E-07
120204054	50	56.823:58.727	none	-	-	-	-	-	-	-	-
120204054	51	58.727:60.943	none	-	-	-	-	-	-	-	-
120204054	52	60.943:65.566	none	-	-	-	-	-	-	-	-
120204054	53	65.566:82.944	none	-	-	-	-	-	-	-	-
120226871	1	-5.120:6.315	COMP	0.0092 ± 0.0017	-0.845 ± 0.066	-	440.20 ± 63.30	-	948.81/479	2.6461±0.35	5.7700E-07±6.6E-08
120226871	2	6.315:7.973	COMP	0.0350 ± 0.0066	-0.777 ± 0.066	-	356.10 ± 40.60	-	555.65/479	8.8034±1.2	1.7732E-06±2.0E-07
120226871	3	7.973:9.516	COMP	0.0409 ± 0.0067	-0.760 ± 0.062	-	381.70 ± 41.90	-	563.13/479	10.452±1.2	2.2241E-06±2.1E-07
120226871	4	9.516:10.871	COMP	0.0363 ± 0.0058	-0.848 ± 0.058	-	442.90 ± 55.70	-	546.28/479	10.423±1.2	2.2752E-06±2.2E-07
120226871	5	10.871:12.645	COMP	0.0389 ± 0.0076	-0.776 ± 0.065	-	307.90 ± 31.30	-	611.62/479	9.1540±1.3	1.6768E-06±2.0E-07
120226871	6	12.645:14.504	COMP	0.0427 ± 0.0085	-0.795 ± 0.066	-	283.10 ± 28.30	-	619.78/479	9.8214±1.4	1.6813E-06±2.0E-07
120226871	7	14.504:16.138	COMP	0.0434 ± 0.0073	-0.905 ± 0.057	-	367.50 ± 44.20	-	627.94/479	12.175±1.4	2.2940E-06±2.2E-07
120226871	8	16.138:17.727	COMP	0.0394 ± 0.0067	-0.829 ± 0.061	-	374.70 ± 43.20	-	600.93/479	10.513±1.3	2.1115E-06±2.1E-07
120226871	9	17.727:18.981	BAND	0.0742 ± 0.0150	-0.589 ± 0.090	-2.183 ± 0.162	257.10 ± 32.00	147.76 ± 21.12	592.19/478	13.943±1.6	2.8074E-06±2.7E-07
120226871	10	18.981:20.915	SBPL	0.0192 ± 0.0032	-0.592 ± 0.183	-1.743 ± 0.070	-	58.77 ± 13.10	594.56/478	6.9714±1.1	1.3403E-06±1.8E-07
120226871	11	20.915:24.363	SBPL	0.0119 ± 0.0022	-0.664 ± 0.182	-1.727 ± 0.074	-	58.38 ± 14.40	651.07/478	4.4776±0.75	8.4773E-07±1.3E-07
120226871	12	24.363:26.893	SBPL	0.0146 ± 0.0025	-0.556 ± 0.206	-1.704 ± 0.066	-	54.17 ± 12.70	654.76/478	5.3799±0.85	1.0508E-06±1.5E-07
120226871	13	26.893:30.008	BAND	0.0270 ± 0.0071	-0.683 ± 0.136	-1.705 ± 0.074	197.80 ± 42.50	80.55 ± 16.63	790.11/478	5.0236±0.77	1.0042E-06±1.4E-07
120226871	14	30.008:31.641	BAND	0.0369 ± 0.0071	-0.799 ± 0.081	-2.010 ± 0.133	355.40 ± 64.00	181.29 ± 33.81	582.89/478	9.5682±1.1	2.0495E-06±2.0E-07
120226871	15	31.641:34.131	BAND	0.0369 ± 0.0081	-0.858 ± 0.095	-1.945 ± 0.102	230.90 ± 40.60	113.16 ± 19.88	707.55/478	8.5162±1.2	1.4825E-06±1.8E-07
120226871	16	34.131:36.820	SBPL	0.0168 ± 0.0024	-1.030 ± 0.058	-1.946 ± 0.100	546.42 ± 205.86	183.70 ± 39.60	706.97/478	6.4954±0.82	1.3280E-06±1.5E-07
120226871	17	36.820:46.150	PL	0.0030 ± 0.0004	-1.414 ± 0.021	-	-	-	1346.3/480	1.6244±0.25	2.9927E-07±4.0E-08

Continued on next page

Table A.1 – continued from previous page

GRB name	spectrum	T_{start}:T_{stop} (s)	BEST model	A (ph s^{-1} cm^{-2} keV^{-1})	α	β	E_p (keV)	E_b (keV)	CSTAT/dof	photon flux (ph s^{-1} cm^{-2})	energy flux (erg s^{-1} cm^{-2})
(1)	(2)	(3)	(4)	(5)	(6)	(7)	(8)	(9)	(10)	(11)	(12)
120226871	18	46.150:54.741	PL	0.0032 ± 0.0005	−1.430 ± 0.022	-	-	-	1151.2/480	1.7192±0.27	3.0880E-07±4.4E-08
120226871	19	54.741:78.848	PL	0.0020 ± 0.0003	−1.433 ± 0.026	-	-	-	2359.7/480	1.0611±0.18	1.8955E-07±2.8E-08
120323507	1	-0.064:0.018	SBPL	0.2631 ± 0.0382	0.042 ± 0.282	−1.849 ± 0.041	-	46.49 ± 6.95	362.47/359	87.252±12.0	1.6488E-05±1.9E-06
120323507	2	0.018:0.034	SBPL	1.5490 ± 0.3130	−0.278 ± 0.219	−2.441 ± 0.120	77.30 ± 13.03	48.01 ± 7.37	298.79/359	661.78±1.2E+02	7.2676E-05±1.2E-05
120323507	3	0.034:0.050	SBPL	1.4050 ± 0.3290	−0.297 ± 0.247	−2.612 ± 0.134	60.86 ± 10.12	42.82 ± 6.70	287.33/359	740.08±1.7E+02	6.7080E-05±1.4E-05
120323507	4	0.050:0.067	SBPL	1.4650 ± 0.2830	−0.514 ± 0.272	−2.393 ± 0.104	57.76 ± 11.47	36.57 ± 6.85	322.02/359	881.88±1.7E+02	7.8715E-05±1.3E-05
120323507	5	0.067:0.081	COMP	2.4220 ± 0.4740	−1.442 ± 0.053	-	206.70 ± 24.40	-	406.74/360	1057.3±1.6E+02	0.00010630±1.4E-05
120323507	6	0.081:0.097	COMP	1.0710 ± 0.1630	−1.598 ± 0.040	-	576.10 ± 165.00	-	380.83/360	628.82±86.0	7.3036E-05±8.4E-06
120323507	7	0.097:0.116	COMP	1.4290 ± 0.2110	−1.476 ± 0.044	-	442.50 ± 90.20	-	348.24/360	717.30±88.0	8.9933E-05±8.8E-06
120323507	8	0.116:0.143	COMP	0.9016 ± 0.1720	−1.560 ± 0.048	-	312.70 ± 71.40	-	289.24/360	484.54±74.0	5.1620E-05±6.4E-06
120323507	9	0.143:0.193	COMP	0.5497 ± 0.1620	−1.519 ± 0.066	-	146.80 ± 22.70	-	297.02/360	252.60±56.0	2.1470E-05±4.1E-06
120323507	10	0.193:0.281	COMP	0.2799 ± 0.1040	−1.496 ± 0.071	-	112.00 ± 12.30	-	319.93/360	117.66±36.0	9.0075E-06±2.6E-06
120323507	11	0.281:0.391	PL	0.0612 ± 0.0132	−2.036 ± 0.033	-	-	-	438.33/361	63.570±16.0	4.5174E-06±9.8E-07
120323507	12	0.391:0.896	none	-	-	-	-	-	-	-	-
120328268	1	-2.048:4.485	BAND	0.0229 ± 0.0039	−0.609 ± 0.079	−1.960 ± 0.104	355.90 ± 50.70	175.79 ± 25.56	544.41/476	5.2467±0.52	1.2874E-06±1.1E-07
120328268	2	4.485:5.252	SBPL	0.0918 ± 0.0081	−0.645 ± 0.056	−2.095 ± 0.089	415.83 ± 136.44	175.70 ± 20.60	583.14/476	29.054±2.1	7.2969E-06±4.3E-07
120328268	3	5.252:5.742	SBPL	0.1168 ± 0.0106	−0.531 ± 0.065	−2.028 ± 0.079	436.22 ± 143.63	152.80 ± 17.30	495.46/476	35.181±2.7	9.0816E-06±5.7E-07
120328268	4	5.742:6.213	BAND	0.1945 ± 0.0309	−0.444 ± 0.076	−2.041 ± 0.088	284.60 ± 28.90	150.03 ± 15.31	547.66/476	35.170±3.0	8.3368E-06±5.8E-07
120328268	5	6.213:6.581	SBPL	0.1505 ± 0.0171	−0.631 ± 0.070	−2.249 ± 0.129	232.80 ± 54.24	127.50 ± 16.30	583.67/476	44.659±4.6	8.8083E-06±7.6E-07
120328268	6	6.581:7.018	BAND	0.3750 ± 0.0737	−0.348 ± 0.098	−2.082 ± 0.094	173.00 ± 15.80	94.69 ± 8.90	553.45/476	43.631±4.6	8.0938E-06±7.2E-07
120328268	7	7.018:7.472	SBPL	0.1104 ± 0.0147	−0.576 ± 0.086	−2.183 ± 0.124	210.37 ± 70.75	101.50 ± 13.70	450.08/476	32.966±4.0	6.0869E-06±6.4E-07
120328268	8	7.472:7.885	BAND	0.3349 ± 0.0679	−0.477 ± 0.089	−2.301 ± 0.155	172.00 ± 15.10	106.41 ± 11.35	529.5/476	43.539±5.6	7.1277E-06±7.7E-07
120328268	9	7.885:8.508	BAND	0.2368 ± 0.0502	−0.536 ± 0.093	−2.193 ± 0.137	157.00 ± 15.00	92.37 ± 10.35	488.71/476	31.044±4.4	4.8559E-06±5.9E-07
120328268	10	8.508:9.381	SBPL	0.0532 ± 0.0084	−0.683 ± 0.147	−1.905 ± 0.072	344.99 ± 119.52	51.85 ± 9.28	452.7/476	21.773±3.2	3.3102E-06±4.2E-07
120328268	11	9.381:10.363	BAND	0.1169 ± 0.0327	−0.640 ± 0.121	−1.962 ± 0.096	123.40 ± 16.20	63.48 ± 8.33	511.13/476	15.240±2.9	2.2301E-06±3.8E-07
120328268	12	10.363:11.725	COMP	0.0948 ± 0.0223	−0.862 ± 0.061	-	187.00 ± 14.80	-	532.02/477	19.272±3.3	2.4026E-06±3.7E-07
120328268	13	11.725:13.242	COMP	0.0877 ± 0.0221	−0.812 ± 0.064	-	180.70 ± 13.60	-	616.04/477	16.534±3.1	2.0512E-06±3.6E-07
120328268	14	13.242:14.882	COMP	0.1285 ± 0.0317	−0.795 ± 0.065	-	161.80 ± 11.10	-	509.34/477	22.417±3.9	2.5884E-06±4.1E-07
120328268	15	14.882:17.500	BAND	0.0674 ± 0.0178	−0.815 ± 0.115	−1.970 ± 0.111	132.60 ± 20.50	68.37 ± 10.82	591.3/476	11.502±2.0	1.6100E-06±2.4E-07
120328268	16	17.500:18.635	COMP	0.0532 ± 0.0080	−0.962 ± 0.048	-	422.80 ± 54.40	-	579.24/477	16.307±1.8	3.1818E-06±3.0E-07
120328268	17	18.635:19.381	SBPL	0.0713 ± 0.0076	−0.688 ± 0.079	−1.854 ± 0.067	-	102.30 ± 14.50	535.94/476	23.234±2.3	4.9800E-06±4.2E-07
120328268	18	19.381:20.035	BAND	0.1674 ± 0.0334	−0.556 ± 0.096	−1.926 ± 0.084	184.40 ± 21.80	91.20 ± 10.71	479.63/476	25.555±3.0	4.7547E-06±4.8E-07
120328268	19	20.035:20.474	COMP	0.1865 ± 0.0317	−0.607 ± 0.058	-	258.30 ± 17.90	-	490.04/477	34.710±4.1	6.1174E-06±6.2E-07
120328268	20	20.474:20.983	COMP	0.2921 ± 0.0553	−0.616 ± 0.061	-	198.40 ± 12.00	-	493.01/477	46.721±5.9	6.6944E-06±7.2E-07
120328268	21	20.983:21.593	COMP	0.1842 ± 0.0382	−0.769 ± 0.060	-	196.00 ± 13.70	-	589.67/477	34.474±5.1	4.6111E-06±6.0E-07
120328268	22	21.593:22.445	BAND	0.1830 ± 0.0481	−0.506 ± 0.109	−2.239 ± 0.159	129.80 ± 12.50	79.03 ± 9.10	583.39/476	20.161±4.0	2.8173E-06±4.9E-07
120328268	23	22.445:23.266	SBPL	0.0455 ± 0.0091	−0.721 ± 0.136	−2.035 ± 0.099	148.82 ± 52.62	58.03 ± 10.60	529.49/476	18.361±3.5	2.5950E-06±4.4E-07
120328268	24	23.266:25.106	COMP	0.1089 ± 0.0321	−1.044 ± 0.065	-	134.60 ± 10.70	-	525.26/477	24.230±5.3	2.2879E-06±4.6E-07
120328268	25	25.106:27.613	COMP	0.0851 ± 0.0289	−1.023 ± 0.069	-	126.40 ± 9.77	-	628.7/477	17.890±4.7	1.6348E-06±4.1E-07
120328268	26	27.613:30.412	SBPL	0.0140 ± 0.0044	−0.652 ± 0.255	−2.076 ± 0.081	79.94 ± 29.60	31.30 ± 6.50	579.08/476	8.2045±2.6	8.5382E-07±2.6E-07
120328268	27	30.412:32.550	COMP	0.1557 ± 0.0583	−0.842 ± 0.076	-	110.80 ± 6.82	-	484.65/477	23.467±6.8	2.0627E-06±5.7E-07
120328268	28	32.550:42.320	PL	0.0062 ± 0.0013	−1.742 ± 0.026	-	-	-	850.47/478	4.4716±0.96	4.8649E-07±9.8E-08
120328268	29	42.320:56.320	none	-	-	-	-	-	-	-	-

Continued on next page

Table A.1 – continued from previous page

GRB name	spectrum	T_{start}:T_{stop} (s)	BEST model	A (ph s^{-1} cm^{-2} keV^{-1})	α	β	E_p (keV)	E_b (keV)	CSTAT/dof	photon flux (ph s^{-1} cm^{-2})	energy flux (erg s^{-1} cm^{-2})
(1)	(2)	(3)	(4)	(5)	(6)	(7)	(8)	(9)	(10)	(11)	(12)
120426090	1	-2.048:0.501	COMP	0.0699 ± 0.0200	−0.579 ± 0.093	-	195.00 ± 15.50	-	368.06/357	10.638±2.1	1.5245E-06±2.7E-07
120426090	2	0.501:0.638	SBPL	0.2352 ± 0.0457	−0.605 ± 0.104	−2.454 ± 0.189	159.36 ± 33.08	106.20 ± 17.40	368.34/356	69.506±12.0	1.1234E-05±1.8E-06
120426090	3	0.638:0.800	COMP	0.4610 ± 0.1450	−0.547 ± 0.081	-	159.70 ± 9.40	-	342.43/357	59.189±15.0	7.3349E-06±1.7E-06
120426090	4	0.800:0.975	COMP	0.5518 ± 0.1770	−0.478 ± 0.082	-	150.10 ± 7.77	-	366.81/357	62.344±16.0	7.5109E-06±1.8E-06
120426090	5	0.975:1.113	SBPL	0.1378 ± 0.0345	−0.484 ± 0.164	−2.271 ± 0.136	120.40 ± 29.45	65.54 ± 11.40	373.06/356	47.844±11.0	6.7033E-06±1.4E-06
120426090	6	1.113:1.236	COMP	0.7735 ± 0.2130	−0.633 ± 0.078	-	160.30 ± 9.53	-	378.42/357	110.16±22.0	1.3327E-05±2.5E-06
120426090	7	1.236:1.366	COMP	1.0080 ± 0.3020	−0.519 ± 0.084	-	148.80 ± 8.45	-	285.01/357	118.92±25.0	1.4062E-05±2.8E-06
120426090	8	1.366:1.496	COMP	0.6545 ± 0.2000	−0.614 ± 0.081	-	161.00 ± 10.10	-	328.93/357	91.338±21.0	1.1150E-05±2.3E-06
120426090	9	1.496:1.636	COMP	0.9192 ± 0.3620	−0.506 ± 0.089	-	123.70 ± 6.02	-	344.78/357	92.797±29.0	9.5469E-06±2.9E-06
120426090	10	1.636:1.796	COMP	0.6313 ± 0.2440	−0.560 ± 0.089	-	133.40 ± 7.33	-	371.75/357	72.395±22.0	7.7838E-06±2.3E-06
120426090	11	1.796:1.952	PL	0.0195 ± 0.0067	−1.557 ± 0.027	-	-	-	583.39/358	11.658±4.1	1.7033E-06±5.8E-07
120426090	12	1.952:2.124	SBPL	0.0974 ± 0.0369	−0.566 ± 0.175	−2.548 ± 0.170	83.34 ± 16.13	59.31 ± 10.40	332.68/356	40.739±15.0	4.3568E-06±1.5E-06
120426090	13	2.124:2.339	none	-	-	-	-	-	-	-	-
120426090	14	2.339:2.703	PL	0.0238 ± 0.0081	−1.870 ± 0.031	-	-	-	601.74/358	19.885±7.0	1.7825E-06±6.1E-07
120426090	15	2.703:4.233	none	-	-	-	-	-	-	-	-
120426090	16	4.233:10.240	PL	0.0076 ± 0.0028	−2.054 ± 0.088	-	-	-	416.98/358	8.0932±3.5	5.6293E-07±2.1E-07
120526303	1	-1.024:6.385	COMP	0.0280 ± 0.0026	−0.578 ± 0.085	-	530.30 ± 42.80	-	270.93/240	7.5835±0.59	2.2218E-06±9.7E-08
120526303	2	6.385:11.512	COMP	0.0248 ± 0.0020	−0.847 ± 0.064	-	986.90 ± 112.00	-	284.15/240	8.9648±0.70	2.7318E-06±1.2E-07
120526303	3	11.512:16.215	COMP	0.0257 ± 0.0019	−0.603 ± 0.071	-	969.40 ± 79.50	-	271.39/240	8.9792±0.62	3.3976E-06±1.2E-07
120526303	4	16.215:20.014	COMP	0.0283 ± 0.0022	−0.919 ± 0.055	-	1313.00 ± 146.00	-	260.07/240	10.978±0.87	3.3377E-06±1.4E-07
120526303	5	20.014:25.264	COMP	0.0260 ± 0.0021	−0.749 ± 0.071	-	857.90 ± 86.50	-	212.97/240	8.8708±0.68	2.8332E-06±1.2E-07
120526303	6	25.264:29.294	COMP	0.0297 ± 0.0023	−0.766 ± 0.065	-	989.40 ± 96.00	-	276.86/240	10.560±0.79	3.4839E-06±1.4E-07
120526303	7	29.294:33.708	COMP	0.0306 ± 0.0026	−0.710 ± 0.074	-	752.20 ± 71.30	-	290.57/240	9.9273±0.77	3.1201E-06±1.3E-07
120526303	8	33.708:37.347	COMP	0.0317 ± 0.0031	−1.022 ± 0.063	-	801.10 ± 120.00	-	276.97/240	11.762±1.0	2.8101E-06±1.5E-07
120526303	9	37.347:41.384	COMP	0.0312 ± 0.0032	−0.863 ± 0.074	-	641.30 ± 77.90	-	251.77/240	10.148±0.90	2.6126E-06±1.4E-07
120526303	10	41.384:45.460	COMP	0.0419 ± 0.0054	−0.760 ± 0.084	-	408.40 ± 41.00	-	232.58/240	11.031±1.0	2.4452E-06±1.5E-07
120526303	11	45.460:66.560	PL	0.0046 ± 0.0009	−1.752 ± 0.059	-	-	-	354.88/241	3.3330±0.83	3.5726E-07±6.8E-08
120624933	1	-270.340:-245.764	COMP	0.0049 ± 0.0004	−1.030 ± 0.024	-	3320.00 ± 490.00	-	766.42/478	2.1178±0.15	6.4160E-07±4.1E-08
120624933	2	-245.764:-229.380	COMP	0.0108 ± 0.0014	−0.981 ± 0.041	-	514.00 ± 59.40	-	692.97/478	3.5540±0.35	7.4840E-07±6.6E-08
120624933	3	-229.380:-221.187	COMP	0.0135 ± 0.0024	−0.949 ± 0.057	-	415.90 ± 55.50	-	553.06/478	4.0675±0.56	7.9379E-07±9.8E-08
120624933	4	-221.187:-167.939	PL	0.0015 ± 0.0002	−1.372 ± 0.019	-	-	-	1342.3/479	0.77190±0.11	1.5194E-07±1.9E-08
120624933	5	-167.939:-114.690	COMP	0.0040 ± 0.0006	−0.962 ± 0.046	-	622.00 ± 90.20	-	1643.9/478	1.3500±0.16	3.1339E-07±3.3E-08
120624933	6	-114.690:-106.498	COMP	0.0135 ± 0.0022	−0.891 ± 0.058	-	454.30 ± 59.20	-	672.88/478	4.0092±0.50	8.5721E-07±9.3E-08
120624933	7	-106.498:-102.402	COMP	0.0194 ± 0.0026	−0.817 ± 0.051	-	542.10 ± 62.70	-	590.37/478	5.8720±0.60	1.4569E-06±1.3E-07
120624933	8	-102.402:-98.306	COMP	0.0253 ± 0.0034	−0.734 ± 0.052	-	441.50 ± 40.30	-	664.01/478	6.7591±0.66	1.5976E-06±1.3E-07
120624933	9	-98.306:-94.209	COMP	0.0269 ± 0.0028	−0.721 ± 0.046	-	564.60 ± 51.20	-	561.26/478	7.9057±0.59	2.1606E-06±1.3E-07
120624933	10	-94.209:-90.113	COMP	0.0257 ± 0.0029	−0.789 ± 0.047	-	544.50 ± 55.30	-	581.57/478	7.6709±0.63	1.9504E-06±1.3E-07
120624933	11	-90.113:-86.017	COMP	0.0278 ± 0.0025	−0.663 ± 0.043	-	631.40 ± 52.50	-	552.56/478	8.3495±0.53	2.5219E-06±1.3E-07
120624933	12	-86.017:-81.921	COMP	0.0267 ± 0.0018	−0.734 ± 0.034	-	958.60 ± 82.10	-	510.97/478	9.3718±0.49	3.1530E-06±1.3E-07
120624933	13	-81.921:-77.825	COMP	0.0252 ± 0.0019	−0.606 ± 0.041	-	818.50 ± 66.10	-	578.81/478	8.2997±0.45	2.9420E-06±1.3E-07
120624933	14	-77.825:-73.729	COMP	0.0175 ± 0.0016	−0.766 ± 0.044	-	988.50 ± 122.00	-	528.81/478	6.2424±0.45	2.0605E-06±1.2E-07
120624933	15	-73.729:-65.537	COMP	0.0137 ± 0.0014	−0.891 ± 0.041	-	799.40 ± 103.00	-	687.66/478	4.8025±0.38	1.3101E-06±8.7E-08
120624933	16	-65.537:-40.961	PL	0.0009 ± 0.0003	−1.364 ± 0.029	-	-	-	947.67/479	0.48755±0.14	9.7197E-08±2.5E-08

Continued on next page

Table A.1 – continued from previous page

GRB name	spectrum	T_{start}:T_{stop} (s)	BEST model	A (ph s^{-1} cm^{-2} keV^{-1})	α	β	E_p (keV)	E_b (keV)	CSTAT/dof	photon flux (ph s^{-1} cm^{-2})	energy flux (erg s^{-1} cm^{-2})
(1)	(2)	(3)	(4)	(5)	(6)	(7)	(8)	(9)	(10)	(11)	(12)
120624933	17	-4.096:9.216	BAND	0.0115 ± 0.0013	-0.877 ± 0.052	-1.937 ± 0.110	681.60 ± 120.00	323.64 ± 59.39	572.89/477	3.8515±0.29	1.0102E-06±6.7E-08
120624933	18	9.216:12.288	COMP	0.0328 ± 0.0029	-0.791 ± 0.037	-	675.20 ± 61.00	-	512.31/478	10.549±0.69	2.9565E-06±1.6E-07
120624933	19	12.288:15.360	COMP	0.0366 ± 0.0040	-1.000 ± 0.036	-	517.90 ± 54.20	-	498.85/478	12.202±1.0	2.5347E-06±1.8E-07
120624933	20	15.360:48.129	COMP	0.0054 ± 0.0012	-0.999 ± 0.071	-	420.30 ± 75.60	-	716.52/478	1.6965±0.28	3.1993E-07±4.6E-08
120707800	1	-3.072:14.407	BAND	0.0658 ± 0.0132	-0.710 ± 0.112	-2.100 ± 0.070	139.60 ± 14.70	79.08 ± 8.18	603.08/357	9.9641±0.79	1.4064E-06±8.8E-08
120707800	2	14.407:20.869	COMP	0.0549 ± 0.0099	-1.398 ± 0.059	-	167.60 ± 16.40	-	523.71/358	21.655±2.6	2.0328E-06±2.0E-07
120707800	3	20.869:23.861	COMP	0.0588 ± 0.0109	-1.271 ± 0.067	-	207.70 ± 22.30	-	447.79/358	20.510±2.6	2.2571E-06±2.3E-07
120707800	4	23.861:26.476	COMP	0.0676 ± 0.0124	-1.325 ± 0.065	-	202.30 ± 22.10	-	399.47/358	25.113±3.1	2.6560E-06±2.7E-07
120707800	5	26.476:27.245	BAND	0.2871 ± 0.0615	-0.782 ± 0.112	-2.400 ± 0.118	209.30 ± 25.10	142.64 ± 18.31	386.21/357	57.423±5.2	8.9138E-06±6.3E-07
120707800	6	27.245:28.225	COMP	0.1584 ± 0.0238	-1.052 ± 0.065	-	237.00 ± 18.70	-	408.1/358	44.056±4.5	5.8465E-06±4.6E-07
120707800	7	28.225:29.105	COMP	0.1970 ± 0.0370	-0.888 ± 0.078	-	196.20 ± 13.90	-	398.78/358	42.266±5.0	5.3776E-06±5.2E-07
120707800	8	29.105:29.682	COMP	0.2502 ± 0.0360	-1.102 ± 0.062	-	239.00 ± 18.90	-	395.41/358	73.853±7.4	9.5823E-06±7.2E-07
120707800	9	29.682:30.360	COMP	0.2656 ± 0.0394	-1.061 ± 0.064	-	215.90 ± 15.60	-	447.01/358	72.374±7.2	9.0430E-06±6.8E-07
120707800	10	30.360:31.395	SBPL	0.1128 ± 0.0144	-1.009 ± 0.164	-2.273 ± 0.112	121.35 ± 30.90	76.71 ± 17.60	412.71/357	48.927±5.8	5.8138E-06±5.4E-07
120707800	11	31.395:34.057	COMP	0.1062 ± 0.0215	-1.245 ± 0.073	-	158.10 ± 13.10	-	431.16/358	33.258±4.3	3.2181E-06±3.4E-07
120707800	12	34.057:63.488	COMP	0.0169 ± 0.0036	-1.756 ± 0.061	-	105.70 ± 14.80	-	936.22/358	10.869±1.6	7.9203E-07±1.0E-07
120711115	1	-2.048:5.120	COMP	0.0070 ± 0.0022	-0.892 ± 0.166	-	563.00 ± 203.00	-	401.33/359	2.2298±0.52	5.2853E-07±9.4E-08
120711115	2	56.320:65.742	COMP	0.0106 ± 0.0009	-0.934 ± 0.045	-	1820.00 ± 250.00	-	500.01/359	4.3283±0.35	1.3751E-06±7.9E-08
120711115	3	65.742:67.273	COMP	0.0420 ± 0.0031	-0.886 ± 0.042	-	1335.00 ± 160.00	-	386.38/359	16.235±1.1	5.1358E-06±2.5E-07
120711115	4	67.273:68.382	COMP	0.0421 ± 0.0031	-0.931 ± 0.036	-	1785.00 ± 209.00	-	356.88/359	17.096±1.2	5.4351E-06±2.9E-07
120711115	5	68.382:69.465	COMP	0.0552 ± 0.0039	-0.929 ± 0.037	-	1479.00 ± 168.00	-	376.93/359	21.841±1.4	6.7298E-06±3.2E-07
120711115	6	69.465:70.467	COMP	0.0551 ± 0.0045	-0.894 ± 0.045	-	1148.00 ± 146.00	-	406.8/359	20.783±1.5	6.2874E-06±3.3E-07
120711115	7	70.467:71.487	COMP	0.0516 ± 0.0035	-0.968 ± 0.034	-	1850.00 ± 191.00	-	378.32/359	21.183±1.4	6.4807E-06±3.1E-07
120711115	8	71.487:72.842	COMP	0.0488 ± 0.0039	-1.035 ± 0.039	-	1289.00 ± 190.00	-	379.96/359	19.591±1.4	5.1945E-06±2.8E-07
120711115	9	72.842:74.417	COMP	0.0459 ± 0.0045	-0.926 ± 0.051	-	785.90 ± 108.00	-	395.56/359	16.214±1.3	4.2473E-06±2.5E-07
120711115	10	74.417:75.673	COMP	0.0594 ± 0.0059	-1.003 ± 0.049	-	738.30 ± 105.00	-	408.4/359	21.472±1.7	5.0957E-06±3.0E-07
120711115	11	75.673:79.045	COMP	0.0252 ± 0.0030	-1.101 ± 0.053	-	834.80 ± 172.00	-	445.19/359	9.8485±0.94	2.1838E-06±1.6E-07
120711115	12	79.045:81.807	COMP	0.0246 ± 0.0020	-1.076 ± 0.037	-	1723.00 ± 269.00	-	408.16/359	10.316±0.83	2.7362E-06±1.7E-07
120711115	13	81.807:85.349	COMP	0.0263 ± 0.0030	-0.994 ± 0.056	-	728.90 ± 121.00	-	410.2/359	9.4315±0.85	2.2488E-06±1.5E-07
120711115	14	85.349:86.744	COMP	0.0423 ± 0.0042	-0.882 ± 0.052	-	885.30 ± 126.00	-	392.54/359	15.082±1.2	4.2901E-06±2.6E-07
120711115	15	86.744:88.189	COMP	0.0427 ± 0.0036	-1.030 ± 0.041	-	1290.00 ± 202.00	-	407.98/359	17.087±1.3	4.5599E-06±2.6E-07
120711115	16	88.189:89.518	COMP	0.0430 ± 0.0033	-0.917 ± 0.040	-	1344.00 ± 172.00	-	336.1/359	16.746±1.2	5.1260E-06±2.7E-07
120711115	17	89.518:90.699	COMP	0.0467 ± 0.0045	-0.871 ± 0.051	-	921.80 ± 128.00	-	357.75/359	16.757±1.3	4.8830E-06±2.9E-07
120711115	18	90.699:91.820	COMP	0.0586 ± 0.0057	-0.942 ± 0.049	-	795.70 ± 108.00	-	370.95/359	20.885±1.6	5.4063E-06±3.1E-07
120711115	19	91.820:92.936	COMP	0.0475 ± 0.0036	-0.966 ± 0.038	-	1450.00 ± 193.00	-	339.61/359	18.907±1.3	5.5629E-06±3.0E-07
120711115	20	92.936:93.925	COMP	0.0541 ± 0.0039	-1.063 ± 0.033	-	1808.00 ± 221.00	-	354.34/359	22.716±1.6	6.1680E-06±3.2E-07
120711115	21	93.925:94.917	COMP	0.0552 ± 0.0037	-0.980 ± 0.034	-	1821.00 ± 183.00	-	376.55/359	22.678±1.5	6.8236E-06±3.2E-07
120711115	22	94.917:95.583	SBPL	0.0584 ± 0.0043	-0.807 ± 0.047	-2.059 ± 0.077	1394.81 ± 506.62	552.90 ± 92.00	370.03/358	24.877±1.6	8.9817E-06±4.1E-07
120711115	23	95.583:96.390	BAND	0.0640 ± 0.0052	-0.938 ± 0.046	-2.272 ± 0.147	1445.00 ± 266.00	903.80 ± 175.18	385.54/358	25.291±1.8	7.6776E-06±3.9E-07
120711115	24	96.390:97.631	COMP	0.0488 ± 0.0034	-0.896 ± 0.038	-	1490.00 ± 163.00	-	404.5/359	19.228±1.3	6.1521E-06±2.9E-07
120711115	25	97.631:98.719	COMP	0.0486 ± 0.0034	-0.910 ± 0.036	-	1713.00 ± 180.00	-	362.07/359	19.565±1.3	6.3268E-06±3.0E-07
120711115	26	98.719:99.870	COMP	0.0449 ± 0.0031	-1.004 ± 0.033	-	2122.00 ± 217.00	-	355.42/359	18.796±1.3	5.6107E-06±2.8E-07
120711115	27	99.870:101.288	COMP	0.0394 ± 0.0028	-0.962 ± 0.035	-	1805.00 ± 195.00	-	352.56/359	16.110±1.1	4.9460E-06±2.5E-07

Continued on next page

Table A.1 – continued from previous page

GRB name	spectrum	T_{start}:T_{stop} (s)	BEST model	A (ph s^{-1} cm^{-2} keV^{-1})	α	β	E_p (keV)	E_b (keV)	CSTAT/dof	photon flux (ph s^{-1} cm^{-2})	energy flux (erg s^{-1} cm^{-2})
(1)	(2)	(3)	(4)	(5)	(6)	(7)	(8)	(9)	(10)	(11)	(12)
120711115	28	101.288:102.122	BAND	0.0618 ± 0.0048	-0.807 ± 0.049	-2.414 ± 0.163	1263.00 ± 183.00	849.68 ± 137.94	366.67/358	23.403±1.5	7.9374E-06±3.7E-07
120711115	29	102.122:103.323	COMP	0.0469 ± 0.0041	-0.965 ± 0.045	-	1117.00 ± 167.00	-	354.33/359	17.990±1.4	5.0084E-06±2.9E-07
120711115	30	103.323:104.716	COMP	0.0488 ± 0.0053	-1.023 ± 0.051	-	767.30 ± 123.00	-	415.34/359	17.988±1.6	4.2310E-06±2.8E-07
120711115	31	104.716:109.230	COMP	0.0205 ± 0.0037	-1.275 ± 0.061	-	535.10 ± 139.00	-	471.01/359	8.5653±1.2	1.3835E-06±1.5E-07
120711115	32	109.230:119.808	PL	0.0053 ± 0.0013	-1.681 ± 0.060	-	-	-	518.13/360	3.6005±1.0	4.2991E-07±9.2E-08

Table A.2: $E_{\rm p}$ evolutionary trends (Ch. 2). Column (1) lists the GRB names. Column (2) lists the numbers of spectra with $E_{\rm p}$. Columns (3), (7), and (11) list the Spearman's Rank Correlation Coefficients between $E_{\rm p}$ and the photon flux and the 90%, 95%, and 99% confidence intervals, respectively. Columns (4), (8), and (12) list the Spearman's Rank Correlation Coefficients between $E_{\rm p}$ and the energy flux and the 90%, 95%, and 99% confidence intervals, respectively. Columns (5), (9), and (13) list the Spearman's Rank Correlation Coefficients between $E_{\rm p}$ and the time and the 90%, 95%, and 99% confidence intervals, respectively. Columns (6), (10), and (14) list the trends as determined by the computer for the 90%, 95%, and 99% confidence intervals, respectively. Column (15) lists the trends as determined by human eyes.

GRB name	N	$\rho_{\rm ph}$(90%)	$\rho_{\rm en}$(90%)	$\rho_{\rm t}$(90%)	trend(90%)	$\rho_{\rm ph}$(95%)	$\rho_{\rm en}$(95%)	$\rho_{\rm t}$(95%)	trend(95%)	$\rho_{\rm ph}$(99%)	$\rho_{\rm en}$(99%)	$\rho_{\rm t}$(99%)	trend(99%)	trend(by eyes)
(1)	(2)	(3)	(4)	(5)	(6)	(7)	(8)	(9)	(10)	(11)	(12)	(13)	(14)	(15)
080817161	15	$0.354^{+0.335}_{-0.459}$	$0.546^{+0.250}_{-0.409}$	$-0.700^{+0.327}_{-0.172}$	undeter.	$0.354^{+0.379}_{-0.547}$	$0.546^{+0.281}_{-0.499}$	$-0.700^{+0.407}_{-0.192}$	undeter.	$0.354^{+0.451}_{-0.711}$	$0.546^{+0.329}_{-0.676}$	$-0.700^{+0.577}_{-0.223}$	h.t.s.	h.t.s.+in.track.
080825593	12	$0.322^{+0.386}_{-0.533}$	$0.538^{+0.279}_{-0.485}$	$-0.832^{+0.263}_{-0.108}$	undeter.	$0.322^{+0.434}_{-0.631}$	$0.538^{+0.311}_{-0.590}$	$-0.832^{+0.338}_{-0.119}$	h.t.s.	$0.322^{+0.509}_{-0.803}$	$0.538^{+0.359}_{-0.789}$	$-0.832^{+0.508}_{-0.135}$	h.t.s.	h.t.s.
080916009	21	$0.168^{+0.338}_{-0.383}$	$0.249^{+0.317}_{-0.382}$	$-0.288^{+0.379}_{-0.306}$	undeter.	$0.168^{+0.391}_{-0.452}$	$0.249^{+0.366}_{-0.454}$	$-0.288^{+0.452}_{-0.352}$	undeter.	$0.168^{+0.483}_{-0.579}$	$0.249^{+0.448}_{-0.588}$	$-0.288^{+0.589}_{-0.430}$	undeter.	undeter.
081009140	0	-	-	-	-	-	-	-	-	-	-	-	-	-
081124060	0	-	-	-	-	-	-	-	-	-	-	-	-	-
081125496	4	-	-	-	-	-	-	-	-	-	-	-	-	-
081207680	9	$0.683^{+0.223}_{-0.521}$	$0.717^{+0.201}_{-0.491}$	$0.367^{+0.418}_{-0.646}$	in.track.	$0.683^{+0.244}_{-0.648}$	$0.717^{+0.219}_{-0.616}$	$0.367^{+0.462}_{-0.760}$	in.track.	$0.683^{+0.272}_{-0.896}$	$0.717^{+0.244}_{-0.866}$	$0.367^{+0.526}_{-0.949}$	undeter.	in.track.
081215784	16	$0.453^{+0.284}_{-0.421}$	$0.538^{+0.247}_{-0.394}$	$-0.650^{+0.341}_{-0.193}$	undeter.	$0.453^{+0.322}_{-0.508}$	$0.538^{+0.278}_{-0.480}$	$-0.650^{+0.422}_{-0.217}$	undeter.	$0.453^{+0.381}_{-0.675}$	$0.538^{+0.328}_{-0.650}$	$-0.650^{+0.589}_{-0.253}$	h.t.s.	h.t.s.+in.track.
081221681	0	-	-	-	-	-	-	-	-	-	-	-	-	-
081224887	11	$0.455^{+0.336}_{-0.545}$	$0.873^{+0.086}_{-0.230}$	$-0.991^{+0.020}_{-0.006}$	undeter.	$0.455^{+0.374}_{-0.654}$	$0.873^{+0.094}_{-0.300}$	$-0.991^{+0.027}_{-0.007}$	undeter.	$0.455^{+0.431}_{-0.851}$	$0.873^{+0.106}_{-0.464}$	$-0.991^{+0.046}_{-0.008}$	undeter.	h.t.s.
090131090	4	-	-	-	-	-	-	-	-	-	-	-	-	-
090328401	8	$-0.238^{+0.695}_{-0.514}$	$0.214^{+0.527}_{-0.690}$	$-0.714^{+0.555}_{-0.212}$	h.t.s.	$-0.238^{+0.799}_{-0.569}$	$0.214^{+0.584}_{-0.792}$	$-0.714^{+0.695}_{-0.230}$	h.t.s.	$-0.238^{+0.959}_{-0.646}$	$0.214^{+0.664}_{-0.947}$	$-0.714^{+0.965}_{-0.253}$	undeter.	undeter.
090424592	32	$0.415^{+0.219}_{-0.280}$	$0.725^{+0.116}_{-0.179}$	$0.078^{+0.288}_{-0.301}$	in.track.	$0.415^{+0.252}_{-0.338}$	$0.725^{+0.132}_{-0.222}$	$0.078^{+0.337}_{-0.356}$	in.track.	$0.415^{+0.311}_{-0.452}$	$0.725^{+0.160}_{-0.312}$	$0.078^{+0.427}_{-0.458}$	in.track.	in.track.
090528516	9	$0.200^{+0.504}_{-0.637}$	$0.450^{+0.370}_{-0.635}$	$-0.933^{+0.167}_{-0.049}$	h.t.s.	$0.200^{+0.563}_{-0.735}$	$0.450^{+0.408}_{-0.755}$	$-0.933^{+0.225}_{-0.053}$	h.t.s.	$0.200^{+0.649}_{-0.890}$	$0.450^{+0.461}_{-0.963}$	$-0.933^{+0.374}_{-0.058}$	h.t.s.	h.t.s.
090530760	5	-	-	-	-	-	-	-	-	-	-	-	-	-
090618353	69	$0.639^{+0.105}_{-0.136}$	$0.812^{+0.058}_{-0.081}$	$-0.773^{+0.095}_{-0.070}$	undeter.	$0.639^{+0.122}_{-0.165}$	$0.812^{+0.068}_{-0.100}$	$-0.773^{+0.117}_{-0.081}$	undeter.	$0.639^{+0.152}_{-0.226}$	$0.812^{+0.083}_{-0.139}$	$-0.773^{+0.162}_{-0.100}$	undeter.	h.t.s.(1st)+in.track.(2nd)
090626189	14	$-0.288^{+0.485}_{-0.372}$	$0.046^{+0.448}_{-0.468}$	$0.332^{+0.354}_{-0.482}$	undeter.	$-0.288^{+0.574}_{-0.422}$	$0.046^{+0.517}_{-0.543}$	$0.332^{+0.401}_{-0.573}$	undeter.	$-0.288^{+0.734}_{-0.503}$	$0.046^{+0.630}_{-0.669}$	$0.332^{+0.476}_{-0.738}$	undeter.	undeter.
090718762	8	$-0.095^{+0.660}_{-0.586}$	$-0.143^{+0.674}_{-0.563}$	$-0.381^{+0.704}_{-0.432}$	undeter.	$-0.095^{+0.749}_{-0.654}$	$-0.143^{+0.768}_{-0.627}$	$-0.381^{+0.823}_{-0.475}$	undeter.	$-0.095^{+0.879}_{-0.752}$	$-0.143^{+0.908}_{-0.718}$	$-0.381^{+1.016}_{-0.533}$	undeter.	undeter.
090719063	20	$0.105^{+0.360}_{-0.390}$	$0.457^{+0.256}_{-0.363}$	$-0.450^{+0.365}_{-0.258}$	undeter.	$0.105^{+0.418}_{-0.459}$	$0.457^{+0.291}_{-0.439}$	$-0.450^{+0.441}_{-0.294}$	undeter.	$0.105^{+0.518}_{-0.582}$	$0.457^{+0.350}_{-0.587}$	$-0.450^{+0.589}_{-0.354}$	undeter.	h.t.s.+in.track.
090804940	2	-	-	-	-	-	-	-	-	-	-	-	-	-
090809978	9	$0.050^{+0.568}_{-0.602}$	$0.433^{+0.380}_{-0.638}$	$-0.950^{+0.129}_{-0.037}$	h.t.s.	$0.050^{+0.641}_{-0.685}$	$0.433^{+0.419}_{-0.757}$	$-0.950^{+0.175}_{-0.040}$	h.t.s.	$0.050^{+0.751}_{-0.812}$	$0.433^{+0.475}_{-0.961}$	$-0.950^{+0.297}_{-0.044}$	h.t.s.	h.t.s.
090820027	83	$0.391^{+0.144}_{-0.166}$	$0.523^{+0.121}_{-0.146}$	$-0.287^{+0.176}_{-0.159}$	in.track.	$0.391^{+0.169}_{-0.200}$	$0.523^{+0.141}_{-0.177}$	$-0.287^{+0.211}_{-0.186}$	in.track.	$0.391^{+0.214}_{-0.267}$	$0.523^{+0.178}_{-0.239}$	$-0.287^{+0.280}_{-0.238}$	in.track.	in.track.
090829672	32	$0.238^{+0.261}_{-0.301}$	$0.489^{+0.197}_{-0.264}$	$-0.257^{+0.300}_{-0.257}$	undeter.	$0.238^{+0.304}_{-0.359}$	$0.489^{+0.227}_{-0.320}$	$-0.257^{+0.358}_{-0.299}$	undeter.	$0.238^{+0.380}_{-0.469}$	$0.489^{+0.278}_{-0.432}$	$-0.257^{+0.469}_{-0.373}$	undeter.	h.t.s.+in.track.
090902462	93	$0.500^{+0.119}_{-0.141}$	$0.741^{+0.069}_{-0.089}$	$-0.636^{+0.115}_{-0.092}$	undeter.	$0.500^{+0.139}_{-0.170}$	$0.741^{+0.080}_{-0.108}$	$-0.636^{+0.139}_{-0.107}$	undeter.	$0.500^{+0.175}_{-0.229}$	$0.741^{+0.100}_{-0.149}$	$-0.636^{+0.190}_{-0.135}$	undeter.	in.track.
090926181	58	$-0.123^{+0.221}_{-0.209}$	$0.365^{+0.175}_{-0.205}$	$-0.654^{+0.146}_{-0.109}$	h.t.s.	$-0.123^{+0.263}_{-0.247}$	$0.365^{+0.205}_{-0.247}$	$-0.654^{+0.178}_{-0.126}$	h.t.s.	$-0.123^{+0.343}_{-0.316}$	$0.365^{+0.258}_{-0.330}$	$-0.654^{+0.244}_{-0.157}$	h.t.s.	h.t.s.+in.track.
091003191	12	$0.056^{+0.484}_{-0.512}$	$0.224^{+0.427}_{-0.534}$	$-0.483^{+0.505}_{-0.309}$	undeter.	$0.056^{+0.554}_{-0.591}$	$0.224^{+0.483}_{-0.626}$	$-0.483^{+0.609}_{-0.345}$	undeter.	$0.056^{+0.667}_{-0.721}$	$0.224^{+0.572}_{-0.782}$	$-0.483^{+0.803}_{-0.399}$	undeter.	h.t.s.(1st)+in.track.(2nd)
091010113	4	-	-	-	-	-	-	-	-	-	-	-	-	-
091120191	5	-	-	-	-	-	-	-	-	-	-	-	-	-
091127976	12	$0.154^{+0.453}_{-0.528}$	$0.350^{+0.373}_{-0.531}$	$0.434^{+0.333}_{-0.517}$	undeter.	$0.154^{+0.515}_{-0.615}$	$0.350^{+0.420}_{-0.630}$	$0.434^{+0.373}_{-0.620}$	undeter.	$0.154^{+0.613}_{-0.760}$	$0.350^{+0.491}_{-0.806}$	$0.434^{+0.434}_{-0.808}$	undeter.	undeter.
091128285	5	-	-	-	-	-	-	-	-	-	-	-	-	-

Continued on next page

Table A.2 – continued from previous page

GRB name	N	$\rho_{\rm ph}(90\%)$	$\rho_{\rm en}(90\%)$	$\rho_{\rm t}(90\%)$	trend(90%)	$\rho_{\rm ph}(95\%)$	$\rho_{\rm en}(95\%)$	$\rho_{\rm t}(95\%)$	trend(95%)	$\rho_{\rm ph}(99\%)$	$\rho_{\rm en}(99\%)$	$\rho_{\rm t}(99\%)$	trend(99%)	trend(by eyes)
(1)	(2)	(3)	(4)	(5)	(6)	(7)	(8)	(9)	(10)	(11)	(12)	(13)	(14)	(15)
100122616	2	-	-	-	-	-	-	-	-	-	-	-	-	-
100322045	19	$-0.263^{+0.404}_{-0.329}$	$0.672^{+0.169}_{-0.289}$	$0.668^{+0.171}_{-0.291}$	in.track.	$-0.263^{+0.480}_{-0.378}$	$0.672^{+0.191}_{-0.359}$	$0.668^{+0.193}_{-0.361}$	in.track.	$-0.263^{+0.621}_{-0.460}$	$0.672^{+0.225}_{-0.503}$	$0.668^{+0.228}_{-0.506}$	in.track.	in.track.(2nd)
100324172	9	$0.200^{+0.504}_{-0.637}$	$0.367^{+0.418}_{-0.646}$	$-0.883^{+0.267}_{-0.085}$	h.t.s.	$0.200^{+0.563}_{-0.735}$	$0.367^{+0.462}_{-0.760}$	$-0.883^{+0.353}_{-0.092}$	h.t.s.	$0.200^{+0.649}_{-0.890}$	$0.367^{+0.526}_{-0.949}$	$-0.883^{+0.556}_{-0.102}$	h.t.s.	h.t.s.
100414097	15	$-0.200^{+0.466}_{-0.390}$	$-0.025^{+0.447}_{-0.437}$	$-0.093^{+0.457}_{-0.421}$	undeter.	$-0.200^{+0.548}_{-0.446}$	$-0.025^{+0.519}_{-0.505}$	$-0.093^{+0.533}_{-0.485}$	undeter.	$-0.200^{+0.693}_{-0.538}$	$-0.025^{+0.641}_{-0.621}$	$-0.093^{+0.665}_{-0.591}$	undeter.	undeter.
100511035	3	-	-	-	-	-	-	-	-	-	-	-	-	-
100612726	4	-	-	-	-	-	-	-	-	-	-	-	-	-
100707032	25	$0.406^{+0.248}_{-0.326}$	$0.770^{+0.109}_{-0.185}$	$-0.936^{+0.061}_{-0.032}$	undeter.	$0.406^{+0.284}_{-0.393}$	$0.770^{+0.123}_{-0.231}$	$-0.936^{+0.078}_{-0.036}$	undeter.	$0.406^{+0.347}_{-0.524}$	$0.770^{+0.147}_{-0.331}$	$-0.936^{+0.116}_{-0.042}$	undeter.	h.t.s.
100719989	14	$0.332^{+0.354}_{-0.482}$	$0.499^{+0.280}_{-0.447}$	$-0.776^{+0.284}_{-0.135}$	h.t.s.	$0.332^{+0.401}_{-0.573}$	$0.499^{+0.315}_{-0.542}$	$-0.776^{+0.359}_{-0.150}$	h.t.s.	$0.332^{+0.476}_{-0.738}$	$0.499^{+0.369}_{-0.724}$	$-0.776^{+0.523}_{-0.172}$	h.t.s.	in.track.
100722096	1	-	-	-	-	-	-	-	-	-	-	-	-	-
100724029	47	$0.397^{+0.187}_{-0.227}$	$0.455^{+0.173}_{-0.217}$	$-0.245^{+0.243}_{-0.216}$	undeter.	$0.397^{+0.217}_{-0.273}$	$0.455^{+0.201}_{-0.262}$	$-0.245^{+0.290}_{-0.252}$	undeter.	$0.397^{+0.272}_{-0.365}$	$0.455^{+0.251}_{-0.353}$	$-0.245^{+0.382}_{-0.319}$	undeter.	in.track.
100728095	21	$0.474^{+0.244}_{-0.347}$	$0.741^{+0.131}_{-0.229}$	$-0.537^{+0.328}_{-0.219}$	undeter.	$0.474^{+0.278}_{-0.421}$	$0.741^{+0.147}_{-0.286}$	$-0.537^{+0.400}_{-0.249}$	undeter.	$0.474^{+0.334}_{-0.565}$	$0.741^{+0.174}_{-0.408}$	$-0.537^{+0.544}_{-0.299}$	in.track.	in.track.
100826957	21	$0.165^{+0.339}_{-0.383}$	$0.318^{+0.297}_{-0.376}$	$0.031^{+0.365}_{-0.373}$	undeter.	$0.165^{+0.392}_{-0.452}$	$0.318^{+0.341}_{-0.450}$	$0.031^{+0.426}_{-0.437}$	undeter.	$0.165^{+0.484}_{-0.579}$	$0.318^{+0.415}_{-0.589}$	$0.031^{+0.532}_{-0.551}$	undeter.	in.track.
100829876	5	-	-	-	-	-	-	-	-	-	-	-	-	-
100910818	5	-	-	-	-	-	-	-	-	-	-	-	-	-
100918863	26	$0.762^{+0.111}_{-0.185}$	$0.843^{+0.075}_{-0.133}$	$0.162^{+0.305}_{-0.340}$	in.track.	$0.762^{+0.125}_{-0.230}$	$0.843^{+0.085}_{-0.167}$	$0.162^{+0.355}_{-0.402}$	in.track.	$0.762^{+0.150}_{-0.329}$	$0.843^{+0.101}_{-0.242}$	$0.162^{+0.443}_{-0.519}$	in.track.	in.track.
101014175	43	$0.236^{+0.227}_{-0.256}$	$0.506^{+0.168}_{-0.217}$	$0.090^{+0.247}_{-0.258}$	in.track.	$0.236^{+0.265}_{-0.305}$	$0.506^{+0.194}_{-0.264}$	$0.090^{+0.290}_{-0.306}$	in.track.	$0.236^{+0.334}_{-0.401}$	$0.506^{+0.240}_{-0.357}$	$0.090^{+0.370}_{-0.397}$	in.track.	h.t.s.+in.track.
101023951	10	$0.709^{+0.197}_{-0.451}$	$0.818^{+0.126}_{-0.333}$	$-0.285^{+0.602}_{-0.439}$	in.track.	$0.709^{+0.216}_{-0.566}$	$0.818^{+0.137}_{-0.429}$	$-0.285^{+0.705}_{-0.491}$	in.track.	$0.709^{+0.243}_{-0.797}$	$0.818^{+0.154}_{-0.642}$	$-0.285^{+0.877}_{-0.568}$	in.track.	in.track.
101123952	39	$0.369^{+0.210}_{-0.256}$	$0.496^{+0.178}_{-0.233}$	$-0.521^{+0.226}_{-0.171}$	h.t.s.	$0.369^{+0.244}_{-0.308}$	$0.496^{+0.206}_{-0.282}$	$-0.521^{+0.275}_{-0.197}$	h.t.s.	$0.369^{+0.304}_{-0.411}$	$0.496^{+0.254}_{-0.382}$	$-0.521^{+0.373}_{-0.243}$	h.t.s.	h.t.s.+in.track.
101126198	11	$-0.536^{+0.519}_{-0.291}$	$-0.273^{+0.566}_{-0.424}$	$-0.264^{+0.566}_{-0.428}$	undeter.	$-0.536^{+0.630}_{-0.323}$	$-0.273^{+0.664}_{-0.477}$	$-0.264^{+0.663}_{-0.482}$	undeter.	$-0.536^{+0.838}_{-0.370}$	$-0.273^{+0.831}_{-0.558}$	$-0.264^{+0.829}_{-0.564}$	undeter.	undeter.
101231067	4	-	-	-	-	-	-	-	-	-	-	-	-	-
110213220	0	-	-	-	-	-	-	-	-	-	-	-	-	-
110301214	27	$-0.042^{+0.328}_{-0.319}$	$0.031^{+0.320}_{-0.327}$	$-0.315^{+0.325}_{-0.265}$	undeter.	$-0.042^{+0.385}_{-0.373}$	$0.031^{+0.375}_{-0.384}$	$-0.315^{+0.389}_{-0.306}$	undeter.	$-0.042^{+0.491}_{-0.472}$	$0.031^{+0.475}_{-0.489}$	$-0.315^{+0.512}_{-0.377}$	undeter.	h.t.s.+in.track.
110407998	5	-	-	-	-	-	-	-	-	-	-	-	-	-
110428388	5	-	-	-	-	-	-	-	-	-	-	-	-	-
110622158	14	$-0.086^{+0.474}_{-0.438}$	$-0.042^{+0.467}_{-0.450}$	$-0.459^{+0.459}_{-0.299}$	undeter.	$-0.086^{+0.552}_{-0.504}$	$-0.042^{+0.542}_{-0.518}$	$-0.459^{+0.554}_{-0.337}$	undeter.	$-0.086^{+0.684}_{-0.612}$	$-0.042^{+0.668}_{-0.632}$	$-0.459^{+0.732}_{-0.395}$	undeter.	undeter.
110625881	38	$-0.007^{+0.272}_{-0.271}$	$0.311^{+0.226}_{-0.267}$	$-0.439^{+0.248}_{-0.196}$	undeter.	$-0.007^{+0.320}_{-0.319}$	$0.311^{+0.263}_{-0.321}$	$-0.439^{+0.300}_{-0.226}$	undeter.	$-0.007^{+0.411}_{-0.408}$	$0.311^{+0.328}_{-0.424}$	$-0.439^{+0.403}_{-0.280}$	undeter.	in.track.
110717319	13	$0.363^{+0.354}_{-0.502}$	$0.615^{+0.229}_{-0.421}$	$-0.011^{+0.480}_{-0.475}$	in.track.	$0.363^{+0.399}_{-0.598}$	$0.615^{+0.256}_{-0.518}$	$-0.011^{+0.554}_{-0.548}$	in.track.	$0.363^{+0.469}_{-0.772}$	$0.615^{+0.295}_{-0.712}$	$-0.011^{+0.677}_{-0.667}$	undeter.	in.track.
110721200	12	$-0.538^{+0.485}_{-0.279}$	$0.049^{+0.486}_{-0.511}$	$-0.490^{+0.502}_{-0.305}$	undeter.	$-0.538^{+0.590}_{-0.311}$	$0.049^{+0.557}_{-0.589}$	$-0.490^{+0.607}_{-0.341}$	undeter.	$-0.538^{+0.789}_{-0.359}$	$0.049^{+0.671}_{-0.718}$	$-0.490^{+0.802}_{-0.394}$	undeter.	h.t.s.
110729142	7	$0.571^{+0.329}_{-0.743}$	$0.607^{+0.303}_{-0.725}$	$-0.107^{+0.721}_{-0.623}$	undeter.	$0.571^{+0.355}_{-0.890}$	$0.607^{+0.326}_{-0.876}$	$-0.107^{+0.810}_{-0.689}$	undeter.	$0.571^{+0.388}_{-1.135}$	$0.607^{+0.356}_{-1.132}$	$-0.107^{+0.935}_{-0.777}$	undeter.	undeter.
110731465	7	$-0.036^{+0.692}_{-0.660}$	$0.643^{+0.277}_{-0.702}$	$0.929^{+0.057}_{-0.251}$	undeter.	$-0.036^{+0.773}_{-0.732}$	$0.643^{+0.298}_{-0.856}$	$0.929^{+0.061}_{-0.345}$	undeter.	$-0.036^{+0.884}_{-0.832}$	$0.643^{+0.325}_{-1.124}$	$0.929^{+0.066}_{-0.583}$	undeter.	undeter.
110817191	4	-	-	-	-	-	-	-	-	-	-	-	-	-
110825102	20	$0.087^{+0.364}_{-0.389}$	$0.720^{+0.143}_{-0.251}$	$0.421^{+0.269}_{-0.371}$	in.track.	$0.087^{+0.423}_{-0.457}$	$0.720^{+0.161}_{-0.313}$	$0.421^{+0.307}_{-0.447}$	in.track.	$0.087^{+0.525}_{-0.578}$	$0.720^{+0.191}_{-0.444}$	$0.421^{+0.370}_{-0.595}$	in.track.	in.track.
110903009	2	-	-	-	-	-	-	-	-	-	-	-	-	-
110920546	17	$0.583^{+0.220}_{-0.359}$	$0.848^{+0.086}_{-0.179}$	$-0.968^{+0.043}_{-0.019}$	undeter.	$0.583^{+0.248}_{-0.441}$	$0.848^{+0.096}_{-0.228}$	$-0.968^{+0.056}_{-0.021}$	undeter.	$0.583^{+0.292}_{-0.604}$	$0.848^{+0.111}_{-0.339}$	$-0.968^{+0.089}_{-0.024}$	undeter.	h.t.s.
110921912	11	$-0.187^{+0.560}_{-0.460}$	$-0.027^{+0.531}_{-0.516}$	$-0.437^{+0.550}_{-0.345}$	undeter.	$-0.187^{+0.652}_{-0.521}$	$-0.027^{+0.609}_{-0.590}$	$-0.437^{+0.658}_{-0.384}$	undeter.	$-0.187^{+0.805}_{-0.613}$	$-0.027^{+0.735}_{-0.707}$	$-0.437^{+0.852}_{-0.443}$	undeter.	undeter.
111003465	6	$0.086^{+0.690}_{-0.784}$	$0.714^{+0.237}_{-0.768}$	$-0.829^{+0.599}_{-0.144}$	h.t.s.	$0.086^{+0.753}_{-0.866}$	$0.714^{+0.252}_{-0.946}$	$-0.829^{+0.777}_{-0.152}$	h.t.s.	$0.086^{+0.832}_{-0.971}$	$0.714^{+0.269}_{-1.245}$	$-0.829^{+1.123}_{-0.162}$	undeter.	h.t.s.+in.track.
111127810	0	-	-	-	-	-	-	-	-	-	-	-	-	-
111216389	9	$-0.167^{+0.631}_{-0.519}$	$0.483^{+0.350}_{-0.627}$	$-0.600^{+0.578}_{-0.277}$	h.t.s.	$-0.167^{+0.726}_{-0.581}$	$0.483^{+0.385}_{-0.750}$	$-0.600^{+0.707}_{-0.304}$	undeter.	$-0.167^{+0.875}_{-0.673}$	$0.483^{+0.435}_{-0.964}$	$-0.600^{+0.944}_{-0.341}$	undeter.	in.track.
111220486	9	$0.483^{+0.350}_{-0.627}$	$0.650^{+0.245}_{-0.547}$	$-0.317^{+0.647}_{-0.445}$	in.track.	$0.483^{+0.385}_{-0.750}$	$0.650^{+0.268}_{-0.675}$	$-0.317^{+0.757}_{-0.494}$	undeter.	$0.483^{+0.435}_{-0.964}$	$0.650^{+0.299}_{-0.919}$	$-0.317^{+0.936}_{-0.564}$	undeter.	in.track.
111228657	1	-	-	-	-	-	-	-	-	-	-	-	-	-
120119170	15	$0.475^{+0.283}_{-0.433}$	$0.743^{+0.149}_{-0.295}$	$-0.450^{+0.440}_{-0.294}$	in.track.	$0.475^{+0.319}_{-0.524}$	$0.743^{+0.166}_{-0.371}$	$-0.450^{+0.531}_{-0.332}$	in.track.	$0.475^{+0.376}_{-0.698}$	$0.743^{+0.193}_{-0.533}$	$-0.450^{+0.703}_{-0.392}$	in.track.	in.track.
120129580	29	$0.390^{+0.236}_{-0.301}$	$0.600^{+0.168}_{-0.246}$	$-0.083^{+0.318}_{-0.302}$	in.track.	$0.390^{+0.272}_{-0.363}$	$0.600^{+0.192}_{-0.301}$	$-0.083^{+0.375}_{-0.353}$	in.track.	$0.390^{+0.335}_{-0.483}$	$0.600^{+0.233}_{-0.414}$	$-0.083^{+0.481}_{-0.446}$	in.track.	in.track.
120204054	44	$0.216^{+0.227}_{-0.253}$	$0.547^{+0.155}_{-0.204}$	$-0.136^{+0.255}_{-0.239}$	in.track.	$0.216^{+0.266}_{-0.302}$	$0.547^{+0.179}_{-0.249}$	$-0.136^{+0.304}_{-0.280}$	in.track.	$0.216^{+0.336}_{-0.397}$	$0.547^{+0.222}_{-0.338}$	$-0.136^{+0.395}_{-0.356}$	in.track.	in.track.

Continued on next page

Table A.2 – continued from previous page

GRB name	N	$\rho_{\rm ph}(90\%)$	$\rho_{\rm en}(90\%)$	$\rho_{\rm t}(90\%)$	trend(90%)	$\rho_{\rm ph}(95\%)$	$\rho_{\rm en}(95\%)$	$\rho_{\rm t}(95\%)$	trend(95%)	$\rho_{\rm ph}(99\%)$	$\rho_{\rm en}(99\%)$	$\rho_{\rm t}(99\%)$	trend(99%)	trend(by eyes)
(1)	(2)	(3)	(4)	(5)	(6)	(7)	(8)	(9)	(10)	(11)	(12)	(13)	(14)	(15)
120226871	13	$0.022^{+0.473}_{-0.483}$	$0.093^{+0.453}_{-0.496}$	$-0.335^{+0.505}_{-0.366}$	undeter.	$0.022^{+0.544}_{-0.557}$	$0.093^{+0.519}_{-0.576}$	$-0.335^{+0.600}_{-0.413}$	undeter.	$0.022^{+0.662}_{-0.682}$	$0.093^{+0.627}_{-0.711}$	$-0.335^{+0.770}_{-0.487}$	undeter.	undeter.
120323507	9	$-0.250^{+0.644}_{-0.479}$	$0.200^{+0.504}_{-0.637}$	$0.450^{+0.370}_{-0.635}$	undeter.	$-0.250^{+0.747}_{-0.534}$	$0.200^{+0.563}_{-0.735}$	$0.450^{+0.408}_{-0.755}$	undeter.	$-0.250^{+0.912}_{-0.613}$	$0.200^{+0.649}_{-0.890}$	$0.450^{+0.461}_{-0.963}$	undeter.	in.track.
120328268	26	$0.361^{+0.256}_{-0.326}$	$0.590^{+0.180}_{-0.267}$	$-0.653^{+0.241}_{-0.156}$	undeter.	$0.361^{+0.295}_{-0.392}$	$0.590^{+0.205}_{-0.327}$	$-0.653^{+0.297}_{-0.177}$	undeter.	$0.361^{+0.362}_{-0.519}$	$0.590^{+0.248}_{-0.450}$	$-0.653^{+0.414}_{-0.213}$	undeter.	h.t.s.+in.track.
120426090	11	$0.064^{+0.505}_{-0.540}$	$0.164^{+0.470}_{-0.558}$	$-0.600^{+0.489}_{-0.255}$	h.t.s.	$0.064^{+0.575}_{-0.621}$	$0.164^{+0.532}_{-0.647}$	$-0.600^{+0.600}_{-0.282}$	h.t.s.	$0.064^{+0.687}_{-0.753}$	$0.164^{+0.628}_{-0.796}$	$-0.600^{+0.814}_{-0.322}$	undeter.	h.t.s.
120526303	10	$0.042^{+0.539}_{-0.565}$	$0.782^{+0.150}_{-0.378}$	$-0.418^{+0.593}_{-0.370}$	in.track.	$0.042^{+0.612}_{-0.646}$	$0.782^{+0.164}_{-0.482}$	$-0.418^{+0.705}_{-0.411}$	in.track.	$0.042^{+0.726}_{-0.773}$	$0.782^{+0.184}_{-0.705}$	$-0.418^{+0.902}_{-0.471}$	in.track.	in.track.
120624933	18	$0.193^{+0.358}_{-0.418}$	$0.358^{+0.306}_{-0.408}$	$0.168^{+0.365}_{-0.418}$	undeter.	$0.193^{+0.412}_{-0.494}$	$0.358^{+0.349}_{-0.489}$	$0.168^{+0.421}_{-0.492}$	undeter.	$0.193^{+0.503}_{-0.631}$	$0.358^{+0.420}_{-0.640}$	$0.168^{+0.515}_{-0.626}$	undeter.	h.t.s.+in.track.
120707800	12	$0.650^{+0.217}_{-0.427}$	$0.748^{+0.160}_{-0.351}$	$-0.189^{+0.532}_{-0.440}$	in.track.	$0.650^{+0.241}_{-0.528}$	$0.748^{+0.177}_{-0.443}$	$-0.189^{+0.621}_{-0.499}$	in.track.	$0.650^{+0.276}_{-0.733}$	$0.748^{+0.201}_{-0.638}$	$-0.189^{+0.772}_{-0.593}$	in.track.	in.track.
120711115	31	$0.324^{+0.246}_{-0.299}$	$0.515^{+0.192}_{-0.262}$	$0.014^{+0.300}_{-0.302}$	in.track.	$0.324^{+0.284}_{-0.358}$	$0.515^{+0.220}_{-0.318}$	$0.014^{+0.353}_{-0.356}$	in.track.	$0.324^{+0.352}_{-0.473}$	$0.515^{+0.269}_{-0.432}$	$0.014^{+0.449}_{-0.454}$	in.track.	in.track.

Table A.3: Best-fit parameters of the identified significant blackbodies of the PLBB model (Ch. 2). Column (1) lists the GRB names. Column (2) lists the spectrum numbers within individual burst. Column (3) lists the start times $T_{\rm start}$ and end times $T_{\rm stop}$ for the time bins. Columns(4) - (7) list the best-fit parameters of the PLBB model. Column (7) lists the values of ΔCSTAT = CSTAT(BEST) − CSTAT(PLBB). [a]We note that for these 2 spectra the BEST models are SBPL (the rest BEST models from this burst are all COMP), CSTAT values between SBPL and PLBB are directly compared without performing any simulations.

GRB name	spectrum	$T_{\rm start}$:$T_{\rm stop}$ (s)	$A_{\rm PL}$ (ph s^{-1} cm^{-2} keV^{-1})	α	$A_{\rm BB}$ (ph s^{-1} cm^{-2} keV^{-1})	kT (keV)	ΔCSTAT
(1)	(2)	(3)	(4)	(5)	(6)	(7)	(8)
090618353	46	79.706:80.155	0.0249 ± 0.0061	-1.70 ± 0.06	$3.135E-04 \pm 1.22E-04$	22.12 ± 1.72	57.57
090618353	77	96.641:110.742	0.0051 ± 0.0010	-1.88 ± 0.03	$1.333E-04 \pm 3.59E-05$	15.59 ± 0.81	128.1
090902462[a]	10	6.433:6.851	0.0216 ± 0.0021	-1.56 ± 0.05	$1.456E-06 \pm 1.79E-07$	181.20 ± 6.14	12.43
090902462[a]	11	6.851:7.218	0.0233 ± 0.0024	-1.58 ± 0.06	$1.600E-06 \pm 2.08E-07$	175.70 ± 6.18	29.47
090902462	12	7.218:7.500	0.0315 ± 0.0031	-1.61 ± 0.05	$2.050E-06 \pm 2.78E-07$	170.50 ± 6.25	82.4
090902462	13	7.500:7.774	0.0387 ± 0.0037	-1.62 ± 0.05	$9.601E-07 \pm 1.28E-07$	222.10 ± 8.40	59.65
090902462	14	7.774:7.958	0.0516 ± 0.0048	-1.63 ± 0.05	$9.149E-07 \pm 1.48E-07$	227.70 ± 10.50	102.04
090902462	15	7.958:8.119	0.0804 ± 0.0069	-1.65 ± 0.04	$9.125E-07 \pm 1.60E-07$	228.50 ± 11.60	67.74
090902462	16	8.119:8.280	0.0635 ± 0.0068	-1.71 ± 0.05	$1.179E-06 \pm 2.15E-07$	204.90 ± 10.40	53.62
090902462	17	8.280:8.424	0.0672 ± 0.0068	-1.76 ± 0.05	$8.905E-07 \pm 1.53E-07$	237.60 ± 11.80	181.34
090902462	18	8.424:8.563	0.0708 ± 0.0065	-1.66 ± 0.04	$1.150E-06 \pm 2.22E-07$	210.40 ± 11.50	125.79
090902462	19	8.563:8.706	0.0681 ± 0.0069	-1.76 ± 0.05	$7.986E-07 \pm 1.42E-07$	240.00 ± 12.30	153.02
090902462	20	8.706:8.874	0.0590 ± 0.0061	-1.75 ± 0.04	$5.968E-07 \pm 1.13E-07$	244.80 ± 13.50	129.94
090902462	21	8.874:9.030	0.0630 ± 0.0063	-1.72 ± 0.05	$1.093E-06 \pm 1.97E-07$	213.70 ± 10.90	148.11
090902462	22	9.030:9.184	0.0772 ± 0.0073	-1.75 ± 0.04	$6.380E-07 \pm 1.05E-07$	264.90 ± 12.90	177.34
090902462	23	9.184:9.315	0.0955 ± 0.0089	-1.71 ± 0.04	$1.088E-06 \pm 2.37E-07$	206.80 ± 12.70	83.87
090902462	24	9.315:9.443	0.0806 ± 0.0088	-1.78 ± 0.05	$1.569E-06 \pm 3.36E-07$	184.40 ± 10.80	536.44

Continued on next page

Table A.3 – continued from previous page

GRB name	spectrum	$T_{\rm start}$:$T_{\rm stop}$ (s)	$A_{\rm PL}$ (ph s^{-1} cm^{-2} keV^{-1})	α	$A_{\rm BB}$ (ph s^{-1} cm^{-2} keV^{-1})	kT (keV)	ΔCSTAT
(1)	(2)	(3)	(4)	(5)	(6)	(7)	(8)
090902462	25	9.443:9.595	0.0890 ± 0.0086	-1.77 ± 0.04	$1.567E-06 \pm 3.22E-07$	184.50 ± 10.40	115.81
090902462	26	9.595:9.721	0.0841 ± 0.0091	-1.78 ± 0.05	$3.432E-06 \pm 7.35E-07$	146.70 ± 8.08	97.97
090902462	27	9.721:9.816	0.1082 ± 0.0117	-1.79 ± 0.05	$7.694E-06 \pm 1.28E-06$	137.40 ± 5.79	110.98
090902462	28	9.816:9.938	0.0940 ± 0.0104	-1.83 ± 0.05	$5.745E-06 \pm 1.18E-06$	128.70 ± 6.56	95.97
090902462	29	9.938:10.059	0.0726 ± 0.0081	-1.73 ± 0.05	$3.282E-06 \pm 6.22E-07$	154.90 ± 7.61	73.25
090902462	30	10.059:10.206	0.0663 ± 0.0076	-1.81 ± 0.06	$2.682E-06 \pm 4.41E-07$	168.50 ± 7.36	126.01
090902462	31	10.206:10.383	0.0550 ± 0.0067	-1.85 ± 0.06	$2.792E-06 \pm 4.81E-07$	155.40 ± 6.97	126.13
090902462	32	10.383:10.561	0.0659 ± 0.0066	-1.78 ± 0.05	$8.862E-07 \pm 1.40E-07$	234.30 ± 10.70	159.15
090902462	33	10.561:10.720	0.0678 ± 0.0068	-1.74 ± 0.05	$1.050E-06 \pm 1.85E-07$	218.80 ± 11.00	136.11
090902462	34	10.720:10.881	0.0826 ± 0.0081	-1.71 ± 0.04	$1.020E-06 \pm 2.25E-07$	199.20 ± 12.30	43.77
090902462	35	10.881:11.011	0.0665 ± 0.0068	-1.71 ± 0.05	$2.275E-06 \pm 4.08E-07$	176.10 ± 8.45	124.71
090902462	36	11.011:11.145	0.0837 ± 0.0080	-1.68 ± 0.04	$3.913E-06 \pm 7.07E-07$	150.70 ± 7.16	54.48
090902462	37	11.145:11.326	0.0505 ± 0.0055	-1.76 ± 0.05	$1.764E-06 \pm 3.30E-07$	171.00 ± 8.50	128.03
090902462	38	11.326:11.521	0.0403 ± 0.0052	-1.83 ± 0.06	$2.410E-06 \pm 5.04E-07$	142.30 ± 7.58	110.62
090902462	39	11.521:11.718	0.0478 ± 0.0051	-1.68 ± 0.05	$2.258E-06 \pm 3.98E-07$	160.60 ± 7.38	83.84
090902462	40	11.718:11.934	0.0448 ± 0.0054	-1.84 ± 0.06	$2.277E-06 \pm 3.93E-07$	158.80 ± 7.21	158.65
090902462	41	11.934:12.204	0.0498 ± 0.0054	-1.72 ± 0.04	$2.949E-06 \pm 8.41E-07$	114.80 ± 8.21	34.59
110622158	13	29.726:31.428	0.0084 ± 0.0024	-1.79 ± 0.07	$7.874E-05 \pm 3.01E-05$	26.23 ± 1.28	155.02
110622158	15	33.430:36.752	0.0046 ± 0.0015	-1.72 ± 0.05	$6.697E-05 \pm 2.49E-05$	21.13 ± 1.10	155.29

Table A.4: The BAND fit parameters for the eight bursts (Ch. 3). The times $t_{\rm start}$ and $t_{\rm stop}$ are relative to the GBM trigger time T_0. CSTAT/dof shows the modified Cash Statistics (Cash 1979), Caster C-Statistics, per degrees of freedom.

$t_{\rm start}$ (s)	$t_{\rm stop}$ (s)	A (ph s^{-1} cm^{-2} keV^{-1})	$E_{\rm p}$ (keV)	α	β	CSTAT/dof
GRB 090902B						
0.000	2.325	0.0681±0.0043	521.5±24.1	−0.307±0.039	−4.168±1.980	539.10/478
2.325	4.207	0.0745±0.0043	589.1±27.2	−0.220±0.041	−3.158±0.365	543.25/478
4.207	5.987	0.0780±0.0041	620.5±24.7	−0.197±0.038	−4.367±1.810	547.67/478
5.987	7.173	0.0885±0.0038	959.9±41.2	−0.366±0.030	−4.600±1.470	662.97/478
7.173	7.892	0.1352±0.0054	1421.0±79.2	−0.782±0.019	−5.175±3.080	799.87/478
7.892	8.340	0.2221±0.0093	1631.0±128.0	−1.099±0.016	< -15.53	826.49/478
8.340	8.738	0.2148±0.0100	1811.0±198.0	−1.153±0.016	−3.457±0.674	938.64/478
8.738	9.176	0.2253±0.0095	1801.0±161.0	−1.169±0.015	< -5.522	974.42/478
9.176	9.554	0.2497±0.0112	1737.0±181.0	−1.279±0.015	< -5.696	764.26/478
9.554	9.878	0.3091±0.0163	1082.0±114.0	−1.201±0.018	−3.909±1.280	867.81/478
9.878	10.262	0.2456±0.0123	1171.0±106.0	−1.123±0.018	< -12.89	843.17/478
10.262	10.730	0.2260±0.0095	1588.0±133.0	−1.147±0.016	< -8.822	1000.1/478
10.730	11.116	0.2432±0.0117	1324.0±123.0	−1.108±0.018	−4.184±1.630	779.39/478
11.116	11.633	0.1634±0.0083	1272.0±119.0	−1.110±0.018	< -12.32	805.70/478
11.633	12.270	0.1398±0.0077	1226.0±137.0	−1.140±0.020	−4.258±2.460	712.95/478
12.270	12.982	0.2276±0.0359	137.4±12.3	−0.969±0.062	−2.214±0.106	557.08/478
12.982	13.337	0.6174±0.0740	212.2±11.7	−0.495±0.051	−2.451±0.110	579.38/478
13.337	13.799	0.2969±0.0318	297.8±20.7	−0.808±0.039	−2.751±0.257	475.17/478
13.799	14.247	0.2260±0.0131	668.4±38.6	−0.776±0.025	< -11.92	536.24/478
14.247	14.773	0.1927±0.0117	676.2±42.1	−0.810±0.025	< -9.535	526.75/478
14.773	15.186	0.2159±0.0117	746.0±39.0	−0.665±0.025	< -11.92	552.70/478
15.186	15.682	0.1805±0.0083	999.9±53.3	−0.628±0.024	−4.202±0.990	622.98/478
15.682	16.280	0.1591±0.0114	603.1±46.8	−0.820±0.029	−2.772±0.268	566.78/478
16.280	16.753	0.2031±0.0118	666.4±37.1	−0.683±0.027	−4.580±2.870	586.40/478
16.753	17.418	0.2017±0.0190	366.7±26.3	−0.705±0.039	−2.562±0.185	557.65/478
17.418	18.232	0.1534±0.0144	382.1±29.3	−0.822±0.037	−2.699±0.284	467.21/478
18.232	18.977	0.1515±0.0136	427.2±34.5	−0.907±0.033	−2.916±0.485	484.31/478
18.977	19.575	0.2776±0.0310	278.2±19.1	−0.570±0.049	−2.285±0.096	491.66/478
19.575	19.995	0.3303±0.0322	343.4±22.5	−0.606±0.041	−2.563±0.156	509.15/478
19.995	20.571	0.1728±0.0161	419.3±36.4	−0.869±0.036	−2.450±0.180	509.15/478
20.571	21.148	0.3419±0.0417	217.2±13.7	−0.645±0.050	−2.397±0.119	548.28/478
21.148	21.843	0.3242±0.0417	197.3±11.6	−0.524±0.055	−2.395±0.121	564.19/478

Continued on next page

Table A.4 – continued from previous page

$t_{\rm start}$ (s)	$t_{\rm stop}$ (s)	A (ph s^{-1} cm^{-2} keV^{-1})	$E_{\rm p}$ (keV)	α	β	CSTAT/dof
21.843	23.098	0.0832±0.0103	342.9±45.0	−1.146±0.040	−2.283±0.192	565.37/478
23.098	33.792	0.0184±0.0055	134.3±19.5	−1.427±0.061	−2.727±0.780	627.70/478
GRB 100724B						
-7.168	10.075	0.0079±0.0005	961.0±129.0	−0.878±0.032	−1.581±0.032	22341./478
10.075	12.503	0.0358±0.0024	570.7±56.3	−0.698±0.043	−1.721±0.035	2558.6/478
12.503	15.016	0.0292±0.0019	662.1±65.9	−0.727±0.040	−1.722±0.037	2459.2/478
15.016	17.022	0.0306±0.0020	1222.0±161.0	−0.877±0.030	−1.790±0.051	1297.9/478
17.022	19.118	0.0301±0.0020	968.7±114.0	−0.793±0.034	−1.744±0.043	1608.2/478
19.118	21.649	0.0249±0.0015	940.3±115.0	−0.882±0.033	−1.648±0.035	3636.6/478
21.649	24.481	0.0262±0.0021	580.1±83.4	−0.847±0.044	−1.580±0.029	4363.6/478
24.481	29.293	0.0208±0.0017	473.6±80.8	−0.862±0.051	−1.494±0.022	10681./478
29.293	38.468	0.0150±0.0017	282.6±49.7	−0.888±0.065	−1.511±0.015	53566./478
38.468	41.089	0.0445±0.0052	286.5±38.3	−0.688±0.067	−1.595±0.024	6721.3/478
41.089	45.942	0.0249±0.0025	298.9±36.6	−0.787±0.058	−1.628±0.020	20827./478
45.942	50.235	0.0184±0.0018	375.9±52.8	−0.890±0.052	−1.636±0.022	20121./478
50.235	55.075	0.0179±0.0017	352.5±44.9	−0.877±0.051	−1.646±0.019	20911./478
55.075	57.006	0.0397±0.0030	525.8±43.7	−0.780±0.039	−1.872±0.030	2355.2/478
57.006	58.742	0.0420±0.0034	499.2±43.7	−0.754±0.041	−1.888±0.028	3499.4/478
58.742	59.914	0.0677±0.0053	436.5±37.5	−0.717±0.044	−1.934±0.043	2615.2/478
59.914	60.965	0.0751±0.0072	364.7±34.8	−0.661±0.052	−1.936±0.049	2171.3/478
60.965	62.298	0.0613±0.0040	457.8±29.2	−0.687±0.040	−1.978±0.021	2335.1/478
62.298	63.162	0.0950±0.0095	454.5±47.1	−0.657±0.048	−1.903±0.050	829.13/478
63.162	64.192	0.0869±0.0099	368.5±38.1	−0.587±0.056	−1.796±0.031	1239.1/478
64.192	65.463	0.0752±0.0075	323.4±30.0	−0.615±0.056	−1.797±0.027	1907.0/478
65.463	66.735	0.0689±0.0056	434.0±39.4	−0.706±0.045	−1.906±0.042	1695.8/478
66.735	67.858	0.0807±0.0082	389.2±38.6	−0.661±0.051	−1.844±0.032	1289.5/478
67.858	69.182	0.0672±0.0064	349.3±32.5	−0.649±0.053	−1.805±0.025	1703.0/478
69.182	70.591	0.0474±0.0051	417.1±56.2	−0.819±0.051	−1.714±0.031	1498.7/478
70.591	72.794	0.0487±0.0061	262.8±30.7	−0.605±0.070	−1.650±0.026	3089.7/478
72.794	74.372	0.0597±0.0061	372.9±37.6	−0.615±0.054	−1.772±0.032	1165.1/478
74.372	75.362	0.0950±0.0105	373.0±36.6	−0.587±0.054	−1.874±0.038	1090.3/478
75.362	76.443	0.1011±0.0112	334.1±31.7	−0.571±0.056	−1.879±0.044	725.08/478
76.443	78.171	0.0513±0.0051	347.2±37.5	−0.759±0.053	−1.791±0.029	1247.7/478
78.171	86.297	0.0109±0.0011	513.8±78.7	−0.982±0.043	−1.634±0.025	15102./478
86.297	123.477	0.0056±0.0038	93.0±49.1	−0.692±0.292	−1.312±0.015	15525./478
123.477	130.458	0.0080±0.0041	143.4±17.6	−0.864±0.083	−2.062±0.134	907.00/478

Continued on next page

Table A.4 – continued from previous page

$t_{\rm start}$ (s)	$t_{\rm stop}$ (s)	A (ph s^{-1} cm^{-2} keV^{-1})	$E_{\rm p}$ (keV)	α	β	CSTAT/dof
130.458	142.336	<0.0018	111.8±53.1	−1.168±0.212	−1.842±0.143	1020.7/478
GRB 100826A						
-2.048	9.547	0.0551±0.0145	144.3±14.5	−0.006±0.160	−1.782±0.055	609.22/356
9.547	11.903	0.0501±0.0099	296.2±42.1	−0.545±0.099	−1.993±0.100	451.52/356
11.903	13.740	0.0650±0.0129	275.8±37.3	−0.543±0.098	−2.032±0.105	412.41/356
13.740	14.495	0.0781±0.0159	323.8±51.6	−0.551±0.100	−1.943±0.094	368.17/356
14.495	15.320	0.0900±0.0178	312.9±47.8	−0.551±0.099	−1.938±0.082	387.25/356
15.320	15.979	0.0629±0.0088	561.2±84.0	−0.814±0.058	−2.813±0.696	349.78/356
15.979	16.622	0.0550±0.0075	693.2±127.0	−0.808±0.061	−2.237±0.195	389.88/356
16.622	17.190	0.0677±0.0093	551.2±81.7	−0.747±0.061	−2.437±0.275	426.53/356
17.190	17.712	0.1054±0.0214	314.5±51.2	−0.582±0.099	−1.891±0.078	359.30/356
17.712	18.294	0.1062±0.0207	328.0±47.5	−0.565±0.092	−2.099±0.120	385.37/356
18.294	18.769	0.1372±0.0264	328.0±45.7	−0.485±0.094	−2.044±0.099	430.26/356
18.769	19.175	0.0908±0.0120	580.0±81.2	−0.696±0.061	−2.502±0.313	397.80/356
19.175	19.580	0.1196±0.0191	433.9±65.9	−0.636±0.077	−2.069±0.102	383.34/356
19.580	19.961	0.0991±0.0137	581.5±92.5	−0.681±0.067	−2.142±0.130	346.77/356
19.961	20.408	0.1155±0.0186	452.9±73.0	−0.676±0.075	−2.070±0.104	359.67/356
20.408	20.825	0.1587±0.0276	353.2±45.8	−0.510±0.085	−2.187±0.120	376.13/356
20.825	21.204	0.1393±0.0220	424.2±57.4	−0.560±0.078	−2.232±0.141	397.45/356
21.204	21.603	0.1282±0.0199	460.3±72.3	−0.696±0.073	−2.130±0.116	375.87/356
21.603	22.059	0.1219±0.0193	424.2±63.6	−0.681±0.074	−2.161±0.130	377.50/356
22.059	22.412	0.1160±0.0161	539.0±81.1	−0.657±0.067	−2.137±0.119	359.72/356
22.412	22.834	0.1335±0.0226	411.0±65.6	−0.604±0.083	−1.952±0.076	391.29/356
22.834	23.301	0.0928±0.0140	549.7±104.0	−0.792±0.067	−1.998±0.099	343.64/356
23.301	23.825	0.0746±0.0112	554.1±96.3	−0.756±0.067	−2.173±0.162	433.43/356
23.825	24.471	0.0710±0.0121	458.0±87.6	−0.754±0.078	−1.938±0.096	402.13/356
24.471	25.169	0.0824±0.0159	355.3±61.4	−0.677±0.088	−1.952±0.095	434.64/356
25.169	25.789	0.0727±0.0137	399.5±79.9	−0.716±0.088	−1.836±0.077	371.05/356
25.789	26.336	0.0907±0.0182	332.9±53.9	−0.636±0.091	−2.004±0.119	424.82/356
26.336	27.189	0.0856±0.0168	309.3±48.8	−0.710±0.088	−2.060±0.120	433.55/356
27.189	28.154	0.0928±0.0210	220.0±33.9	−0.564±0.115	−1.895±0.093	364.10/356
28.154	28.989	0.1055±0.0222	266.2±37.2	−0.628±0.094	−2.128±0.124	438.88/356
28.989	29.888	0.0709±0.0148	316.4±57.6	−0.830±0.086	−2.067±0.133	427.39/356
29.888	31.139	0.0452±0.0098	336.6±75.2	−0.937±0.086	−1.991±0.144	394.69/356
31.139	32.985	0.0408±0.0092	262.2±53.6	−0.812±0.102	−1.837±0.092	399.37/356
32.985	35.735	0.0365±0.0085	228.4±37.4	−0.723±0.103	−1.956±0.126	387.28/356

Continued on next page

Table A.4 – continued from previous page

$t_{\rm start}$ (s)	$t_{\rm stop}$ (s)	A (ph s^{-1} cm^{-2} keV^{-1})	$E_{\rm p}$ (keV)	α	β	CSTAT/dof
35.735	37.794	0.0868±0.0321	126.6±21.1	−0.321±0.199	−1.765±0.071	393.57/356
37.794	40.792	0.0496±0.0189	121.6±25.3	−0.542±0.195	−1.722±0.068	407.95/356
40.792	46.181	0.0710±0.0216	117.2±15.9	−0.526±0.154	−1.963±0.094	424.55/356
46.181	60.975	0.0493±0.0150	108.4±13.3	−0.328±0.159	−1.777±0.051	520.17/356
60.975	62.775	0.0614±0.0135	232.6±35.3	−0.768±0.094	−2.094±0.147	442.50/356
62.775	64.610	0.0456±0.0105	258.6±45.7	−0.951±0.082	−2.221±0.236	402.38/356
64.610	70.330	0.0254±0.0057	211.1±35.6	−0.917±0.088	−2.016±0.150	426.15/356
70.330	72.515	0.0279±0.0041	549.0±85.8	−0.968±0.051	< -12.27	410.69/356
72.515	73.736	0.0520±0.0106	346.4±73.5	−0.941±0.080	−2.020±0.136	395.10/356
73.736	76.263	0.0455±0.0106	209.4±31.9	−0.813±0.094	−2.101±0.170	375.69/356
76.263	78.063	0.0561±0.0134	231.3±34.0	−0.889±0.083	−2.472±0.365	377.34/356
78.063	80.235	0.0354±0.0087	263.8±56.3	−1.199±0.070	−2.476±0.547	392.60/356
80.235	83.975	0.1548±0.2100	45.8±12.1	−0.143±0.553	−1.672±0.042	412.44/356
83.975	89.057	0.1167±0.1011	51.3±10.5	−0.384±0.364	−1.805±0.049	386.98/356
89.057	90.011	0.0838±0.0258	169.4±21.9	−1.043±0.082	−3.072±1.090	380.52/356
90.011	91.665	0.1179±0.0450	82.9±11.8	−0.950±0.151	−2.301±0.192	400.87/356
91.665	98.549	0.0659±0.0566	46.9±9.6	−0.552±0.343	−1.857±0.050	440.67/356
98.549	121.856	<1.5170	29.0±6.8	< -1.102	−1.791±0.053	581.38/356
GRB 101123A						
38.912	43.589	0.0179±0.0033	497.5±98.7	−0.549±0.101	−1.926±0.100	447.95/356
43.589	44.391	0.0380±0.0033	1635.0±295.0	−0.717±0.048	−2.026±0.114	370.62/356
44.391	44.844	0.0770±0.0104	683.7±129.0	−0.583±0.073	−1.753±0.057	380.88/356
44.844	45.250	0.1016±0.0166	506.6±90.5	−0.606±0.077	−1.884±0.075	372.85/356
45.250	45.628	0.1530±0.0276	374.4±54.5	−0.486±0.088	−1.989±0.086	345.89/356
45.628	45.949	0.1407±0.0267	380.9±67.5	−0.541±0.093	−1.777±0.060	372.09/356
45.949	46.255	0.1001±0.0148	577.7±98.7	−0.728±0.064	−2.132±0.150	399.98/356
46.255	46.552	0.1173±0.0179	544.2±94.3	−0.726±0.067	−2.088±0.125	366.58/356
46.552	46.836	0.1243±0.0206	467.8±75.3	−0.605±0.076	−2.044±0.118	414.08/356
46.836	47.262	0.1339±0.0303	278.5±47.1	−0.702±0.095	−2.040±0.128	404.28/356
47.262	47.831	0.0808±0.0155	416.5±84.7	−0.825±0.077	−2.061±0.144	337.31/356
47.831	48.538	0.0739±0.0137	423.0±84.1	−0.826±0.076	−2.059±0.134	374.63/356
48.538	49.070	0.0923±0.0173	388.3±61.6	−0.679±0.078	−2.255±0.207	382.10/356
49.070	49.701	0.1666±0.0424	198.2±25.3	−0.482±0.114	−2.196±0.167	396.86/356
49.701	50.067	0.1229±0.0174	453.2±50.6	−0.515±0.068	−2.815±0.522	368.62/356
50.067	50.332	0.1673±0.0188	533.5±49.6	−0.582±0.055	−3.884±2.3	364.11/356
50.332	50.600	0.1184±0.0151	616.6±83.3	−0.711±0.056	−2.630±0.367	394.00/356

Continued on next page

Table A.4 – continued from previous page

$t_{\rm start}$ (s)	$t_{\rm stop}$ (s)	A (ph s^{-1} cm^{-2} keV^{-1})	$E_{\rm p}$ (keV)	α	β	CSTAT/dof
50.600	51.027	0.1445±0.0320	267.1±41.8	−0.662±0.095	−2.042±0.117	383.01/356
51.027	51.565	0.0824±0.0136	443.1±68.5	−0.915±0.059	−3.471±2.750	368.09/356
51.565	51.904	0.1089±0.0123	648.0±74.4	−0.770±0.049	< −9.740	348.95/356
51.904	52.133	0.1842±0.0233	457.0±42.2	−0.659±0.055	< −14.27	331.89/356
52.133	52.444	0.1727±0.0318	374.4±56.8	−0.641±0.079	−2.204±0.145	412.50/356
52.444	52.701	0.1704±0.0201	518.0±51.0	−0.705±0.052	< −14.90	394.79/356
52.701	53.008	0.1605±0.0253	420.4±56.2	−0.672±0.069	−2.523±0.283	437.42/356
53.008	53.355	0.0999±0.0127	565.9±68.1	−0.737±0.054	−4.167±5.450	401.64/356
53.355	53.681	0.1462±0.0230	425.7±54.1	−0.617±0.068	−2.588±0.329	333.49/356
53.681	54.170	0.0849±0.0157	410.1±71.3	−0.823±0.071	−2.294±0.240	377.17/356
54.170	55.513	0.0225±0.0047	688.9±240.0	−1.053±0.068	−2.049±0.248	394.51/356
55.513	55.962	0.1402±0.0264	346.1±51.1	−0.663±0.081	−2.230±0.161	419.37/356
55.962	56.334	0.0982±0.0124	559.1±60.4	−0.630±0.057	−7.559±264.0	357.26/356
56.334	56.672	0.1198±0.0194	431.7±60.8	−0.708±0.067	−2.483±0.324	346.27/356
56.672	58.101	0.0776±0.0235	199.9±32.8	−0.972±0.093	−2.768±0.627	430.97/356
58.101	62.873	0.0291±0.0105	171.3±42.3	−0.865±0.149	−1.996±0.187	449.63/356
62.873	67.584	0.2631±1.4600	68.4±43.5	< −1.497	−1.418±0.111	489.31/356
81.920	89.903	0.0113±0.0025	568.6±175.0	−1.146±0.069	< −17.00	518.16/356
89.903	92.126	0.0323±0.0090	288.3±53.7	−0.946±0.084	−3.685±5.650	419.32/356
92.126	93.570	0.0327±0.0095	283.1±62.0	−0.968±0.090	−2.350±0.504	466.08/356
93.570	94.965	0.0610±0.0217	140.1±31.2	−0.902±0.146	−2.005±0.173	360.96/356
94.965	100.352	0.0131±0.0087	109.2±50.4	−0.925±0.281	−1.778±0.142	441.31/356
140.288	143.695	0.0172±0.0051	407.7±149.0	−1.208±0.080	−2.602±1.250	373.85/356
143.695	145.029	0.0200±0.0050	537.8±161.0	−1.095±0.069	−2.940±2.800	388.75/356
145.029	146.541	0.0360±0.0137	158.5±42.3	−0.944±0.142	−1.936±0.187	375.53/356
146.541	149.288	0.0444±0.0203	109.1±26.4	−0.847±0.192	−1.997±0.176	393.57/356
149.288	155.648	<0.0793	55.3±19.2	−0.435±0.982	−1.746±0.132	365.35/356
GRB 120526A						
-2.048	3.367	0.0144±0.0023	625.6±100.0	−0.610±0.145	< −8.973	277.98/239
3.367	5.382	0.0430±0.0069	457.2±57.8	−0.647±0.128	< −12.32	248.49/239
5.382	7.254	0.0339±0.0041	720.7±79.8	−0.533±0.122	< −10.83	256.79/239
7.254	8.973	0.0262±0.0030	1389.0±221.0	−0.893±0.083	< −6.327	302.93/239
8.973	11.365	0.0214±0.0032	865.8±203.0	−0.954±0.106	< −5.560	288.98/239
11.365	13.269	0.0340±0.0042	711.4±88.2	−0.630±0.118	< −11.92	236.42/239
13.269	15.565	0.0224±0.0027	954.3±144.0	−0.521±0.129	−2.691±0.380	271.67/239
15.565	16.889	0.0220±0.0029	1463.0±369.0	−0.724±0.113	−2.174±0.194	263.50/239

Continued on next page

Table A.4 – continued from previous page

$t_{\rm start}$ (s)	$t_{\rm stop}$ (s)	A (ph s^{-1} cm^{-2} keV^{-1})	$E_{\rm p}$ (keV)	α	β	CSTAT/dof
16.889	18.729	0.0288±0.0034	1224.0±198.0	−0.894±0.090	< −6.337	264.96/239
18.729	20.182	0.0334±0.0042	1100.0±236.0	−0.911±0.098	−2.885±0.660	248.03/239
20.182	22.412	0.0302±0.0044	683.2±132.0	−0.693±0.134	−2.410±0.271	214.16/239
22.412	24.484	0.0214±0.0028	984.4±163.0	−0.698±0.117	< −6.364	241.56/239
24.484	26.325	0.0300±0.0037	936.3±158.0	−0.768±0.109	−3.186±0.976	234.93/239
26.325	28.016	0.0331±0.0042	781.7±114.0	−0.743±0.108	< −11.92	247.35/239
28.016	29.555	0.0278±0.0035	1119.0±238.0	−0.791±0.108	−2.533±0.347	285.22/239
29.555	30.980	0.0337±0.0052	640.2±109.0	−0.653±0.129	−3.159±1.240	257.64/239
30.980	33.168	0.0298±0.0039	746.7±117.0	−0.695±0.125	−3.105±0.903	285.57/239
33.168	34.993	0.0280±0.0042	853.7±219.0	−0.918±0.112	−2.499±0.407	246.47/239
34.993	36.553	0.0366±0.0062	697.4±204.0	−0.994±0.115	−2.269±0.253	255.41/239
36.553	37.691	0.0362±0.0079	475.6±109.0	−0.991±0.120	< −9.537	246.99/239
37.691	39.667	0.0253±0.0037	821.6±166.0	−0.825±0.115	−3.497±2.140	215.69/239
39.667	41.306	0.0374±0.0061	532.0±86.7	−0.813±0.119	< −14.64	242.91/239
41.306	42.977	0.0404±0.0074	466.1±77.8	−0.757±0.131	−3.940±4.880	204.96/239
42.977	44.596	0.0452±0.0110	342.3±56.5	−0.771±0.141	< −5.606	240.63/239
44.596	46.530	0.0407±0.0083	395.0±62.2	−0.781±0.132	< −14.90	253.36/239
46.530	56.166	0.0064±0.0047	<227.1	−1.568±0.307	−1.966±0.374	298.50/239
56.166	67.584	<0.0052	<21.2	< −1.847	−1.963±0.212	301.17/239
GRB 130427A						
-0.064	0.145	0.0821±0.0080	1246.0±126.0	−0.386±0.081	−2.916±0.359	1489.3/357
0.145	0.214	0.1936±0.0197	918.8±73.1	−0.116±0.089	−3.719±0.799	1275.0/357
0.214	0.268	0.3744±0.0374	764.6±62.0	−0.363±0.074	−4.031±1.280	1246.8/357
0.268	0.313	0.4275±0.0506	657.9±63.1	−0.319±0.085	−3.400±0.702	1168.7/357
0.313	0.358	0.5104±0.0558	569.5±42.7	−0.332±0.078	−4.889±3.570	1163.6/357
0.358	0.398	0.4528±0.0510	734.1±75.3	−0.560±0.070	−3.750±1.090	1169.3/357
0.398	0.434	0.7357±0.1020	486.6±47.5	−0.593±0.075	−3.979±1.580	1115.3/357
0.434	0.472	0.5783±0.0660	617.0±60.7	−0.610±0.066	< −11.92	1119.4/357
0.472	0.505	0.5876±0.0804	572.7±69.1	−0.676±0.072	−3.286±0.834	1090.3/357
0.505	0.541	0.9841±0.2210	319.3±42.3	−0.466±0.111	−2.721±0.281	1098.2/357
0.541	0.575	0.6740±0.1011	465.0±53.0	−0.647±0.077	−3.512±1.050	1100.0/357
0.575	0.614	0.8132±0.1500	379.0±47.8	−0.593±0.089	−2.949±0.408	1113.6/357
0.614	0.656	0.4534±0.0718	505.2±65.4	−0.800±0.070	−3.815±2.120	1107.9/357
0.656	0.696	0.5599±0.0885	423.0±44.6	−0.726±0.072	< −6.620	1089.5/357
0.696	0.736	0.5940±0.1160	366.3±50.1	−0.762±0.087	−3.075±0.656	1123.8/357
0.736	0.780	0.4775±0.1011	383.8±65.1	−0.746±0.095	−2.593±0.350	1170.2/357

Continued on next page

Table A.4 – continued from previous page

$t_{\rm start}$ (s)	$t_{\rm stop}$ (s)	A (ph s^{-1} cm^{-2} keV^{-1})	$E_{\rm p}$ (keV)	α	β	CSTAT/dof
0.780	0.824	0.6696±0.1150	339.6±32.5	−0.732±0.077	< -9.537	1075.6/357
0.824	0.870	0.4616±0.0926	348.3±43.1	−0.813±0.078	< -9.537	1040.5/357
0.870	0.927	0.8204±0.2170	244.9±32.2	−0.686±0.108	−3.027±0.448	1008.3/357
0.927	0.994	0.6554±0.1690	234.1±28.2	−0.696±0.104	−3.118±0.554	1156.6/357
0.994	1.064	0.5467±0.1660	210.9±33.9	−0.732±0.132	−2.504±0.252	1107.2/357
1.064	1.147	0.4542±0.1370	204.3±31.1	−0.766±0.126	−2.591±0.311	1168.0/357
1.147	1.226	0.9292±0.3080	162.6±19.5	−0.489±0.154	−2.652±0.261	1155.7/357
1.226	1.300	0.9699±0.2980	169.2±13.3	−0.577±0.109	< -7.937	1052.7/357
1.300	1.378	0.8825±0.2450	182.0±14.9	−0.660±0.100	< -5.563	1102.9/357
1.378	1.447	1.3581±0.4850	144.9±13.9	−0.400±0.150	−3.036±0.384	1034.1/357
1.447	1.529	0.5947±0.1870	176.2±18.9	−0.663±0.123	−3.338±0.738	1125.5/357
1.529	1.619	0.5603±0.1870	170.0±15.6	−0.670±0.112	< -4.840	1127.0/357
1.619	1.708	0.8494±0.3490	131.1±10.0	−0.591±0.126	−5.137±5.110	1071.8/357
1.708	1.795	0.5043±0.1810	148.3±16.4	−0.632±0.140	−2.950±0.470	1144.4/357
1.795	1.903	1.0900±0.4041	129.2±10.3	−0.493±0.137	−3.475±0.607	1103.9/357
1.903	2.002	0.6567±0.2420	133.3±13.8	−0.613±0.143	−2.994±0.482	1120.9/357
2.002	2.123	0.8216±0.3150	123.5±11.7	−0.600±0.143	−3.164±0.519	1116.5/357
2.123	2.249	0.7220±0.3370	102.8±12.0	−0.344±0.218	−2.675±0.320	1145.5/357
2.249	2.405	0.5713±0.2600	119.9±9.0	−0.660±0.128	< -6.759	1165.1/357
2.405	2.613	0.7771±0.3810	99.5±7.5	−0.748±0.143	−4.253±1.560	1255.3/357
2.613	2.752	<1.4110	87.3±6.5	−0.302±0.222	−4.909±3.920	1049.3/357
GRB 130504C						
-6.144	14.601	0.0074±0.0008	969.0±180.0	−0.892±0.049	−2.236±0.208	593.56/359
14.601	15.059	0.0640±0.0071	952.5±164.0	−0.784±0.057	−2.420±0.259	388.66/359
15.059	15.467	0.0539±0.0049	2096.0±454.0	−0.945±0.041	−2.312±0.261	383.17/359
15.467	15.851	0.1054±0.0126	681.7±103.0	−0.732±0.064	−2.311±0.169	368.60/359
15.851	16.140	0.1040±0.0108	959.4±158.0	−0.824±0.052	−2.388±0.220	372.68/359
16.140	16.485	0.1134±0.0170	565.5±101.0	−0.757±0.073	−2.122±0.131	358.14/359
16.485	16.926	0.0876±0.0120	596.3±104.0	−0.813±0.067	−2.210±0.177	414.67/359
16.926	17.368	0.0700±0.0087	727.6±114.0	−0.911±0.053	−3.828±3.170	418.61/359
17.368	18.042	0.0528±0.0080	586.7±112.0	−0.853±0.068	−2.246±0.232	459.53/359
18.042	18.791	0.0594±0.0103	522.2±120.0	−1.011±0.068	−2.189±0.217	380.92/359
18.791	20.215	0.0354±0.0067	487.2±121.0	−1.025±0.073	−2.169±0.238	340.56/359
20.215	24.224	0.0283±0.0067	245.2±49.0	−0.834±0.109	−1.954±0.130	437.97/359
24.224	25.900	0.0468±0.0112	266.8±55.3	−0.933±0.100	−2.079±0.165	422.51/359
25.900	27.775	0.0189±0.0056	300.3±105.0	−1.204±0.096	−2.016±0.276	399.99/359

Continued on next page

Table A.4 – continued from previous page

$t_{\rm start}$ (s)	$t_{\rm stop}$ (s)	A (ph s^{-1} cm^{-2} keV^{-1})	$E_{\rm p}$ (keV)	α	β	CSTAT/dof
27.775	28.549	0.0482±0.0089	517.4±124.0	−1.142±0.063	−2.707±0.891	449.85/359
28.549	28.831	0.1072±0.0143	793.9±190.0	−1.011±0.058	−2.103±0.151	420.52/359
28.831	29.323	0.0781±0.0139	538.3±141.0	−0.999±0.074	−2.022±0.130	428.27/359
29.323	30.661	0.0274±0.0046	758.2±222.0	−1.133±0.059	−2.451±0.566	433.24/359
30.661	30.978	0.1087±0.0164	552.3±93.0	−0.686±0.076	−2.160±0.147	399.00/359
30.978	31.173	0.1219±0.0150	951.2±196.0	−0.818±0.059	−2.054±0.124	354.79/359
31.173	31.397	0.1399±0.0207	640.3±131.0	−0.818±0.070	−2.024±0.106	404.81/359
31.397	31.654	0.1717±0.0338	376.4±72.8	−0.852±0.085	−2.142±0.148	356.74/359
31.654	32.002	0.1825±0.0460	237.5±44.7	−0.766±0.117	−2.022±0.117	389.46/359
32.002	32.962	0.0626±0.0172	217.8±66.2	−0.990±0.132	−1.812±0.095	440.69/359
32.962	49.001	0.0522±0.0785	44.9±17.8	−0.553±0.602	−1.718±0.044	784.55/359
49.001	51.264	0.1290±0.1560	66.4±23.7	−0.234±0.542	−1.584±0.046	382.04/359
51.264	52.063	0.6384±1.0200	53.7±15.7	−0.189±0.688	−1.603±0.046	388.96/359
52.063	63.008	<1.0260	29.5±8.3	−0.475±1.250	−1.771±0.042	670.35/359
63.008	64.051	0.0517±0.0100	429.3±88.0	−1.060±0.069	−2.845±1.050	407.86/359
64.051	64.571	0.0582±0.0099	693.2±196.0	−1.172±0.058	−2.556±0.564	393.54/359
64.571	66.126	0.0371±0.0088	349.0±75.8	−1.232±0.067	< −5.742	423.05/359
66.126	67.813	0.0287±0.0073	344.8±84.0	−1.137±0.079	−2.623±0.944	399.31/359
67.813	69.496	0.0292±0.0063	463.6±138.0	−1.182±0.073	−2.324±0.441	467.87/359
69.496	69.836	0.0896±0.0105	725.0±88.0	−0.743±0.056	< −8.680	372.08/359
69.836	70.212	0.1048±0.0141	553.5±73.1	−0.834±0.060	−3.928±3.460	369.74/359
70.212	70.748	0.1316±0.0328	243.4±40.1	−0.724±0.112	−2.167±0.156	363.61/359
70.748	76.011	0.0163±0.0054	235.3±43.6	−1.217±0.078	< −7.767	557.39/359
76.011	78.210	0.0354±0.0115	160.4±51.4	−1.229±0.130	−2.021±0.185	373.22/359
78.210	121.856	< 0.0177	<35.0	−0.898±1.300	−1.684±0.040	1483.3/359
GRB 130606B						
-3.072	8.039	0.0406±0.0034	314.8±19.8	−0.561±0.046	−2.012±0.048	592.26/476
8.039	9.019	0.1460±0.0139	370.0±31.6	−0.730±0.044	−2.092±0.064	515.85/476
9.019	9.424	0.1393±0.0070	1951.0±234.0	−1.011±0.021	−2.173±0.107	569.35/476
9.424	9.815	0.1949±0.0139	699.7±72.4	−0.846±0.033	−2.018±0.062	569.74/476
9.815	10.220	0.2004±0.0145	672.6±69.5	−0.846±0.033	−2.005±0.059	539.28/476
10.220	10.764	0.1765±0.0146	507.0±48.0	−0.848±0.036	−2.175±0.082	531.91/476
10.764	11.459	0.1997±0.0205	325.2±26.5	−0.686±0.048	−2.106±0.065	550.81/476
11.459	12.253	0.1464±0.0132	415.6±37.5	−0.808±0.040	−2.154±0.081	539.34/476
12.253	12.859	0.1434±0.0107	651.6±70.3	−0.887±0.033	−2.016±0.059	526.98/476
12.859	13.366	0.2035±0.0156	588.3±64.5	−0.859±0.036	−1.931±0.046	640.58/476

Continued on next page

Table A.4 – continued from previous page

$t_{\rm start}$ (s)	$t_{\rm stop}$ (s)	A (ph s^{-1} cm^{-2} keV^{-1})	$E_{\rm p}$ (keV)	α	β	CSTAT/dof
13.366	13.791	0.1857±0.0129	841.1±108.0	−0.962±0.030	−1.922±0.053	534.27/476
13.791	14.244	0.1794±0.0163	582.8±95.4	−0.992±0.039	−1.749±0.038	514.99/476
14.244	14.643	0.1721±0.0118	1066.0±188.0	−1.131±0.027	−1.880±0.057	512.53/476
14.643	15.140	0.1476±0.0109	974.4±181.0	−1.190±0.027	−1.945±0.069	508.88/476
15.140	15.815	0.1257±0.0093	839.6±146.0	−1.279±0.025	−2.154±0.111	556.16/476
15.815	16.659	0.1009±0.0076	732.4±103.0	−1.327±0.024	−3.402±1.230	521.86/476
16.659	17.717	0.0904±0.0094	409.8±58.2	−1.402±0.029	−2.917±0.751	546.90/476
17.717	19.180	0.0648±0.0064	457.8±65.5	−1.418±0.027	< -4.091	536.98/476
19.180	26.218	0.0566±0.0115	63.0±6.1	−1.419±0.078	−2.290±0.085	568.75/476
26.218	36.930	0.0266±0.0042	124.2±18.0	−1.316±0.062	−2.010±0.068	725.95/476
36.930	38.530	0.0848±0.0078	392.3±33.1	−0.938±0.036	−2.682±0.290	591.78/476
38.530	40.034	0.1075±0.0106	330.0±25.9	−0.821±0.042	−2.380±0.128	547.79/476
40.034	41.440	0.2016±0.0274	175.3±11.3	−0.691±0.060	−2.374±0.109	531.31/476
41.440	43.824	0.1237±0.0176	165.6±9.2	−0.858±0.049	−2.774±0.222	446.06/476
43.824	46.694	0.0996±0.0167	153.8±7.5	−0.885±0.047	−3.717±0.974	531.36/476
46.694	49.917	0.1140±0.0179	130.0±7.6	−0.648±0.067	−2.360±0.111	571.19/476
49.917	50.937	0.1577±0.0173	274.3±19.5	−0.763±0.046	−2.476±0.144	516.05/476
50.937	51.685	0.2721±0.0325	214.4±13.0	−0.534±0.055	−2.285±0.085	497.29/476
51.685	52.584	0.2729±0.0332	211.8±11.0	−0.604±0.049	−2.789±0.177	569.27/476
52.584	54.244	0.1599±0.0212	186.7±10.7	−0.708±0.053	−2.617±0.162	574.81/476
54.244	56.959	0.1294±0.0185	156.2±8.9	−0.739±0.057	−2.570±0.161	579.22/476
56.959	77.824	0.0809±0.0246	63.0±4.2	−0.590±0.129	−2.309±0.072	1006.3/476

Table A.5: Comparison between the average time-resolved and the time-integrated sharpness angles for the bursts (Ch. 4). Column (1) lists the GRB names using the *Fermi* GBM trigger designation that is assigned for each new trigger detected. Column (2) lists the numbers of spectra used in averaging θ and $\theta_{\rm left}$, N, for individual bursts. Columns (3) and (5) list the average time-resolved sharpness angles $\langle\theta\rangle$ and left angles $\langle\theta_{\rm left}\rangle$, and Cols. (4) and (6) list their respective standard deviations $SD = \sqrt{\langle\theta^2\rangle - \langle\theta\rangle^2}$ and $SD_{\rm left} = \sqrt{\langle\theta^2_{\rm left}\rangle - \langle\theta_{\rm left}\rangle^2}$. Columns (7) and (9) list the time-integrated sharpness angles $\theta^{\rm int}$ and left angles $\theta^{\rm int}_{\rm left}$, and Cols. (8) and (10) list their respective errors.

GRB name	N	$\langle\theta\rangle$	SD	$\langle\theta_{\rm left}\rangle$	$SD_{\rm left}$	$\theta^{\rm int}$	$\sigma^{\rm int}$	$\theta^{\rm int}_{\rm left}$	$\sigma^{\rm int}_{\rm left}$
(1)	(2)	(3)	(4)	(5)	(6)	(7)	(8)	(9)	(10)
080817.161	14	113.72	11.40	58.10	6.09	141.78	3.11	57.02	0.53
080825.593	12	104.97	17.79	50.46	5.20	125.47	3.03	50.57	0.68
080916.009	12	97.13	7.84	52.77	3.85	158.31	8.04	65.02	4.35
081125.496	4	79.65	9.23	43.98	4.68	125.60	5.95	48.77	1.37
081207.680	7	102.97	21.57	50.74	7.73	134.76	3.85	49.36	0.67
081215.784	16	113.42	20.45	51.99	4.89	128.58	2.33	53.27	0.35
081224.887	11	88.08	11.32	48.23	5.65	97.49	0.89	52.98	0.44
090131.090	1	125.13	-	66.06	-	149.10	2.88	63.36	2.07
090328.401	7	109.53	9.37	58.74	4.45	115.07	0.90	61.40	0.42
090424.592	27	94.86	8.24	51.65	4.05	121.41	2.46	59.76	0.40
090528.516	9	113.35	8.92	60.55	4.21	122.99	1.15	65.08	0.53
090530.760	4	74.46	3.24	41.34	1.68	122.69	1.43	58.23	0.74
090618.353	47	118.12	9.18	61.19	4.17	140.99	0.93	62.03	0.39
090626.189	10	110.62	10.07	55.91	7.11	146.27	2.43	63.82	0.64
090718.762	7	98.76	7.02	53.58	3.43	117.73	1.39	62.65	0.65
090719.063	19	80.31	7.63	44.33	3.92	96.27	0.77	52.38	0.38
090804.940	1	81.78	-	45.12	-	90.82	1.23	49.69	0.61
090809.978	7	102.46	13.01	51.64	4.24	141.06	3.46	54.05	0.87
090820.027	82	95.73	10.20	49.91	4.23	114.84	1.32	51.12	0.23
090829.672	32	130.12	13.03	67.80	5.62	153.69	2.56	72.83	0.38
090902.462	60	98.14	17.93	50.32	6.40	96.89	1.05	56.00	0.85
090926.181	56	104.08	20.17	50.84	4.76	136.77	1.80	55.01	0.42

Continued on next page

Table A.5 – continued from previous page

GRB name	N	$\langle\theta\rangle$	SD	$\langle\theta_{\rm left}\rangle$	$SD_{\rm left}$	$\theta^{\rm int}$	$\sigma^{\rm int}$	$\theta^{\rm int}_{\rm left}$	$\sigma^{\rm int}_{\rm left}$
(1)	(2)	(3)	(4)	(5)	(6)	(7)	(8)	(9)	(10)
091003.191	11	111.50	21.26	59.10	8.73	114.55	1.02	61.16	0.48
091010.113	3	87.61	14.55	47.94	7.25	114.84	1.81	61.30	0.85
091120.191	5	104.85	6.26	56.53	3.03	113.75	1.39	60.79	0.65
091127.976	4	136.45	11.17	71.11	4.98	147.43	2.08	63.86	2.56
091128.285	5	92.07	6.28	50.28	3.11	109.96	1.42	59.00	0.67
100322.045	17	101.47	8.81	54.31	4.86	150.77	0.97	46.10	0.51
100324.172	9	83.40	13.16	45.83	6.68	90.10	0.83	49.33	0.41
100414.097	14	94.27	22.51	46.01	6.45	91.59	0.55	50.07	0.27
100511.035	2	107.98	3.59	58.05	1.71	132.58	1.06	69.44	0.48
100612.726	4	98.33	7.75	46.38	3.58	120.01	3.33	52.36	0.96
100707.032	21	96.00	24.53	39.00	4.37	145.17	2.17	55.78	0.52
100719.989	13	111.32	23.61	45.57	8.05	126.63	2.91	52.48	0.53
100724.029	40	128.33	21.23	53.66	8.31	146.58	1.07	54.59	0.22
100728.095	20	87.19	4.95	47.85	2.48	111.12	4.14	50.33	0.39
100826.957	14	131.98	19.54	53.98	4.89	149.83	0.91	55.65	0.30
100829.876	4	88.51	7.22	48.49	3.63	141.16	3.82	52.67	1.64
100910.818	5	103.49	10.35	55.83	5.01	130.08	4.46	57.44	1.01
100918.863	26	101.71	8.23	55.00	4.02	99.82	0.58	54.12	0.28
101014.175	37	122.80	16.43	62.07	6.07	148.72	1.09	61.83	0.28
101023.951	10	111.86	7.84	58.76	4.30	138.19	2.83	59.73	0.86
101123.952	30	113.28	18.37	55.25	5.31	140.21	1.95	56.06	0.29
101126.198	11	116.00	5.50	61.82	2.58	129.69	1.25	68.13	0.57
101231.067	3	92.98	13.39	50.64	6.66	127.74	6.73	51.13	1.44
110301.214	21	105.55	9.15	54.71	4.33	119.12	1.28	56.21	0.47
110407.998	4	95.66	9.52	52.03	4.68	107.89	1.19	58.01	0.57
110428.388	5	78.48	8.18	42.80	4.64	101.69	3.00	44.70	0.54
110622.158	9	104.27	17.11	54.30	3.55	123.40	1.64	58.65	0.54
110625.881	37	101.15	14.11	51.18	5.87	128.70	1.67	53.85	0.44

Continued on next page

Table A.5 – continued from previous page

GRB name	N	$\langle\theta\rangle$	SD	$\langle\theta_{\rm left}\rangle$	$SD_{\rm left}$	$\theta^{\rm int}$	$\sigma^{\rm int}$	$\theta^{\rm int}_{\rm left}$	$\sigma^{\rm int}_{\rm left}$
(1)	(2)	(3)	(4)	(5)	(6)	(7)	(8)	(9)	(10)
110717.319	12	106.86	11.01	57.45	5.26	143.11	3.61	57.38	0.69
110721.200	9	123.02	11.45	58.32	11.02	160.99	1.31	58.56	0.51
110729.142	6	113.66	10.91	60.67	5.08	114.58	1.15	61.18	0.54
110731.465	7	90.09	13.06	49.21	6.50	113.45	6.95	52.88	0.77
110817.191	3	96.32	13.85	46.54	3.21	151.33	2.06	55.12	1.14
110825.102	18	95.10	10.12	51.74	4.95	117.89	0.81	62.72	0.38
110920.546	11	85.26	18.09	38.35	1.06	112.64	2.66	46.85	0.38
110921.912	9	109.51	6.17	57.30	3.38	128.10	4.55	56.72	0.49
111003.465	5	101.43	10.22	51.49	4.69	140.55	3.51	58.05	0.84
111216.389	7	112.41	15.99	57.59	2.28	111.91	1.23	59.92	0.58
111220.486	9	109.50	8.12	58.74	3.86	114.75	0.82	61.26	0.38
120119.170	14	107.72	10.16	57.87	4.81	129.94	3.60	57.56	0.67
120129.580	26	97.85	8.05	52.85	4.05	119.18	2.69	53.05	0.41
120204.054	39	111.53	13.74	59.63	6.46	126.38	2.02	63.29	0.31
120226.871	9	113.08	11.90	56.78	2.98	145.26	2.20	53.93	0.56
120328.268	22	125.40	22.21	53.35	4.62	145.76	1.12	52.85	0.43
120426.090	10	99.11	21.79	48.54	1.58	110.01	2.42	52.02	0.67
120526.303	10	97.10	7.83	52.75	3.80	110.52	3.43	51.15	0.48
120624.933	18	103.02	16.19	54.30	5.48	143.06	4.30	57.26	1.26
120707.800	12	130.08	17.19	63.49	8.75	145.04	2.13	62.19	0.93